# Actuation of DNA cages and their potential biological applications


**Aiman Entwistle**

Department of Physics

University of Oxford

This dissertation is submitted for the degree of

*Doctor of Philosophy*

St. Anne's College 2015

I would like to dedicate this thesis to my loving family and friends.

# Acknowledgements

I would like to thank the DNA group for supporting me in the past three years. I am very grateful for all your help and friendship. I would like to thank my supervisor, Prof Turberfield for your advice, guidance and discussions. I am in awe of your sharp mind and grateful to be able to work with you in the past few years. I would like to thank Dr Jon Bath, for all your time, patience and practical advice, always letting me 'externally processed' through a few things. Thanks for the amazing brownies and parties at your house. I would like to thank you Alex Lucas, Natalie Haley, Flo Benn and Mike Boemo for proofreading my chapters. I don't know what my thesis would be like without your help. I am so grateful for that. Alex, I will miss your jellyfish and crazy ideas. Natalie, though you are only a recent addition to the group, but I am so grateful for your encourage and promise will make an effort to keep in touch. For the rest of the group: Helen Carstairs, Adam Wollman, Carlos Sanchez, Robert Machinek, Katherine Dunn, Anthony Walsh, Wenjing Meng, Ibon Santiago, Celine Journot, Antonio, Robert Schreiber and Sam Tusk), thanks for being great colleagues and all the fun.

I would like to thank Prof Wood for the tissue culture facilities, to thank Samir El Andaloussi, Imre Mager, Fiona Lee and the Wood group for all the valuable advice and scientific discussions. Fiona, you are amazing. You are my molecular biology guru, my tennis and food buddy.

I would like to thank Alan Wainman for teaching me how to use the microscope and Nigel Rust for the flow cytometry.

I would like to thank the DTC, particularly Prof Garman for all the teaching opportunities and guidance. I would like to thank Federico Garza de Leon for the board game nights organised and meat feasts. I would like to thank EPSRC for funding my DPhil.

I would like to thank the Postgrad group at St. Aldates Church, for being a wonderful and encouraging community.

Finally, I would like to thank my family and Phil, for all your unconditional support through the highs, lows and tantrums.

# Abstract

DNA cages are polyhedra self-assembled from synthetic oligonucleotides in a one-pot process. The main system described in this thesis is a reconfigurable, wire-framed DNA tetrahedron in nanometre-scale. On one of its vertices this tetrahedron has an overhang that can hybridise with a specific sequence of nucleic acids and open the cage.

We describe the design of a reconfigurable cage that remained closed under physiological conditions and only opened in the presence of an appropriate signal in solution. Fluorescence techniques were employed to distinguish the open and closed states of the cage.

We used flow cytometry and confocal microscopy to successfully established the open and closed states of the cage inside live cultured mammalian cells. Further experiments revealed that the DNA cage could be opened by a separately transfected signalling strand. Hybridisation between two separately transfected systems was possible. The DNA cage was then simplified to a DNA duplex so that the intracellular interactions between the two nucleic acids systems could be studied more efficiently. Microscopy images showed that the interaction occurred in membrane-bound compartments.

We describe an investigation into the use of various cellular RNAs, including full-length mRNA and tRNA-RNA fusion, to actuate the DNA cages. Choosing an appropriate cellular opening signal remains a challenge. Analysis showed that bulky cellular RNA experienced steric hindrance with the rigid DNA cage. Finally, other potential biological applications of

DNA cages, such as using DNA nanostructures as the carriers for genetic therapeutic agents, were also presented.

# Contents

# Chapter 1 Introduction

The overarching goal of this project is to develop a DNA-based targeted drug delivery system. Targeted delivery is an important aspect of a drug delivery system because therapeutic agents often have adverse effect on both normal and diseased cells. A targeted system would reduce the side effects of the therapeutic agents. Ideally, the drug would only be released upon the detection of a disease marker. The success of many potential gene therapies and cancer treatments is dependent on their targeted drug delivery strategies.[1]

Recent development in DNA nanotechnology enables us to design and assemble sophisticated nanodevices. Since nucleic acids interact in a highly specific manner based on the Watson-Crick complementary base-pairing, this property offers an opportunity to design nanodevices that can respond to cellular nucleic acid signal, and hence a targeted system. In addition, DNA is a biopolymer that can be functionalised with a wide range of chemical groups and therefore, additional functionalities can be introduced into the structures. Furthermore, recent studies show that DNA nanostructures can be internalised into cells alone.[2–4] All these properties pave the way to develop a DNA-based drug delivery system.

In this chapter, I will first introduce some basic properties of DNA and then highlight the milestones in static and dynamic DNA nanostructures. Next, I will present studies on DNA nanostructures inside cells and their potential biomedical applications. Finally, I will discuss some DNA-based nanomaterials other than DNA nanostructures.

## 1.1 DNA as a building material

DNA is a biopolymer formed from a sequence of four natural bases: adenine (A), cytosine (C), guanine (G) and thymine (T). A short single-stranded DNA is sometimes called an oligonucleotide. A & T and G & C form hydrogen bonds with each other and this interaction is called Watson-Crick complementary base-pairing. Two oligonucleotides with complementary sequences will hybridise to form a double helix because this is a more energetically favourable formation than two single-stranded DNA.

Because of this highly selective interaction between the bases, the information required to assemble nanometre-scale structures can simply be coded into the sequence of the oligonucleotides, giving us precise control over their geometry at the nanoscale. DNA nanostructures can be rationally designed to suit a specific purpose. In the past decade, there has been rapid development of DNA as a nanomaterial and considerable advances in potential biological and biomedical applications have been made. In this Chapter, I will highlight the milestones of DNA nanotechnology and some of the current developments.

## 1.2 DNA structural nanotechnology

### 1.2.1 Wire-framed polyhedra

The construction of a closed DNA polyhedron was first reported in 1991, but it required multiple steps and the yield was low.[5] In 2004, Goodman et al.[6] demonstrated the first three-dimensional DNA structure that was self-assembled in a one-pot reaction with high yield. The synthesis of this tetrahedron is simple: it only requires equimolar quantities of the four

component strands to be annealed in the presence of magnesium ions. In this tetrahedron, each strand runs round one face and each edge is 7 nm in length (Figure 1-1). This study demonstrates that it is possible to have a robust one-step synthesis process for rigid polyhedral DNA structures with simple design principles.

Since then, many different wire-framed polyhedra have been constructed. They all have double helices as edges with open faces. He et al.[7] used three-point-star tiles that can connect to other identical tiles via complementary base pairing to build supra-molecular polyhedra of up to 100 nm in size (Figure 1-2). For the rest of the thesis, an enclosed DNA polyhedron is considered as a DNA cage. The two terms will be used interchangeably.

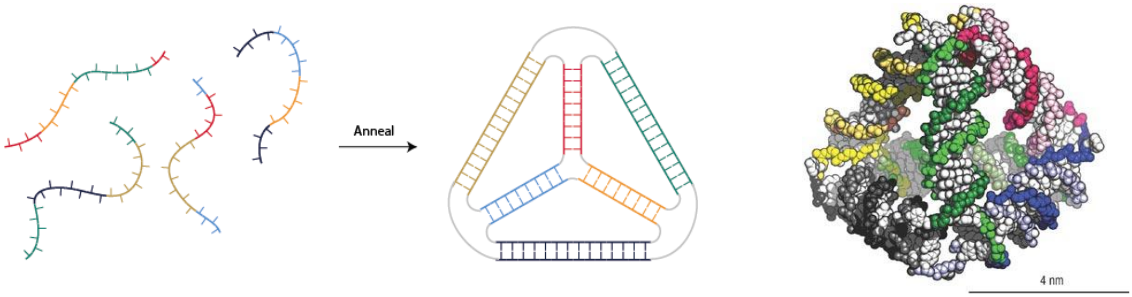


Figure 1-1: The formation scheme of a DNA tetrahedron (left). The molecular model of a DNA tetrahedron (right). Taken from Reference 8.

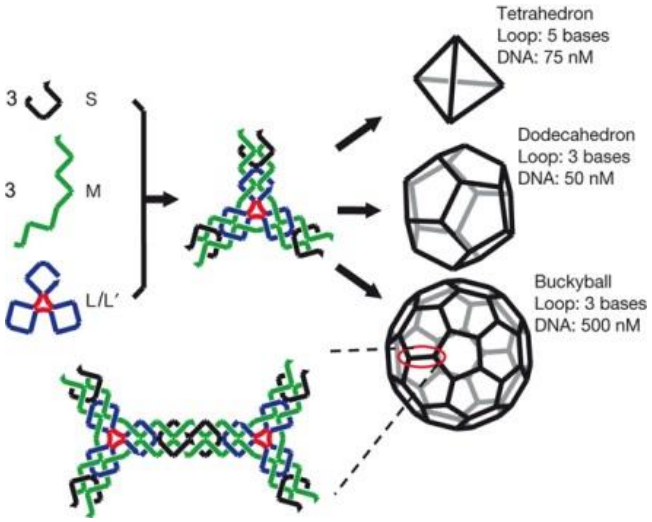


Figure 1-2: DNA polyhedra self-assembled from three-point tiles at various concentrations. Taken from Reference 7.

### 1.2.2 DNA Origami

In 2006, Rothemund reported the DNA origami method to synthesise DNA nanostructures.[9] This led to a paradigm shift in the design strategy of structural DNA nanotechnology because more complicated structures could be constructed. The origami method involves a long single-stranded DNA (the "scaffold") self-assembled into pre-designed shape by many short DNA strands ("staples") in a one-pot synthesis process (Figure 1-3a). The first reported origami structures are a range of two-dimensional patterns of 100 nm in size (Figure 1-3b).

The DNA origami structure consists of bundles of DNA helices and these bundles are held together by staple strands that run through two adjacent helices. Figure 1-3b shows a section of two helices within an origami structure, being held together by two staple strands (orange and purple) that are part of both helices. The black triangles point to a crossover. The positions of crossovers are very important in the design of origami structure because they control the curvature of the folded object. For the two-dimensional structures, such as tiles, the spacing between crossovers needs to be an odd number of half helical turn, so that the crossover strands will experience least strain. Curvature and twist (Figure 1-3c) can be introduced via engineered insertions or deletions of base pairs between adjacent crossovers.[10,11]

With the DNA origami method, we have increased control over the geometry of the designed nanostructure at the nanoscale. This makes DNA is a fantastic nanomaterial from a structural point of view.

In 2012, Ke et al.[12] presented a simple and modular framework to self-assemble three-dimensional structures with only short, synthetic DNA strands ("DNA bricks"), without the

need of a scaffold strand. The major advantage is that the shape can be customised by switching in and out component strands from a bank of strands. This further diversifies the approaches available to form complex three-dimensional structures.

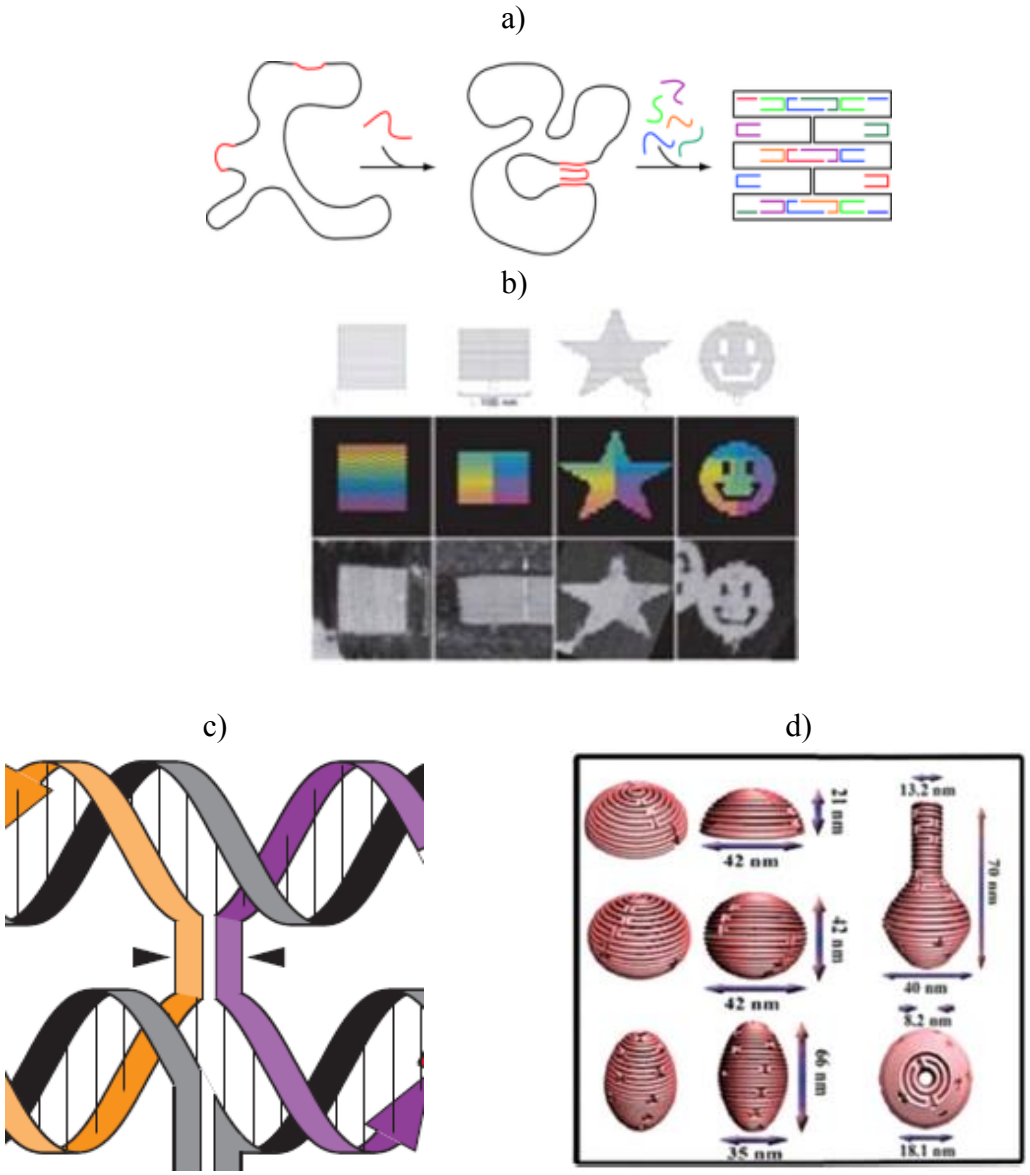


Figure 1-3: Examples of DNA origami structures. a) illustrates the formation principle of DNA origami structures. A long scaffold (black) is folded into the desired shapes by many short staple strands. Taken from [1]. b) shows the designs and AFM images of some two-dimensional origami structures. Taken from Reference 9. c) Similar to a), but with strands drawn as helices. The black triangles highlight the position of a crossover within a generic origami structure d) shows three-dimensional strcutures with complex curvature self-assembled by the origami method. Taken from Reference 11.

[1] http://www.softmatter.physik.uni-muenchen.de/liedl_group/index.html

## 1.3 DNA nanostructures with functional properties

DNA itself has limited chemical and optical functionality, but DNA nanostructures can act as scaffolds for building nanoparticles with new properties. Erben et al.[13] covalently attached a protein (cytochrome *c*) to a DNA strand through a surface amine to form a protein-DNA conjugate. This DNA strand is one of the four component strands of a tetrahedron. When the DNA tetrahedron is assembled with this protein-DNA conjugate, the tetrahedron will have a protein attached to it (Figure 1-4a). The position of the protein relative to the cage, i.e. whether it is inside or outside the cage, can be controlled by altering the sequence of the strand bound to the protein.

Furthermore, molecules can also be attached to the DNA nanostructure through non-covalent interactions. Crawford et al.[14] encapsulated a transcription factor by incorporating a sequence-specific DNA recognition site into one of the edges of the DNA tetrahedron (Figure 1-4b). By shifting the binding site along the edge, they could also control the orientation of the protein.

Compared to wire-framed DNA nanostructures, DNA origami structures provide us with even more freedom to spatially address the nanostructures. Voigt et al.[15] used a DNA origami tile as a pegboard for single-molecule chemical reactions at predetermined positions and imaged them by atomic force microscopy. Fu et al.[16] arranged horseradish peroxidase and glucose oxidase enzyme pairs on the DNA origami tiles with specific inter-enzyme distances, in order to study the distance-dependent kinetic process (Figure 1-4c). Fu et al.[17] attached the same enzyme pair to the interior of DNA nanotubes to study the coupling efficiency of an enzyme cascade in confined space.

All these examples confirm that DNA is a highly versatile nanomaterial because functional properties can be introduced. Moreover, DNA nanostructures have the potential to create an artificial system for studying chemical reactions in a highly organised crowded environment. This is a more realistic model of the cellular environment, where proteins are often present in confined areas. This could alter their interactions and behaviours drastically due to changes in equilibrium constants and reaction rates.[18,19]

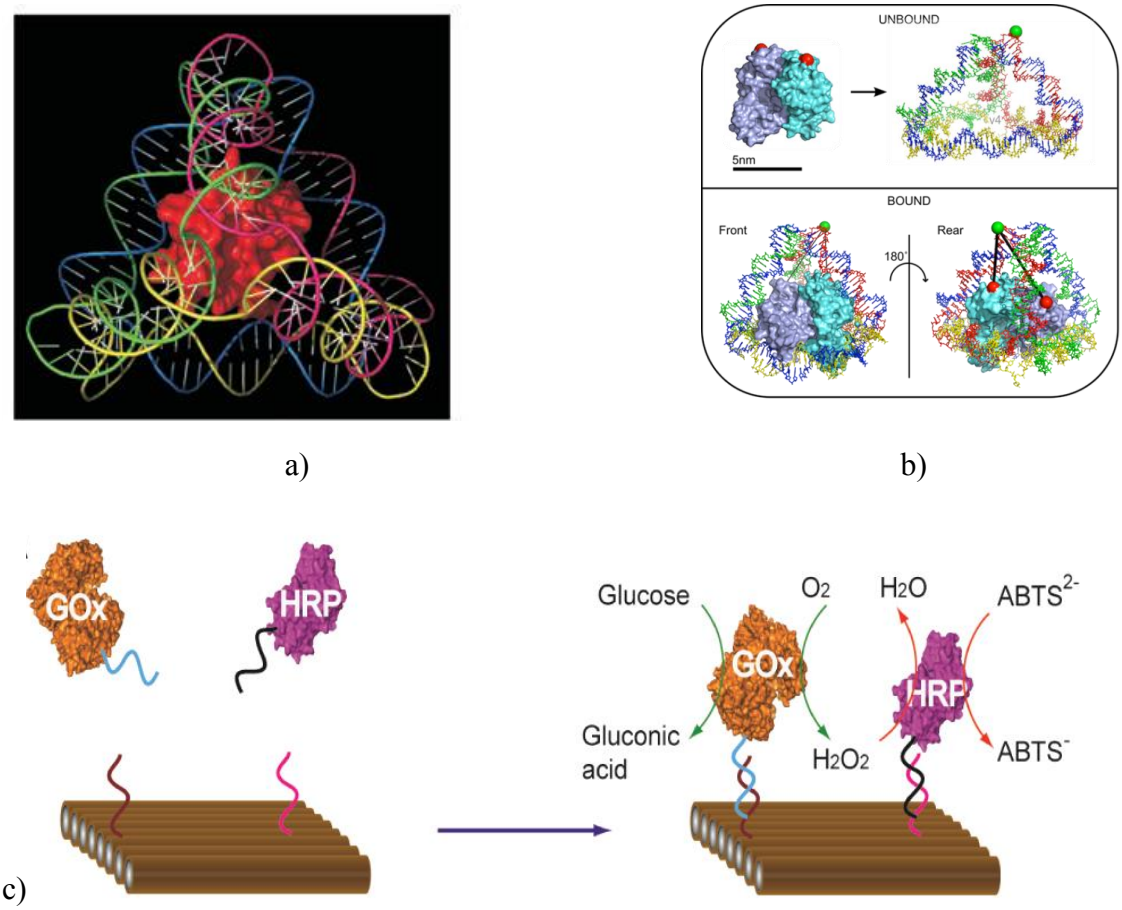


Figure 1-4: Example of DNA nanostructures with functional properties. a) is a molecular model showing cytochrome *c* encapsulated inside a DNA tetrahedron. Taken from Reference 13. b) shows the encapsulation of a transcription factor into a tetrahedral structure. Taken from [14] c) is a schematic diagram of an enzyme pair attached to an origami tile. Taken from Reference 16.

## 1.4 Dynamic DNA nanostructures

Other than having precise control over the structural design of the DNA nanostructures, dynamic properties can also be introduced. Herein, I will focus on dynamic DNA nanostructures with conformational changes that can be triggered by a variety of stimuli.

### 1.4.1 Conformational changes controlled by strand displacement

Firstly, I will talk about conformational changes of DNA nanostructures triggered by toehold-mediated strand displacement reaction (Figure 1-5). In its most basic form, the process involves a duplex and an invader strand. The duplex consists of a short and a long strand, so the duplex has a single-stranded overhang region called the toehold (red) and a double-stranded region called the displacement domain (black).

The invader strand and the long strand are fully complementary, so the long strand has more complementary bases with the invader strand than with the short strand. Therefore, a duplex between the invader strand and the long strand is thermodynamically favourable and this is the driving force of the strand displacement reaction.

In the first stage of strand displacement, the invader strand hybridises to the toehold domain of the long strand. Then, the invader strand displaces the short strand base by base via branch migration. This is modelled as an unbiased stochastic process[20,21] and the branch point of the three-strand complex can either advance along the displacement domain or return to the beginning. When the branch point is sufficiently advanced, the short strand disassociates from the long strand. This marks the end of a strand displacement reaction and this cannot be

reversed because the invader strand and the long strand have formed a fully complementary duplex.

On the other hand, the branch point could return to the beginning of the displacement region. Depending on the toehold strength, there are two possibilities: the invader strand might completely dissociate from the long strand or the invader strand might remain bound to the toehold and re-initiate the displacement of the short strand. The later case will increase the probability of successful strand displacement. Therefore, the rate of strand displacement reaction is highly dependent on the toehold stability, which is influenced by its sequence and length.


Figure 1-5: Toehold-mediated strand displacement. The long and short strands are hybridised to each other to form Duplex 1 because they are complementary in the black region. The invader strand is fully complementary to the long strand (black and red). The invader strand first hybridises to the toehold region in the long strand and eventually displaces the short strand from Duplex 1 to form Duplex 2 with the long strand.

Yurke et al.[22] constructed the first dynamic DNA nanomachine: a DNA tweezers (Figure 1-6). They went beyond using DNA only as a structural material, but also used DNA as the 'fuel' to power the motion. The tweezers can be opened or closed reversibly by the addition of appropriate strands that lead to strand displacements. The closed and opened states are reported by a fluorescence read-out. Dittmer et al. extended the idea to using mRNA as the 'fuel' to induce conformational changes in the tweezers.[23] The mRNA is transcribed from the *in vitro* transcription reaction of an artificial gene, so the mRNA is not a full length transcript that codes for a protein. It is a proof of concept, rather than using a relevant biological signal to trigger changes in DNA nanomachines.

Strand displacement reaction has also been incorporated into three-dimensional DNA polyhedral structures. Bujold et al.[24] constructed a sequence-responsive DNA cube (Figure 1-7). It has overhangs that can hybridise with specific opening strands and this unzips the cube into a flat two-dimensional structure.

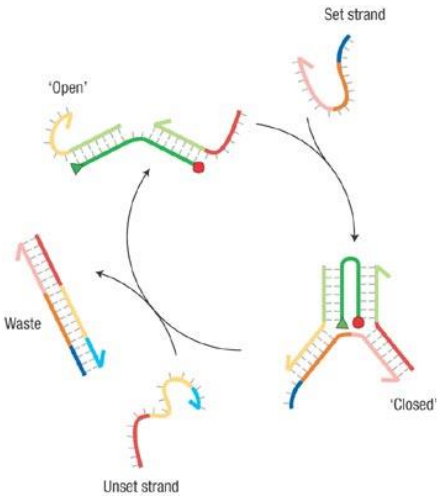

Figure 1-6: Schematic diagram of DNA tweezers undergoing reversible conformational changes. Taken from Reference 8.

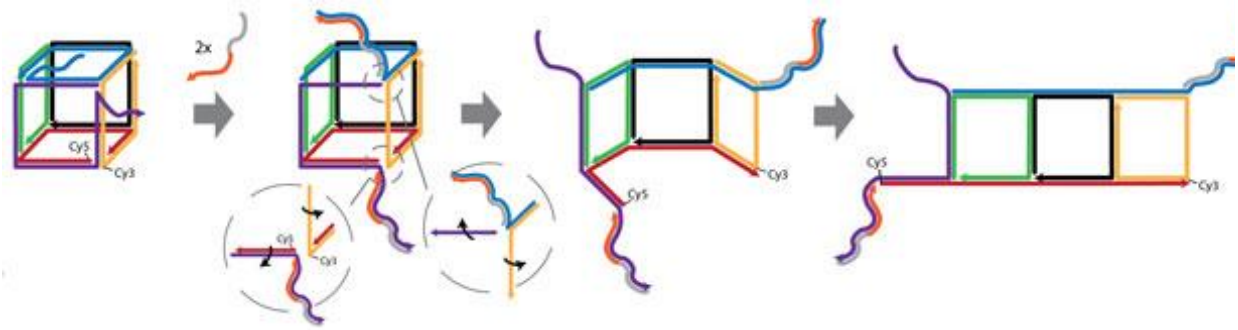


Figure 1-7: Schematic diagram of the conformational change of a sequence-responsive DNA cube. Each cube has two overhangs, so it requires two identical opening strands to unzip the three-dimensional cage into a flat two-dimensional structure. When the cage is closed, Cy3 and Cy5 are adjacent to each other at a vertex, so they are in close proximity. Due to fluorescence resonance energy transfer (FRET) from Cy3 and Cy5, when the construct is under excitation at 550 nm, the emission at 570 nm by Cy3 would reduce, but the signal from Cy5 at 670 nm would increase. When the opening strand unzips the cage, the two fluorophores are at the opposite end, so the FRET signal is low. This increases the emission at 570 nm by Cy3 and decreases the emission at 670 nm by Cy5 when the construct is excited at 550 nm. Taken from Reference 24.

### 1.4.2 Conformational changes controlled by chemicals and aptamers

Other than using nucleic acids to displace another strand from a duplex, small molecules that target particular aptameric oligonucleotides have also been used.

Aptamers are specific sequences of nucleic acids that bind strongly to their target molecules.[25] The selection of aptamers is based on the systematic evolution of ligands by exponential enrichment (SELEX) procedure.[26] It began with a library of over $10^{15}$ random oligonucleotides, followed by 8 – 15 cycles of binding-separation-amplification, and finally identified an aptamer with high affinity towards a specific substrate. Aptamers can bind with

a wide range of molecules, such as thrombin,[27] cocaine[28] and ATP[29], in micro- to nanomolar concentration. Due to the binding strength and specificity of aptamers to their targets, they are often compared with antibodies, but one of the distinctive properties of aptamers is that they undergo drastic conformational changes upon binding with their targets. Based on this characteristic, a wide range of electrochemical[30,31] and optical[32–34] aptamer-based biosensors have been developed. For example, a thrombin-binding aptamer functionalised with an electroactive group was tethered covalently to the surface of a gold electrode. In the absence of thrombin, the flexible single-stranded aptamer prevented electrical contact of the electroactive group with the electrode. Upon binding with thrombin, the aptamer formed a G-quadruplex, which brought the electroactive group into proximity with the electrode. This led to electron transfer between the electroactive group and the electrode and hence an electrical signal upon the detection of thrombin. Other than extracellular detection, aptamers have been incorporated into antiswitches that modulate gene expression in yeast in response to a specific ligand.[35] The antiswitch has two domains: an antisense RNA domain and an aptamer domain. In the absence of the ligand, the antisense domain cannot interact with the mRNA because it is hybridised with another part of the structure. The protein encoded by the mRNA is expressed. In the presence of the ligand, the aptamer domain binds with the ligand and induces a conformational change that exposes the antisense domain. Then, the antisense RNA can bind with the mRNA and inhibit gene expression.

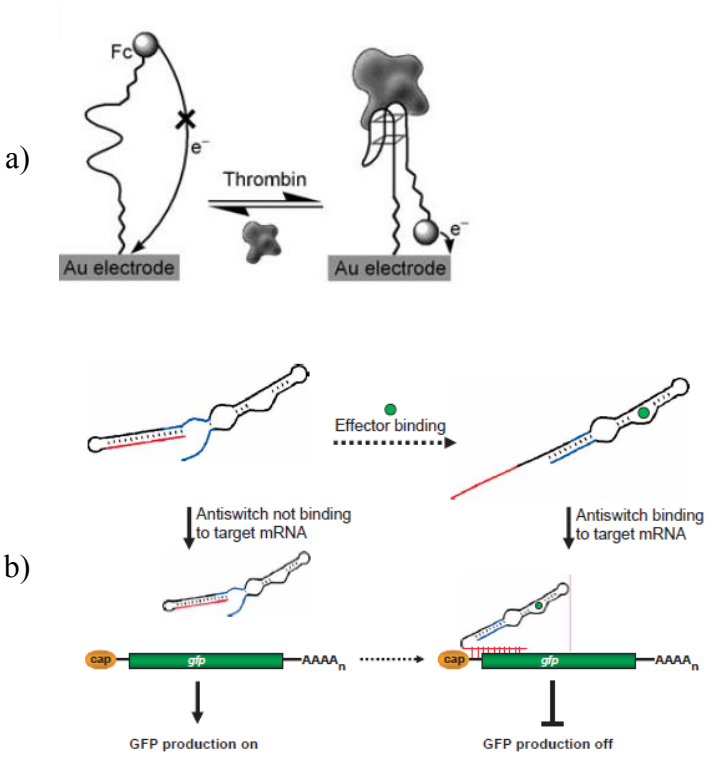


Figure 1-8: Designs of an aptamer-based biosensor and an antiswitch. A) A thrombin-binding aptamer is tethered to the surface of the gold electrode. The other end of the aptamer is functionalised with an electroactive group ferrocene (Fc). Upon binding with thrombin, the aptamer forms a G-quadruplex and brings Fc close to the gold surface. This results in an electric signal. Taken from Reference 31. b) illustrates the mechanism of a antiswitch that regulates gene expression. In the absence of the ligand, the antisense domain (red) is hybridised to part of the antiswitch and the antiswitch is not active. In the presence of the ligand, the aptamer domain (blue) binds with the ligand and displaces the antisense. The antisense becomes single-stranded and therefore, the antiswitch is active. The antisense can bind to the target mRNA and inhibit the gene expression. Reference taken from Reference 35.

Furthermore, aptamers can be incorporated into the DNA nanostructures as dynamically responsive units. Pei et al.[3] built a DNA tetrahedron that can respond to changes in the chemical environment. One or two edges of the tetrahedron contain a special single-stranded

region (ssDNA). These regions contain an i-motif, ATP aptamer or T-rich mercury-specific sequences, which are dynamic and respond to the presence of different chemicals (Figure 1-9). For example, in the presence of ATP, the ssDNA region will bind to ATP and form a well-defined conformation, hence shorten the edge of the tetrahedron. They also showed that these structures can enter cells and remain responsive to the ATP environment inside cells.

Banerjee et al.[36] constructed a DNA icosahedron that separates into two halves in the

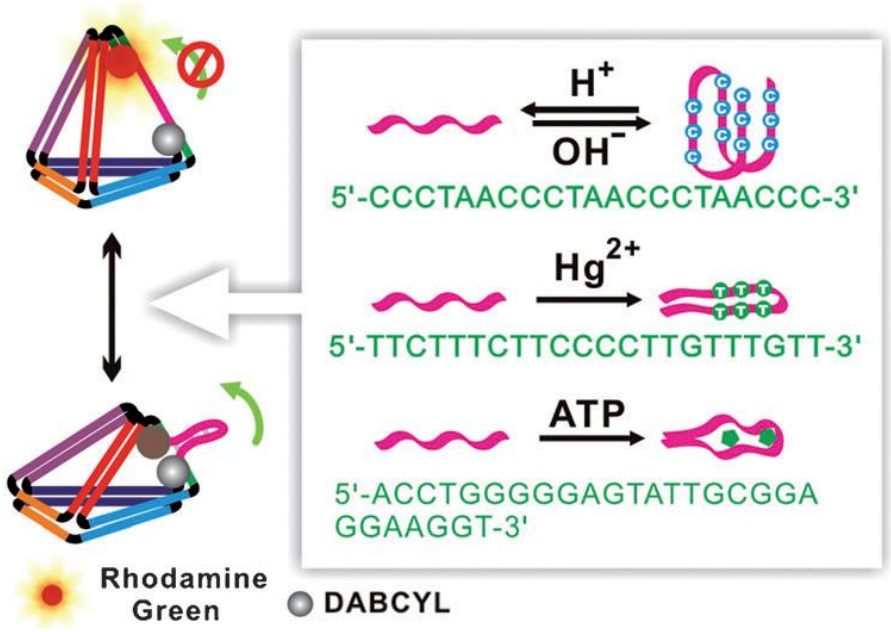


Figure 1-9: Schematic diagram of the reconfigurable tetrahedron. By incorporating a dynamic sequence into one of the edges, the tetrahedron is reconfigurable, depending on the chemical environment. Three dynamic sequences are used. They are aptameric sequences that bind strongly to their corresponding target molecules and undergo conformational changes. Taken from Reference 3.

presence of cyclic-di-GMP (cdGMP). The two halves are initially held together via ten identical lock sites (Figure 1-10). Each lock site consists of one cdGMP aptamer sequence. In

the absence of cdGMP, the aptamer sequence binds to the complementary strand that links to the other half of the icosahedron and this keeps the two halves together. In the presence of cdGMP, the responsive unit binds to cdGMP instead of its complementary counterpart and releases the other half of the icosahedron.

Through this conformational change, cargoes that are encapsulated inside the icosahedron can be released. The two halves of the icosahedron are joined together in the presence of a high concentration of cargo. The cargoes are encapsulated as the icosahedron closes. The cargoes are not covalently linked to any part of the nanostructure, but because each cargo is bigger than the open faces of the icosahedron, they cannot escape. The separation of the two icosahedral domains leads to the release of the cargoes.

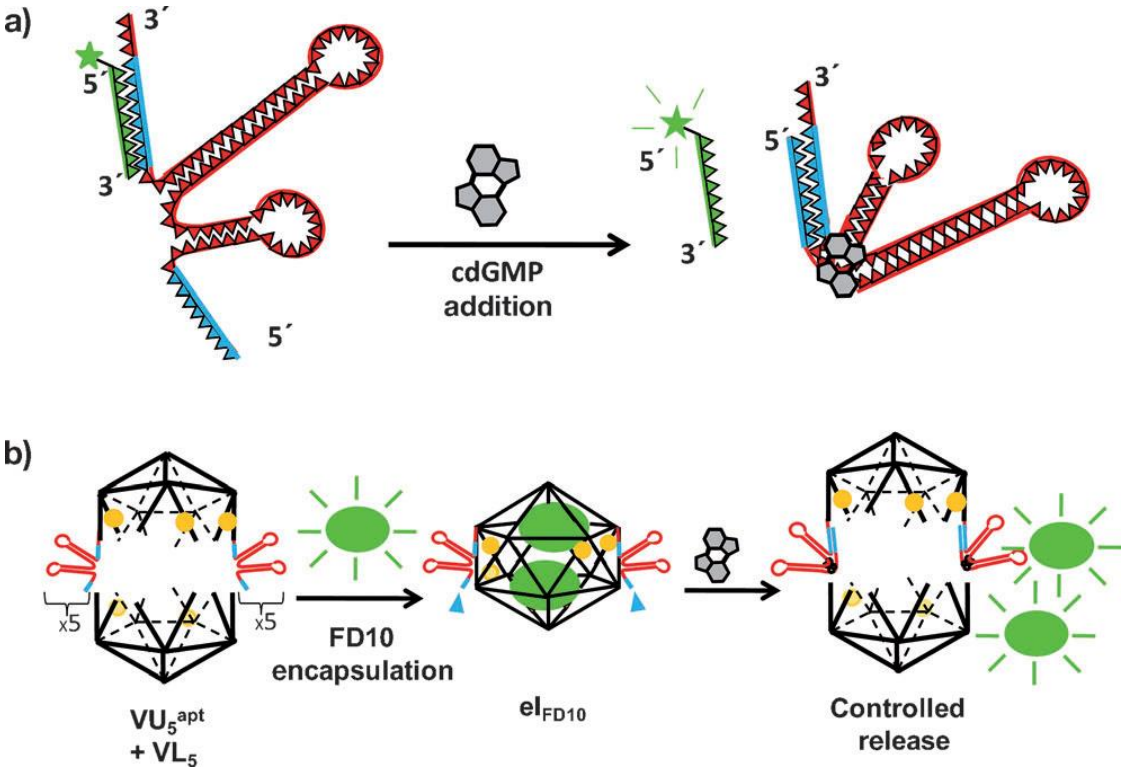


Figure 1-10: a) is the design of the lock sites of the DNA icosahedron. Upon binding with the cdGMP, the responsive unit undergoes conformational changes and displaces its complementary oligonucleotide. b) is a schematic diagram showing the encapsulation of the cargoes (10 kDa FITC dextran FD10, green) by two halves of an icosahedron held together by 10 cdGMP responsive units. The cargoes are released in the presence of cdGMP. Taken from Reference 36.

More complicated dynamic structures have started to emerge with the advance of DNA nanostructure design. Douglas et al.[37] assembled DNA nanorobots that can detect cell surface antigens, triggering a conditional opening of the structure and exposing the molecular payloads (Figure 1-11). The closed nanorobot has two domains that close to form a hexagonal barrel and is held closed by two lock sites. The lock sites consist of aptamer sequences that undergo structure-switching in the presence of the targets.

Compared to the icosahedron, the molecular payloads are loaded into the nanorobot via Watson-Crick base pairing between complementary strands. Each payload is covalently linked to the 5' end of a short oligonucleotide that is complementary to the extended region of a staple strand that is pointing into the barrel of the nanorobot. Therefore, when the nanorobot is open, it exposes the payloads. In this study, the payloads were a combination of antibody and induced growth arrest in leukemic cells. Since there is no particular mechanism for this DNA nanorobot to be taken into cells, this system neither enters the cells nor delivers the payloads into the cells, it only exposes the payloads to the cell surface; whereas for most drugs to be effective, the payloads need to be delivered into the cytosol. Nevertheless, this is the most complicated system described so far.

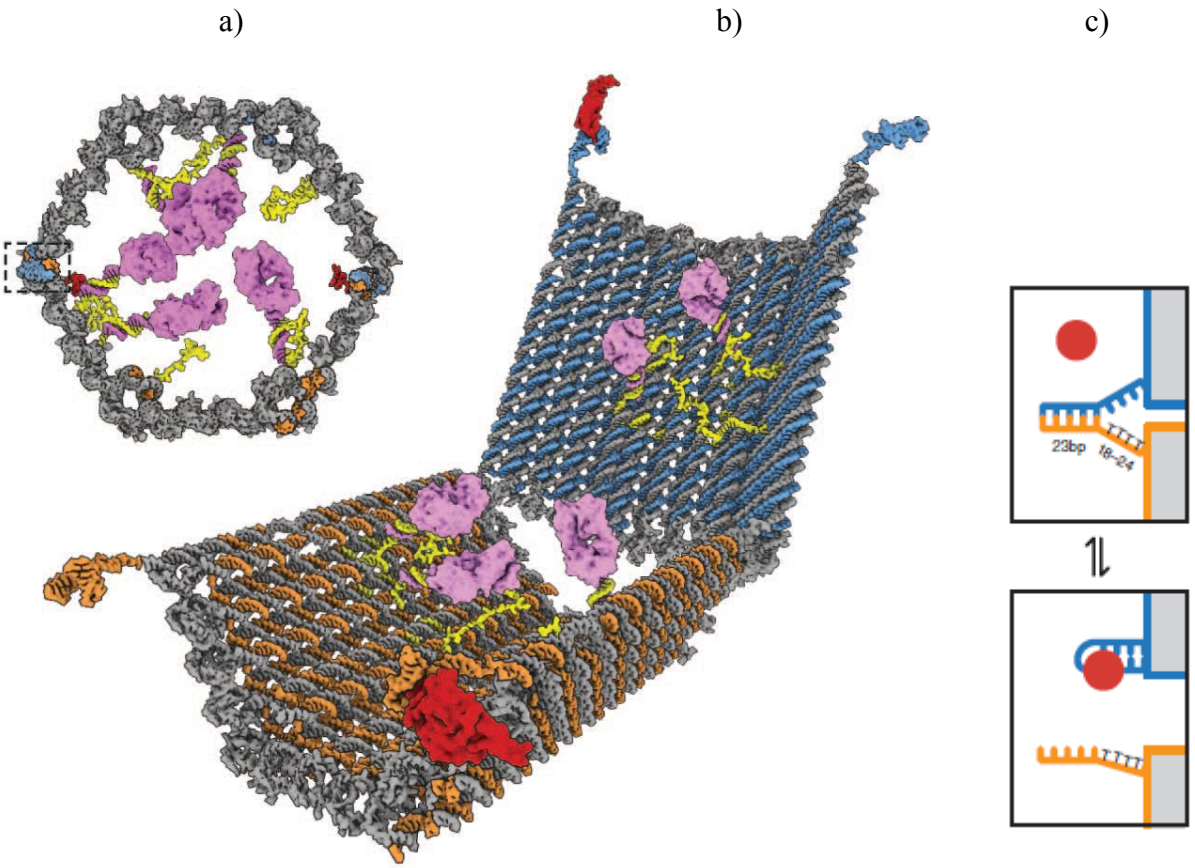


Figure 1-11: The schematic diagram of the design of the aptamer-gated DNA nanorobot. a) shows the front orthographic view of a closed nanorobot. It is held closed by two aptamer lock sites (blue and orange). One of them is highlighted in a rectangular dotted box. The nanorobot has a hexagonal barrel shape and is loaded with multiple molecular payloads (purple). b) is the open nanorobot and the hexagonal barrel is split into two domains. c) shows the aptamer lock mechanism. The blue strand has the aptamer sequence and is complementary to the orange strand. In the presence of the aptamer (red circle), the blue strand undergoes a conformational change and displace from the orange strand to bind with the aptamer molecule (red). This releases the other half of the barrel, opening the nanorobot. Taken from Reference 37.

### 1.4.3 Conformational changes controlled by temperature

Juul et al.[38] constructed a DNA nanocage that responded to temperature changes reversibly (Figure 1-12). The cage is based on a truncated octahedron. One of the six corners is composed of four DNA strands that can be folded into four hairpins. At 4˚C, the hairpin structures are stable and the cage is closed. As the temperature increases to 37˚C, the hairpin structure is no longer stable and the nanocage becomes opened. The pre-assembled cage is then incubated in a molar excess of horseradish peroxidase at 37˚C (open cage) and gradually cooled to 4 ˚C (closed cage). This temperature-controlled conformational transition of the DNA nanocage successfully encapsulates the enzyme with a maximum yield of 30%. Similar to the icosahedron, this example of controlled encapsulation and release of a protein cargo is not facilitated by any form of covalent or non-covalent attachment of the cargo to the DNA structure.

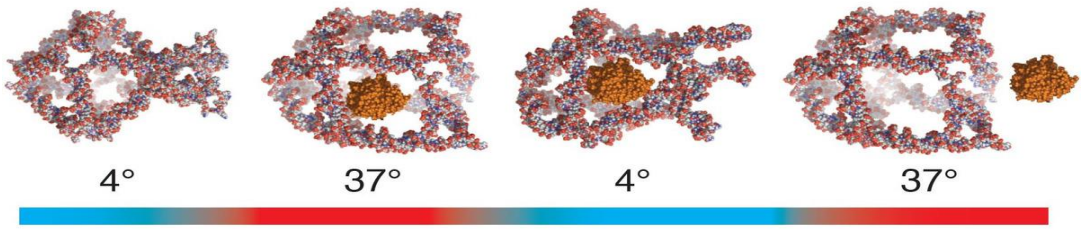


Figure 1-12: The schematic diagram of the temperature-controlled DNA nanocage. It undergoes a conformational change when the temperature varies between 4˚C and 37˚C. At 4˚C, the cage is held closed by 4 hairpin structures at one of the corners. At 37˚C, the hairpin structures are not stable and the corner relaxes and an enzyme (orange) can diffuse into the central cavity of the nanocage. This process is reversible. When the temperature returns to 4˚C, the hairpin structures re-form and close the cage. The enzyme is trapped inside the cage, because it is larger than the open faces. If the temperature increases again, the cage reopens and the enzyme can diffuse out of the cage. Taken from Reference 38.

## 1.5 DNA nanostructures in cells

Studying DNA nanostructures inside cells is the main theme of this thesis. Effective cellular delivery of such structures is crucial to their biomedical applications. Therefore, before describing possible biomedical applications of DNA nanostructures inside cells, it is important to briefly discuss how cellular uptakes of extracellular materials occur and ways to deliver DNA nanostructures across the plasma membrane barrier.

In this section, I will first introduce endocytosis, the process of how cells internalise extracellular materials, then describe the trafficking of those materials inside cells. Finally, I will highlight different methods used in the literature to deliver DNA nanostructures.

### 1.5.1 Endocytosis

### 1.5.2 Crossing the plasma membrane

The plasma membrane is the first barrier that separates the intra- and extra-cellular environment. Endocytosis is a process by which eukaryotic cells engulf extracellular materials into cells.[39] An area of the plasma membrane first surrounds the extracellular material to be internalised, and then the membrane buds off inside the cell. A vesicle with the ingested material is therefore formed. Through endocytosis, cells can internalise large particles such as bacteria, small solutes and proteins.

There are four main endocytotic pathways: clathrin-dependent endocytosis, caveolae-dependent endocytosis, micropinocytosis and phagocytosis.[39] The best-characterised one is the clathrin-mediated endocytosis.[40] Clathrin is a protein that coats the plasma membrane and

they assemble to form a basket-like structure (clathrin-pits) which encourages vesicle budding. Hence, the internalisation of extracellular materials occurs. Similarly, caveolae-dependent pathway involves the formation of pits in the plasma membrane via caveolin, a cholesterol-binding protein.[41] However, the caveolin-pits tend to be smaller than those formed by clathrin.

Furthermore, endocytosis can be receptor-mediated or non-receptor-mediated. In the former case, receptors will first be concentrated in the clathrin- or caveolin-pits. Then, the receptors bind to the target molecules and trigger the pits to bud off and form intracellular vesicles. The latter pathway results in some uptake of unwanted particles because the mechanism is non-specific.

### 1.5.3 Trafficking of internalised materials

There are three principal components of the endocytic pathway after internalisation: early endosomes, late endosomes and lysosomes (Figure 1-13).[42] The vesicles that bud off from the plasma membrane are first fused with the early endosomes. They are the first sorting stations for the internalised materials. Some molecules are recycled back to the plasma membrane, either through the Golgi network or the recycling endosomes. Early endosomes are mildly acidic with pH 6. The early endosomes gradually mature to late endosomes and they contain multiple vesicles. The pH further decreases to pH 5.5. Late endosomes are the second sorting stations in this pathway. Molecules can be recycled to the Golgi network or remain trapped in the late endosomes. Finally, the late endosomes become lysosomes, with pH 4.8 and they are bigger than the endosomes. They contain enzymes to degrade the unwanted internalised extracellular materials.

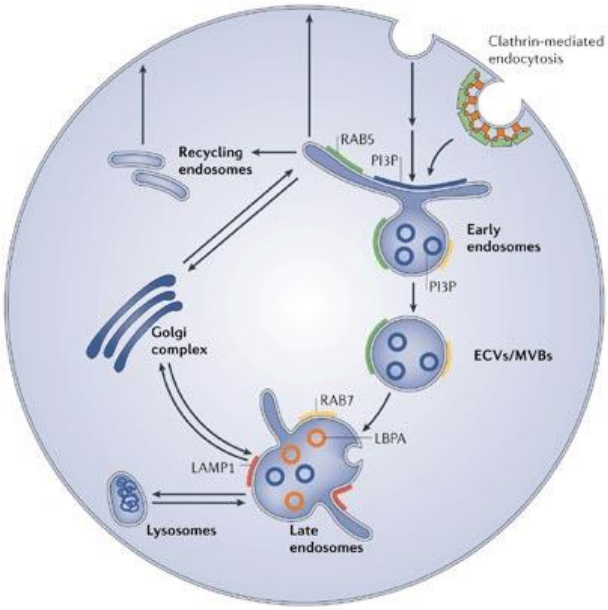


Figure 1-13: Schematic view of the endocytic pathway. Extracellular materials are internalised via Clathrin-mediated endocytosis. The internalised substances are transported to the early endosomes, which are the sorting stations in cells. As the early endosomes mature, multiple vesicles fuse together to form endosomal carrier vesicles (ECVs) or multi-vesicular bodies (MVBs). The vesicles become bigger and more acidic in the late endosomes. Finally, the late endosomes become lysosomes and the pH drops to pH 4.8. The trapped materials are destined for degradation. Important endosomal markers (RAB, P|3P and LBPA) are also included in the diagram. Taken from Reference 42.

### 1.5.4 Delivery methods for DNA nanostructures

DNA is negatively charged and hence does not cross the hydrophobic plasma membrane effectively. It is not internalised into cells via endocytosis effectively. In addition, for DNA nanostructures to perform their desired functions inside cells once they have crossed the plasma membrane, it is important for the structures to escape from the endosomes into the cytosol. Otherwise, they will eventually be degraded by enzymes in the lysosomes

In this section, I will focus on approaches that have been used to deliver various DNA nanostructures into cells.

### 1.5.4.1 Transfection reagents

Transfection reagents are commonly used to deliver genetic materials into cells. They are cationic chemicals that form a complex with negatively-charged nucleic acids. They can be liposomal-, polymer- or peptide-based. Lipofectamine® 2000 (LF) is considered to be the gold standard for gene delivery. The exact composition of LF is unavailable, but it contains liposomes formed by a mixture of cationic and neutral lipids.[43] The positively charged head groups from the lipids form complexes with the negatively charged sugar-phosphate backbone of the nucleic acids. This complexation enables the nucleic acids to overcome the electrostatic repulsion from the cell membrane and facilitates the contacts between the nucleic acids and cell membrane. The neutral lipid then promotes the liposomes to fuse with the cell membrane and this improves the uptake of the complexes containing nucleic acids.

However, transfection reagents are far from ideal because such chemicals are often toxic to cells[44,45] and most materials remain trapped in membrane-bound compartments after the uptake. Nevertheless, it is a simple and convenient method to deliver genetic material that does not require special equipment.

Hemphill et al.[46] delivered DNA duplexes with X-tremeGene HP transfection reagent into mammalian cells to perform logic gate operations; and Afonin et al.[47] delivered a pair of inactive RNA-DNA hybrids using Lipofectamine® 2000. Fakhoury et al.[48] used a DNA triangular prism to carry six antisense strands into HeLa cells with the aid of transfection

reagent Oligofectamine™. The antisense strands induced a knockdown of luciferase expression in the HeLa cells.

### 1.5.4.2 Chemical modifications

Another approach to promote internalisation of DNA nanostructures is to functionalise the structures with molecules that enhance uptake, for example, folate and unmethylated cytosine-phosphate-guanosine (CpG) oligonucleotides. Both of them can bind to receptors on the cell surface be internalised.

Ko et al.[49] functionalised DNA nanotubes with folate molecules. Since cancer cells overexpress folate receptors on the plasma membrane, the folate molecules on the DNA tubes can promote the uptake of the nanotubes into cancerous cells. Nanotubes without any folate had no significant uptake when compared to single-stranded DNA. The extent of delivery was measured via the Cyanine fluorescence (Cy3) because the DNA nanotubes were also functionalised with Cy3 fluorophores.

Similarly, Lee et al.[50] functionalised a DNA tetrahedron with folate molecules. The DNA tetrahedron was also used as a siRNA carrier and it achieved silencing effects on the target genes in both tissue culture experiments and in the tumours of mice. In addition, they screened another 27 tumour-targeting ligands and selected the most effective ligand to facilitate the delivery of the nanostructures. Functionalising the DNA tetrahedra with some cationic peptides was not stable and aggregation was observed. They also found that at least three folate molecules per tetrahedron were required for optimal delivery of the siRNA into cells and that spatial orientation of the folate molecule influenced the gene silencing

efficiency. The gene silencing effect of the tetrahedron functionalised with folate was comparable to their transfection with Lipofectamine. Both treatments induced over 50% knockdown of GFP expression when compared to untreated cells.

CpG oligonucleotides are recognised by Toll-like receptor (TLR9) as a signal for pathogen invasion, activating the immune response. Jiang et al.[51] showed that appending multiple CpG oligonucleotides to their DNA nanostructures can promote uptake into macrophage-like RAW264.7 cells, inducing an enhanced immune-stimulatory effect.

Bujold et al.[24] constructed a DNA cube, modified with hydrophobic and hydrophilic dendritic chains. Hydrophobic chains promote cellular uptake in the first 48 hours and hydrophilic chains induce slightly higher uptake after 72 hours. However, these uptakes are at least 10-fold less than those transfected with Lipofectamine® 2000.

Another option to enhance the cellular uptake of DNA nanostructures is to incorporate aptamers because they can bind strongly to receptors on the cell surface and be internalised. For example, three AS1411 aptamers have been incorporated into a DNA tetrahedron to enhance the intracellular uptake into cancerous cells[52]. AS1411 is a DNA aptamer that binds to the plasma membrane glycoprotein nucleolin,[53] which is up-regulated in some cancer cell lines.[54]

### 1.5.4.3 Microinjection

Microinjection is a process that injects liquid directly into a living cell or intercellular space using a glass micropipette. The liquid can contain genetic materials, proteins and other chemicals of study. It is performed under a microscope with a micromanipulator. It is an

effective~~, but labour intensive,~~ method to introduce material into either the nucleus or the cytoplasm. However, microinjection is labour intensive, operator dependent and it is not convenient for a large number of cells. These limit the potential biological applications for DNA cages, for example drug delivery.

Surana et al.[55] demonstrated the possibility to introduce intact DNA nanostructures into *Caenorthabditis elegans* via microinjection. As *C. elegans* is transparent, it is appropriate for fluorescence imaging to track the DNA nanostructures after microinjection.

Although there are not many studies that use this method to deliver DNA nanostructures, it is worth noting that microinjection is a common delivery method for DNA hybridisation probes in live cell mRNA imaging.[56–58] The mRNA imaging experiments showed that the delivered probes were in the cytosol and could hybridise with cytosolic mRNA. These results indicated the probes were not trapped in membrane-bound compartments and they confirmed successful cytosolic delivery via microinjection. Therefore, microinjection could be a very useful method to deliver DNA nanostructures to the cytosols.

#### 1.5.4.4 Simple incubation

There have been multiple publications reporting that three-dimensional wire-framed DNA nanostructures have the ability to enter mammalian cells without the aid of any transfection reagent.[2–4,24] Unlike their DNA component strands, the three-dimensional structures might lead to distinct property that enables the nanostructures to cross the plasma membrane. If DNA nanostructures can indeed cross the plasma membrane and enter cells at a reasonable concentration, this will give an incredible advantage for DNA nanostructures in

nanomedicine. Walsh et al.[2] observed a substantial uptake of DNA tetrahedra into HEK-293 cells and the amount is comparable to that being taken up with the aid of the transfection reagent Lipofectin®. This is the first reported unaided entry of DNA nanostructures into mammalian cells.

Pei et al.[3] also reported on a reconfigurable tetrahedron with an ATP aptamer that responded to the changes in ATP concentration in an intracellular environment. This implies that the tetrahedra are in the cytoplasm. However, the authors did not speculate the mode of entry of such structures into cells. Apart from the tetrahedral structure, Bujold et al.[24] also reported the uptake of DNA cubes in LNCaP cells and HeLa cells.

None of the above examples concluded on the uptake pathway of the DNA nanostructures, but Le et al.[4] used single-particle tracking methods to investigate the uptake pathway of a DNA tetrahedron labelled with Cy3 fluorophores. By introducing endocytotic chemical inhibitors and observing the uptake process at 4˚C instead of 37˚C, they concluded that the DNA tetrahedron is internalised through caveolin-dependent endocytosis. However, the DNA tetrahedron was trapped in the endocytic pathway and failed to have cytosolic access.

## 1.6 DNA nanostructures with biomedical applications

DNA is a biocompatible polymer, which makes DNA nanostructures an attractive candidate for biomedical applications.[50,59–62] In this section, I will outline some of the examples in literature in which DNA nanostructures were used to perform biomedical functions inside cells. DNA nanostructures have mainly been utilised as carriers for a cancer drug or genetic therapeutic agents.

## 1.6.1 Carriers

### 1.6.1.1 Doxorubicin

Doxorubicin (Dox) is a chemotherapy drug that is used to treat many different types of cancer.[60] It intercalates DNA double helices, interfering with many cellular processes, such as DNA replication. This induces apoptosis when cells are exposed to Dox. DNA nanostructures are ideal carriers to deliver a large quantity of Dox into cells because Dox has a natural affinity for binding to the DNA helices that make up the structures, and so Dox can be loaded by simple incubation.

Zhao et al.[60] loaded Dox onto twisted DNA bundles and observed enhanced cytotoxicity when compared to free Dox in solution. In addition, the drug release kinetics can be controlled by the degrees of twist in the DNA nanostructures. Both Jiang et al.[61] and Kim et al.[62] reported that by loading Dox onto DNA nanostructures (both origami structures and DNA tetrahedra), they can overcome the drug resistance of the cells. However, the underlying principles of the observed enhancement effects are currently unclear.

### 1.6.1.2 Genetic therapeutics

DNA can hybridise with other nucleic acids via Watson-Crick base pairing and so therapeutics oligonucleotides can be readily loaded on the DNA nanostructures. Such genetic therapeutics includes unmethylated cytosine-phosphate-guanosine (CpG) oligonucleotides, small interfering RNA (siRNA) and antisense RNA.

It has already been mentioned in section 1.5.4.2 that Jiang et al.[51] showed that appending multiple CpG oligonucleotides to their DNA nanostructures can promote uptake into macrophage-like RAW264.7 cells with an enhanced immune-stimulatory effect. Furthermore, Liu et al.[63] used a DNA tetrahedral structure as a platform to bring multiple antigens and CpGs together to build a synthetic vaccine complex that resembles a natural viral particle. The tetrahedral vaccine complex was incubated with RAW264.7 and it induced a strong and long-lasting antibody response when compared to antigens alone or antigens mixed with CpG in solution. DNA nanostructures can, therefore, serve as a general template for the rational design and construction of vaccines.

Antisense strands are single-stranded and siRNAs are double-stranded.[64] They act on different parts of the RNA interference pathway, but they both suppress the expression of their targeted genes. They are important genetic therapeutic agents because they can alter gene expression. Lee et al.[50] self-assembled a modified tetrahedral structure to carry one siRNA and observed gene silencing in both tissue culture and tumours in mice. Fakhoury et al.[48] developed a cage that carried six antisense RNA strands into HeLa cells and induced a knockdown of the luciferase expression.

### 1.6.2 Intracellular pH mapping

Beside using DNA nanostructures as carriers for therapeutic agents, Surana et al.[65] used a DNA nanodevice to map spatiotemporal pH changes in the endocytic pathway in *C. elegans*. The device has two oligonucleotides with cytosine-rich regions and a third strand that holds them together in the non-cytosine-rich regions (Figure 1-14). At neutral pH, the cytosine-rich regions are single stranded and the device is in the linear conformation. A fluorophore is

attached at each of the free end of the cytosine-rich overhangs. In this conformation, the fluorescence resonance energy transfer (FRET) between the two fluorophore is low. In an acidic environment, cytosines can undergo protonation and form base pairs with unprotonated cytosines. These base pairs intercalate and causes the cytosine-rich overhangs of the device to fold into a special quadruplex structure called "i-motif".[66] This transforms the device from a linear conformation to a triangular conformation, which brings the two fluorophores attached at the far ends closer and the FRET signal increases. The extent of conformational change can be quantified by (FRET).

Modi et al.[67] applied a similar concept to map pH changes inside live HeLa cells. Their dynamic DNA nanomachines reveal the morphology and pH of intracellular organelles. In addition, they tagged the DNA nano-devices with specific trafficking proteins, furin and transferrin, in order to study different endocytotic pathways with different destinations. One of the DNA nano-devices reached the trans-Golgi network and the other one reached the early endosomes. This study utilised the programmable nature of DNA nanostructures to achieve both organelle targeting and chemical mapping simultaneously in mammalian cells. This demonstrates the potential of DNA nanostructures in biomedical sensing and diagnostics in live cells.

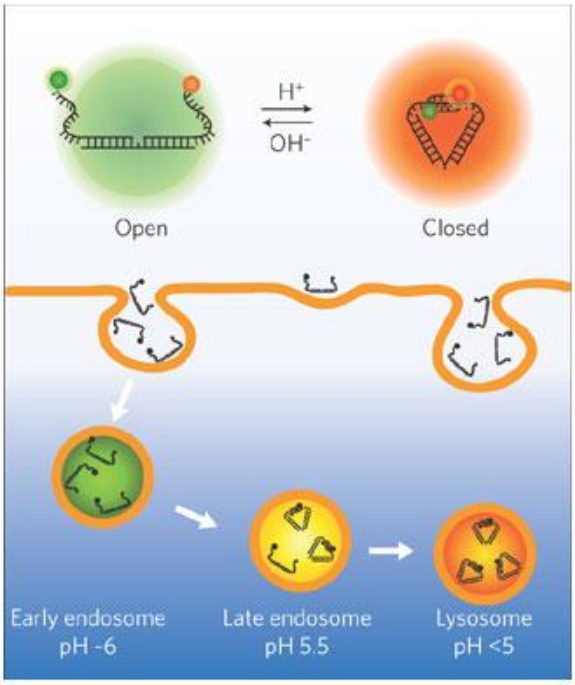


Figure 1-14: The schematic diagram of how the pH mapping nanomachine works. At high pH, the nanomachine is open and the FRET signal is low. At acidic pH, the nanomachine becomes closed because the two cytosine-rich oligonucleotides form an i-motif structure. The FRET signal increases. As the nanomachines enter the cell (middle), they undergo conformational changes and the FRET signal corresponds to the pH of the environment. This enables monitoring of the maturation of endosomal compartments. Taken from Reference 68.

## 1.7 Other DNA nanomaterials

### 1.7.1 DNA hydrogel

Developing nanomaterials for biomedical applications is a very exciting field of research. DNA nanostructure is the focus of this thesis, but it is only one of the many other candidates, even within the realm of DNA-based materials. DNA hydrogels formed from ligating X-shaped DNA have been utilised to deliver both CpG oligos and Dox to a co-culture of cancer

and macrophage-like cells. [69] These nanoparticles effectively inhibit the tumour growth because CpG stimulates an enhanced immune-stimulatory response and Dox is released from the hydrogel in a slow and sustained manner that induces apoptosis of a larger proportion of cancer cells than the free Dox.

### 1.7.2 Spherical nucleic acid

Another class of nucleic acids is spherical nucleic acid (SNA).[70] SNA is constructed from multiple DNA strands that are covalently attached to the surface of an inorganic core, such as gold nanoparticle. Oligonucleotides are arranged into highly-orientated, densely-packed spherical structures (Figure 1-15). This arrangement introduces distinct properties that are absent in either the core or the nucleic acids alone. Firstly, SNA is nuclease-resistant and it can cross the plasma membrane barrier and enter most cell types through the scavenger receptor pathway, which is known to mediate endocytosis.[71–73] Secondly, SNA has a polyvalent shell and because of cooperative binding, it can detect target molecules at a low concentration. The target can be nucleic-acid based, antibodies or proteins. A wide variety of *in vitro* molecular diagnostic assays based on SNAs have been developed.[74,75] For example, a SNA-based assay can detect prostate-specific antigens at attomolar concentrations in human serum.[76] By combining the first two properties, SNA can also be used to detect molecules inside cells.[77] For example, sequences that target specific mRNA can be incorporated into the SNA. Initially, those sequences are hybridised to shorter, complementary, fluorophore-labelled 'flare' strands. The fluorescence signal of the "flare" strands is quenched because they are close to the gold core. In the presence of the target mRNA inside cells, the strands bind to the complementary mRNA target because they can form more base pairs with it, and

this displaces the ‘flare’ strands. As the ‘flare’ strands diffuse away from the SNA, their fluorescence increases as it is no longer quenched by the gold core. Furthermore, SNA can cross the skin[78] and blood-brain barrier[79]. With all these properties, SNA is a strong candidate for future biomedical applications.

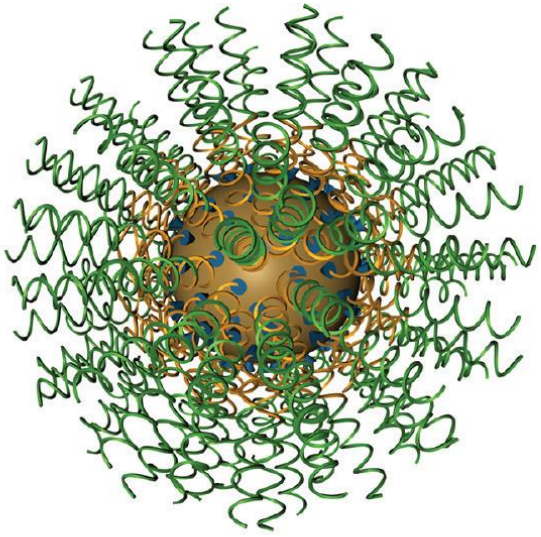

Figure 1-15: The schematic diagram of a spherical nucleic acid nanoparticle. It consists of an inorganic core that is densely covered with oligonucleotides. The end of each oligonucleotide has an amine or thiol group, so that the oligo can covalently link to the core. Functional groups, for example, aptamers, can be attached to parts of the oligonucleotides. Taken from Reference 80.

## 1.8 Summary and aim of the project

My DPhil has been developed under the overarching goal to build a DNA-based targeted drug delivery system that detects a specific disease marker and releases a cargo. For example, there is a specific gene translocation in prostate cancer which results in a unique fusion transcript.[81] Therefore, prostate cancer cells have a unique RNA marker.

My main focus is to investigate the potential ways to trigger a conformational change in a reconfigurable DNA tetrahedron inside cells with a specific signal. The actuation of the DNA tetrahedron is based on the toehold-mediated strand displacement reaction.

In Chapter 2, I discuss the stability of this reconfigurable DNA tetrahedron under physiological conditions. I designed a tetrahedron with a closing mechanism that is strong enough to keep the cage closed despite the magnesium ion depletion in tissue culture medium.

In Chapter 3, I establish the open and closed state of the tetrahedron inside mammalian cells as the positive and negative controls with the aid of transfection reagent. I also show that a proportion of tetrahedra can be open via a separately transfected, chemically-modified, synthetic oligonucleotide.

In Chapter 4, I simplify the DNA tetrahedron system into a DNA duplex in order to gain more insight into the interaction between the DNA nanostructure and the signalling strand.

In Chapter 5, I explore the possibility of using cellular RNA rather than synthetic nucleic acids to open DNA cages. Three candidates were tested: mRNA, modified tRNA and short RNA. They all have a complementary region that can in principle reconfigure the DNA tetrahedron.

Chapter 6 continues the results of associated experiments: I investigate the benefits of using DNA nanostructures as a carrier to deliver antisense RNA, the synthesis of a smaller tetrahedron and the potential of using DNA cages as a chemical reactor that regulates the activity of its cargo.

# Chapter 2 Design and stability of the reconfigurable DNA tetrahedron system

## 2.1 Introduction

In this project, the aim is to build a targeted drug delivery system with DNA nanostructures. In order to be a targeted system, the DNA nanostructures need to be able to respond to specific signals and this is the area I will focus on in this thesis. My main system is a reconfigurable DNA tetrahedron with an overhang and it can be opened in the presence of a specific signalling strand.

In this chapter, I will first describe the operation principle of this opening mechanism. Then, I will discuss different designs of the DNA tetrahedron; follow by the stabilities of the cage and the signalling strand under physiological conditions. Their stabilities under physiological conditions are very important because this is a system designed to be delivered and to function inside cells. The lack of structural integrity of the DNA nanostructure will compromise its engineered functions. There are two main factors that influence the stability of such nanostructures: cation concentration and nuclease activity, which I will investigate in Sections 2.3.3 and 2.3.4 respectively.

For the signalling strand, if it gets degraded, then it will not be able to interact with the DNA tetrahedron. Therefore, I will examine its stability in tissue culture medium and inside cells.

In the remainder of the introduction of this chapter, I will explain the important role of cations in the assembly of DNA nanostructures and I will highlight publications that studied the nuclease resistance of various DNA nanostructures.

### 2.1.1 The role of cations in the assembly DNA nanostructures

In order for the DNA nanostructures to fold into the designed structures, the sample mix is annealed in the presence of magnesium ions. This is because the phosphodiester backbone of the nucleic acid is negatively charged, so it requires the presence of cations to overcome the repulsive forces between the backbones, in order for a DNA strand to hybridise with the complementary strand to form a double helix. The $Mg^{2+}$ is essential for the formation and stability of the DNA nanostructures.

During the assembly, the sample mix is in buffer that has the desired concentration of $Mg^{2+}$, typically of 5-20 mM.[82] The exact $Mg^{2+}$ concentration is structure dependent. However, experiments will involve DNA nanostructures incubating with cells in tissue culture medium, in which the $Mg^{2+}$ concentration is at least five-fold lower than the typical buffer for DNA nanostructures. It is therefore important to test if these structures are stable in such environment. It is possible that although DNA nanostructures require a high $Mg^{2+}$ concentration during the folding, they could remain stable at a lower cation concentration after the assembly. In addition, tissue culture media have other cations, such as sodium, potassium and calcium ions and these cations also contribute to screening backbone charges and supporting the integrity of the nanostructures. It has been shown that DNA origami structures can be formed in molar concentration of $Na^{+}$, without $Mg^{2+}$.[83]

### 2.1.2 Nuclease resistance of DNA nanostructures

The second factor which might affect the stability of DNA nanostructures is nuclease degradation. Fetal bovine serum (FBS) is often added as a supplement to tissue culture medium. It contains nucleases[84] that would degrade DNA nanostructures during the incubation. Such nuclease degradation is also a problem for gene therapy. For example, DNA plasmids have a half-life in serum of 20 minutes.[85] The fully ligated DNA tetrahedra demonstrate some degree of nuclease resistance[86] when compared to the linear counterparts. The DNA tetrahedra have been shown to be stable in serum for up to four hours.[51] It is possible that the binding and catalytic activity of nucleases is inhibited by steric hindrance imposed on the enzyme from the three-dimensional structure of the DNA tetrahedra.

Mei et al.[87] incubated various DNA origami structures in cell lysate and examined their structural integrity under atomic force microscope (AFM) and transmission electron microscope (TEM) techniques. The images showed that those structures were stable in cell lysate for 12 hours.

Hahn et al.[88] reported two ways to reduce the nuclease activity: heat inactivation of FBS at 75˚C, and the addition of actin in the culture medium. However, the first method damages some of the serum proteins and is therefore likely to affect the cell growth. For the second method, actin competes against DNA nanostructures for binding with nucleases and hence reduces degradation of the nanostructures. Serum stability of DNA nanostructures can be further increased by chemical modifications of the component strands. Conway et al.[89] functionalised the ends of the component strands of a triangular prism with small chemical groups, such as hexaethylene glycol, and the prism's mean lifetime in serum increased from 2

hour to 62 hours. However, such modified oligonucleotides are not commercially available and utilising this technique would significantly increase the costs of the materials.

Another way to improve stability is to protect the DNA nanostructures with a membrane. Perrault et al.[90] elegantly encapsulated DNA nanostructures in PEGylated lipid bilayers to protect the structures against nuclease digestion. This also significantly improved the pharmacokinetic bioavailability of the nanostructures when they were injected into mice. However, these structures were not taken up by cells, and it would be difficult to communicate information across the artificial PEGylated membrane.

Summing up all these findings, some DNA nanostructures show evidence of being able to withstand physiological conditions. Chemical modifications could be introduced to extend the lifetimes of the nanostructures. Serum-free media could also be used during the experiments to prevent DNA nanostructures from degradation. This is the most direct way of avoiding nuclease activity whilst minimising the impact upon cell metabolism and phenotype.

## 2.2 Design of the reconfigurable DNA tetrahedron system

The reconfigurable DNA tetrahedron system consists of two components: the DNA tetrahedron and the signalling strand.

The reconfigurable tetrahedron is based on the DNA tetrahedron reported by Goodman et al.[6] It is typically assembled from four component strands, each of which runs around one face of the tetrahedron. In this reconfigurable DNA tetrahedron, one of the component strands of the tetrahedron (S4) has a single-stranded extension that serves as a toehold for hybridisation with a complementary single-stranded signalling strand.

The tetrahedron has two configurations: open and closed. Figure 2-1 illustrates the opening mechanism of the system: the closed tetrahedron (grey) hybridises with the single-stranded signalling strand (blue) and the product of this reaction is the open tetrahedron. The open state is energetically more favourable than the closed state because more nucleotides are paired.

### 2.2.1 Fluorescence read-out to determine the state of the configuration

Fluorescent labels and quenchers on the tetrahedron can report the different configurations of the system. A fluorophore (Cy3) and a quencher (Iowa Black® FQ) are used to indicate the state of the tetrahedral cage. On the left of Figure 2-1, the tetrahedron is in the closed state and the quencher (black circle) is held immediately adjacent to the fluorophore (pink circle), so that the Cy3 fluorescence is quenched. Where specified, Cy3 was replaced with Alexa-488 due to instrument requirement. Both Cy3 and Alexa-488 are effectively quenched by

quencher Iowa Black® FQ. According to the IDT website, Iowa Black® FQ absorbs from 420 to 620nm, with a peak absorbance at 531 nm. Since the peak emission for Cy5 is 665 nm, it is not quenched by Iowa Black® FQ.

On the right of Figure 2-1, the DNA tetrahedron becomes opened and the average separation between the quencher and Cy3 is bigger. Therefore the Cy3 fluorescence is brighter when the tetrahedron is open. Since the uptake of nanostructures varies between cells in live cell experiments, a second fluorophore, Cy5 (green circle), is used to report the level of uptake; the Cy5 fluorescence does not depend on the open or closed state of the tetrahedra. The Cy3:Cy5 ratio is used to report the fraction of open cages.

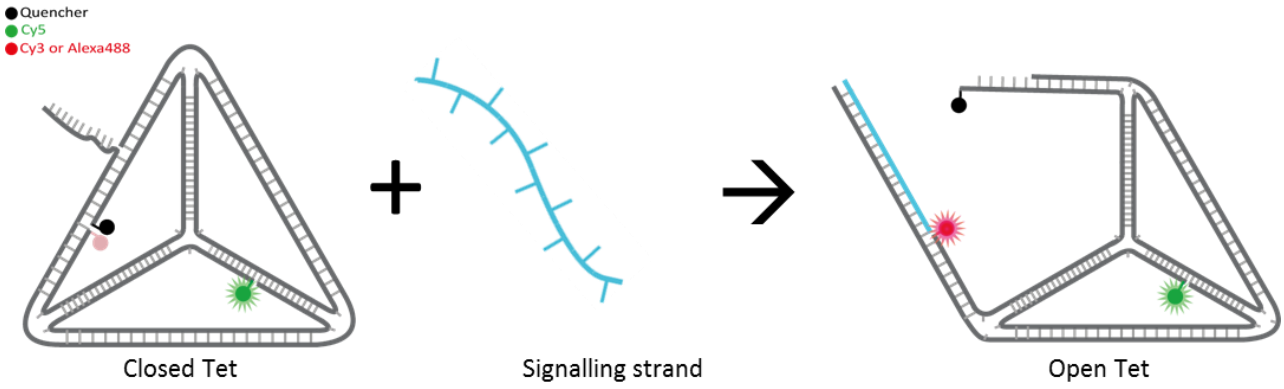


Figure 2-1: Schematic diagram for the opening mechanism. The reconfigurable tetrahedron is opened upon addition of a complementary signalling strand via strand displacement reaction.

Stein et al.[91] reported the Förster radius for the Cy3-Cy5 pair to be 5.3 nm. Within the closed tetrahedron, Cy3 and Cy5 dyes is 5 nm apart. Therefore, there could be some Förster Resonance Energy Transfer (FRET) between the Cy3-Cy5 pair in this tetrahedral system. However, the spectrometer used was not sensitive enough to detect significant amount of FRET between Cy3 and Cy5. The FRET signal was very low in both the closed and open state of the tetrahedron (Appendix C.1). Therefore, it is valid to use the Cy3:Cy5 ratio to determine the fraction of open cages.

The open tetrahedron is a more flexible structure than the closed one. Firstly, the two arms that formed as a result of the opening strand are hinged on the vertices and they move around them. Secondly, the end with the quencher becomes single stranded. The single stranded region is also flexible and will have a persistence length of approximately 1 nm.[92] It is possible that there is some fluorescence transfer from Cy3 to the quencher within the open cage. One can design more cages with appropriate fluorophores to gain additional information about the dynamics and average distances between fluorophores and quencher in the open configuration.

## 2.3 The reconfigurable DNA tetrahedron

### 2.3.1 Synthesis

A standard DNA tetrahedron has four component strands, S1, S2, S3 and S4. For a reconfigurable tetrahedron (Figure 2-2), there are two modifications. Firstly, S4 has an overhang that serves as a toehold for a complementary signalling strand, so that the

tetrahedron can be opened. Secondly, S2 of the reconfigurable tetrahedron is split into two parts, the S2 quencher and the 5' phosphorylated strand S2 Cy3. This is because the full length dual-labelled oligonucleotide is not commercially available from Integrated DNA Technologies (IDT). In the current design, the two strands can be ligated after the tetrahedron has been assembled.

The reconfigurable tetrahedron was formed by annealing the five component strands at a final concentration of 2.5 µM in Buffer A (10 mM Tris-HCl and 15 mM $MgCl_2$, pH 7.4) and then the sample was ligated overnight at room temperature. The tetrahedron was gel-purified by extracting the band corresponding to well-formed tetrahedra from a polyacrylamide gel, crushing the gel fragment with a pipette tip, and then soaking it overnight in Buffer A. The full protocol is given in Appendix A.2.

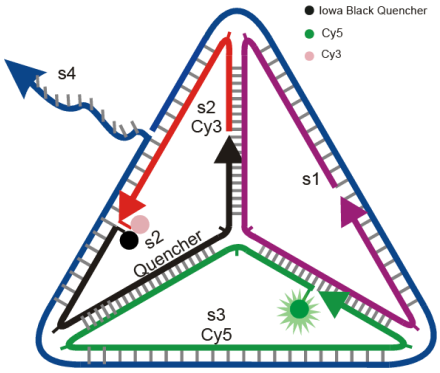


Figure 2-2: Schematic diagram of a reconfigurable tetrahedron before ligation, showing all the component strands. The arrorws are the 3’ end of the oligonucleotides

### 2.3.2 Opening

Ensemble fluorescence measurement was used to determine the conformational state of the tetrahedron in the buffer solution (Appendix A.6). Figure 2-3 shows the Cy3 and Cy5 fluorescence of a sample of 20 nM reconfigurable tetrahedron in 120 µl of Buffer A. The tetrahedron used in this experiment was OT2.2, which will be discussed in detail in the next section. During the first 25 minutes, the reconfigurable tetrahedron was in the closed configuration, so the Cy3 signal was low. Then, 10µl of 10µM of signalling strand was added into the sample mix. The signalling strand hybridised with the overhang and opened the tetrahedron. Hence, this led to a 20-fold increase in the Cy3 signal while the Cy5 signal remained at a similar level. The slight drop in Cy5 signal was due to the dilution effect of the addition of 10µl of the signalling strand. The fluorescence measurement agreed with the design principle of the DNA tetrahedron.

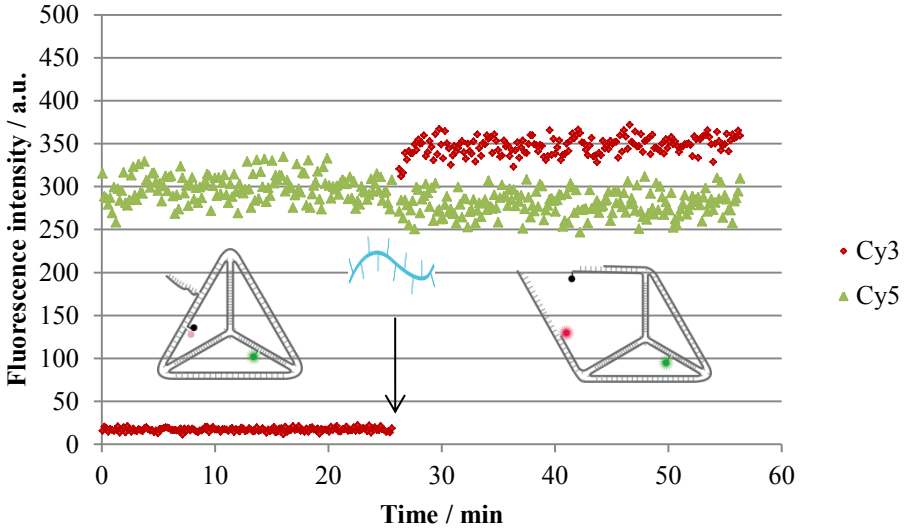


Figure 2-3: Fluorescence measurement of the reconfigurable tetrahedron. Initially, the tetrahedron is in Buffer A (10 mM Tris-HCl and 15 mM $MgCl_2$, pH 7.4) and it is closed. At 25 minutes, the opening strand in molar excess is added into the sample mix and it opens the tetrahedron, which leads to the increase in Cy3 signal.

### 2.3.3 Stability at low magnesium ions concentrations

Cations are necessary for a DNA strand to hybridise with its complementary strand to form a double helix. The reconfigurable DNA tetrahedron is therefore self-assembled in the presence of 15 mM $Mg^{2+}$ ions. However, in tissue culture medium, the $Mg^{2+}$ concentration is much lower (around 1 mM) and this causes unintentional opening of the first design of the tetrahedron (OT2.2). It becomes open in the absence of the signalling strand because the closing mechanism is not strong enough to keep the cage closed at physiological level of magnesium ions.

### 2.3.3.1 OT2.2

In the initial design, OT2.2 (Figure 2-4) has an overhang of ten nucleotides (nt) long and is held closed by the six base pairs (bp) segment (sequences see Appendix B.1.1). When the cage is closed, a low Cy3:Cy5 ratio is expected and when it is opened, a high Cy3:Cy5 ratio is expected. This ratio can also be used to reflect the stability of the cage in different environments. The ensemble fluorescence measurements and native gel electrophoresis experiments were used to measure the fluorescence read-out and hence assess the stability of the cage.

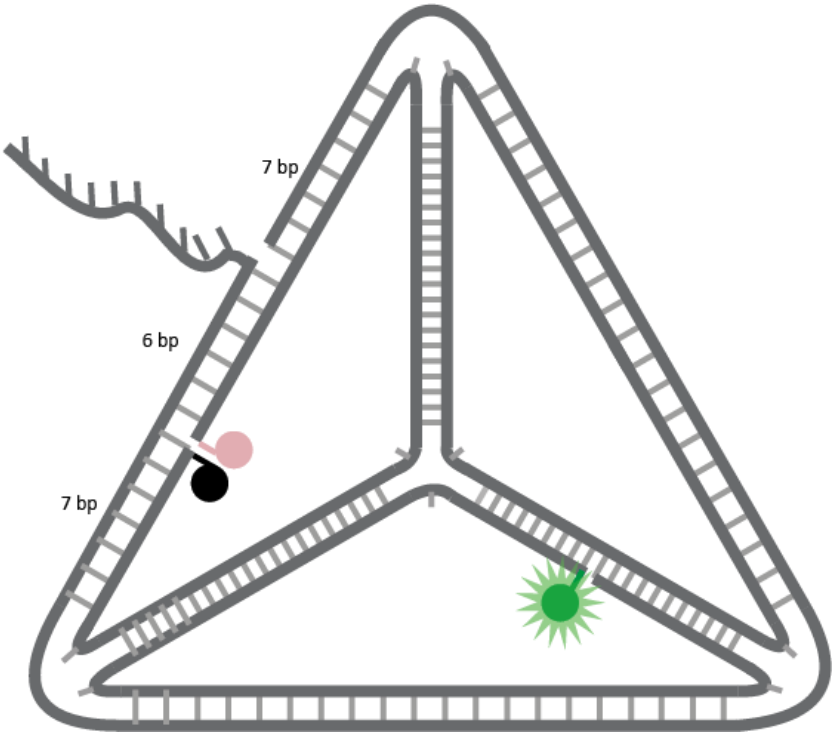


Figure 2-4: Schematic diagrams of OT2.2

#### 2.3.3.1.1 OT2.2 in tissue culture medium

20 µl of gel purified OT2.2 was added into a cuvette containing either 120 µl of Buffer A or the tissue culture medium, Opti-MEM® (Appendix A.1.1). The ensemble Cy3 and Cy5 signals were measured by the fluorimeter (Appendix A.6). The gel purified OT2.2 was originally in the assembly buffer, Buffer A and the purified concentration ranged from 300 nM to 800 nM. The exact concentration of the sample was not measured, but in this experiment the same batch of sample was used, so it was a fair comparison.

Figure 2-5 shows that the Cy3:Cy5 ratio of OT2.2 in Opti-MEM® (red) and in Buffer A (blue). In Buffer A, all OT2.2 was assumed to be closed because the buffer had 15 mM $Mg^{2+}$. The corresponding Cy3:Cy5 ratio of the sample therefore represented the minimum level of Cy3:Cy5 ratio. If a sample has a Cy3:Cy5 ratio that is above this level, this means that a proportion of OT2.2 is opened.

At the beginning, the Cy3:Cy5 ratio of the sample in Opti-MEM® was twice as high as that of OT2.2 in Buffer A. This indicated a proportion of OT2.2 was unintentionally opened. The opening was against the design principle because the cage was opened in the absence of the signalling strand.

Between 20 and 45 minutes, $Mg^{2+}$ in the Opti-MEM® sample was increased in 10 mM step. After each addition, the Cy3:Cy5 ratio decreased, which suggested that some of the opened OT2.2 became closed again. This suggested that the unintentional opening was due to the low magnesium ion concentration in Opti-MEM® and the process was reversible. At 30 mM $Mg^{2+}$, the Cy3:Cy5 ratio in Opti-MEM® was decreased to a level similar to the one in Buffer A, so all the cages in Opti-MEM® was closed in the presence of the extra $Mg^{2+}$.

Interestingly, the final magnesium ion concentration in Opti-MEM® was twice as high the one in Buffer A. This implied that once the cage was open at 37˚C, it required a higher concentration of cations to close it again. The difference might be due to the fact that the tetrahedron was assembled in an annealing process, which temperature decreased from 91˚C to 4˚C. This cooling process encouraged the closed configuration to form. This experiment was conducted at 37˚C and there were more dynamic structural fluctuations. These might explain the difference between the final magnesium ion concentration in Opti-MEM® and Buffer A.

A molar excess of the signalling strand (1 μM final concentration) was added at 70 minutes and both samples had over 5-fold increases in their Cy3:Cy5 ratios. Therefore, OT2.2 was responsive to the signalling strand in both Opti-MEM® and Buffer A.

For the Opti-MEM® sample, the Cy3:Cy5 ratio was 0.65 for the fully opened, 0.1 for the fully closed and 0.25 at the beginning, so it can be deduced that approximately 30% of OT2.2 was open in the original Opti-MEM®, before the addition of $Mg^{2+}$. This showed that it was necessary to redesign the reconfigurable tetrahedron to strengthen the closing mechanism. Otherwise, the cage would likely become open under physiological conditions.

Unintentional opening of DNA cages was further investigated by stepwise addition of EDTA to a sample of DNA cages (Appendix C.2). EDTA has a high binding affinity towards $Mg^{2+}$, so it competes for $Mg^{2+}$ binding with the DNA. The addition of EDTA decreases the concentration of $Mg^{2+}$ in the environment. EDTA has a binding constant with $Mg^{2+}$ in the order of $10^8$ $M^{-1}$ and DNA's binding constant with $Mg^{2+}$ is in the order of $10^5$ $M^{-1}$.[93,94] Due to the relatively higher binding affinity of EDTA towards $Mg^{2+}$, it is assumed that $Mg^{2+}$ is

completely removed by EDTA despite of the presence of competitions with DNA. One EDTA molecule chelates with one $Mg^{2+}$. The experiment showed the Cy3:Cy5 ratio increased as $Mg^{2+}$ concentration decreased. The observation was in agreement to the hypothesis that magnesium ion depletion led to cage opening.

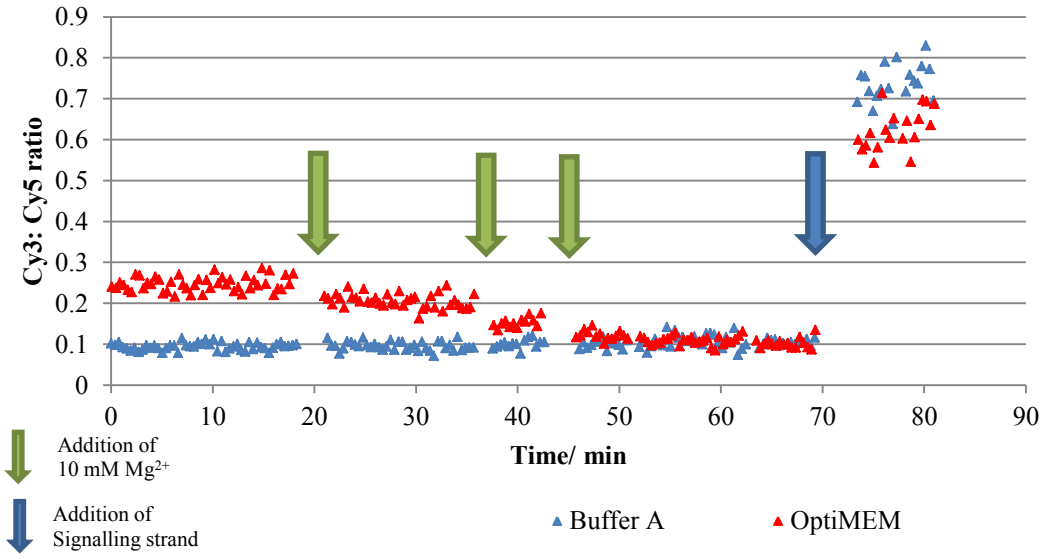


Figure 2-5: Fluorescence measurement of the closed tetrahedron (OT2.2). One sample was incubated in a low $Mg^{2+}$ buffer (Opti-MEM®, red triangles) and the other sample was incubated in a high $Mg^{2+}$ buffer (Buffer A, blue triangles). The Cy3:Cy5 ratio in the low $Mg^{2+}$ sample indicates that ~30% of the tetrahedra are open even in the absence of the complementary opening strand. The $Mg^{2+}$ concentration was increased by the addition of 10 mM magnesium chloride at the times indicated by green arrows. The Cy3:Cy5 ratio decreased as the concentration of magnesium ions increased, which suggests that the cages became closed as the $Mg^{2+}$ concentration increased. At 70 minutes, the opening strand of 1 μM final concentration was added into both samples (blue arrow). The increase in the Cy3:Cy5 ratio indicates that the cages in both buffers were opened.

#### 2.3.3.1.2 OT2.2 in Polyacrylamide Gel Electrophoresis (PAGE)

In addition to ensemble fluorescence measurement, native polyacrylamide gel electrophoresis (PAGE – Appendix A.7.1) was used to compare the configurations of OT2.2 in different magnesium concentrations. For standard PAGE, the gel and running buffer are prepared with 1x TAE buffer, which contains 40 mM Tris, 20 mM acetic acid and 1 mM EDTA and so it has no $Mg^{2+}$ ions. However, in this case, samples of OT2.2 were run in PAGE under two conditions: with or without $Mg^{2+}$ ions.

Figure 2-6 shows two gels that were run at different conditions. On the left is '15mM $Mg^{2+}$', which means 15 mM of MgCl were added to both the gel and the running buffer, in order to give the same $Mg^{2+}$ concentration as the assembly buffer, Buffer A. Since there was only 1 mM EDTA in the 1x TAE buffer, $Mg^{2+}$ was in excess with the addition of 15 mM of MgCl. On the right is the standard PAGE without $Mg^{2+}$ ions; hence it is labelled as 'no $Mg^{2+}$'.

In both gels, lane 1 was the open tetrahedron and lane 2 was the closed tetrahedron. The open tetrahedron was a sample of closed tetrahedron with the addition of the signalling strand, so the cage was already opened before loading into the gel. In both cases, the gels were run on ice or at 4 ˚C to prevent the cages from opening as a result of heating of the gel.

The Cy5 channel was shown in green and the Cy3 channel was shown in red. As expected, the closed tetrahedron in 15 mM $Mg^{2+}$ buffer had a low Cy3 signal and a high Cy5 signal and therefore appeared as a green band (Figure 2-6a, lane 2). Similarly, when the closed cage was opened by the complementary signalling strand, the Cy3 signal increased and the band in lane 1 appeared yellow for both conditions. However, in the absence of magnesium ions, the

originally closed OT2.2 had a high Cy3 signal (Figure 2-6b, lane 2) indicating that it was open even in the absence of the complementary signalling strand.

In view of all the experimental data, a new design of tetrahedron that does not open at low magnesium ion concentration is needed.

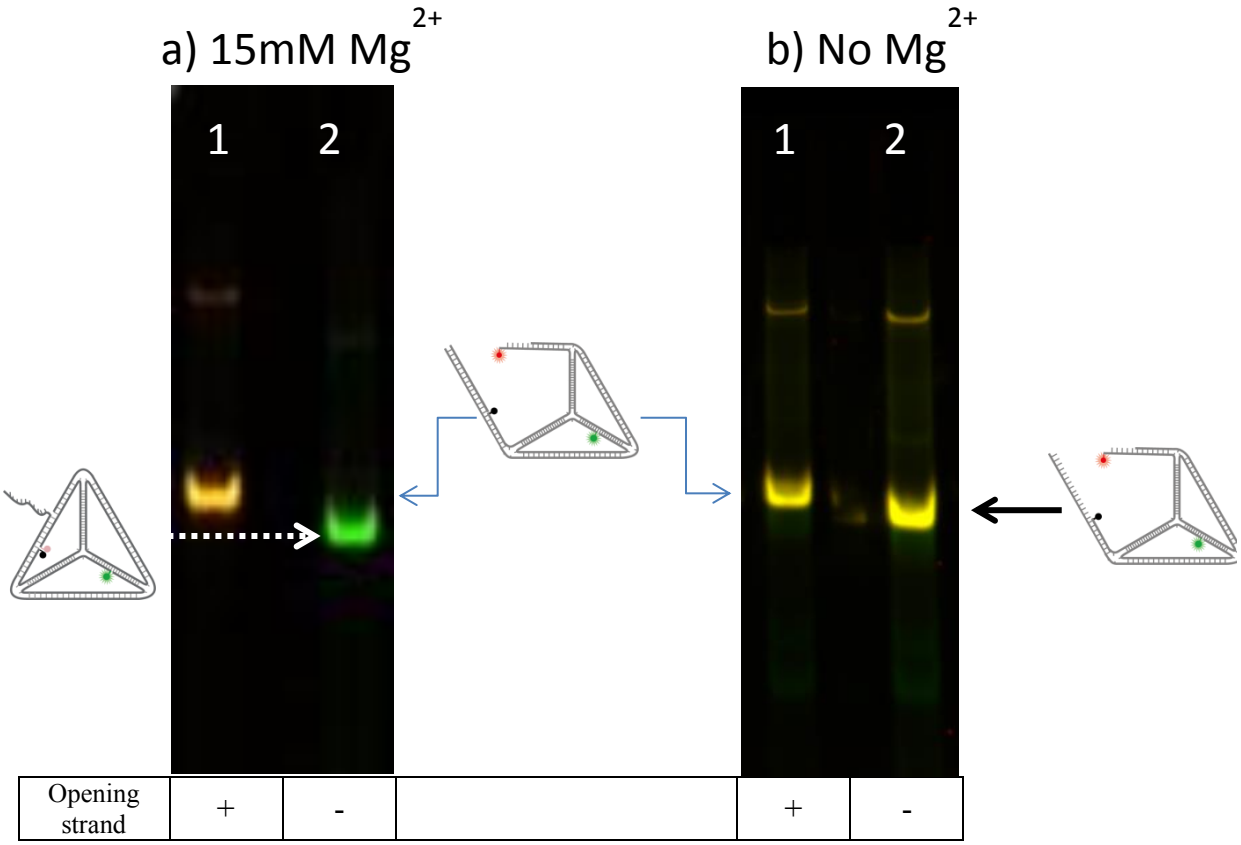


Figure 2-6: 29:1 6% Native PAGE. a) shows the system with 15 mM $MgCl_2$ added to the gel mix and the running buffer; b) shows the system with no magnesium ions in gel or the running buffer. The Cy5 scan was in green, and the Cy3 scan was in red. Therefore, when the tetrahedron sample is in the open state, both the Cy5 and Cy3 signals are strong and the tetrahedral band appears yellow; when the sample is in the closed state, Cy3 signal is weak due to the close proximity of Cy3 to its quencher, so the band appears green. Lane 1 shows OT2.2 with the opening strand and lane 2 shows OT2.2 without the opening strand.

### 2.3.3.2 OT6.3

In order to improve the closing mechanism so that the tetrahedra remained closed in the physiological level of $Mg^{2+}$, the overhang was moved from the middle of the edge to the vertex, and away from the fluorophore. Figure 2-7 shows the modified design OT6.3, which has the overhang at the vertex. The overhang is 6 nt long and is held closed more tightly by the hybridization of an additional 7 bp along the tetrahedral edge. OT6.3 is therefore closed by 13 bp, instead of 6 bp (sequences of the component strands see Appendix B.1.2).

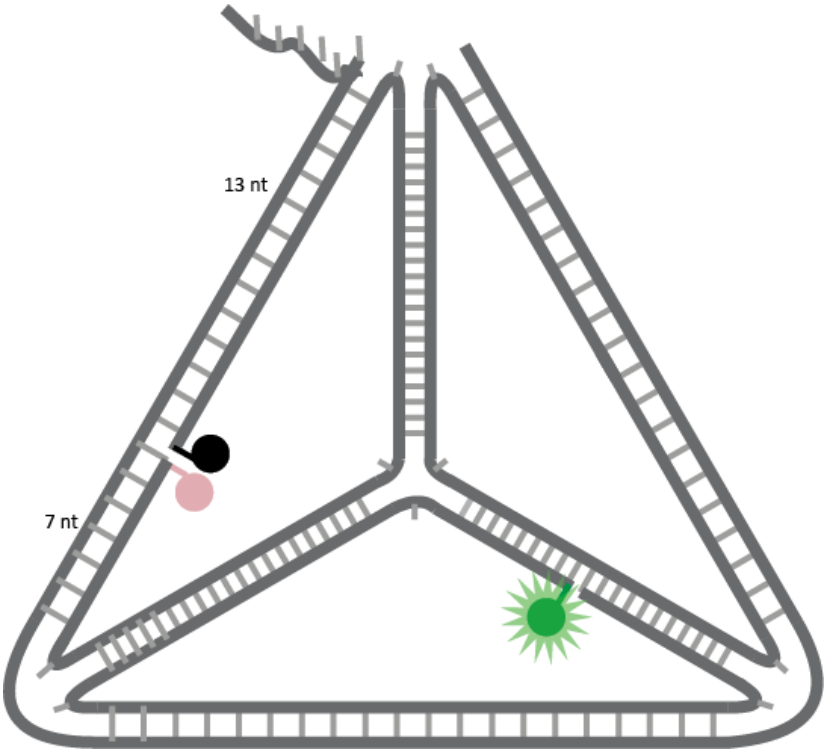


Figure 2-7: Schematic diagram of OT6.3.

Next, I will examine the stability of OT6.3 by monitoring its Cy3:Cy5 ratio in the fluorimeter while decreasing the $Mg^{2+}$ concentration with EDTA, and in the standard PAGE without $Mg^{2+}$.

#### 2.3.3.2.1 Effect of EDTA on OT6.3

Figure 2-8 shows the Cy3:Cy5 ratio of 40 nM of OT6.3 in 120 µl of Buffer A. The initial $Mg^{2+}$ concentration was 15 mM and all the cages were closed. Over the course of the first 200 minutes, the $Mg^{2+}$ concentration was decreased by 1 mM every 15 minutes by the addition of EDTA. The final $Mg^{2+}$ concentration at 200 minutes was 3 mM and the Cy3:Cy5 ratio remained low. Then, EDTA was continually added for another 50 minutes and the $Mg^{2+}$ concentration reached 0 mM. There was only a slight increase in the Cy3:Cy5 ratio between 200 and 250 minutes, corresponding to the opening of a small proportion of cages. This showed that the new design of tetrahedron could withstand the low $Mg^{2+}$ concentration.

At 250 minutes, an excess of signalling strands was added to the sample and the Cy3:Cy5 ratio increased rapidly to 0.85, indicating that all the cages were opened and OT6.3 was responsive to the signalling strand.

If the EDTA had chelated all the magnesium ions, then DNA hybridisation would not have been possible and the cages should have fallen apart. However, Hahn et al.[88] speculate that the assembled DNA nanostructures might sequester the magnesium ions so that they do not fall apart at low magnesium ion concentrations. The experimental result in Figure 2-8 agrees with this hypothesis. This result also suggests that the assumption of complete $Mg^{2+}$ removal

by EDTA in the presence of DNA is likely to be over simplistic, especially when the concentration of $Mg^{2+}$ is low.

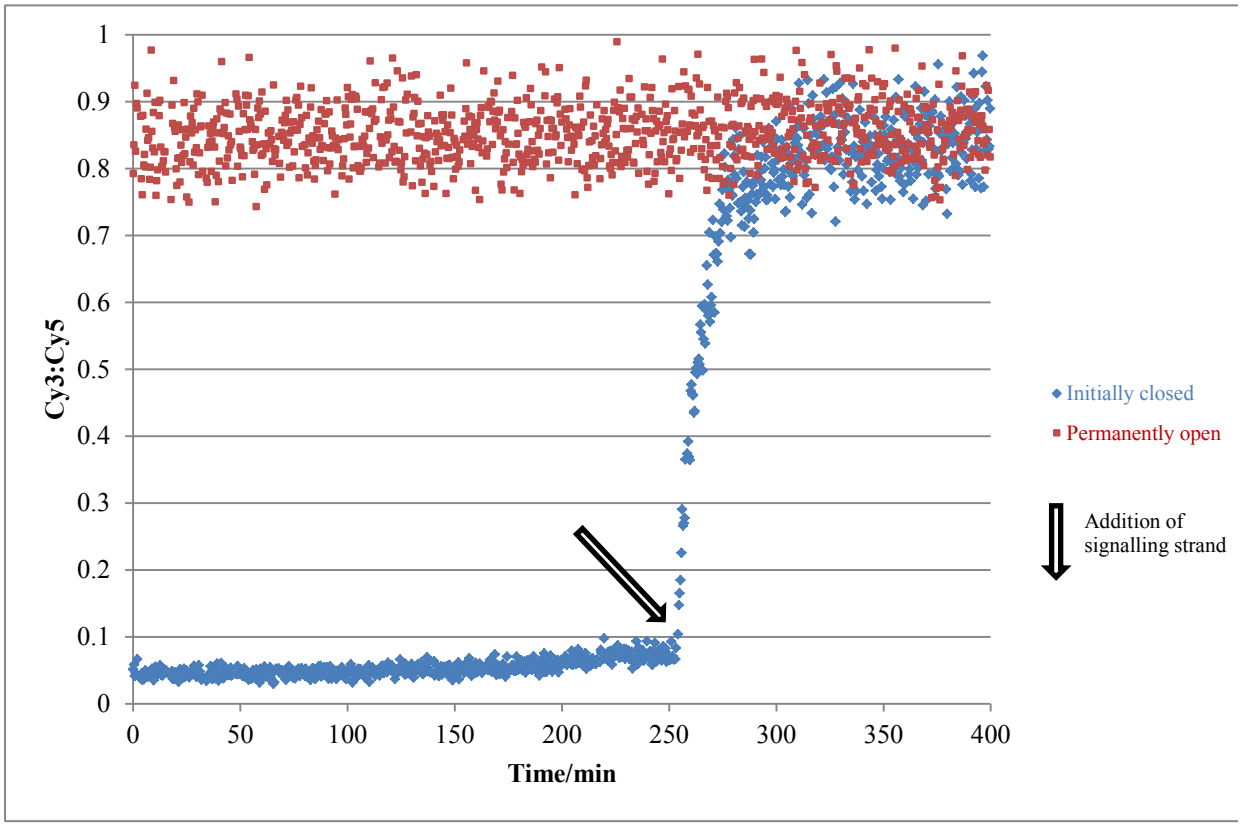


Figure 2-8: Fluorescence measurement of OT6.3 in two different states: initially closed (the blue diamonds) and permanently open (the red squares). In the first 250 min, EDTA was gradually added to the samples, and this resulted in a slight increase in the Cy3:Cy5 ratio, but the majority of cages remained closed. At 250 min, the signalling strand (the black arrow) was added to the sample with closed OT6.3, and this led to the opening of all cages.

During 200 and 250 minutes, a small proportion of cages were opened due to magnesium ions depletion. There were insufficient amount of magnesium ions to shield the negative charges on the phosphate backbones of the DNA strand. The double helix structure became less stable, particularly at the reconfigurable edge because there were two break points on the same edge, 13 bp apart. There were disruptions of base pairs at the vertex with the overhang.

The zipping and unzipping of each base pair was a stochastic process. It was a competition between the repulsion of the negative charges on the backbone and the attraction between the nucleobases via the hydrogen bonds. In some cases, the overhang frayed and the cage became open.

In this ensemble measurement, it was impossible to determine the rate of the exchange between the open and closed state. For future experiments, one could use single molecule techniques, such as fluorescence correlation spectroscopy (FCS), to investigate this. Firstly, we would need to measure the distribution of the Cy3:Cy5 ratio in the 'always closed' and 'always open' tetrahedra; then with the reconfigurable tetrahedra in the low magnesium ions condition. If the zipping and unzipping is a rapid process relative to the diffusion time, two distinct populations that correspond to the 'always closed' and 'always open' state would be observed. On the other hand, if the process is much faster than diffusion, then we would expect to observe a distribution of Cy3:Cy5 signal centred between the 'always closed' and 'always open' distributions.

#### 2.3.3.2.2 OT6.3 in PAGE

Figure 2-9 shows the closed (lane 1) and the open (lane 2) OT6.3 in a polyacrylamide gel. The gel was run in the standard conditions, without magnesium ions. In the absence of the signalling strand, the Cy3 signal was quenched, indicating that the tetrahedra were closed. The addition of the opening strand caused an increase in the Cy3 signal, which was consistent with the opening of the tetrahedra.

Both the fluorimeter (Figure 2-8) and the gel (Figure 2-9) results suggested that the modified OT6.3 was likely to be able to withstand magnesium ion depletion and remained closed in physiological conditions.

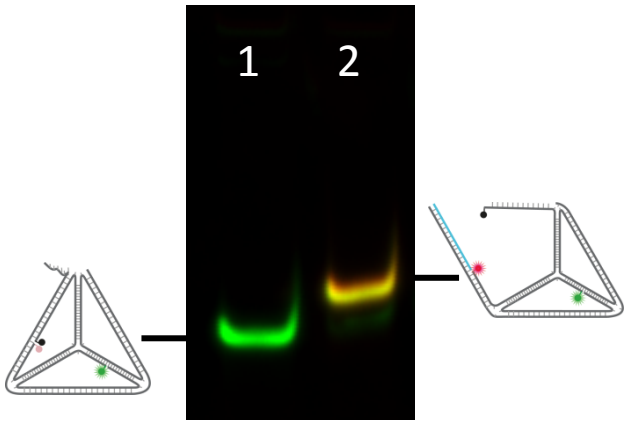


Figure 2-9: 29:1 10% Native PAGE to verify the formation of OT6.3. Lane 1 is the closed cage and lane 2 is the open cage. Red is the Cy3 scan and green is the Cy5 scan.

### 2.3.4 Stability in complete medium

The next area of stability I will look into is the degradation of tetrahedra in tissue culture medium in the presence of serum. Cells are incubated in Dulbecco's Modified Eagle's Medium (DMEM-Appendix 1.2), supplemented with 10% heat inactivated fetal bovine serum (FBS) at 37˚C. For the rest of this thesis, DMEM medium with the supplemented FBS is referred to as 'complete medium'. FBS provides the growth factors and hormones required to support cell growth. However, FBS also contains nucleases that degrade DNAs, which might therefore compromise the structural integrity of DNA nanostructures.

In this section, I will examine and compare the stabilities of a tetrahedral component strand, a closed tetrahedron and an open tetrahedron in complete medium using PAGE and fluorimeter measurements. Then, I will discuss the variation of nuclease activity between different batches of FBS.

All three samples were incubated in complete medium at 37°C over the course of 5.5 hours (Appendix A.8). As all the samples were labelled with Cy5, their integrities were examined in native PAGE with Cy5 scans (Figure 2-10). The incubation periods were in ascending order from lane 1 to lane 5.

#### 2.3.4.1 Degradation of the component strand (S3 Cy5) of the tetrahedron

Figure 2-10a shows the results of the tetrahedral component strand S3 Cy5. Lane 1 contained the intact S3 Cy5 and it had a sharp band. However, the sharp band was digested into multiple fragments from lane 2 onward and no intact S3 Cy5 remained. There was significant degradation within the first hour of incubation.

The position of a band in electrophoresis is influenced by both the charge and the size of the molecule. The black arrow in Figure 2-10a points to a band that has a lower mobility than the intact S3 Cy5. Its intensity increases with incubation time, so it is likely a product of nuclease degradation, which should be smaller than those of the intact S3 Cy5. This may be because Cy5 fluorophore is positively charged (Figure 2-11). Due to nuclease degradation, fragments conjugated to Cy5 have a smaller average charge to mass ratio which may explain the reduced mobility towards the positive end of the gel of this indicated band.

### 2.3.4.2 Degradation of a closed and a reconfigurable tetrahedron

Figure 2-10b & c show the results of a closed tetrahedron and the open tetrahedron respectively. The closed tetrahedron was a fully ligated closed cage without an overhang, so that is unamenable to strand opening. By visual inspection, after six hours, there was still a visible band for the closed tetrahedron, but for the open tetrahedron, the band was smeared.

In Figure 2-10d, the extent of degradation for all three samples was quantified in terms of the difference between the relative intensities of the tetrahedral band at different time points and the initial intensity in lane 1. The approximate initial rate of degradation of the open tetrahedron was 3 times higher than that of the closed tetrahedron. Chemical modifications, such as a phosphorothioate backbone, could further enhance such resistance.

For the open tetrahedra (Figure 2-10c), there were some aggregates in the wells in lanes 2 to 5. This suggested that some non-specific binding occurred between the DNA cages and the proteins in the serum. In Section 2.3.5, non-specific binding is shown to be a significant problem when the DNA tetrahedra were incubated with the cell lysate.

In summary, S3 Cy5 had the shortest life-time in the complete medium, followed by the open tetrahedron and the closed tetrahedron was the most stable structure. DNA cages were therefore more resistant to nuclease degradation than their component strands alone. However, for the reconfigurable tetrahedron, nicks were introduced into the structure, which made the structure more vulnerable to nuclease attack. A fully ligated tetrahedron was more stable in the presence of serum because it was less prone to exonuclease digestion.

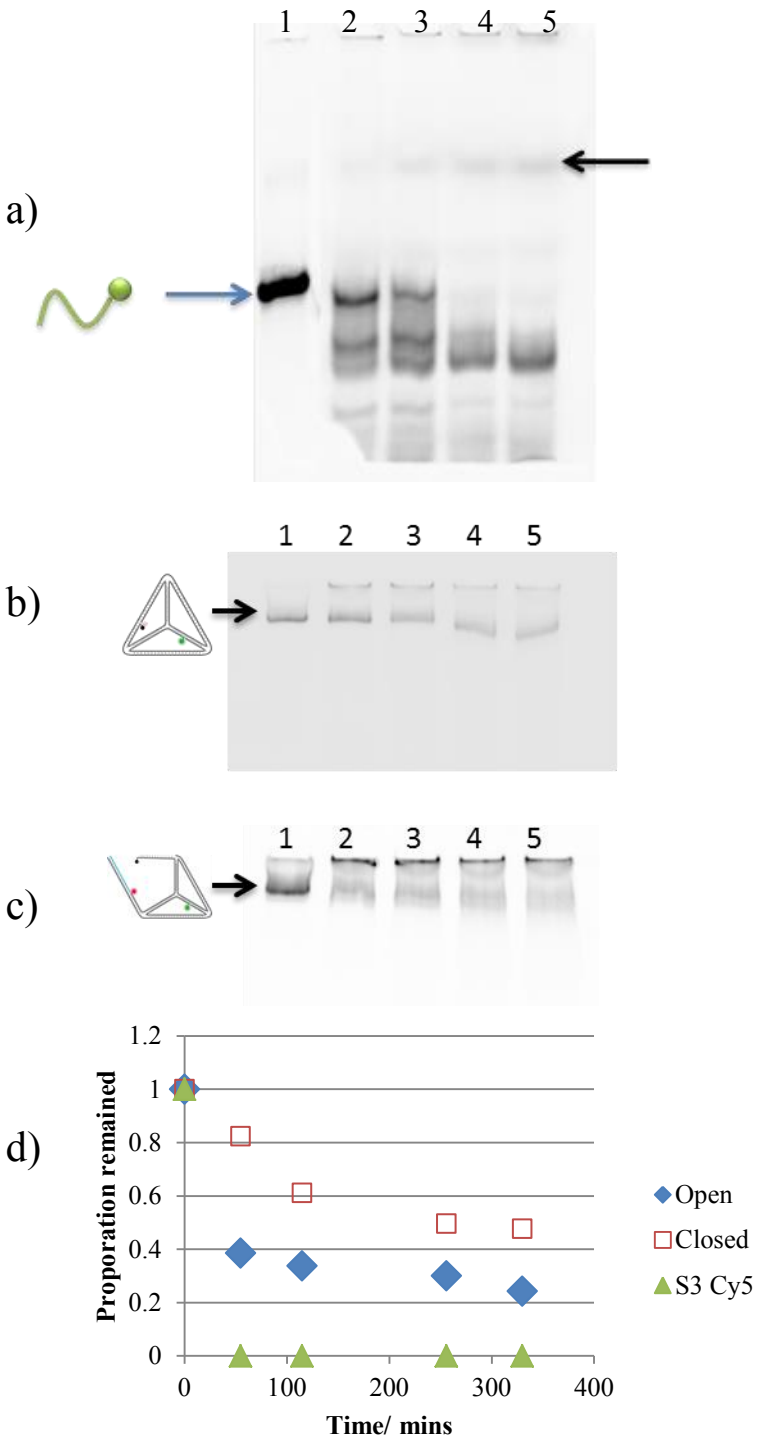


Figure 2-10: (a)-(c) are 29:1 10% native PAGE ran at the same time to examine the stability of various DNA materials in complete medium at 37˚C with different incubation periods. Lane 1: 0 min; lane 2: 55 min; lane 3: 115 min; lane 4: 256 min; lane 5: 330 min. a) is S3 Cy5, one of the tetrahedral component strands; b) is the closed tetrahedra and c) is the open tetrahedra. The images were taken in the Cy5 channel. d) shows the degradation time curves for open (the blue diamonds), closed (the red rectangle boxes) tetrahedra and S3 Cy5 (the green triangles) based on data in a) to c). The intensities of the tetrahedral bands were measured and divided against their initial intensity in lane 1.

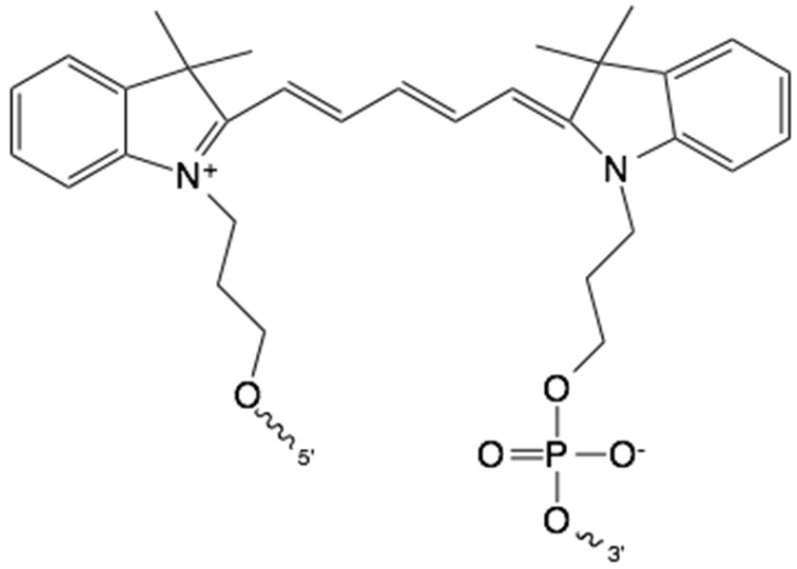


Figure 2-11: Chemical structure of a phosphate based linked to a Cy5 fluorophore.

### 2.3.4.3 Degradation monitored by ensemble fluorescence measurement

The stability of the tetrahedra in tissue culture medium was also assessed using ensemble fluorescence. 20 µl of OT6.3 was incubated in 120 µl of complete medium at 37˚C, and the Cy3 and Cy5 signals were measured over a period of time (Appendix A.6).

Figure 2-12 shows the change of Cy3:Cy5 ratio of OT6.3 over 33 hours. At the beginning, the ratio was low. This was because the majority of the cages were intact, so the Cy3 signal was quenched. The Cy3:Cy5 ratio gradually increased, indicating an increasing proportion of OT6.3 was digested. Interestingly, the Cy3:Cy5 ratio increased at a slower rate in the first 180 minutes than over the period between 180 and 800 minutes. This might have been due to the co-operative protection of the three-dimensional tetrahedral structures, which imposed some steric hindrance upon the enzymes, preventing the enzymes from binding to the DNA

cages. Hence, at the beginning, when the majority of the structures were intact, the degradation was slower. However, when parts of individual cages began to be digested, the cages lost their three-dimensional rigidities, and the rate of degradation increased.

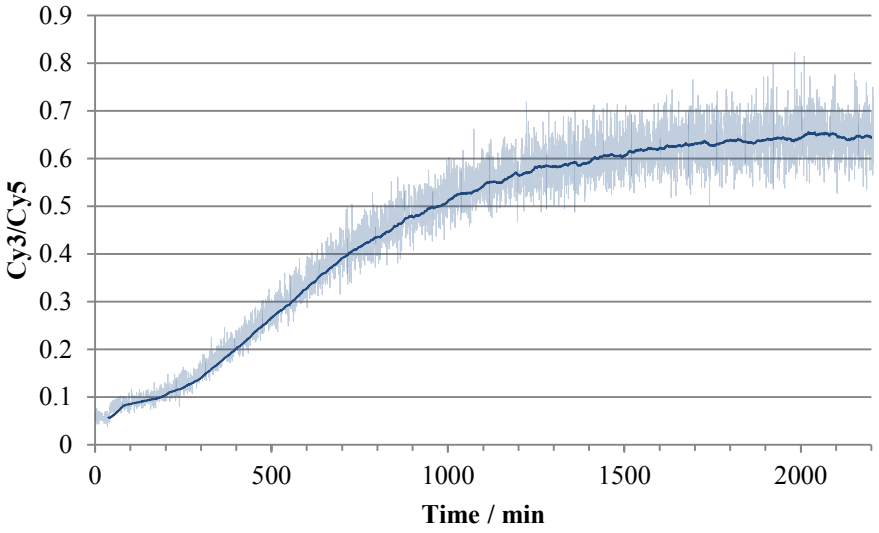


Figure 2-12: Fluorescence measurement of the closed tetrahedron (OT6.3) incubated in complete medium at 37˚C overnight.

### 2.3.4.4 Variations between different aliquots of FBS

The level of nuclease activity in the FBS varied between frozen aliquots. In Figure 2-13, the tetrahedra were incubated with two different aliquots of complete media at 37˚C over the period of six hours (Appendix A.8). The complete medium in a) contained freshly thawed serum and the one in b) was one-week-old.

In Figure 2-13a, degradation was visible after two hours of incubation (lane 2) and the tetrahedral band was very faint by the end of the experiment (lane 4). In contrast, there was

no visible degradation fragment after six hours in Figure 2-13b. Both a) and b) had the same batch of DNA tetrahedra, but different aliquots of FBS in the complete medium. This suggested that, in agreement with Hahn et al.,[88] nuclease activity between different batches and aliquots of FBS could be quite variable, and this in turn affected the rates of degradation. The inconsistency was likely to be related to how long the serum has been thawed. In addition, FBS is a blood product from fetal bovines, it is reasonable to expect differences between batches, including nuclease activities. Therefore, when comparing stabilities of different DNA nanostructures, it is important to account for this variability. Experiments discussed in Sections 2.3.4.1 and 2.3.4.2 were conducted at the same time with the same batch of fresh complete medium, so they were fair comparisons.

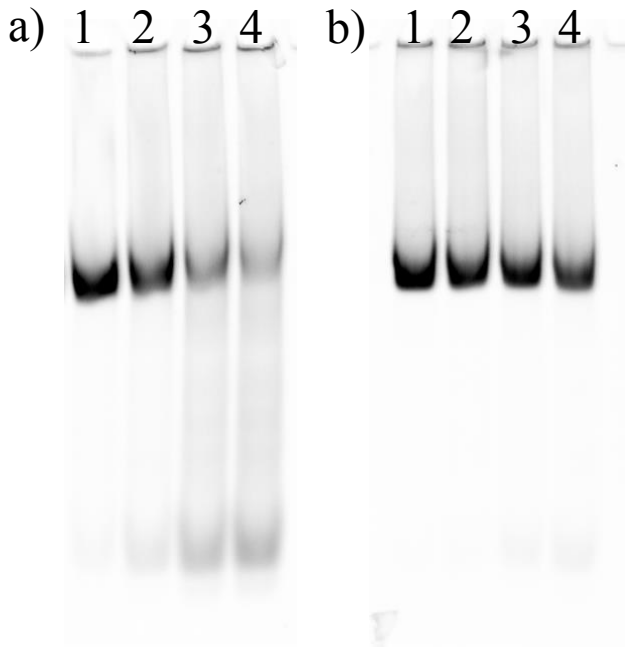


Figure 2-13: 29:1 6% native PAGE. The closed tetrahedra were incubated in complete medium with a) freshly thawed FBS and b) one-week-old FBS at 37 ˚C. Samples were incubated for different durations. Lane 1: 57 min; lane 2: 123min; lane 3: 280 min; lane 4: 364 min.

### 2.3.5 Degradation in cell lysate

Besides stability in tissue culture medium, it is important to evaluate the stability of DNA nanostructures in an intracellular environment. Mei et al.[87] examined the stability of DNA origami nanostructures in cell lysate mainly via AFM imaging of the sample. They reported that the DNA origami structures were intact and this validated the suitability of DNA nanostructures in biological applications.

However, the tetrahedra (7 nm) are smaller than most origami structures (10s nm), so it would be difficult to image the degradation of tetrahedra by AFM. In this section, PAGE was used to examine the structural integrity of tetrahedra, but due to the aggregations between the DNA cages and the cell lysates, the experiment was unsuccessful.

$10^5$ MCF-7 cells were lysed using 300 µl of 1x Cell Culture Lysis Reagent (CCLR). 6 µl of purified OT6.3 was then incubated with 6 µl of cell lysate at 37˚C (see Appendix A.10 for details). It contains protease inhibitors and protects proteins from degradation. The lysis reagent breaks the plasma membranes and other membrane-bound features in cells, and releases nucleases into the lysate.

Figure 2-14 is a native PAGE gel with three samples. Lane 2 was the tetrahedra incubated with the CCLR for three hours and the tetrahedral band ran to the expected position, so CCLR did not aggregate with the DNA tetrahedra.

Lane 1 contained the sample of tetrahedra incubated with the cell lysate for half an hour. The tetrahedral band was absent and there were aggregates in the well. The aggregation was most

likely caused by the non-specific interactions between the proteins in the cell lysate and the DNA cages.

Lane 3 contained OT6.3 that was incubated with the cell lysate for three hours. The quantity of cages remaining accumulated in the well reduced significantly, indicating that they had been degraded. Fragments of the digested products were also visible in lane 3. Therefore, the non-specific bindings did not protect the DNA cages from enzymatic attacks.

In view of this preliminary experimental result, the transfection time for naked DNA cages inside cells should be limited to the order of hours, rather than tens of hours.

Future experiments could investigate the cause of aggregation. Aggregation may have been caused by the fluorophores rather than the DNA nanostructures themselves. Some hydrophobic fluorophores cause non-specific binding in cells.[95] The aggregation might also influence the uptake of such structures inside cells. Once we understand the underlying mechanism, we will be able to use it to our advantage.

| | 1 | 2 | 3 |
|---|---|---|---|
| MCF-7 cell lysate | + | - | + |
| CCLR (lysate buffer) | - | + | - |
| Incubation time / hr | 0.5 | 3 | 3 |

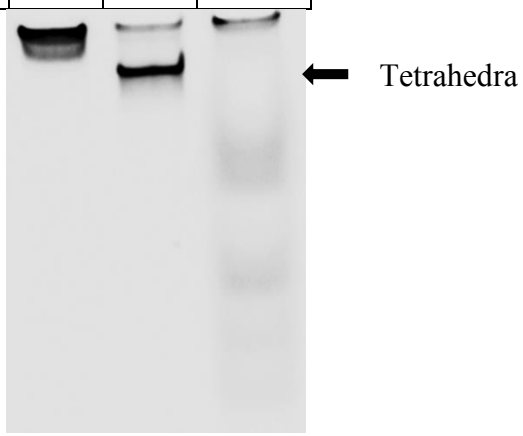


Figure 2-14: OT6.3 was incubated with different media and resulted in degradations in some cases. Lane 1: MCF-7 cell lysate and OT6.3 were incubated for 30 minutes and aggregation was observed in the well; Lane 2: CCLR and OT6.3 were incubated for three hours and the tetrahedral band migrated as a single band to the expected position, which implied the sample was intact; Lane 3: MCF-7 cell lysate and OT6.3 were incubated for three hours and the multiple smeared bands appeared, which implied the tetrahedra were degraded. This was a 29:1 10% native PAGE in the Cy5 scan.

## 2.3.6 OT6.3SCO

There are various versions of OT6.3 because several signalling molecules with different sequences were investigated and some of them will be discussed in Chapter 5. Nevertheless, all OT6.3 have the same structural design (a 6 nt overhang and 13 bp to keep the cage closed), but the sequences of the component strands are different.

Herein, I would like to introduce a specific version of OT6.3 - OT6.3SCO, which is designed to be opened by a synthetic oligonucleotide with chemical modifications called $O_c$. $O_c$ was originally based on a splice correcting oligonucleotide, hence the abbreviation of SCO for the

related tetrahedron. The characteristic of $O_c$ will be discussed in Section 2.4. This is the key system in this thesis because OT6.3SCO is the focus of Chapter 3 and $O_c$ is used Chapter 3, 4 and 6. Sequences of the component strands and $O_c$ are found in Appendix B.1.3.

Figure 2-15 shows the fluorescence measurement that demonstrates the opening of OT6.3SCO by $O_c$. At the beginning, there was 15 nM of closed tetrahedra inside the cuvette (Appendix A.6). Alexa-488 was next to the quencher, and hence, a low intensity was measured for the Alexa-488 emission. There were occasions that Cy3 was replaced by Alexa-488 because of instrument requirement for the flow cytometry experiments. The flow cytometer (BD FACSCALIBUR) used was equipped with a 488 nm blue laser. It would therefore excite Alexa-488 more effectively than Cy3. The relevant experiments will be discussed in chapter 3 and 4. Nevertheless, for the fluorimeter experiments described in this section were not affected by the choice of fluorophores and both Alexa-488 and Cy3 were used. In each case, the fluorophores used were stated explicitly.

At 12 minutes, an excess of $O_c$ was added into the sample (45nM final concentration) and this resulted in an increase in the fluorescence of Alexa-488. This was because the signalling strand hybridised with the toehold and eventually opened the cage. The addition of the opening strand $O_c$ resulted in a 5-fold increase of the Alexa-488:Cy5 ratio.

The Alexa-488 signal reached its level of half-maximum at around ten minutes, which was two minutes after the addition of $O_c$. The strand displacement was modelled as a second-order reaction,[20,96] which gave a rate constant of $6 \times 10^5$ $M^{-1}$ $s^{-1}$. This is comparable to the rate constants reported in the literature for toehold-mediated strand exchange reactions, which are in the range of $10^6$ $M^{-1}$ $s^{-1}$.[96] For details of fitting see Appendix A.31.

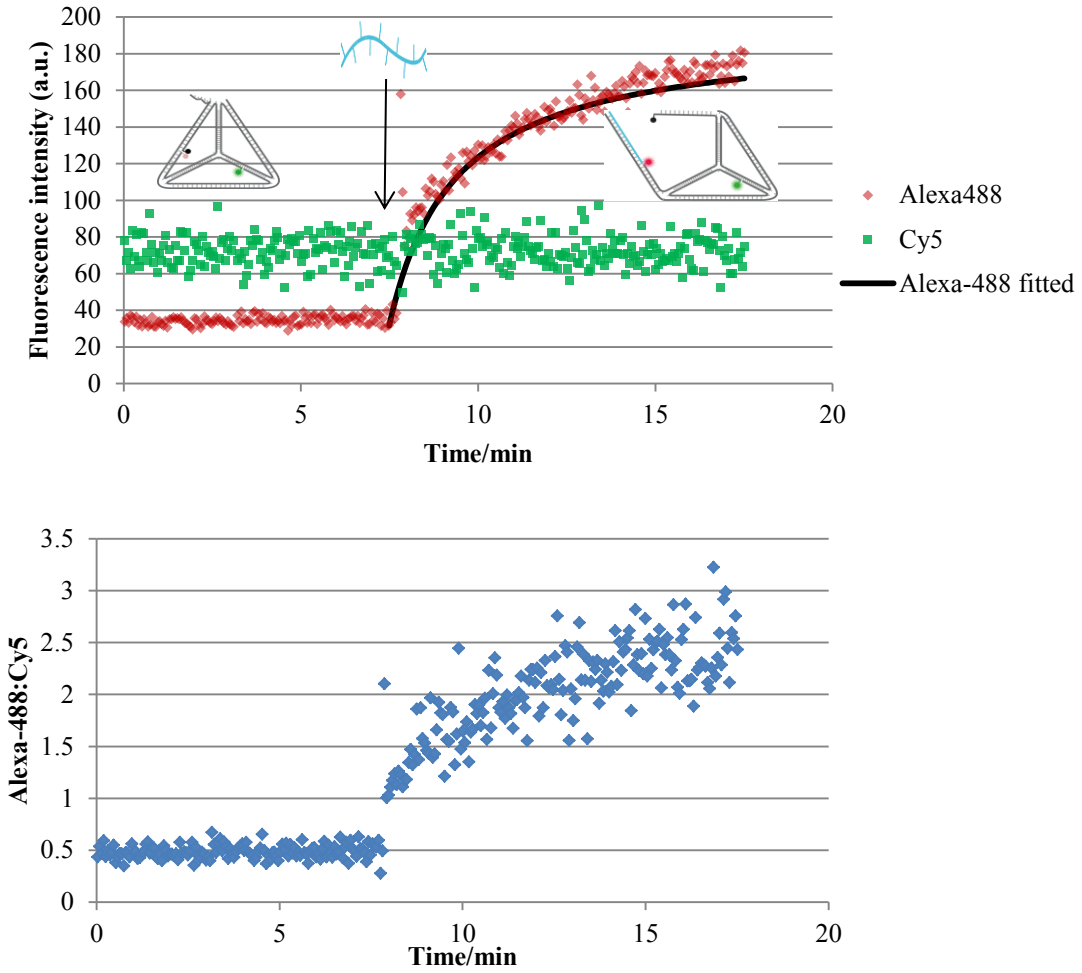


Figure 2-15: Ensemble fluorescence measurement shows the effect of the addition of the signalling strands on the fluorescence of the closed tetrahedra. The top and bottom graphs are based on the same data set. The top graph shows the fluorescence of Cy5 and Alexa-488 separately, while the bottom graph shows the Alexa-488:Cy5 ratio. The quenched Alexa-488 fluorescence was measured in the first 12 minutes. The increase in Alexa-488 fluorescence intensity was due to the hybridisation of the signalling strand with the DNA tetrahedra. The Alex-488 signal (red diamond) is fitted assuming second-order kinetics with a rate constant of 6 x $10^6$ $M^{-1}$ $s^{-1}$, this is shown as a black line in the top graph.

## 2.4 Signalling strand

The signalling strand $O_c$ can hybridise with the overhang of OT6.3SCO and open the DNA cage. $O_c$ has 2′ O-methyl and phosphorothioate modifications to increase its resistance to nuclease degradation. This is an important characteristic of $O_c$ because if it were prone to degradation, it would not have been able to trigger opening of the DNA cages inside cells. The chemical modification is shown in Figure 2-16a. The sequence is based on a well-established antisense RNA strand that induces luciferase expression in HeLa pLuc705 cells.[97,98] $O_c$ also has additional unmodified DNA bases at its 5'end for some other experiments in Chapter 6. The term 'signalling strand' is used interchangeably with 'opening strand' throughout this thesis.

### 2.4.1 Stability of the signalling strand in complete medium

In order to examine the stability of $O_c$ in the presence of serum, it was incubated at 37˚C overnight with complete medium, which was supplemented with 10% FBS. Native PAGE was used to examine its integrity (Appendix A.8).

In Figure 2-16b, lane 1 was $O_c$ in PBS, so there was no degradation and $O_c$ was intact. Lanes 2 to 4 were samples of $O_c$ incubated with complete medium over the course of 18 hours. In all four lanes, there was a distinct band that represented $O_c$ and they ran to the same position. This suggested that $O_c$ remained intact after an overnight incubation with complete medium and it was stable in the presence of nucleases from the serum. The band in lane 2 was smeary and that was postulated due to the degradation of the unmodified DNA deoxynucleotides in

$O_c$, but these bases were not involved in the opening of cages, so this should not compromise the interaction between the signalling strand and the DNA cages.

(a) (b)

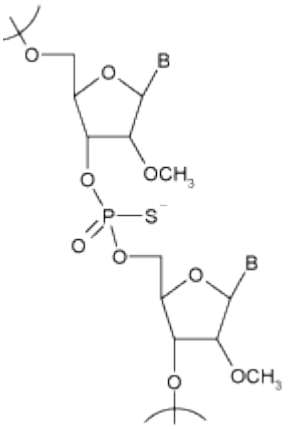


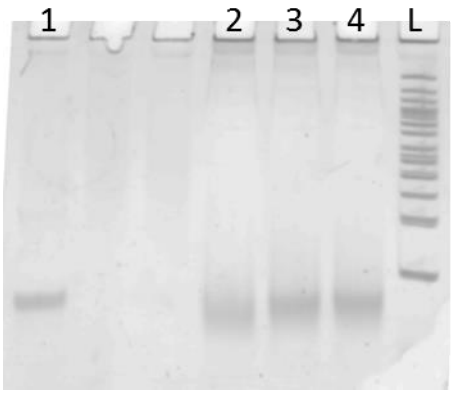


ACCCTCGCATGATT**GCCUCUUACCUCAGUUACA**

Figure 2-16 a) Chemical structures of 2′ O-methyl and phosphorothioate bases (B) , taken from[2]. The $O_c$ sequence is underneath. The region with the chemical modifications is in bold, and the region involved in opening is underlined. b) Native PAGE 29:1 10% to verify the integrity of $O_c$ in complete medium. Lane 1: $O_c$ in PBS, the rest are $O_c$ incubated at 37 ˚C with complete medium for 18 hours (lane 2), 4 hours (lane 3) and 3 hours (lane 4); L: NEB 50 bp ladder

[2] http://www.trilinkbiotech.com/cart/scripts/prodView.asp?idproduct=3304

## 2.4.2 Stability of the signalling strand inside cells

### 2.4.2.1 RNA extract examined in PAGE

Once the stability of $O_c$ in complete medium was established, its stability inside cells was assessed. The delivery of $O_c$ into cells was achieved with the aid of transfection reagent Lipofectamine® 2000 (Appendix A.11). 300 pmol of $O_c$ was first transfected into the mammalian cells overnight in a 35 mm petri dish. The following day, the cells were thoroughly washed with PBS in order to remove any $O_c$ that were not taken up by cells. Then, the RNA extract from the transfected cells was collected with a miRNeasy mini kit (Qiagen, details see Appendix A.12). The RNA extract was examined in native PAGE.

Figure 2-17 shows various samples of the RNA extract. Lane 1 was the control, which contained the RNA extract from the untreated MCF-7 cells. All the bands in lane 1 were the intracellular RNA materials collected, such as mRNA and tRNA. Lane 2 and lane 3 were extracts from the cells transfected with $O_c$. The blue arrow highlighted the position of the faint band corresponding to $O_c$ in both lane 2 and 3. This suggested that $O_c$ was resistant to nuclease degradation inside cells. It was of great importance that $O_c$ remained intact inside cells, so that it could interact with the DNA cages.

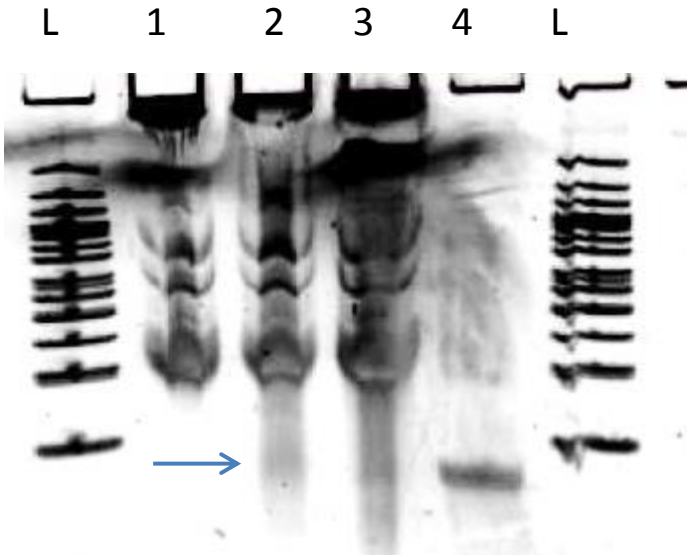


Figure 2-17: RNA extracts with $O_c$. Native PAGE 29:1 10% of MCF-7 cell lysate. L: NEB 50 bp ladder; Lane 1: cell lysate of MCF-7; lane 2: cell lysate of MCF-7 transfected with $O_c$; lane 3: cell lysate of HEK-293 transfected with $O_c$; Lane 4: $O_c$ in buffer A.

### 2.4.2.2 RNA extract open DNA cages

A further experiment was conducted to confirm the integrity of $O_c$ after the overnight transfection. 20 µl RNA extract was added to a solution of 30 nM DNA cages in Buffer A with a final volume of 150 µl. The Cy3 and Cy5 signals of the DNA cages were measured in the fluorimeter. If the $O_c$ is sufficiently intact, it will open the DNA cages and an increase in Cy3:Cy5 signal will be observed.

In Figure 2-18, there were three traces: the light blue trace was the sample with the addition of RNA extract containing $O_c$, the purple trace was the sample with RNA extract without $O_c$ and the grey trace was DNA cages in Buffer A, with the addition of $O_c$ at 85 minutes. The initial Cy3:Cy5 ratios of all samples containing closed cages were around 0.5.

For the grey trace, the addition of a molar excess of $O_c$ (3 µM) to the sample at 85 minutes induced opening of all the cages. Therefore, the Cy3:Cy5 ratio for a sample with complete opening was approximately 3.5.

For the purple trace, it contained RNA extract from cells without any transfection, so $O_c$ was absent. The Cy3:Cy5 ratio in this sample remained around 0.5 throughout the experiment. This demonstrated that there was no nonspecific interaction between the native cellular RNA extract and the closed cages.

For the light blue trace, the addition of RNA extract at the beginning induced opening of cages and hence an increase in Cy3:Cy5 ratio. The ratio stabilised just above 2, which was a 4 times increase in the ratio. This experiment therefore demonstrated that the $O_c$ in the RNA extract was sufficiently intact to interact with the reconfigurable part of the DNA cages.

Since the ratio stabilised below the grey trace, this indicated that only 60% of the cages were open and so, there was insufficient amount of $O_c$ in the lysate.

From this set of experimental data, I estimated the amount of $O_c$ in the RNA extract. There was a total of 4.5 pmol of OT6.3SCO in the solution and only 60% of which were open, so it was deduced that there was approximately 3 pmol of $O_c$ in the mix. Since I added 20µl of RNA extract, which was 13% of the total volume of the extract, the total amount of $O_c$ extracted was 20 pmol. This was approximately 7 % of the 300 pmol transfected into the cells. This was an underestimate of the amount of $O_c$ taken up by cells because some $O_c$ would be lost through the extraction process. Nevertheless, it provided us with a rough estimate.

A second-order rate constant was also fitted for the reaction in the cell lysate sample (black line in Figure 2-18). The rate constant was 1 x $10^5$ $M^{-1}$ $s^{-1}$ and the time to half completion was thirteen minutes. This strand exchange reaction was slower, but the rate constant was in the same order of magnitude as the one discussed in Section 2.3.6, where $O_c$ from the stock was added to OT6.3SCO in Buffer A. In that case, the rate constant was 6 x $10^5$ $M^{-1}$ $s^{-1}$ and the time to half completion was two minutes.

A direct comparison of those numerical values should be taken with cautions because there were variations between the two experiments. For example, the $Mg^{2+}$ concentration of the final mix was lower in the cell lysate experiment because of a bigger volume of RNA extract, eluted in water, was added. When $O_c$ was added from the stock, a smaller volume of $O_c$ was added because it was more concentrated than $O_c$ in the RNA extract. Nevertheless, $O_c$ before and after transfection into cells interacted with the DNA cages in a similar fashion. Therefore,

$O_c$ is a promising opening signal to trigger conformation changes of the DNA cage inside cells.

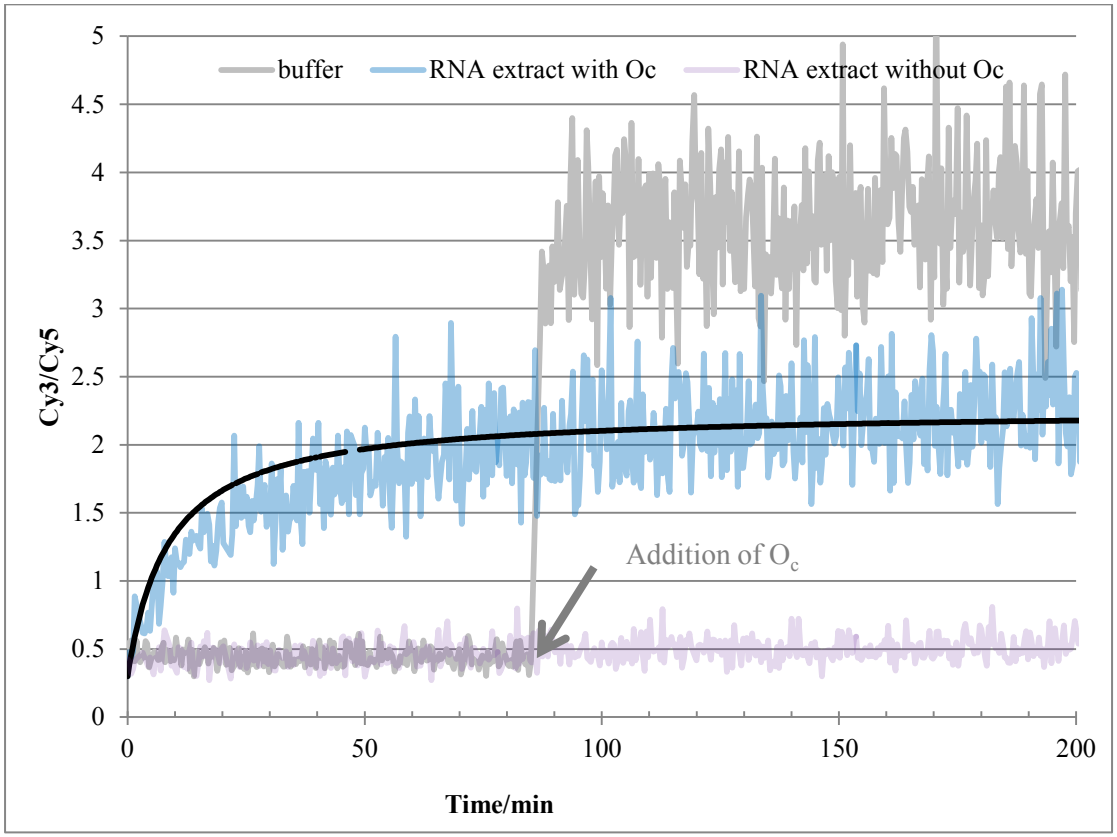


Figure 2-18: Fluorimeter measurement of cage opening by addition of RNA extract from cells transfected with $O_c$ the night before (light blue). Purple is the sample with DNA cages in RNA extract from cells without the $O_c$ transfection. It acted as a negative control to demonstrate that there was not non-specific opening of the cages by the cellular RNA extract. Grey is the sample with DNA cages in buffer A and when signalling strand $O_c$ is added, all cages become open. Maximum Cy3:Cy5 ratio occurs when all the cages are open. The actuation of the cages by the cell lysate is fitted assuming second-order kinetics with a rate constant of 1 x $10^6$ $M^{-1}$ $s^{-1}$ and this is shown as a black line in the graph.

## 2.5 Conclusion

In this chapter, I have introduced the opening mechanism of the reconfigurable DNA tetrahedron, which can be triggered by a signalling strand. I then investigated the extent to which magnesium ion concentration and nuclease degradation affect structural stability of the tetrahedron and the signalling strand.

In the initial design (OT2.2), there were only six base pairs holding the cage closed (Figure 2-4a) and the cage was closed in the presence of 15 mM $MgCl_2$ in the buffer. However, in tissue culture medium, which mimicked the physiological conditions, the cage was opened unintentionally, in the absence of the opening strand. In the new design (OT6.3), the 5' end of S4 was shifted to the vertex and there were thirteen base pairs rather than six base pairs keeping the cage closed (Figure 2-7). The cage remained closed when the concentration of $MgCl_2$ was dropped below 1 mM. Therefore, the modified OT6.3 is likely to be able to withstand the magnesium ion depletion in physiological conditions.

Next, I investigated the stability of DNA tetrahedron in complete medium. The fully ligated tetrahedron was reported to be stable in cell medium for at least four hours.[51] However, the process of configuring the cage to open unavoidably introduces extra nicks into the structure, and these comprise the tetrahedron's weak points for exonuclease attacks. These changes affect the stability of the structure and it becomes more prone to nuclease degradation. The serum stabilities of a single-stranded tetrahedral component strand, a closed and an open tetrahedron were compared. The closed tetrahedron demonstrated the highest resistance to nuclease degradation (Figure 2-10). Overall, OT6.3 is stable in physiological concentrations of $Mg^{2+}$, but it is prone to nuclease degradation within hours. In future chapters, the

transfections of DNA cages in tissue culture were therefore always conducted in serum-free medium to avoid degradation.

After establishing experimental evidence that a reconfigurable tetrahedron is stable under physiological level of magnesium ion, I moved on to discuss the other important component of the system: the signalling strand $O_c$. It was shown to be stable overnight in complete medium (Figure 2-16b). Its stability inside cells was then examined through the RNA extract from cells transfected with $O_c$. $O_c$ was sufficiently intact that the RNA extraction actuated the DNA cages (Figure 2-18). In conclusion, I have described a system that responds to a specific signal with conformational changes in buffer and tissue culture medium conditions. More importantly, this system has the potential to behave in a similar manner inside cells.

# Chapter 3 Reconfigurable DNA tetrahedra inside cells

## 3.1 Introduction

In the previous chapter, I introduce the reconfigurable tetrahedron that can be opened by a signalling strand in solution. Fluorescent labels and quenchers on the DNA tetrahedron enable us to distinguish the open and closed configuration of the DNA tetrahedron. In this chapter, I will show that the two configurations remain distinguishable inside mammalian cells because the fluorescence signals continue to give robust read-outs of the states of the system inside cells. Confocal microscopy and flow cytometry are used to measure the fluorescence signals in order to monitor the states of the system. In the final section, I will present data demonstrating a small proportion of DNA cages being opened by the signalling strand transfected separately into cells several hours after the cages.

## 3.2 Open and closed tetrahedron inside cells

In order to observe opening of DNA cages inside cells, firstly, the DNA cages have to be delivered into cells. The DNA cages were transfected into cells with the aid of transfection reagent. Secondly, the open and closed cages need to be distinguishable inside cells from the fluorescence measurement. The closed tetrahedron represents the negative control and the open tetrahedron is the positive control. The open tetrahedron is assembled in the presence of the signalling strand, so that the tetrahedron is already opened before the transfection.

There are several factors that might affect the fluorescence measurement from the tetrahedra inside cells. Due to differences in pH and ion concentrations inside cells compared to the assembly buffer, fluorophores and quenchers might exhibit different brightness in the cellular environment. As discussed in the previous chapter, the DNA cages could be degraded by both exo- and endo- nucleases and the DNA cages might not remain closed under different ionic concentrations. Therefore, it is important to establish the positive and negative controls with caution.

The cellular fluorescence was measured by confocal microscopy and flow cytometry. Live-cell confocal microscopy enables imaging of the uptake of fluorescently labelled DNA tetrahedra in living cells with optical sectioning. The focal plane of the microscope can be varied with a range of Z-axis positions. This sectioning allows one to image focal planes that span through the interiors of cells and enables one to determine whether the fluorescent labelled materials are inside cells or just attached to cell surfaces.

Flow cytometry is a fluidic system that can hydro-dynamically focus cells in suspension, so that they pass through the laser beam one cell at a time. It is equipped with fluorescent detectors to measure the fluorescence signal of each cell. Flow cytometry is a complementary investigative method to confocal microscopy because it allows high throughput analysis. Flow cytometry can analyse $10^4$ cells in minutes. Since it measures the fluorescence of the whole cell, so the information provided is different to that obtained from confocal microscopy.

### 3.2.1 Experimental outline

In brief, cells were seeded in a 24-well plate the night before(Appendix A.9). The following day, 0.2 µg of the DNA cage was incubated with 2 µl of transfection reagent Lipofectamine® 2000 (LF) in 100 µl of Opti-MEM® for one hour. Meanwhile, the medium in the 24-well plate was removed and the cells were washed with PBS three times. The medium was replaced with 400µl of Opti-MEM®. Then, the LF-DNA mix was added into the cells for several hours. Cells were washed once prior any further examinations. For the full protocol of transfection, please refer to Appendix A.15.1.1.

Cellular fluorescence was determined by confocal microscopy (Appendix A.13) and flow cytometry (Appendix A.14). In both methods, the incubation medium was removed and the cells were washed with PBS three times in order to remove any DNA nanostructures that remained in the medium. For confocal microscopy, colourless imaging medium was added to the washed sample and replaced the pink Opti-MEM® to optimise the imaging conditions. For the flow cytometry measurement, the washed samples were then incubated with trypsin

replacement so that the cells would detach from the surface. The cell-suspensions were taken for flow cytometry measurement.

### 3.2.2 Choice of cell lines

Breast cancer cell line MCF-7 is the main cell line used in the work of this thesis because MCF-7 cells are adherent to untreated surfaces even after multiple washes and the cell line has a good transfection efficiency with the transfection reagent LF.

HeLa and HEK-293 cells were also tested. The HEK-293 cell line had a similar uptake to MCF-7, but HEK-293 cells could be lifted from the growth surface easily during washes. Rinsing is particularly important for the later experiments in Section 3.3 because cells need to be thoroughly washed to ensure the DNA cages are removed from the medium before the addition of the signalling strands. Therefore, positive (open) and negative controls (closed) were established in HEK-293 cells because there was only one round of transfection (Appendix C.3). However, HEK-293 cells were not used for experiments with two rounds of transfection (one for the DNA cage and the other for the signalling strand) because the cells became detached during the washes and this resulted in loss of cells for the second round of transfection.

As for HeLa cells, LF was not an effective transfection reagent for this cell line. When both HeLa and HEK-293 cells were transfected with the Cy5-labelled DNA cages for three hours, HeLa cellular fluorescence was approximately half of that in HEK-293, according to the flow cytometry measurement (Appendix C.4). In addition, the distinction between positive and negative control in HeLa cells was small, which I will discuss further in Section 3.2.4. With

such small difference between the controls, it would be difficult detect the openings of the cages. The use HeLa cells was therefore discontinued.

### 3.2.3 Confocal Microscopy

Confocal microscopy was used to follow the uptake of fluorophore-labelled DNA tetrahedra into MCF-7 cells. The Cy5 dye was used to report the uptake and cellular localisation of the tetrahedra and the Cy3/quencher pair was used to report the state of the tetrahedra.

#### 3.2.3.1 Qualitative analysis

Figure 3-1 shows the typical live-cell confocal micrographs after eight hours of incubation with two tetrahedra samples. (a) was the cells transfected with the closed tetrahedra and (b) was with the open tetrahedra. The cell nuclei were stained with fluorescent nucleic acid stain Hoechst (Appendix A.13.1) and its channel was shown in blue. In order to avoid Hoechst binding to the DNA tetrahedra in addition to the nuclei, Hoechst was added to the tissue culture media for 30 minutes to stain the cell nuclei at least two hours before the transfection began, and then the media was replaced with fresh one. The Cy3 channel was shown in red and Cy5 channel was shown in green. In both (a) and (b), the Cy5 signals were observed within the cytoplasm and this suggested that there were successful uptake of the Cy5-labelled tetrahedra into cells, not merely on the cell surface.

The Cy3 signal in (a) was relatively weaker than in (b). This agreed with the design of the tetrahedra because (a) was treated with the closed tetrahedra and (b) was treated with the open tetrahedra. When the tetrahedron was closed, Cy3 was in close proximity to the quencher, and hence the Cy3 signal was low. On the other hand, when the tetrahedron was

open, Cy3 was no longer next to the quencher and the Cy3 signal increased. Furthermore, the Cy3 and Cy5 signals in (b) were co-localised in the same structures in the cytoplasm.

With these two observations, I concluded that the DNA tetrahedra were stable within cells for at least eight hours. Cy3 remained quenched in the images for the closed tetrahedra and Cy3 and Cy5 were co-localised in the images for the open tetrahedra. Fluorescent labels and quenchers therefore allowed robust read-out inside cells. Positive and negative controls were established in cells with confocal microscopy.

The punctate distributions of the Cy5 signal in both (a) and (b) suggest that the cages were confined within membrane-bound compartments, which could be endosomes and lysosomes. This meant that the DNA nanostructures could be trapped and they were unlikely to be in the cytosol. Furthre experiments, such as labelling the endosomes and lysosomes with LysoTracker, are required to confirm this hypothesis.

DNA nanostructures that were unable to escape from the endosomes into the cytosol were likely to be degraded and excreted out of the cells. Unsuccessful endosomal escape therefore limits the interactions of the DNA nanostructures with the cellular materials, and hence reduces their potential in biomedical applications. One possible way to overcome this limitation is the funcationalise the DNA nanostructures with endosomal escape signals, such as folate acid and transferrin.

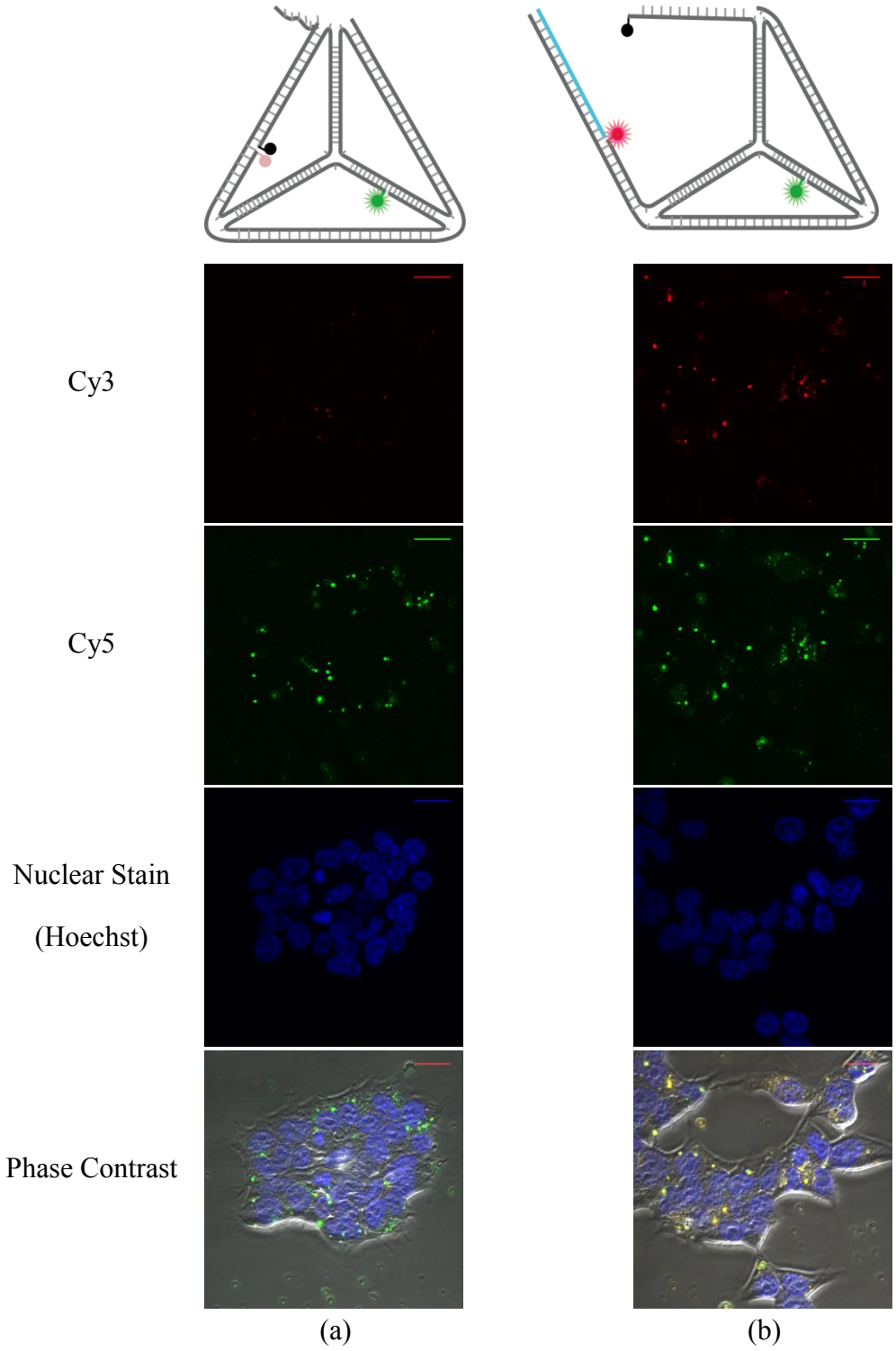


Figure 3-1: Confocal micrographs of DNA cages when transfected with Lipofectamine® 2000 in closed (a) and open (b) states in MCF-7 cells. Red is the Cy3 channel, green is the Cy5 channel, and blue is the Hoechst channel. Hoechst is a live-cell nuclear stain. It is clear that Cy3 signal in the closed tetrahedra sample is weaker than in the sample transfected with the open tetrahedra. The scale bar is 20 μm.

#### 3.2.3.2 Quantitative analysis

Confocal micrographs were also analysed quantitatively (Appendix A.32) because brightness of different colours could be subjective and a quantitative approach allows objective comparison between samples. In the case of the positive and negative controls, a quantitative analysis may seem redundant because the distinction between the two is obvious. However, for future experiments, when one is examining opening of cages, the changes in Cy3:Cy5 ratio may be more subtle and a quantitative analysis can be more reliably detect any small changes.

In MATLAB, the thresholds of Cy3 and Cy5 were determined separately and only pixels with both Cy3 and Cy5 intensities above the background, but not saturated were selected. Then the Cy3:Cy5 ratios for each selected pixel were calculated, and the frequency of each Cy3:Cy5 value was weighted with the Cy5 intensity. This was necessary because the number of tetrahedron is proportional to the Cy5 intensity, so a higher Cy5 signal represented more tetrahedra, hence a higher frequency. Figure 3-2 shows the distributions of the Cy3:Cy5 ratio of opened and closed tetrahedra. The quantitative analysis was based on the confocal micrographs Figure 3-1. The distribution for the open tetrahedra was centred on 0.3 while the one for the closed tetrahedra is centred on 0.1. Therefore, the Cy3:Cy5 ratio for the sample transfected with open cages was three times higher than the one with the closed cage. This is in agreement with the qualitative analysis.

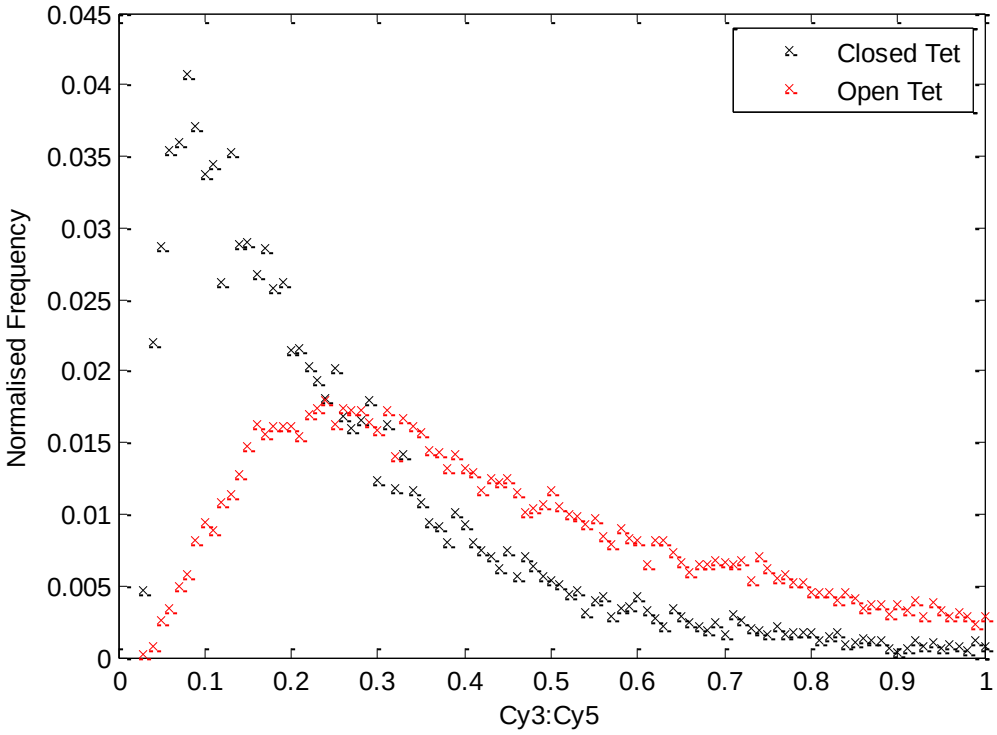


Figure 3-2: Quantitative analysis of confocal micrographs. The two traces are the distributions of the Cy3:Cy5 ratio of the pixels in of the confocal images in Figure 3-1. The black crosses correspond to the closed tetrahedra in Figure 3-1(a) and the red crosses correspond to the open tetrahedra in Figure 3-1(b). The frequency is scaled with the cy5 intensity of each pixel. The sample transfected with the closed tetrahedra has a distribution that is centred to the left of the sample with the open tetrahedra. This suggests that overall cells with the closed tetrahedra have a lower Cy3:Cy5 ratio.

### 3.2.4 Flow cytometry

Flow cytometry is a complementary investigative method to confocal microscopy because it allows high throughput analysis. It can measure the fluorescence signals of thousands individual cells within a few minutes. The punctate distribution observed in Figure 3-1 showed that LF transfection was not very effective in aiding the DNA cages to escape the endosomes. It was likely that only a small proportion of cages would be opened by the separately transfected signalling strand, resulting in minute changes in fluorescence. Flow cytometry has a wider dynamic range and with its large sample size, it is more reliable way to measure small changes.

The cellular fluorescence signals for Alexa-488 and Cy5 were collected in the flow cytometer and the histograms of the ratio of Alexa-488:Cy5 were plotted in Figure 3-3. It shows the data of MCF-7 cells transfected with closed (black) and opened (red) cages. The sample with the closed tetrahedra is the negative control and the sample with the open tetrahedra is the positive control.

The graph on the top shows the data collected four hours after the transfection of cages and the bottom graph shows the data ten hours after the transfection. After four hours of incubation, the sample treated with the closed tetrahedra (black crosses) had a distribution of Alexa-488:Cy5 ratio centred around 1.5, while the sample with the open tetrahedra (red crosses) had a distribution centred on 3, which was approximately twice of that with the closed tetrahedra. These fluorescence read-outs agreed with the design of the open and closed configurations of the DNA cages.

The bottom graph in Figure 3-3 shows similar distributions to the one above. After ten hours of incubation, the sample treated with the closed tetrahedra (black circles) had a distribution centred just above 1 and the sample with the open tetrahedra was centred on 3. This distinction between the positive and negative control was maintained throughout the course of the experiment. The DNA tetrahedra were therefore stable for at least ten hours within cells because the Alexa-488 signals were consistently lower in cells transfected with the closed tetrahedra than those with the open tetrahedra. Fluorescent labels and quenchers allowed robust read-out inside MCF-7 cells.

Establishment of the positive and negative controls were not successful with HeLa cells. The distinction between positive and negative controls in HeLa cells was small (Figure 3-4) in comparison to MCF-7 cells, so the use HeLa cells is discontinued. With such small difference between the controls, it would be difficult detect the openings of the cages.

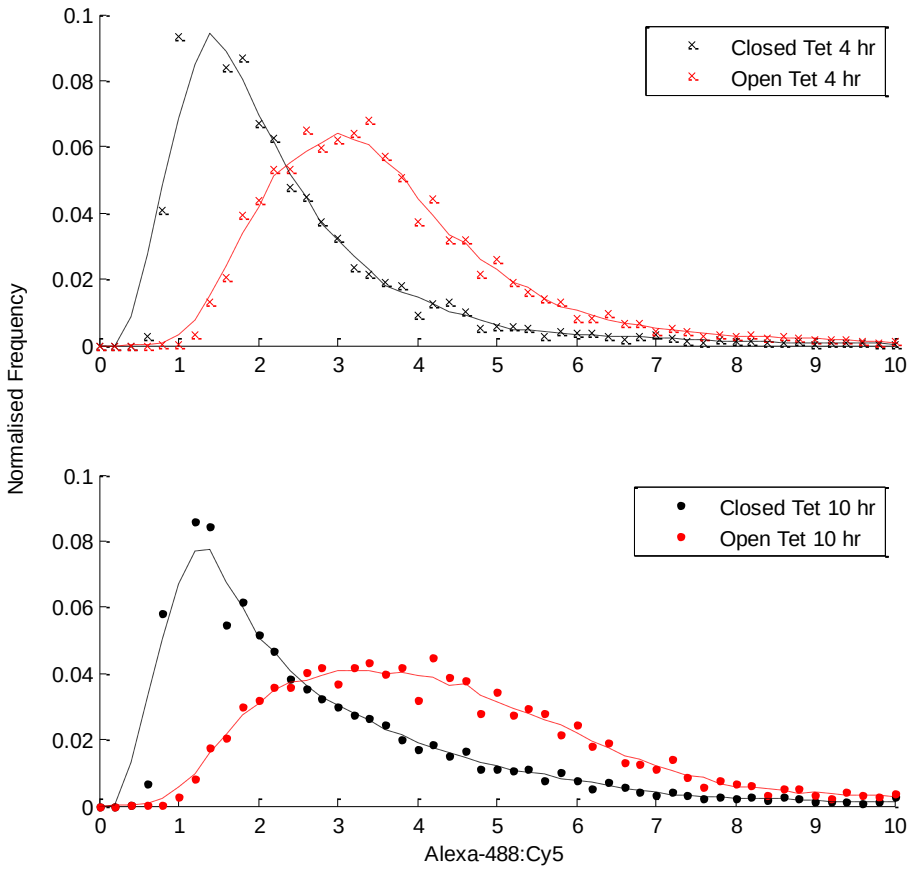


Figure 3-3: Histograms of the cellular Alexa-488: Cy5 ratio with open and closed tetrahedra. The closed tetrahedra are in black and the open tetrahedra are in red. The histograms are based on the flow cytometry data of MCF-7 cells incubated with the DNA tetrahedra for 4 hr (top) and 10 hr (bottom). The two configurations are clearly distinguishable inside cells over 4 to 10 hours.

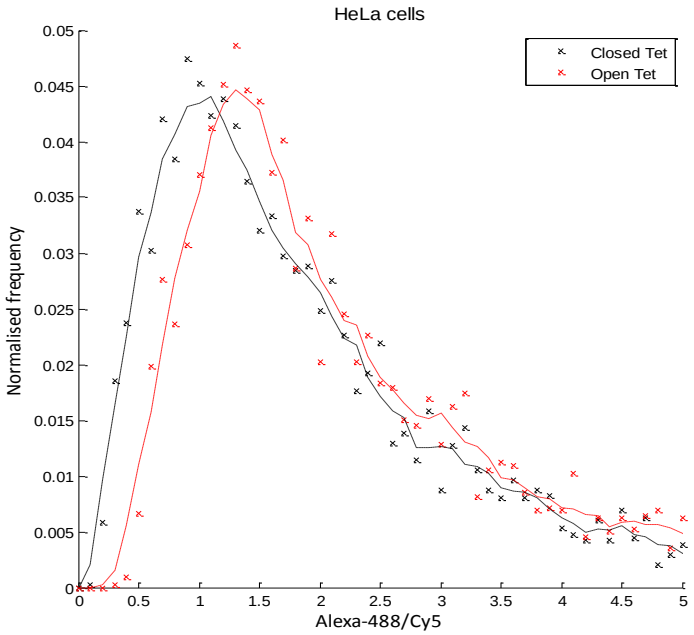


Figure 3-4: Histograms of the Alexa-488:Cy5 in HeLa cells. The histograms are based on flow cytometry data of HeLa cells transfected with the open tetrahedra (red) and the closed tetrahedra (black). There is only a small distinction between open and closed tetrahedra, so the use of HeLa cells was discontinued.

### 3.2.5 LF potentially enhances DNA cages nuclease resistance

According to the fluorescence measurement in confocal micrographs and flow cytometry data, Cy3 or Alexa-488 remained quenched inside cells for at least eight hours, indicating that the integrity of the cages was preserved. This was longer than that was observed in complete medium and cell lysate discussed in Chapter 2. Degradation fragments of the DNA tetrahedra were visible after two hours of incubation. The difference in the stability may be due to the extra protection from the transfection reagent LF against nuclease degradation. In the previous chapter, the DNA tetrahedra were naked. However, in this case, they are in complex with LF. The complex may hinder the nucleases from binding to the DNA nanostructures.

This hypothesis could be tested by comparing the Cy3:Cy5 ratios of tetrahedra that were in complex with LF and without, in the presence of nucleases at various time points. If LF enhances DNA cages nuclease resistance, there will be a delay in the increase in the Cy3:Cy5 ratio because the cages remain intact for a longer period of time. This could be measured in the fluorimeter or gel scanner.

## 3.3 Opening DNA tetrahedra inside cells

In the previous chapter, I have shown that the signalling strand $O_c$ was detectable in the cell lysate after an overnight transfection. In Section 3.2, the negative (closed) and the positive (open) controls were established in cellular measurements. According to the fluorescence measurement in confocal micrographs and flow cytometry data, the open and closed cages were clearly distinguishable for at least eight hours. We are therefore in the position to test if reconfiguration of DNA cages inside cell with a biological signal is possible.

Two different transfecting agents were used: Lipofectamine® 2000 (LF) and X-tremeGene HP DNA transfection reagent (XG). The former is cationic-lipid based and the latter is non-liposomal based. XG has been shown to be a more effective transfection reagent.[99] More importantly, DNA logic gate operations were reported to be possible inside mammalian cells when the nanostructures were delivered by XG.[46] A comparison between LF and XG will be discussed in Section 3.4.

### 3.3.1 Experimental outline

The experimental procedure is similar to the one described in Section 3.2.1, but for experiments described here, there are two rounds of transfection rather than one. DNA cages were transfected first and then 4 hours later, the signalling strand $O_c$ was transfected.

In brief, 0.2 μg of the closed tetrahedron was transfected into MCF-7 cells using either LF (Appendix A.15.1.2) or XG (Appendix A.15.2) in Opti-MEM®. After 3 hours, the samples were washed with PBS three times, and the old medium was replaced with the fresh medium. After an hour, the medium was replaced again and 10 times molar excess of $O_c$ were transfected with the same transfection reagent as the first round. Cells were incubated with $O_c$ for several hours. Finally, the cells were trypsinised for flow cytometry measurement.

### 3.3.2 Delivering DNA materials with LF

Figure 3-5a shows the Alexa-488:Cy5 distributions of cells transfected with open or closed DNA tetrahedra for three hours. The two distributions were clearly distinguishable, so the positive and negative controls were established. Figure 3-5b shows the cellular fluorescence of cells first transfected with the closed DNA tetrahedra, then four hours later, $O_c$ was transfected. Measurements were taken after one hour and six hours of transfection of $O_c$. The total incubation periods were therefore five and ten hours respectively.

In Figure 3-5b, after one hour of incubation with $O_c$, the Alexa-488:Cy5 ratio remained similar to the closed tetrahedra in Figure 3-5a. Both distributions centred at the same position and this suggested most cages in (b) remain closed. At this point, $O_c$ was still in the early

stage of the transfection. It might not have escaped the endosomes or reached the same cellular locations as the DNA cages, which began the incubation four hours earlier.

After six hours, there was a slight increase in Alexa-488:Cy5 ratio and the peak of the distribution shifted slightly to the right. This indicated the opening of some DNA cages. Though the proportion that became opened was small, this did not come as a surprise because the two products were transfected at different time points, so they might not be trafficked into the same locations. Even when they were in the same locations, the strand displacement reaction might be slow because they were in low concentrations. The DNA cages and the signalling strands were likely to have been internalised into different compartments. In addition, the steric hindrance imposed by the tetrahedral structure might further reduce the rate of strand displacement when compared to a similar reaction on a simple duplex. It would be interesting to measure the cellular trafficking timescale, the locations of the transfected DNA materials and where the opening of cages took place. Once we understand the system better, then we can target the bottle neck of this reaction and make the system more target responsive.

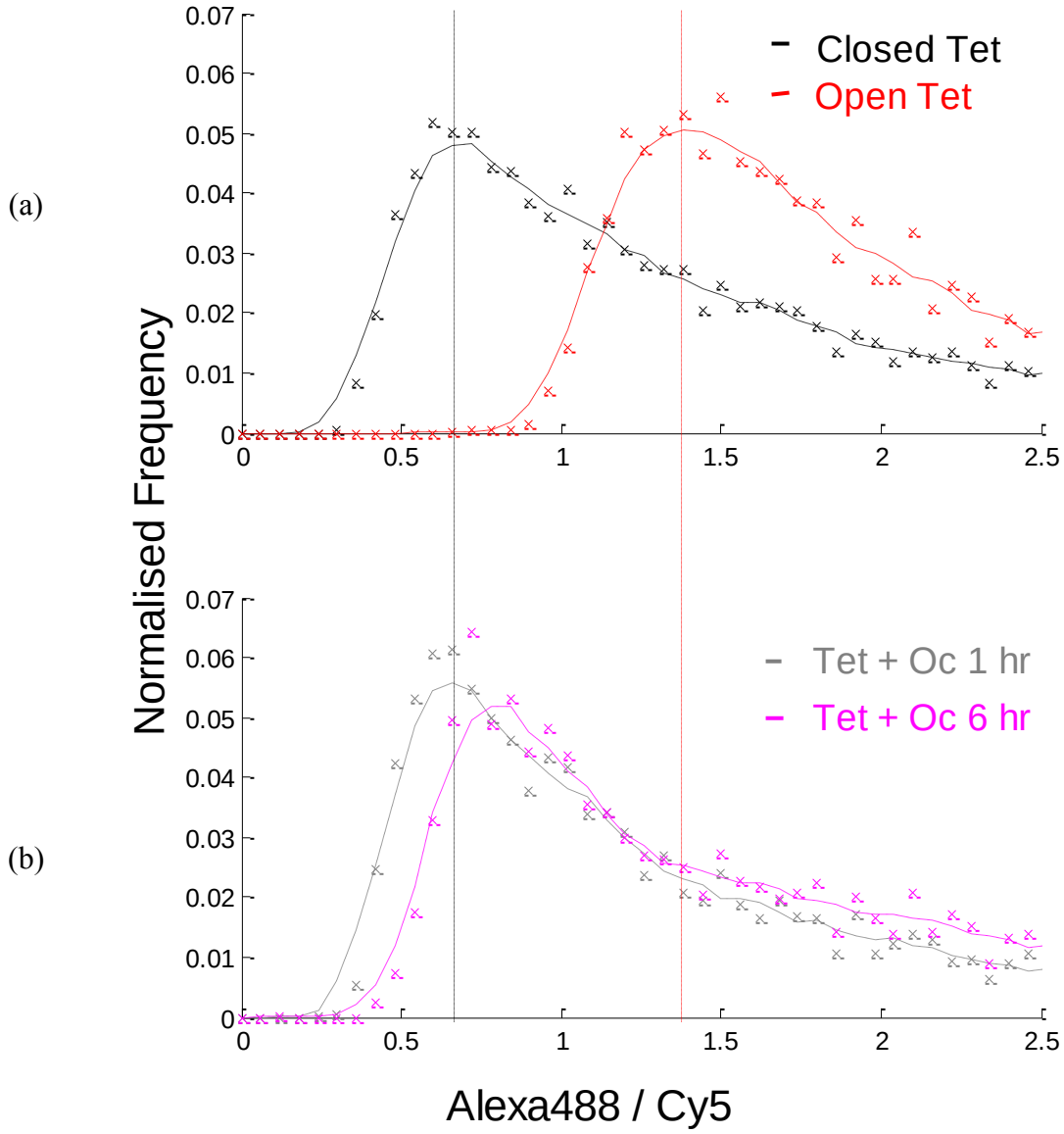


Figure 3-5: Flow cytometry data of fluorescence read-out of DNA cages. LF was the transfection reagent used. Histogram of Alexa-488: Cy5 ratio (a): closed and open tetrahedra after incubation of three hours; (b): in addition to the three hours incubation with the closed tetrahedra, cells were followed by an incubation with Oc for one hour (grey) and six hours (magenta). The experimental data indicates the opening of a small proportion of DNA cages after 6 hr of incubation with $O_c$.

### 3.3.3 Delivering DNA materials with XG

When LF was used to deliver the tetrahedra and the $O_c$, only a small proportion of cages were opened by $O_c$. A potential way to improve the system is to test another transfection reagent. Hemphill et al.[100] demonstrates the operations of nucleic acid AND gates that interact with external DNA strands and specific endogenous miRNAs inside mammalian cells. The nucleic acid AND gates were transfected into cells with X-tremeGene HP DNA transfection reagent (XG). This publication motivated me to test XG after the initial experiments with LF.

Herein, XG was used as the transfection reagent instead of LF. The negative control was also modified slightly. Rather than simply using the closed tetrahedra as the negative control, a random strand $O_{neg}$ was transfected into the cells with closed tetrahedra as a negative control at the second round of transfection, so that any addition effect of an extra round of transfection would be accounted for and this ensured a fair comparison between the negative control and the test sample. $O_{neg}$ was the opening strand for OT6.3 in Chapter 2 (for sequences see Appendix B.2) and it was not expected to interact with OT6.3SCO, which was the DNA tetrahedron used here.

Figure 3-6 shows the cellular fluorescence for three samples. The red one was the positive control, which cells were transfected with the open tetrahedra for seven hours. The black and pink ones were cells transfected with the closed tetrahedra for the first three hours. Then the tetrahedra were removed and at the forth hour, the black sample was transfected with $O_{neg}$ and the pink sample was transfected with $O_c$. Therefore, the black sample was the negative control and the pink sample was the test case. The cellular fluorescence was measured three hours later. The total incubation period for all three samples was seven hours.

The red sample had the highest Alexa-488:Cy5 ratio and the black sample had the lowest ratio. This was expected because the red one is the positive control, which shows the maximal level of Alexa-488:Cy5 ratio and the black sample is the negative control, which shows the minimal level of Alexa-488:Cy5.

The Alexa-488:Cy5 ratio of the sample transfected with $O_c$ (pink) is twice as high as the sample transfected with $O_{neg}$ (black). The difference in the ratio indicates opening of some DNA cages due to the presence of the signalling strand $O_c$.

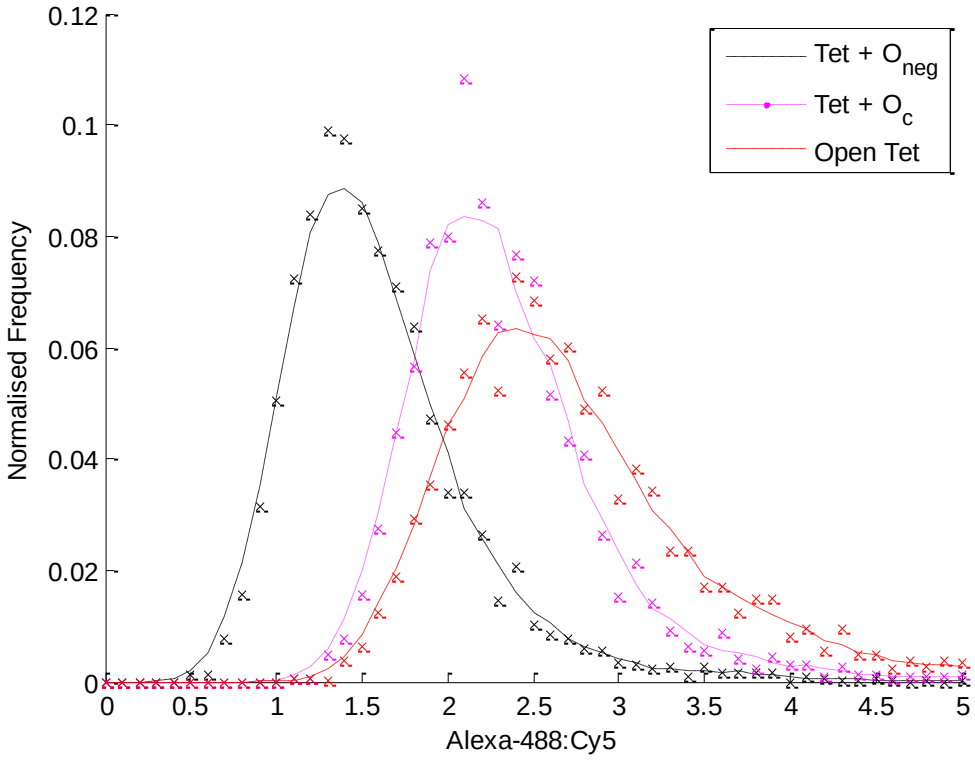


Figure 3-6: Histograms of Alexa-488: Cy5 ratio with XG transfections. The histograms are based on flow cytometry data of cells transfected with the aid of XG. The black trace is the sample transfected with closed tetrahedra for three hours and then followed by three hours incubation with Oneg. The pink trace is the sample transfected with closed tetrahedra for three hours and then followed by three hours incubation with the opening strand Oc. The red trace is the sample transfected with the open tetrahedra for seven hours. Therefore, the data set in black represents the negative control and the one in red is the positive control. Since the sample with the opening strand has an Alexa-488:Cy5 distribution between the negative and positive control, this suggests that some DNA cages are opened by $O_c$.

## 3.4 XG is a better transfection reagent than LF

When either LF or XG was used as the transfection reagent to deliver the DNA cages and the signalling strands into the cells, the experimental results revealed opening of DNA cages. This implied that strand displacement could take place within cells.

When XG was used, a more significant proportion of cages were opened when compared to LF (Figure 3-5 & Figure 3-6). XG is therefore a more promising transfection reagent in the current experimental design. The difference is likely due to the transfection efficiency of the two chemicals. I therefore conducted a comparison between LF and XG. Each well of MCF-7 cells were transfected with 0.2 μg of the Cy5-labelled tetrahedra in a 24-well plate (Appendix A.15). The cellular fluorescence was measured by flow cytometry 3 hours after the transfection.

Figure 3-7 shows the Cy5 distribution of individual cells from three different samples: untreated cells (top), cells transfected with XG (middle) and cells transfected with LF (bottom). The top histogram of untreated cells indicated the level of background fluorescence of the cells, which was below 10 arbitrary units (au). When the Cy5 fluorescence was above this background level, this implied that the cell had taken up some Cy5-lablled tetrahedra.

When transfected with XG, all the cells took up the Cy5-labelled tetrahedra, with the distribution centred around 600 au. On the other hand, when LF was used as the transfection reagent, there were two distributions: one centred at around 5 au and another broad distribution centred on 800 au. The first distribution consisted of cells without a measurable amount of the DNA tetrahedra inside and that was approximately half of the total sample. For

the other half of the sample, which was the second distribution, there was a broad distribution in the amount of DNA tetrahedra inside them.

The property of transfecting cells evenly is particularly important for microscope experiments because only a relatively small numbers of cells are imaged. If all the cells take up similar amount of DNA nanostructures, experiments are less likely to be distorted by the images of a small number of cells. Therefore, XG is a more effective transfection agent and this explains why a larger proportion of cages were opened in the previous section. Furthermore, if more nanostructures are taken up by the cells, then the Cy5 signal will be strong enough even with low laser power. This reduces photocytotoxicity during imaging.

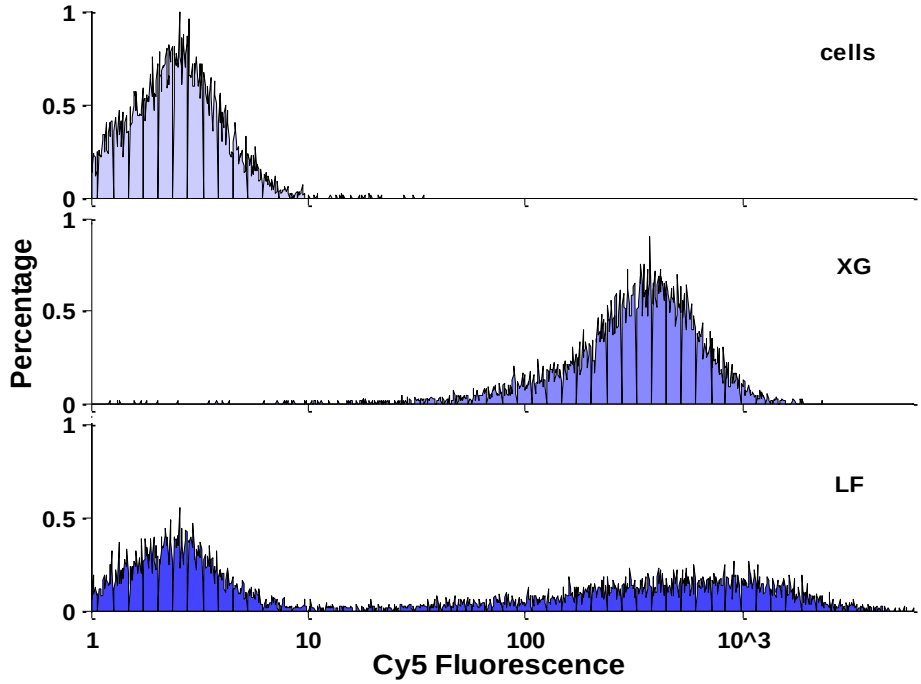


Figure 3-7: Comparing cellular uptake with different transfection reagents. Histograms of cellular fluorescence after transfection of the Cy5-labelled tetrahedra with different transfection reagents: untreated cells (top), X-tremeGene (middle), Lipofectamine® 2000 (bottom). XG transfects cells more evenly than LF, so it is a better transfection reagent in this experimental design.

## 3.5 Conclusion

Positive and negative controls inside cells were established. In confocal microscopy, there was a clear difference between the closed and the open tetrahedra. Cy3 remained quenched inside cells (Figure 3-1) for eight hours, indicating that the integrity of the cages was preserved. This was longer than the reported stability of DNA tetrahedron in complete medium[51] and it was attributed to additional protection from the transfection reagent. However, the delivery into the cytosol was not very effective and nanostructures likely trapped within membrane bound compartments. Flow cytometry was also used to provide a more quantitative approach and to analyse a larger sample size. The Alexa-488:Cy5 ratio in sample transfected with the open tetrahedra was over twice the ratio for the closed tetrahedron. Two distinct histogram distributions Alexa-488:Cy5 are shown in Figure 3-3.

Following this, $O_c$ was transfected four hours after the DNA cages and triggered opening of the cages. LF had been used as the transfection reagent for the majority of experimental data discussed in this chapter and only a very small proportion of cages were open (Figure 3-5). On the other hand, preliminary data on the XG transfection with the cages and $O_c$ showed a more significant portion of cages being opened (Figure 3-6). A comparison between the level of DNA tetrahedral uptake with LF and XG revealed that XG transfected cells more evenly (Figure 3-7). To a greater extent, XG is more suited in this experimental design and will be used in Chapter 4.

Pei et al demonstrated conformational changes of DNA nanostructures induced by a change in cellular ATP concentrations,[3] but this is the first experiment that used an externally transfected signal to actuate the DNA cage inside cells.

# Chapter 4 Model System: DNA duplex

## 4.1 Introduction

In the previous chapter, experimental results showed promise in the actuation of the DNA cages with synthetic oligonucleotides transfected several hours after the DNA cages. In this chapter, a simplified duplex model system is used rather than the DNA cages, because the duplex has a better formation yield than the DNA tetrahedron and it can be transfected into cells at a higher concentration, giving a stronger fluorescence signal.

In this chapter, I show that experiments where cells were first transfected with the duplex DNA and then subsequently transfected with a signalling strand. The results reveal that strand displacement can take place within cells. The extent of strand displacement increases with the incubation time of the signalling strand. Two-colour experiments designed to simultaneously track both the DNA duplex and signalling strand were unsuccessful because aggregation outside of the cells was observed, demonstrating the need for a more effective washing protocol to remove extracellular DNA nanostructures that remained after the first transfection.

## 4.2 The motivations for simplifying the DNA nanostructure

The reconfigurable DNA tetrahedron is reduced to a simplified model system: a DNA duplex. At the current stage of investigation, the focus is on the interaction between the DNA nanostructure and the signalling strand. A DNA duplex is a suitable model nanostructure for this purpose.

There are additional disadvantages in using the cage at this stage. Firstly, the synthesis of the DNA tetrahedron with fluorophores and quenchers modifications is more expensive than a duplex and it is more time consuming to synthesise than a DNA duplex. By using duplexes, we can first understand the basic system better, before moving on to a more complicated system involved cages. Secondly, using cages limits the number of the DNA nanostructures that can be transfected into cells. The transfection reagent is not cytotoxic when used in low dose, but it still puts cells under stress.[99] Therefore, optimising transfection is a balance between maximising the uptake of DNA and minimising the quantity of transfection reagent required. The ratio of DNA to transfection reagent is maintained at 0.1 μg:1 μl in the previous experiments with the DNA tetrahedra. In that experimental design, there is only one reconfigurable edge, so only one sixth of the cage is involved in the interaction with the signalling strand. The majority of the transfection reagent is in complex with the other five-sixths of the DNA cages that are not interacting with the signalling strand. If a duplex is used instead, we can transfect 6 times more duplexes with the same amount of transfection reagent and this will give a stronger signal.

In the bigger picture, the tetrahedral structure is vital in the carrying and protecting of the drug molecule, but at this stage, the focus is on the interaction between the reconfigurable

edge and the signalling strand, so it is appropriate to simply the DNA system to a duplex DNA.

## 4.3 Strand exchange reactions in cells using double-stranded DNA

### 4.3.1 Design of duplex L•Q

The design of duplex L•Q is based on the reconfigurable tetrahedron in the previous chapter. Figure 4-1a illustrates the design of L•Q, which is formed by the hybridisation of strand L (purple and grey) and strand Q (grey). Stand L is labelled with Cy5 (green circle) at the 3' end and strand Q is labelled with Iowa Black RQ quencher (black circle) at the 5'end. Upon hybridisation of L and Q, the Cy5 signal is quenched by the quencher beside it. There is a six nucleotides (nt) single-stranded domain (purple) at the 5' end of strand L, which has the same length as the overhang in the reconfigurable tetrahedron in the previous chapter.

The purple domain serves as a toehold to facilitate a strand exchange reaction in which strand Q is displaced by the signalling strand $O_c$ to generate the product L•$O_c$ (Figure 4-1b). The strand exchange reaction triggered by $O_c$ separates Cy5 and the quencher; therefore, the Cy5 signal reports the extent of the strand displacement reaction. Figure 4-2 shows the schematic diagram of the strand exchange reaction. For sequences of the strands, please refer to Appendix B.3.

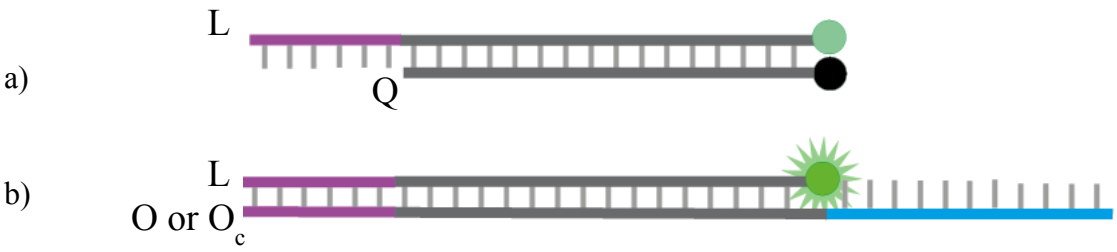


Figure 4-1: Schematic diagrams of the model system a) L•Q and b) L•O or L•Oc, which is the duplex after the strand displacement reaction between L•Q and Oc.

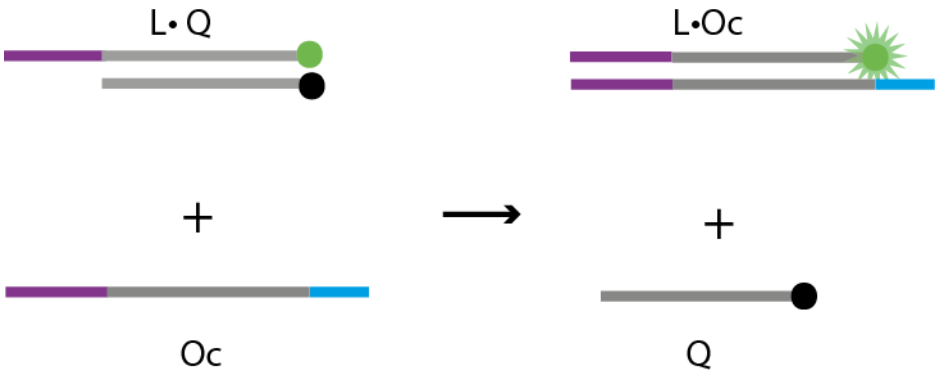


Figure 4-2: Schematic diagram of the strand displacement reaction between L•Q and Oc. Oc displaces Q to form L•Oc, which leads to an increase in the fluorescence signal of the system.

### 4.3.2 Signalling strand: with and without chemical modifications

The signalling strand $O_c$ is the same strand used in the previous two chapters. $O_c$ has 2'O-methyl and phosphorothioate modifications, so it is resistant to nuclease degradation. With enhanced nuclease resistance, the lifetime of $O_c$ inside cells increases, extending the opportunity for it to interact with the DNA nanostructures. This was important in Chapter 3 because the percentage of actuation of the DNA cages inside cells by the externally transfected $O_c$ was small (Section 3.3).

On the other hand, in this chapter, the preliminary data with the simplified design showed a clear trend of the duplex L•Q interacting with the signalling strand $O_c$ as the incubation period increased. I will further discuss this in Section 4.3.4. Based on this observation, I decided to test if it would also work with the unmodified signalling strand O, as it is 10 times cheaper than $O_c$. O has the same sequence as $O_c$.

### 4.3.3 Experimental Outline

The experimental design described here is similar to the one in the previous chapter, except for two changes. Firstly, X-tremeGene HP DNA transfection reagent (XG) is used rather Lipofectamine® 2000 (LF) as the transfection reagent. Secondly, the DNA nanostructure is duplex L•Q instead of the reconfigurable tetrahedron.

In brief, L•Q was synthesised by annealing strand L and strand Q at 4 μM final concentration in Buffer A (Appendix A.2). 50 nM of L•Q was transfected into MCF-7 cells with transfection reagent XG in Opti-MEM®. Then the cells were washed with PBS three times and fresh medium was added. After an hour, the medium was replaced again and cells were

then transfected with 200 nM of the signalling strands with XG. As for the negative control, $O_{neg}$ that was not expected to interact with L•Q, was used in the second round of transfection. For the full protocol of transfections, see Appendix A.15.2.

Cellular fluorescence was determined at a defined time after the second transfection by either flow cytometry or confocal microscopy. The tissue medium was removed and cells were washed with PBS three times. For flow cytometry measurement, the washed samples were trypsinised so that the cells were in suspension and the fluorescence of individual cells was measured (Appendix A.14). For confocal microscopy, the colourless imaging medium was added to the washed cells and replaced the Opti-MEM®. The cells were then ready to be imaged (Appendix A.13).

### 4.3.4 Measuring the extent of strand exchange with flow cytometry

Flow cytometry was used to measure the extent of strand exchange between L•Q and the signalling strands in cells. When duplex L•Q interacts with the separately transfected signalling strand, strand Q with the quencher will be displaced from strand L and this leads to an increase in Cy5 signal.

Figure 4-3 shows the Cy5 cellular fluorescence at three different time points after the second transfection. i) was the negative control, in which $O_{neg}$ was transfected instead of the signalling strands for three hours. It represented the background cellular fluorescence because $O_{neg}$ did not interact with L•Q. The distribution centred around 30 arbitrary units (au).

Figure 4-3a ii - iv represented the samples transfected with $O_c$ with increasing time period (0.5, 1.0 and 3.0 hours). Gradual increases in the Cy5 fluorescence signal were observed as

time progressed. After three hours, the average fluorescence for the cells transfected with $O_c$ increased to approximately 540 (au), which was an 18-fold increase in the Cy5 signal when compared to the negative control.

A similar pattern was observed with the opening strand O without the chemical modifications. Figure 4-3 b ii - iv show gradual increases in the Cy5 fluorescence signal at the same time periods, but the increase was smaller when compared to $O_c$ (Figure 4-3a). After three hours, the average fluorescence for the cells transfected with O increased to around 250 au. An approximate 10-fold increase in the Cy5 signal was observed compared to an 18-fold increase in the case of $O_c$. The difference of fold-increase between the two cases might be due to the increased nuclease resistance of $O_c$, leading to a higher concentration of $O_c$ that were able to hybridise with L•Q.

All samples transfected with the signalling strands, both $O_c$ and O, had higher Cy5 fluorescence than the sample treated with the negative control strand $O_{neg}$, including the first time point (0.5 hour). This suggested that the strand exchange between L•Q and the signalling strand took place as soon as 30 minutes after the second transfection. This was faster than what was observed with the DNA tetrahedron system transfected with LF in the previous chapter. In that case, a very small proportion of DNA cages were opened six hours after the second transfection. This difference was due to XG having a better transfection efficiency and L•Q was transfected at a higher concentration than the DNA cages. This result demonstrated that changing the transfection reagent from LF to XG and simplifying the DNA nanostructures from a tetrahedron to a duplex increased the extent of strand exchange.

(a)

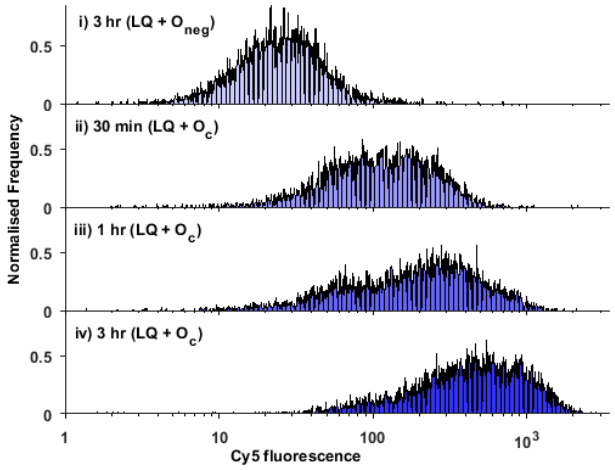


(b)

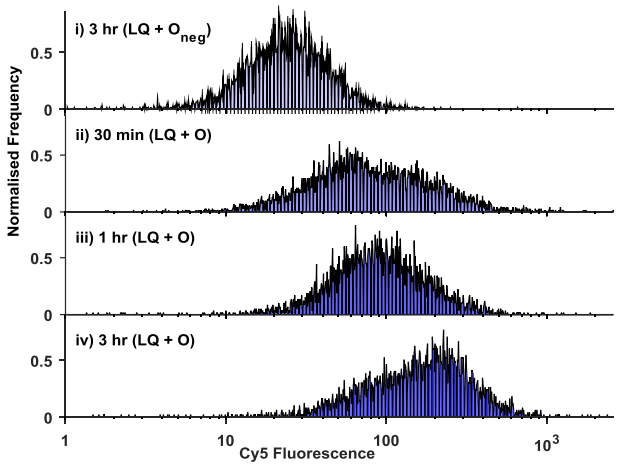


Figure 4-3: Flow cytometry measurements of cells at different time point. MCF7 cells were first transfected with L•Q and then with the opening strands for ii) 30 min, iii) 1 hr and iv) 3 hr. i) is the negative control, which strand $O_{neg}$ was transfected for 3 hr instead of either of the opening strand. (a) is the time course for L•Q + Oc. (b) is the time course for L•Q + O.

### 4.3.5 Determining the subcellular location of duplex strand exchange with confocal microscopy

Flow cytometry measurements are quantitative and particularly useful in the early stage of this investigation because the fluorescence of over $10^4$ cells can be measured in minutes. It has a wide dynamic range and small fluorescence changes could be detected due to the large sample size. However, one crucial piece of information that is not available from flow cytometry measurements is where the interaction between duplex L•Q and the signalling strand takes place. Therefore, confocal imaging is used to provide this piece of information. Flow cytometry and confocal microscopy are complementary investigative methods.

In confocal microscopy, cells were imaged after 1, 3, or 5 hours after the second transfection. Figure 4-4 shows the images of the negative control, in which $O_{neg}$ was transfected. When the sample was transfected with $O_{neg}$, the Cy5 signal remained low throughout the time course and therefore, the degradation of the duplex, which would also lead to separation of the fluorophore and the quencher, did not contribute significantly to the fluorescence signal increase.

Figure 4-5 shows images of cells transfected with the chemically modified signalling strand $O_c$ in the second transfection. After one hour of transfection, the Cy5 signal was relatively weak and only observable in less than half of the cells (Figure 4-5a). After five hours, the Cy5 signal inside cell was significantly stronger and it was present in most of cells (Figure 4-5c). Figure 4-6 shows the images of cells transfected with the unmodified signalling strand O and a similar pattern to $O_c$ was observed.

Since the Cy5 signal remained low throughout the 5-hour-period in the case of $O_{neg,}$ the gradual increases in the Cy5 signal upon transfection of $O_c$ and O were therefore due to the strand exchange between the duplex and the signalling strands, not simply because of the degradation of the duplex.

In both Figure 4-5 & Figure 4-6, the distributions of the Cy5 signal were punctate at all three time points. This suggested that the labelled DNA is in subcellular compartments. As time progressed, the Cy5 signal increased and a larger amount of DNAs accumulated in those compartments. In order to show the punctate distribution clearly, Figure 4-7 shows the zoom-in views at each time point from Figure 4-6. In addition to the punctate nature of the Cy5 signals, the locations of these compartments were mostly juxtanuclear. Late endosomes and lysosomes fuse and exchange materials in this region of the cytoplasm.[101] It was possible that both L•Q and the signalling strand were initially in different endosomes but when the late endosomes fused, they were mixed and the strand displacement reaction takes place.

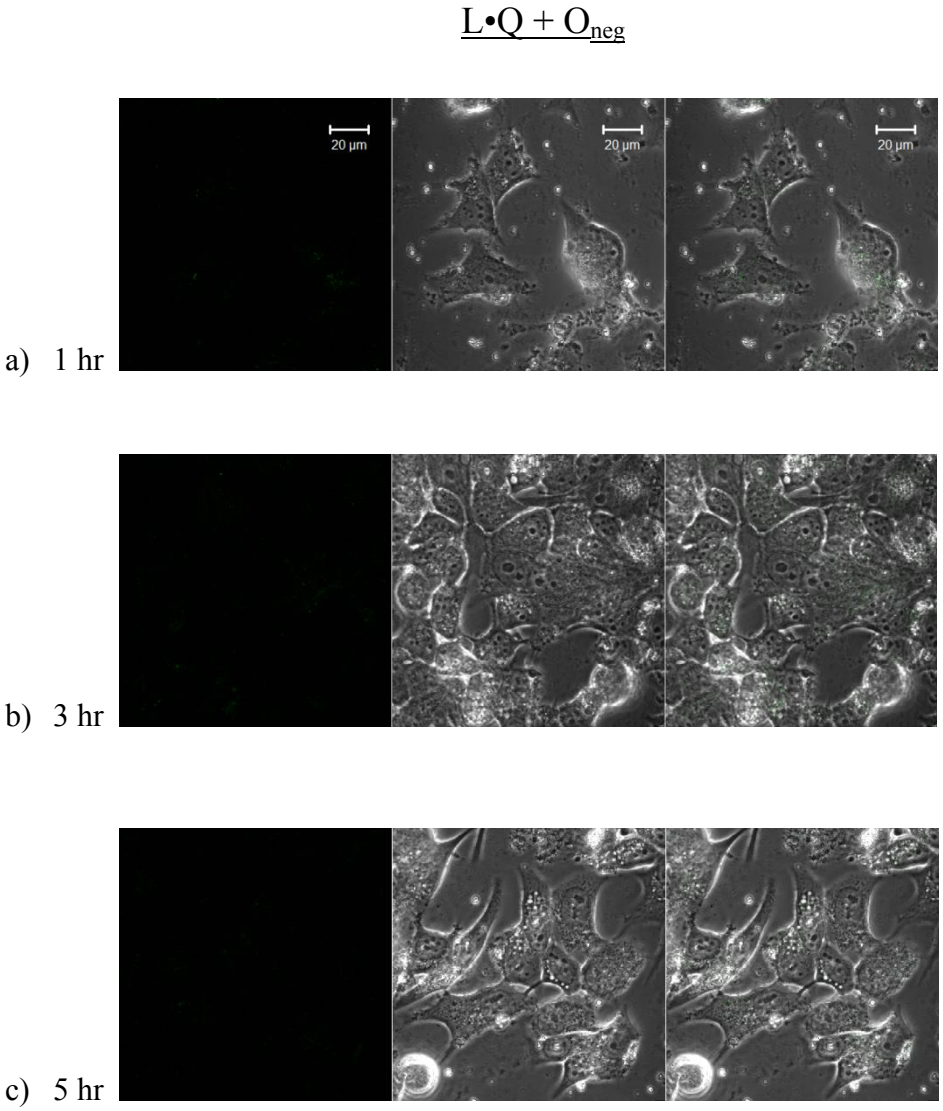


Figure 4-4: Confocal images of MCF7 cells transfected with Oneg. This is the negative control because Oneg does not interact with L•Q. The left panel is the Cy5 channel, the middle is phase contrast and on the right is the overlay. L•Q was first transfected into cells for 3 hours, then the medium was removed and cells were washed with PBS. Cells were then transfected with Oneg for a) 1 hr, b) 3 hr and c) 5 hr. The scale bar is 20 µm

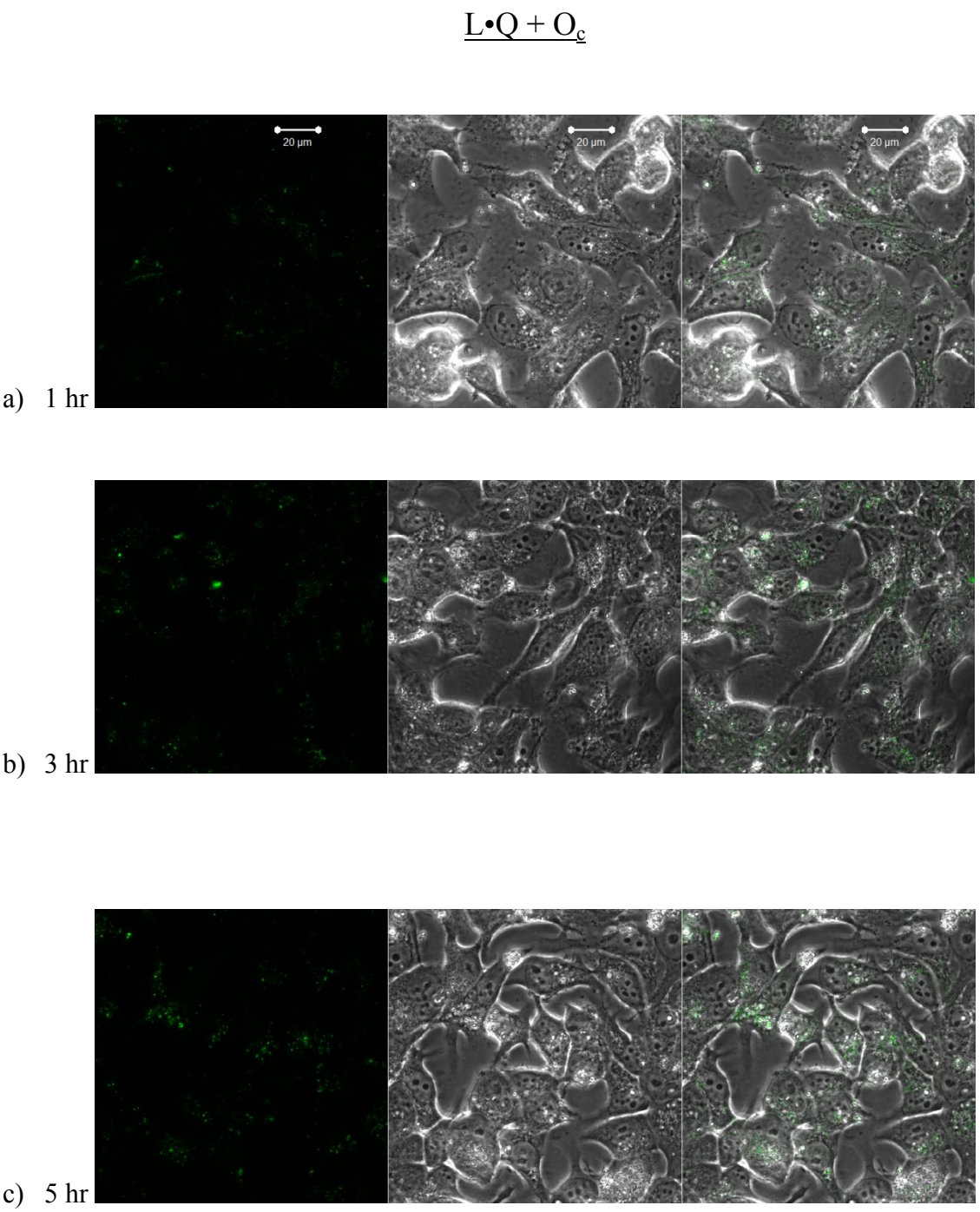


Figure 4-5: Confocal images of MCF7 cells transfected with Oc. The left panel is the Cy5 channel, the middle is phase contrast and on the right is the overlay. L•Q was first transfected into cells for 3 hours, then the medium was removed and cells were washed with PBS. Cells were then transfected with Oc for a) 1 hr, b) 3 hr and c) 5 hr. The scale bar is 20 µm.

L•Q + O

a) 1 hr

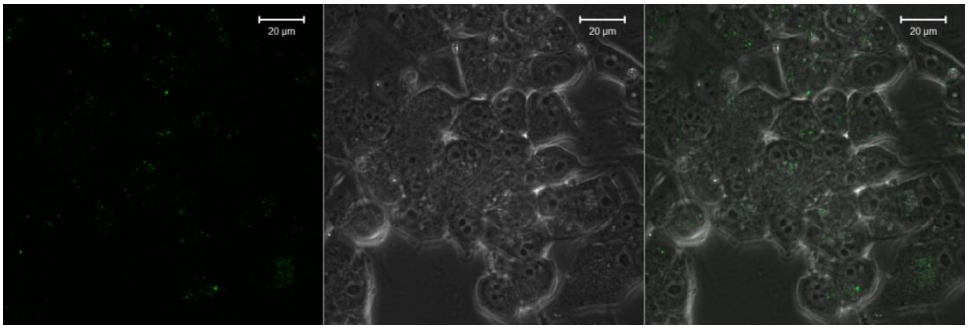


b) 3 hr

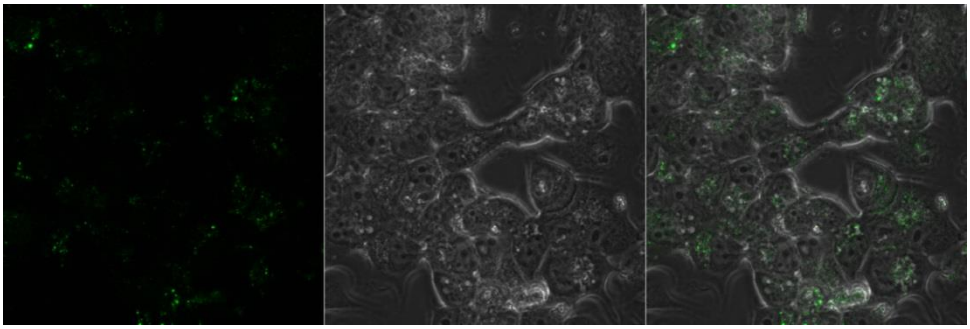

c) 5 hr

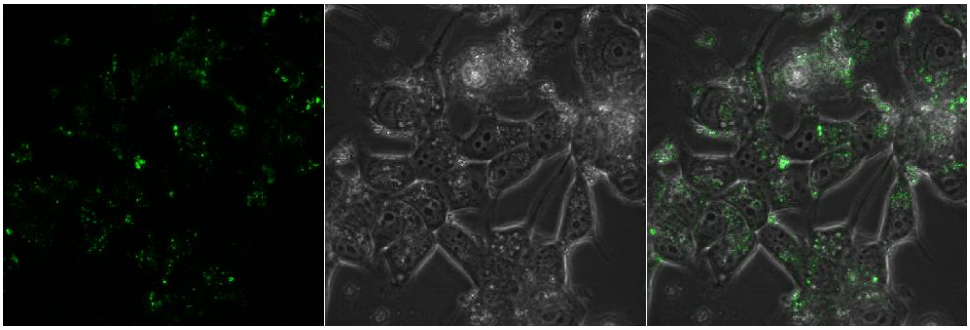

Figure 4-6: Confocal images of MCF7 cells transfected with O. The left panel is the Cy5 channel, the middle is phase contrast and on the right is the overlay. L•Q was first transfected into cells for 3 hours, then the medium was removed and cells were washed with PBS. Cells were then transfected with O for a) 1 hr, b) 3 hr and c) 5 hr. The scale bar is 20 µm.

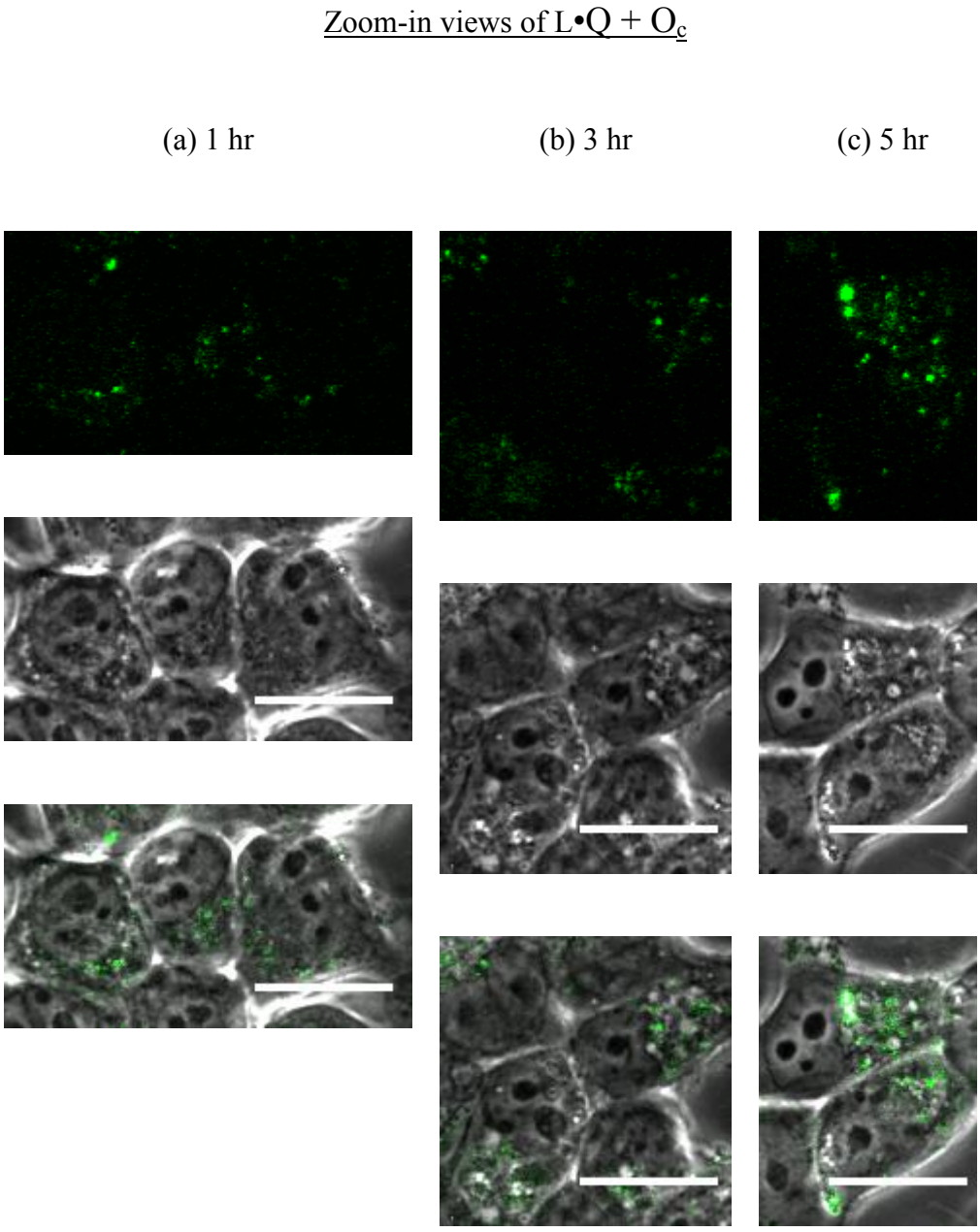


Figure 4-7: Zoom-in views of the confocal images in Figure 4-5 at a) 1 hr, b) 3 hr, c) 5hr incubation with the opening strand O from the previous figure. The top panel is the Cy5, the middle panel is phase contrast and bottom one is the overlay of the phase contrast and the Cy5 channel. The scale bar is 20 μm.

#### 4.3.5.1 Comparing Confocal and Cytometry data

In ImageJ,[102] regions of interest (ROI) were drawn around the cell boundaries in Figure 4-5 and the Cy5 intensities inside the ROIs at 1, 3, and 5 hours were measured. The mean intensities of the cellular Cy5 signal were 740, 920 and 950 respectively. The negative control (Figure 4-4a) had a mean intensity of 500 and that was treated as the background level of cellular fluorescence and hence the intensity at the beginning of the signalling strand incubation. Figure 4-8 shows the mean Cy5 intensities from the microscopy and the cytometry data. They both showed similar trends of gradual increases in the Cy5 signal with the incubation period. This supported the conclusion that hybridisation between L•Q and $O_c$ was possible within cells. In addition, the rate of fluorescence increase was higher at the beginning and then it slowed down. Furthermore, the background Cy5 level of the negative control from the microscopy was higher than that from the flow cytometry. This suggested that the latter was more reliable and convenient in measuring small changes at the beginning of the signalling strand incubation.

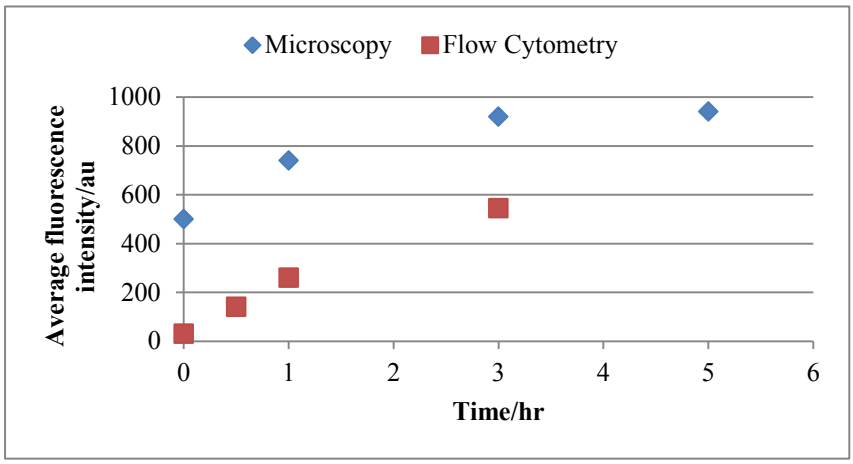


Figure 4-8: Average Cy5 fluorescence at different time points from microscopy and cytometry data. For both sets of data, L•Q was first transfected into cells for 3 hours, and then $O_c$ was transfected later and incubated for different length of time. Blue diamonds are measurement based on the data from Figure 4-5; Red rectangles are measurements based on the data from Figure 4-3a. They both showed a gradual increase in Cy5 signal inside cells as the signalling strand was incubated for a longer period.

### 4.3.6 Introducing the opening strand O labelled with Cy3

So far, I have shown that the simplified duplex L•Q systems can interact with the separately transfected opening strand and identified the locations of the hybridised products in relation to the nucleus. In order to obtain more information about the process, a Cy3 fluorophore is introduced at the 3' end of O so that the uptake of the signalling strand can be tracked and the subcellular location of the interaction between the signalling strand and L•Q can be determined. The new strand is called O_Cy3 and the product of the strand displacement is L•O_Cy3 (Figure 4-9). The Cy3 and Cy5 are at the opposite ends of the duplex, 22 base pairs apart. They are sufficiently distant that there is no significant FRET detected between the two fluorophores in the fluorimeter (Further discussion see Appendix C.5).


Figure 4-9: The schematic diagram of the duplex L•O_Cy3. Cy3 is introduced at the 3’ end of the opening strand. This new strand is called O_Cy3.

Figure 4-10 shows the confocal images of cells transfected with O_Cy3 in the second transfection at different time points (1hr, 3hr and 5 hr after the second transfection). All images had green and red blobs co-localised in the extracellular regions. These blobs were aggregations of the hybridised product L•O_Cy3. The introduction of Cy3 therefore resulted in a significant increase in aggregation of the Cy5 signal outside cells or at the cell peripheral, even at early time points. A major limitation of this observation was that this experimental design was only repeated once. In both times, there was extracellular aggregation of the hybridised product.

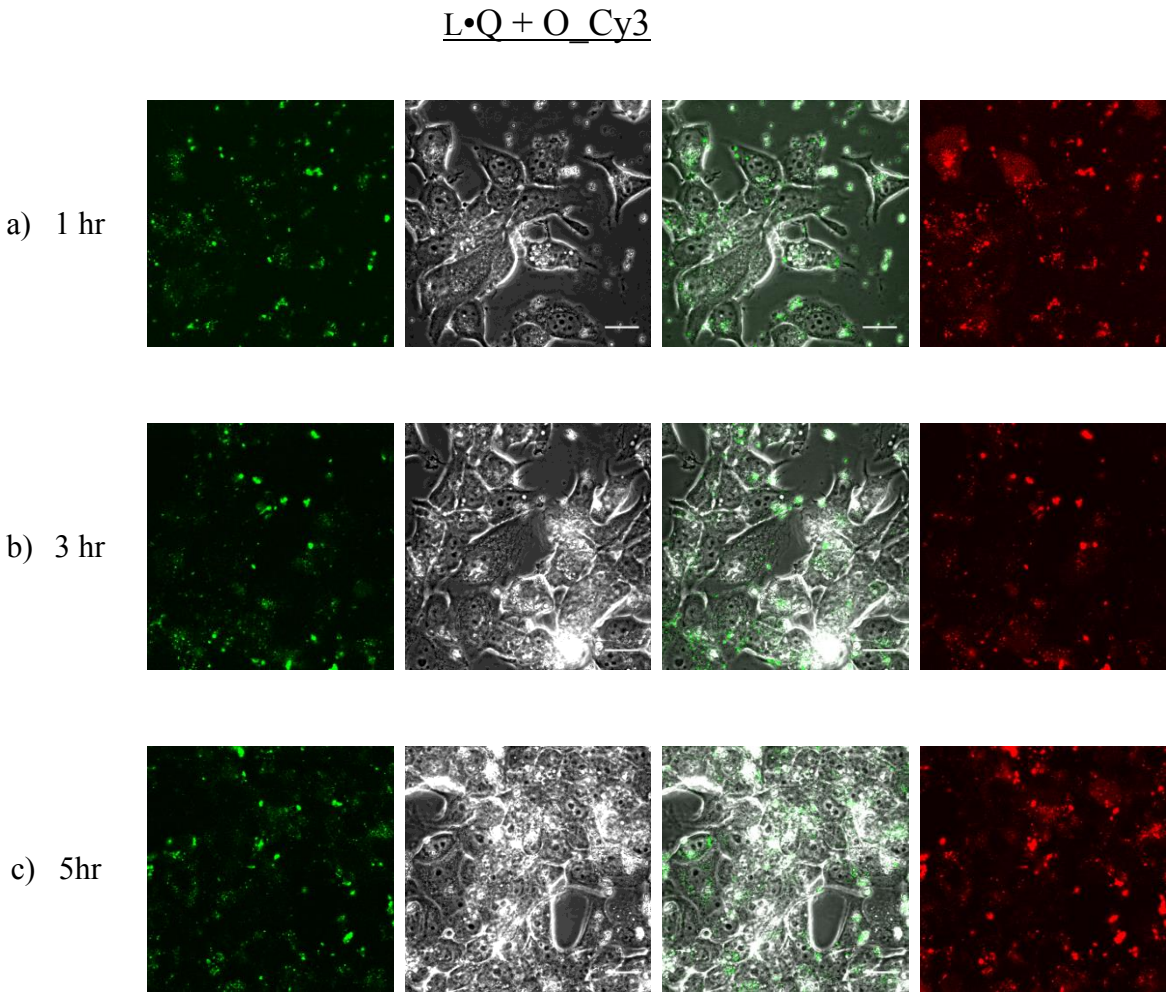


Figure 4-10: Transfect with O_Cy3. The left panel is the Cy5 channel (green), the middle is phase contrast (grey) and on the right is the overlay of the phase contrast and Cy5, on the far right is the Cy3 channel (red). L•Q was first transfected into cells for 3 hours, then the medium was removed and cells were washed with PBS. Cells were then transfected with O_Cy3 for a) 1 hr, b) 3 hr and c) 5 hr. The scale bar is 20 μm.

Cellular materials present in the media might have caused the observed aggregation. In Section 2.3.5, tetrahedra were shown to form aggregates with cell lysates, so aggregations had been observed between DNA nanostructures and cellular materials. In addition, there might be previously internalised L•Q in the extracellular environment. The possible sources of such L•Q could be dead cells releasing L•Q or excreted extracellular vesicles from recycling endosomes expelled L•Q into the extracellular area, and allowing the previously internalised L•Q to hybridise with extracellular O_Cy3.

Another possible explanation was that in the presence of an addition fluorophore, which is Cy3 in this case, accelerated the aggregation process. As a note of clarification, I am not suggesting that Cy3 is much more hydrophobic than Cy5. Before the introduction of Cy3 to the signalling strand, there was only one fluorophore - Cy5 in the system. Aggregation might be accelerated in the presence of an additional fluorophore, which is Cy3 in this case. If Cy5 is replaced by Cy3 on strand L, and the opening strand is O (with no fluorophore), aggregation is not expected to occur. On the other hand, if Cy3 and Cy5 are swapped, so that Cy3 is attached to strand L and Cy5 is attached to the signalling strand, I predict aggregation will still occur. The additional hydrophobicity[95] introduced by modifying the signalling strand with Cy3 perhaps altered the way that the signalling strand formed complexes with the XG. As a consequence, the presence of Cy3 accelerated its interaction with the remaining extracellular L•Q and formed aggregations. However, this is highly speculative and it is unlikely that an introduction of a fluorophore could cause such aggregation. Further experiments are necessary to investigate the cause of aggregation.

One way to determine the cause of aggregation would be to conduct this experiment in a perfusion chamber that allows imaging during the addition of the opening strand O_Cy3 in

the second round of transfection and then continue to image the sample throughout the next few hours. If O_Cy3 hybridised with L•Q that were remained in the media after the washing steps, then L•O_Cy3 would be present very soon after the addition of O_Cy3. However, if the source of L•Q were from previously internalised materials, aggregation would be expected to occur more gradually.

In addition, a control of O_Cy3 without transfection reagent could be introduced. O_Cy3 without transfection reagent would not enter cells efficiently, so that would significantly reduce hybridisation between Strand L and O_Cy3 inside cells. On the other hand, O_Cy3 without transfection reagent could still hybridise with Strand L in the extracellular environment. With this control in place, we could compare the signals in both cases and then infer how much co-localisation of Strand L and O_Cy3 took place inside cells.

Furthermore, one might reconsider the choice of fluorophores and quenchers. For example, Cy5 and Iowa Black RQ quencher on duplex L•Q could be replaced by a FRET pair, such as Alexa488 and Alexa546. The signalling strand could be labelled with Alexa750 instead of Cy3.These alternations would allow tracking for all components within the system throughout the experiment.

Figure 4-11 displays the images and overlays of the different channels of a zoom-in region from Figure 4-10a, in which O_Cy3 was transfected one hour before imaging (Figure 4-10a).

Figure 4-11b is the overlay of Cy3 (red), Cy5 (green) and the phase contrast (grey) images. Firstly, all the Cy5 signals were colocalised with the Cy3 signals. The blue and red arrows pointed to regions that Cy3 and Cy5 were co-localised. The co-localisation between Cy3 and Cy5 signal was expected because the Cy5 signal should be quenched when the duplex remained as L•Q. The quencher strand would be displaced in the presence of O_Cy3 and the Cy5 signal would become unquenched; therefore, this observation implied that Strand Q was only displaced from Strand L by the signalling strand O_Cy3. On the other hand, not all Cy3 signals colocalised with the Cy5 signal. This was because O_Cy3 was 4 times in excess to the duplex L•Q and it is fluorescent on its own. The white arrows in (b), (d) and (f) pointed to the same region that only the Cy3 signals were present, without the Cy5 signals.

The object highlighted by the red arrow was in the extracellular region. Features like this could potentially interfere with observations at later time points. Hybridisation might have happened outside cells, subsequently being taken up by the cells, giving an artefact of hybridisation inside cells. On the other hand, it is not certain that those extracellular colocalised objects originated from the inside or outside of cells. As discussed before, they could be duplexes secreted or expelled by the cells. However, since these colocalised objects were observed at the earliest time point 1 hr, it was likely that they had an extracellular origin rather than intracellular. This hypothesis could be tested with shorter time lag imaging experiments that track both L•Q and O_Cy3 to verify the location of interaction. Alternatively, a negative control of O_Cy3 without transfection reagent could be introduced. If a majority of interactions between L•Q and O_Cy3 occur inside cells, having a control of

O_Cy3 without transfection reagent should significantly reduce the co-location of Cy5 signal from Strand L and Cy3 signal form the signalling strand O_Cy3.

It was not clear whether the features highlighted by the blue arrows were inside cells, or on the cell membrane. In the phase contrast image of the same view (Figure 4-11c), those regions showed plasma membrane irregularities, so they could be aggregates at the peripherals of the cells. This aggregation phenomenon was severe when O_Cy3 was used, but not so the case in the previous experiments with O or $O_c$.

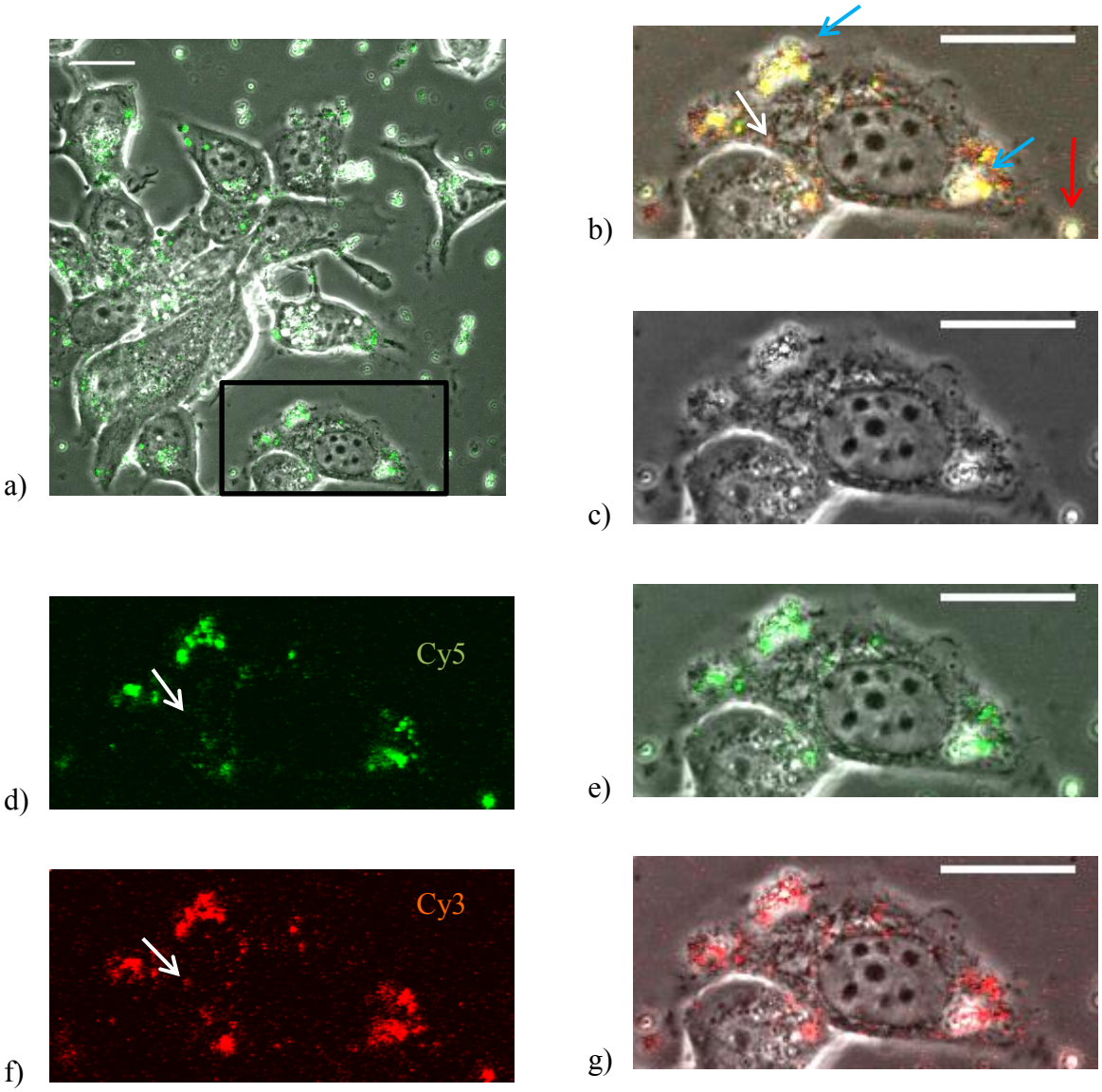


Figure 4-11: a) is the image of L•Q in incubation with O_Cy3 for 1 hr in Figure 4-8; (b)-(g) are the zoom-in views of the area inside the black box in (a). Green is the Cy5 channel and red is the Cy3 channel, b) the overlay of the phase contrast, Cy3 and Cy5, c) the phase contrast, d) the Cy5 channel, e) Cy5 with phase contrast, f) the Cy3 channel, g) Cy3 with phase contrast. Scar bars are all 20 μm. The blue and red arrows highlighted objects with both Cy3 and Cy5 signals. The white arrow highlighted a region with Cy3 signal, but without the Cy5 signal, indicating the presence of O_Cy3 on its own.

## 4.4 Discussion

In Sections 4.3.4 and 4.3.5, flow cytometry data and confocal images supported the conclusion that L•Q could interact with the signalling strand inside cells. The experimental design described in this chapter is comparable to the following two publications, Afonin et al.[47] and Hemphill et al.[46] They both showed that externally transfected nucleic acids can hybridise inside cells.

Afonin et al.[47] demonstrated that two DNA-RNA hybrids could interact inside cells when they were transfected with transfection reagent LF separately in two consecutive days. One of the products of the strand exchange reaction was an asymmetric Dicer substrate siRNA which led to a reduction in luciferase expression. In one of their systems, each hybrid was labelled with a fluorophore (Alexa-488 and Alexa-546), but no aggregation was reported. This might due to the choice of ~~fluorophores and~~ the transfection reagent used.

Hemphill et al.[46] delivered DNA logic gates into mammalian cells using transfection reagent XG, which was the same one used in this chapter. They showed that they could operate the logic gates with endogenous miRNAs and externally transfected synthetic photosensitive DNA strands. In contrast to Afonin et al. and the experiments described in this chapter, the externally transfected synthetic photosensitive DNA strands were co-transfected at the same time as the logic gates, instead of separately. However, the synthetic DNA strand would not interact with the logic gate until photochemical activation by UV irradiation. The read-out of the experiment was the fluorescence from the fluorophores attached to the DNA strands. Confocal microscopy images confirmed the behaviour of the logic gates inside cells. The

incubation period of the logic gate prior imaging was 4 hours, which was comparable to the period of the incubation described in this chapter.

In both of these publications, confocal imaging of fixed cells showed that the hybridisations of the transfected nucleic acids occurred in membrane-bound compartments, mainly in the cytoplasm. This was consistent with the live cell confocal images showed in Section 4.3.5. Additional flow cytometry data from this study also supported the conclusion that interaction occurred inside cells. Furthermore, the flow cytometry data provided clear evidence for interactions in the early time points.

In order to further understand the intracellular interaction, the Cy3-labelled signalling strand was introduced. One of the major drawback of the current experimental design was that neither L•Q nor the signalling strand were fluorescent before their interactions with each other. However, the modification of the signalling strand led to aggregations or revealed that a significant amount of L•Q remained outside the cells after the transfection and the multiple washing steps. A substantial amount of extracellular L•Q were subject to strand displacement by O_Cy3. This result poses questions on the conclusion made previously: hybridisation between L•Q and the signalling strand occur inside cells. If the current washing procedure was insufficient to remove L•Q in the experiment, then it is possible that there were also extracellular L•Q subjected to strand displacement by O or $O_c$ in the previous experiments, which could have led to an increase in the Cy5 signal outside cells. However, this was not observed in Section 4.3.5, either because it did not happen or because it was not as obvious without the aggregation, and hence was not reported.

At this stage, distinctions cannot be made between the intra- or extra- cellular interactions. In either case, it would show an increase in Cy5 fluorescence inside cells as the incubation period increases and this would give similar results in flow cytometry and confocal images.

The two-colour experiment also highlights the fundamental disadvantage of solely using fluorescence measurement in this experimental design. If the interaction between L•Q and the signalling strand could be coupled to a biological output, such as a knockdown of luciferase expression, then the result would be less prone to artefacts.

## 4.5 Further Experiments

More investigations are therefore needed for interesting conclusions to be made. I have the following suggestions:

1) Real time confocal imaging: One way to distinguish between intra and extra- cellular interactions is to track the Cy5 fluorescence for the same view of cells over a period of time. I would suggest first using the signalling strand without the fluorophore to avoid aggregations. If the hybridisation occurred outside cells, Cy5 signals would appear in the extracellular environment and then being internalised into the cells. On the other hand, if hybridisation took place inside cells, there would be no Cy5 signals outside cells and they would only appear inside cells. A microscope with drift-compensation function is very important to maintain the same view of cells for fair comparison.
2) Effective washing protocols: the aggregation of the hybridised product L•O_Cy3 demonstrates the need for a more effective washing protocol to remove the extracellular DNA nanostructures that remain after the transfection. Dextran sulphate[53] or acidic

glycine buffer[103] have been used to remove the extracellular nucleic acids in tissue culture, but they have not been used to remove DNA nanostructures that are in complex with transfection reagent. Therefore, their effectiveness in removing nucleic acids in this experimental design requires further examination. In addition, Dextran sulphate or acidic glycine buffer might affect the uptake in the second round of transfection with the signalling strands. In future experiments, it is necessary to evaluate the effectiveness and potential undesired effects of the suggested washing methods carefully.

3) Labelling cell organelles: It will be informative to know the locations of the DNA nanostructures inside cells, for example in cytosols, endosomes or lysosomes. This would give clues as to where the duplex interacts with the signalling strand. By using cells organelles marker, such as LysoTracker® which is a lysosomal marker, we will be able to use confocal microscopy to find out if the nanostructures co-localised with lysosomes, if the transfection affects the size of lysosomes, and to what extend the nanostructures could endosomal escape. Besides using chemical labels, in the long term, it would be better to create a stable cell line that expresses fluorescent protein with different endosomal markers, such as RAB-7, RAB-12 because chemical labels might non-specifically bind with the transfection complex due to their hydrophobicity. The chemical labels might also alter the hybridisation process. With the use of endogenous endosomal markers, it enables us to observe the process with the least disturbance.
4) Uptake pathway: are the DNA structures being taken up via endocytosis? One way to investigate this is to incubate the sample with the nanostructures at 4 ˚C because endocytosis is an energy dependent process, so there will be minimal uptake at 4 ˚C.[104]

All the mediums and solutions involved will also need to be at 4 ˚C to prevent any unwanted uptake.

5) Using lysosomal/endocytotic inhibitors to interfere with the uptake and trafficking pathways. It would be informative to see how the inhibitors affect the destinations of the DNA nanostructures and how the DNA duplexes interact with the signalling strands. For example, if the hybridisation occurs in the cytosol, the use of lysosomal inhibitors (such as chloroquine, bafilomycin A and methyl-β-cyclodextrin)[105,106] might promote endosomal escapes and more hybridisation would take place. If the hybridisation mainly occurs in lysosomes, chloroquine will impair fusion between endosomes and lysosomes, and this may delay or reduce hybridisation between duplex L•Q and the signalling strand. However, careful planning is required because all of these inhibitors affect multiple stages of the uptake pathways and are often cell line dependent.[105] Therefore, studies of these inhibitors with cells without transfections are essential and they should be conducted first, before moving on to studying their effects on the interactions between the DNA nanostructures. It is also possible to introduce different temperature blocks, which interfere with different stages of the endocytosis; for example, at 16 ˚C to 22 ˚C, the delivery of materials from endosomes to lysosomes is inhibited.[107]

## 4.6 Conclusion

Experiments where cells are first transfected with duplex L•Q and then subsequently transfected with a signalling strand reveal that strand displacement can take place within cells. Both flow cytometry and confocal microscopy show a gradual increase in the Cy5

signal upon transfection with a signalling strand, consistent with strand displacement. The increase is larger when the opening strand has been chemically modified to increase nuclease resistance. It is tempting to speculate that the DNA nanostructure and the signalling strand are initially localised to separate endosomes which fuse at the periphery of the nucleus and trigger the strand exchange reaction.

Two-colour experiments designed to simultaneously localise the DNA nanostructure and the opening strand were unsuccessful because of the aggregations observed outside cells. The experimental results posed questions on the conclusion that L•Q could interact with the separately transfected signalling strand within cells. Furthermore, a substantial amount of extracellular L•Q remained after the multiple washes and this demonstrates the need for a more effective washing protocol to remove the extracellular DNA nanostructures that remain after the transfection. This result poses questions on the conclusion made previously that hybridisation between L•Q and the signalling strand occur inside cells. Further investigation is necessary for conclusion to be made.

I have also made some suggestions for future experiments. Labelling cell organelles can provide information about the locations of duplex L•Q and the signalling strand. Changing incubation temperature and using chemical inhibitors can provide insight of the uptake pathway of the DNA nanostructures.

# Chapter 5 Opening of DNA tetrahedra with biological signals

## 5.1 Introduction

In the previous chapters, the focus was on using a synthetic oligonucleotide to trigger conformational changes. In this chapter, the focus will be shifted from the synthetic signal to cellular RNAs. I will explore how cellular RNA might be used to actuate DNA cages. This is one step towards the main goal of triggering the release of the cargoes from DNA nanostructures via some disease-related endogenous nucleic acids. Some examples will be given in the next section. Three cellular RNAs are discussed as the potential opening signals: mRNA, modified tRNA and the short single-stranded RNA.

The rationale behind using cellular RNAs is simple: Firstly, cells are full of ribonucleic acid materials in cytosol. They have a wide range of sizes, shapes and functions, ranging from protein-coding mRNA with thousands of nucleotides to non-coding small RNA of the order of 20 nucleotides in length. RNA can bind specifically to their DNA or RNA complementary sequences via Watson-Crick base pairing. In principle, the cytoplasm is full of potential signals to trigger conformational changes of the DNA nanostructures. According to the

internal genetic program in cells, RNA levels and their subcellular distributions are regulated. Therefore, the proportion of cages actuated will correspond to the states of the cells.

## 5.2 Messenger RNA (mRNA)

A large proportion of mRNA is present throughout the cytoplasm[108] and the expression level of mRNA is closely linked to the state of the cells. These properties make mRNA an excellent candidate for signalling because cages can be designed to become open only when there is an elevated level of disease-related mRNAs. For example, the level of mRNA for an antioxidant enzyme, manganese superoxide dismutase, increases in malignant cells because antioxidants can suppress tumour proliferation.[109] In some cases, there is a unique mRNA marker as a result of a mutation and that could be used as a signal to trigger opening. A specific gene translocation mutation in prostate cancer results in the production of a new fusion transcript and hence a unique RNA marker in LNCaP prostate cancer cell.[81]

Messenger RNAs have secondary structures and a large proportion of them are double-stranded. However, those double-stranded regions are not suitable targets to open DNA cages, because they are not likely to interact with the overhangs of the cages. Therefore, regions with weak secondary structures, such as hairpins and loops, were selected.

### 5.2.1 Renilla luciferase mRNA

In this section, Renilla luciferase mRNA is the target signal to trigger opening of the DNA cages. It is used as the model system because assays are available to quantify the level of cellular expressions.

Figure 5-1 shows the secondary structure of the mRNA, predicted by the Sfold web server.[110,111] It is a computational tool that is based on statistical sampling algorithms to predict mRNA secondary structures. The program also evaluates the accessibilities of various regions in the mRNA. The selection is based on the following criteria: low GC contents, average unpaired probability and the binding site disruption energy, which is the free energy cost for the target site to alter its local structure in order to bind with a complementary strand.

Since mRNAs exist as a population of structures,[112] some regions that are in hairpin configurations in one structure might have a different configuration in a different structure. Therefore, two regions were chosen as the potential targets for hybridisation, i.e. to open the DNA cages. The two regions were named by the positions of their starting nucleotide, so they were denoted 744 (red box) and 990 (black box).

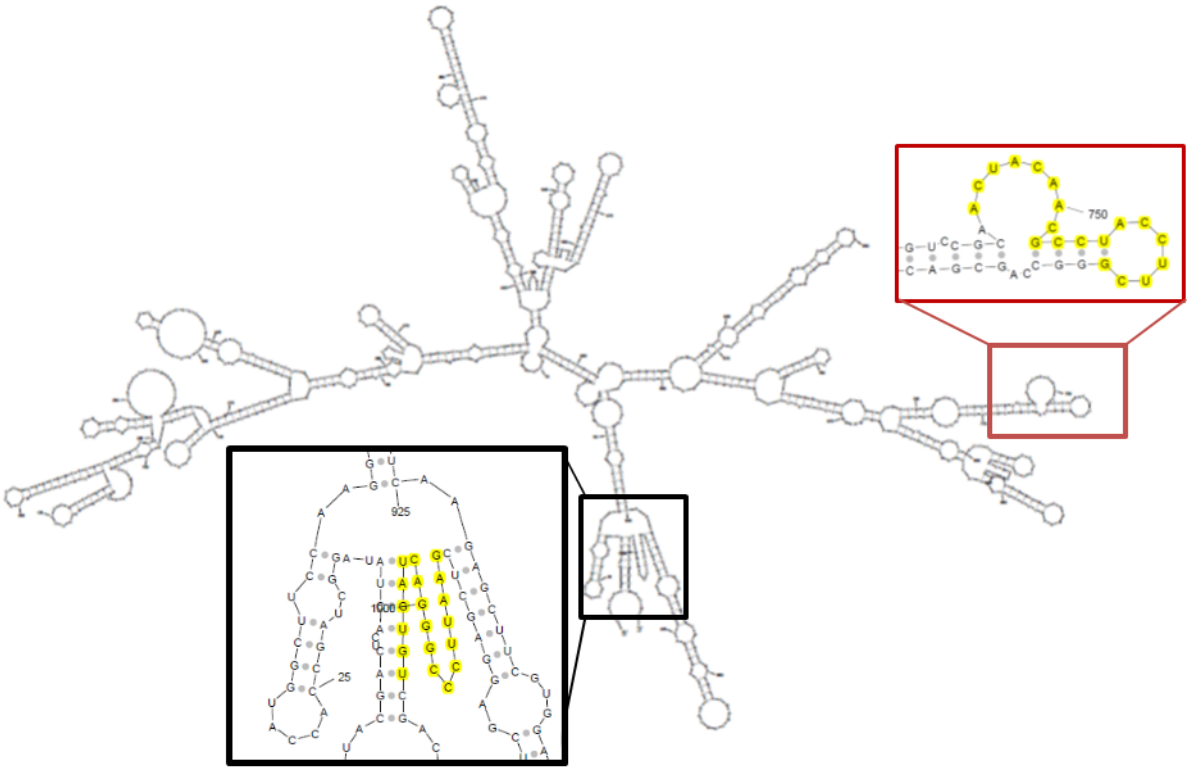


Figure 5-1: One of the predicted secondary structure of Renilla luciferase mRNA by Sfold.[16] The red and black boxes highlight and zoom in on the two selected regions to target opening of DNA cages. The two regions are named by the positions of their starting nucleotide, so they are denoted 744 (red box) and 990 (black box). The hybridisation targets are highlighted in yellow; these sequences are largely unhybridised in the predicted secondary structures.

#### 5.2.1.1 Synthesis of mRNA

The Renilla luciferase gene is embedded in a plasmid called psiCheck 2.2 (Appendix B.4.1). By transfecting the plasmid into mammalian cells, the luciferase mRNA can be transiently expressed. Therefore, it can be expressed inside cells. However, in this first stage of investigation, the luciferase mRNA was produced outside cells, by a T7 *in vitro* transcription kit, MEGAscript® kit (Appendix A.16). It is important to first establish whether the selected regions in the mRNA can interact with the DNA cages outside cells. Such environment is well-defined, so it reduces the number of factors that may affect the experimental outcome.

### 5.2.1.1 Design of the DNA cages

The design of the DNA cage is based on OT6.3 described in Section 2.3.3.2. It has a 6 nucleotides (nt) overhang and 13 base pairs (bp) in the reconfigurable edge to keep the cage closed. When the cage is closed, the Cy3:Cy5 ratio is low and when it is opened, Cy3:Cy5 ratio increases.

The sequences of the two tetrahedral component strands, S2 quencher and S4, were redesigned to form OT744 and OT990, so that part of the tetrahedron would be complementary to the corresponding selected region in the luciferase mRNA. The mRNA sequences for region 744 and region 990 are ACUACAACGCCUACCUUCG and GAAUUCCCGGGACUAGUGU respectively.

#### 5.2.1.1 mRNA hybridisation with a tetrahedral component strand

2 μM of mRNA was incubated with 400 nM of the component strand of the tetrahedron (S4_744 or S4_990) at 37 ˚C for 1 hour. An agarose gel shift experiment (Appendix A.7.2.1) was used to verify the accessibilities of the two target sites.

The tetrahedral component strand is 63 nt long and the luciferase mRNA has over 1000 nt. Therefore, in an agarose gel, the tetrahedral strand alone has a higher mobility than the luciferase mRNA and the former travels farther in the gel. If the mRNA is accessible to the tetrahedral component strand for hybridisation, this will decrease the mobility of the tetrahedral band significantly, but this is unlikely to have a detectable effect on the mRNA. As a result, the position of the tetrahedral band in the agarose gel will be shifted.

The result is shown in Figure 5-2. Lanes 1 and 2 are controls containing the mRNA and S4_744 respectively. Lane 3 contains the sample which the mRNA was incubated with S4_744. The band corresponding to the tetrahedral component strand was absent. S4_744 was therefore successfully bound by luciferase mRNA and the target region was accessible.

On the other hand, S4_990 was not displaced by the mRNA. Lane 4 is S4_990 and lane 5 is the sample which the mRNA was incubated with S4_990. The bands corresponding to S4_990 were present in both lanes, so S4_990 did not interact with the mRNA. The selected region on the mRNA was not accessible to S4_990.

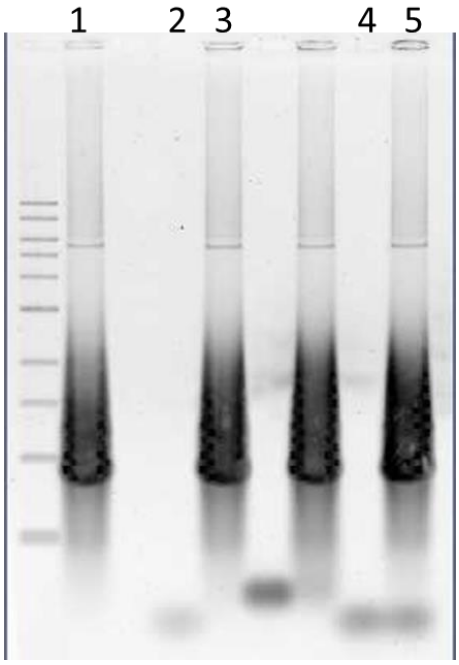


Figure 5-2: Interactions between tetrahedral component strand and Renilla luciferase mRNA. Native 1% agarose gel was used to examine the interactions between S4_744 or S4_990 with the mRNA. The samples were incubated at 37˚C for 1 hour before loading into the gel. If there are any interactions between the tetrahedral component strand and the mRNA, then the band for the tetrahedral strand will be displaced. Lane 1: Renilla luciferase mRNA only. Lane 2: S4_744. Lane 3: S4_744 + mRNA. Lane 4: S4_990. Lane 5: S4_990 + mRNA. On the left of lane 1 is the NEB 1 kb DNA ladder. There are two lanes between lanes 3 and 4 that are not relevant to the discussion here.

#### 5.2.1.2 Unsuccessful interaction between the luciferase mRNA and DNA tetrahedron OT744

Since only S4_744 was able to hybridise to the mRNA, but not S4_990, this meant that only region 744 in the mRNA was the accessible target. Therefore, only tetrahedron OT744 was synthesised (Appendix B.4.2) and used in the next stage.

30 nM of OT744 was incubated with 700 nM of luciferase mRNA at 37 ˚C in 180 μl of Buffer A. Opening of the DNA cages was measured by ensemble fluorescence measurement in the fluorimeter (Appendix A.6). If the cages were opened, there would have been an increase in Cy3:Cy5 ratio.

Figure 5-3 shows the Cy3:Cy5 ratios of three samples: tetrahedra mixed with luciferase mRNA (blue), tetrahedra (red) and opened tetrahedra (green). The tetrahedra were closed in the buffer condition, so the red trace was the negative control. The opened tetrahedra were formed by the addition of the complementary signalling strand in molar excess after the assembly of the tetrahedra, so the green trace was the positive control. It represents the maximum level of Cy3:Cy5 ratio.

For the sample that contained both the tetrahedra and the mRNA (blue), the Cy3:Cy5 ratio stayed at a similar level to the negative sample. This implied that there was very little opening of the DNA cages by the mRNA.

Even though that particular region of the mRNA was accessible to the single-stranded DNA (S4_744), it was not be able to open the DNA cage. The lack of opening observed was likely to be due to the steric interference between the cage and the mRNA. The DNA cage might

not be able to unwind around the mRNA. After the hybridisation with the overhang (6 nt) of the cage, the mRNA must undergo strand exchange around a tetrahedral edge for another 13 nt, which was over a turn in the DNA helix. The space inside the cage was compact compared to the massive mRNA and this could hinder the opening of the DNA cages. Therefore, there is a balance between a strong closing mechanism to keep the cage closed and how accessible it would be for the cage to be opened by biological signals.

With the experimental data shown thus far, this particular region of the luciferase mRNA is unlikely to open the DNA cages inside cells.

a)

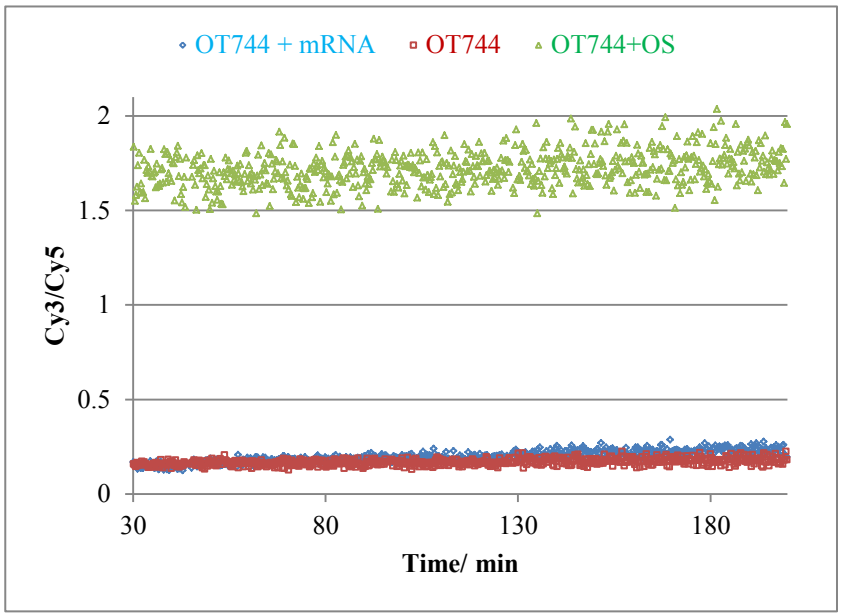


b)

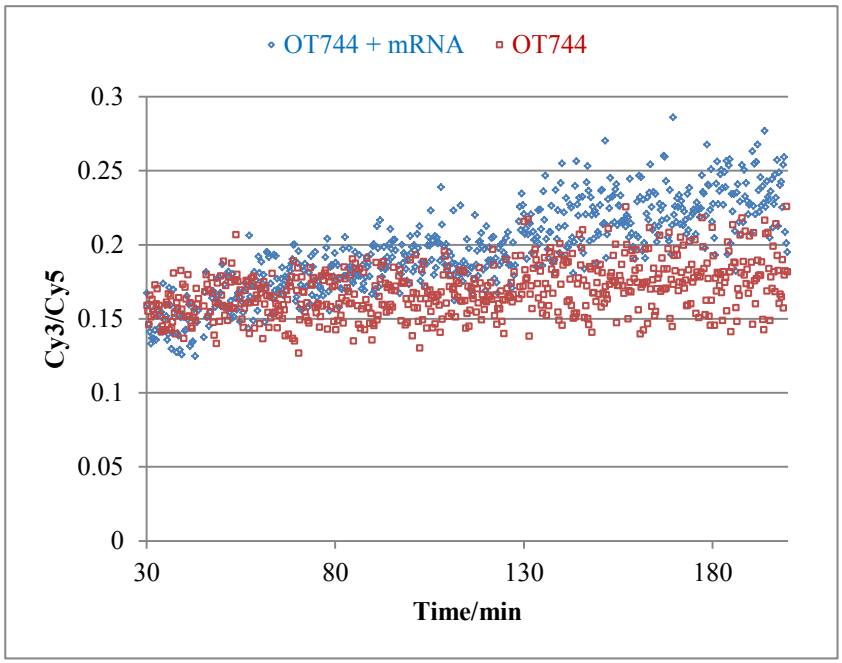


Figure 5-3: Fluorescence measurement of OT744. The cage was incubated with luciferase mRNA (blue), buffer (red) and the opening strand (green) at 37˚C. a) has a scale that is suitable for all three samples. A high Cy3/Cy5 ratio indicates the cage is open and a low Cy3/Cy5 ratio means the cage is closed. b) displays the same set of data, with an adjusted Cy3/Cy5 scale that highlights the changes in the sample incubated with mRNA. The ratio for the blue sample increases from 0.15 to 0.23. This is far below 1.7, which is the ratio for the fully opened sample. It was therefore concluded that there was very little opening of the DNA cages over the course of three hours and this target region is unlikely to open DNA cages inside cells.

### 5.2.2 Discussion and suggestions for future experiments

The selected region of the luciferase mRNA failed to trigger opening of the DNA cages. However, evidence shows that hybridisations between externally transfected DNAs and endogenous mRNAs inside cell are possible.[113–115] This is indeed the basis for mRNA imaging in live cells with fluorophore-labelled DNA hybridisation probes. There are various moieties, but the basic principle is to obtain fluorescence signals when the probes hybridise to a specific region of the target mRNAs. For example, the DNA molecular beacon[56,57,116] is a common category of probe and it is an oligonucleotide in a hairpin conformation with a fluorophore and a quencher at each end. They are next to each other in the stem part of the hairpin structure. The sequence of the loop is complementary to a target region of the mRNA. Upon hybridisation with the mRNA, the quencher is no longer next to the fluorophore and it will result in an increase in fluorescence. The transport and localisation of *oskar* mRNA was successfully imaged by the use of molecular beacons with a confocal fluorescence microscope in live cells.[56] Therefore, the idea of using mRNA to trigger opening of the externally transfected DNA cages inside cells should in principle be a feasible one.

Endogenous RNA should therefore be able to interact with the DNA cages, just as they do with the DNA probes. I therefore suggest that future experiments should start from systems that have been shown to work, namely publications that demonstrate successful live cell imaging data for mRNA.

Once the result is shown to be replicable with the same experimental design, it will then be appropriate to first test the system on a DNA duplex (similar to Chapter 4). This is because probes are often in the form of hairpin structures, with loops of over 20 nt in length and the

DNA cages described in this thesis have overhangs of 6 to 10 nt long. Therefore, it is important to optimise the overhang length. A duplex will be more suitable than a DNA tetrahedron because the former is cheaper and easier to synthesise. The duplex system will enable us to check for a few more parameters, such as hybridisation kinetics and transfection mechanisms in a more efficient manner. After the duplex system has confirmed hybridisation with the cellular target, it can then be tested on the DNA cages. If it were to fail at this stage, then it could be concluded that the actuation had been prevented by the steric hindrance imposed by the three-dimensional structure of the DNA cages. Cages could then be redesigned accordingly.

## 5.3 Transfer RNA

A tRNA is typically made of 65 – 90 ribonucleotides which fold into a conserved three-dimensional structure (Figure 5-4a) under physiological conditions. The anticodon loop (orange) within the tRNA is complementary to part of the mRNA. Being the link between the mRNA and the amino acid sequence, tRNA plays a vital role in protein synthesis.

As a consequence of their three-dimensional structures, tRNAs are stable to both nucleases attack and heat unfolding.[117] When overexpressed from a recombinant plasmid, it can accumulate inside cells without severe degradation, unlike other RNA materials. Typically, RNA is not as stable as DNA because RNA is more prone to hydrolysis than DNA due to its hydroxyl groups.

### 5.3.1 tRNA-RNA fusion

With the exceptional cellular stability of tRNA, tRNA can be used as a protective scaffold for other RNA strands. Additional sequences can be inserted into the anticodon region in the tRNA expression plasmid while maintaining the synthesis, the folding and the stability of the modified tRNAs inside cells. The product is called a tRNA-RNA fusion. Genetically engineered tRNA is an established protocol to produce specific RNA sequences in large scale.[117] This technique has been used to express a fluorophore-binding aptamer *in vivo* in *E. coli* and achieved live cell RNA imaging.[118] The feasibility of using recombinant tRNAs to open DNA cages will be discussed in this section.

#### 5.3.1.1 Construction of the plasmid

I first constructed a tRNA expression plasmid (ptRNA6cut2) that could be expressed inside an *E. coli* host via the T7 promoter. The plasmid ptRNA6cut2 was modified from psi-Check2.2 by standard cloning techniques (Appendix A.17).

The plasmid has a unique restriction site EagI in the anti-codon region of the tRNA scaffold. Therefore, additional sequence can be cloned into the plasmid via this restriction site to create the tRNA-RNA fusion plasmid. The sequence inserted into the tRNA scaffold was based on the signalling strand in Chapter 3 and 4 (Appendix B.4.4). Before creating the tRNA-RNA fusion plasmid, the sequence of the fusion product was first checked in the web server NUPACK[119] that the insert would not alter the tertiary structure of the tRNA scaffold.

Figure 5-4b shows the predicted structure of the fusion product. It has three stem loops and one stem, which is similar to the native form of tRNA (Figure 5-4a). This implies the inserted

sequence is unlikely to interfere with the tRNA structure. In addition, the inserted region remains as a loop without any secondary structures. This is desirable because the loop is the signalling region that is designed to hybridise with the overhang of the DNA tetrahedron and to induce cage opening.

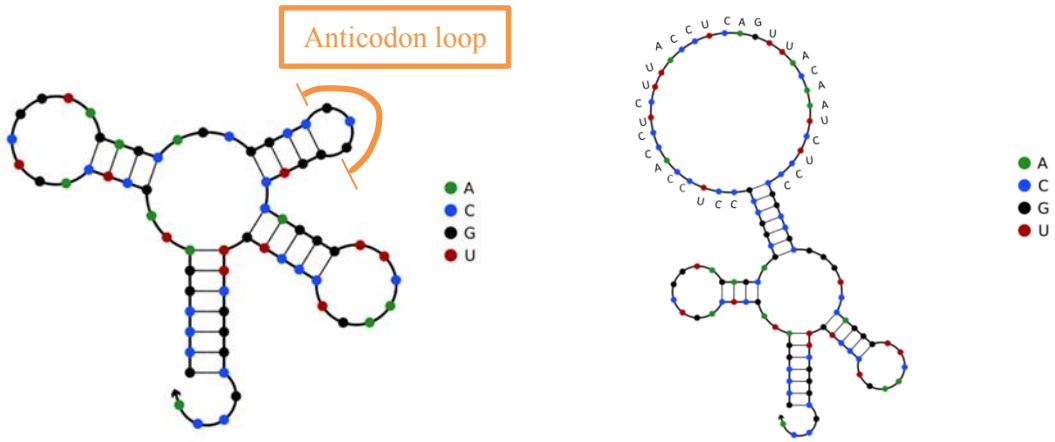


(a)

(b) Inserted sequence:
CCUCCACCUCUUACCUCAGUUACAAUCUCC

Figure 5-4: Secondary structures of tRNA predicted by Nupack.[119] a) is the unmodified tRNA, b) is the tRNA-RNA fusion. The inserted sequence is labelled. In a), the tRNA adopts a cloverleaf structure with the three stem-loops. The anticodon region is marked in orange and it has a sequence of GAG. The black arrow is the 5' end. The anticodon region in (a) is replaced with the inserted opening sequence. The structure of the tRNA is preserved after insertion of the opening sequence.

#### 5.3.1.2 Experimental outline

A T7 expression host, BL21 (DE3) *E. coli* was used to express the tRNA-RNA fusion product. The *E. coli* was transformed with the plasmid via heat shock and plated on an agar plate. It was incubated at 37 °C overnight. A colony was picked and grew in LB medium for another 18 hours at 37°C (Appendix A.20). RNA contents from the bacteria were extracted using the miRNeasy kit (Appendix A.12).

The RNA extract was examined with Agilent 2100 Bioanalyzer (Appendix A.21) to verify the synthesis of the tRNA-RNA fusion product in the bacteria.

#### 5.3.1.3 Results

Figure 5-5 shows the RNA extracts of the bacteria. Lane 1 is the single-stranded RNA (ssRNA) ladder and the lengths of each band are marked on the right. Lane 2 is the extract of bacteria transformed with tRNA-RNA fusion plasmid and lane 3 is the one transformed with the tRNA scaffold plasmid. The red arrow in lane 3 (just below the 80 nt marker) points to the expected position of the tRNA scaffold. The blue arrow in lane 2 (just above the 100 nt marker) shows the position for the tRNA-RNA fusion product, which agrees with the design.

In addition, there are some smeared bands around 20 nt that are only present in lane 2. They are likely to be the cleaved and degraded products from the inserted RNA sequence. Since the insert has no secondary structure, there might still be some degradation despite of the protection from the three-dimensional tRNA scaffold.

These results suggest that both the tRNA and the tRNA-RNA fusion plasmids were being expressed and the desired products were present in the extract.

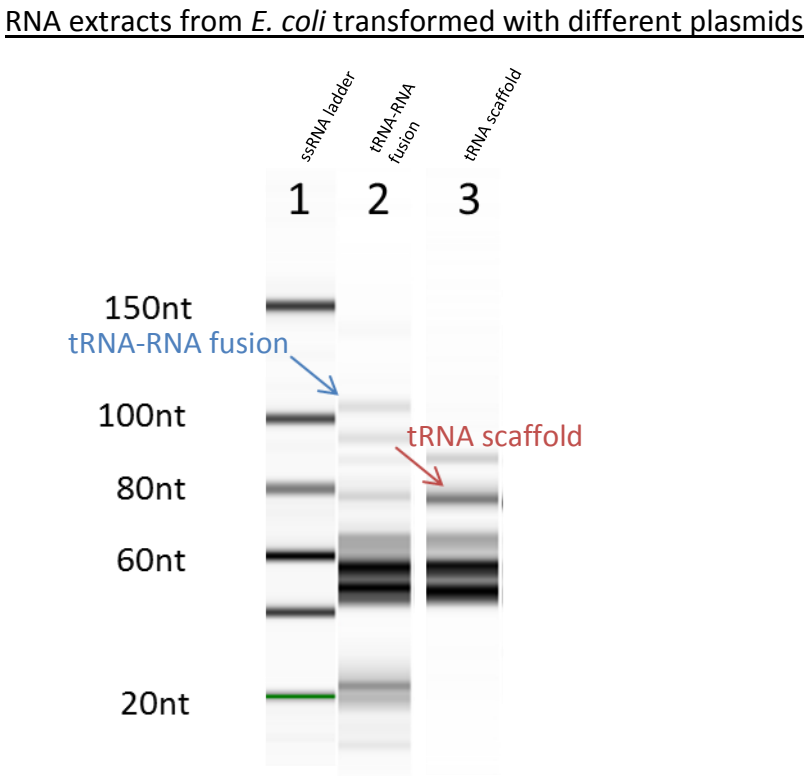


Figure 5-5: Data from Agilent 2100 Bioanalyzer. This is to examine whether the plasmid transformed was expressed inside *E. coli*. Lane 1: ssRNA ladder, with corresponding lengths marked on its left; lane 2: small RNA extraction from *E.coli* transformed with tRNA-RNA fusion plasmid; lane 3: small RNA extractions from *E.coli* transformed with the tRNA scaffold. The blue and red arrows indicates the expected lengths of the overexpressed recombinant tRNAs in the corresponding lanes. In lane 2, there are some smeary bands around 20 nt. They might be the degraded fragments from the loop of the tRNA-RNA fusion. Without any secondary structure within the insert, it is more prone to nuclease

### 5.3.2 Hybridisation with a tetrahedral component strand

To verify that the inserted sequence in the tRNA-RNA fusion product was indeed the intended one, hybridisation between the RNA extract and a shorter version of the tetrahedral component strand (FAM-SCO') was tested and examined in native PAGE. The component strand was labelled with a fluorophore (FAM) so that the position of the strand could be visualised by FAM rather than SYBR® Gold nucleic acid stain. Such staining was avoided because it would stain all the other nucleic acid materials in the cell extract. It would be unlikely to be able to distinguish the component strand from the cellular nucleic acid materials. Therefore, SYBR® Gold staining would not provide a clear analysis of whether the hybridisation had occurred.

10µl of RNA extract was mixed with FAM-SCO'(1 µM final concentration) and the sample was incubated at 37 ˚C for 2 hours. RNase inhibitor was added to reduce the extent of degradation because RNA is prone to nuclease degradation (Appendix A.22).

Figure 5-6 shows the results for the incubation in a native PAGE gel, which was scanned in the FAM channel. There was a band near the bottom of the gel in all the lanes corresponding to FAM-SCO' because it was in excess.

If there is any hybridisation between the RNA extract and the FAM-SCO', then some of the FAM-SCO' will be shifted to higher positions in the gel. In lane 2, FAM-SCO' was incubated with RNA extract containing the tRNA scaffold. It was the negative control and it had no extra bands, so there was no displacement of FAM-SCO' by any other cellular RNAs. In another words, there were no non-specific bindings between the FAM-SCO' and any other RNAs in the extract. In lane 1, FAM-SCO' was incubated with the extract containing the

tRNA-RNA fusion product and there were three displacement positions for FAM-SCO'. Since these displacements were absent in lane 2, this suggested that they were due to the inserted sequence in the tRNA-RNA fusion. The top one was the hybridisation with the intact tRNA-RNA fusion. The other two below were proposed to be the bindings between the fragments of the fusion construct and FAM-SCO'.

Experimental evidences so far support the possibility of utilising tRNA-RNA fusion as the cellular opening signal for the DNA cages. However, due to time constraints of the project, the opening of the tetrahedra by tRNA-RNA fusion products was not tested. For future experiments, further testing on the interactions between the tRNA-RNA fusion and the model duplex system described in Chapter 4 would be informative. After that, opening with the complete tetrahedron by the fusion product should be possible.

| | 1 | 2 | 3 |
|---|---|---|---|
| tRNA-RNA | + | - | - |
| tRNA scaffold | - | + | - |
| FAM-SCO' | + | + | + |

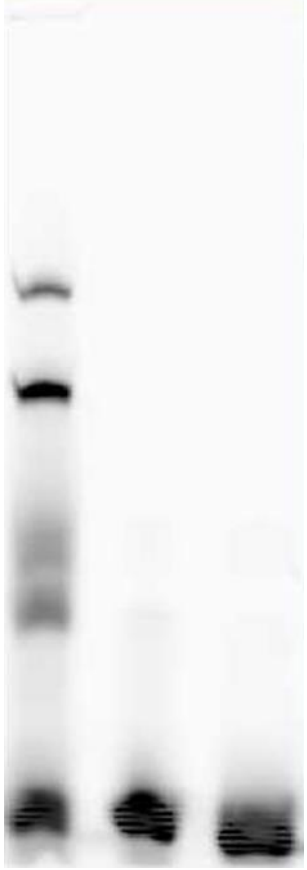

Figure 5-6: 29:1 10% native PAGE. It shows the position of FAM-SCO' after their incubations with various RNA extracts at 37˚C for 1 hour. Lane 1: RNA extract containing the tRNA-RNA fusion product + FAM-SCO'; lane 2: RNA extract containing the tRNA scaffold + FAM-SCO'; lane 3: water + FAM-SCO'. The result in lane 1 shows that FAM-SCO' can hybridise with the tRNA-RNA fusion product in the RNA extract. The gel was scanned in the FAM channel.

### 5.3.3 Discussion

This system is based on *E. coli* rather than mammalian cells. At this stage, only cell lysate was used, so the host of the cellular RNA was not the most important criterion. However, it

would be useful to investigate the applications of DNA nanostructures in *E. coli*. This could potentially be a simpler system for the targeted drug delivery system because *E. coli* has no nucleus and fewer membrane-bound structures. However, the method of delivery will be different from mammalian cells because *E.coli* has a cell wall. The DNA nanostructures cannot be transfected into *E. coli* by Lipofectamine® 2000. The delivery of DNAs, such as plasmids and duplexes, into *E. coli* are achieved via heat shock and electroporation.[120] These conditions might compromise the integrity of the DNA nanostructures. Nevertheless, it could be an interesting system to investigate, but it is beyond the scope of this project.

I speculate that tRNA is more likely to actuate the DNA cages than mRNA because tRNA has fewer bases and so it is smaller. In Section 5.2, the tetrahedral strand (S4_744) hybridised with the targeted region of mRNA, but the luciferase mRNA failed to open the cages. I contributed the main reason to be the steric hindrance imposed on the mRNA by the three-dimensional structure of the DNA cage. The luciferase mRNA is a massive molecule (over 1000 nt) relative to the space within the cage. The tRNA-RNA fusion is 103 nt long, and there are extra nucleotides in the loop to aid its flexibility. It should therefore have less steric hindrance and it should stand a better chance of opening the cage.

In the current design, the opening sequences are incorporated in bulky cellular RNA structures. Neither the mRNA nor tRNA is interacting with the overhang of the DNA tetrahedron via a free end. This might make the interaction between the tetrahedra and cellular RNAs difficult. Green et al.[121] studied the topological constraint imposed by the secondary structure of a hairpin on hybridisation between complementary structures. They reported that the opening of a hairpin loop by a free end adjacent to the neck of the hairpin is 10-100 times faster than via complementary bases located inside the loop. Therefore, the lack

of free ends adjacent to the opening sequence on the cellular targets might hinder hybridisation between the cage and the cellular RNA. One could investigate using the 5' untranslated region of the mRNA as a target because this would provide a free end for hybridisation and the 5' end is capped to prevent degradation by exonucleases.

Alternatively, another way to overcome these two challenges is to avoid direct interaction between the two. An intermediate structure can be introduced into the system. This is a concept based on the translator gate proposed by Seelig et al.,[122] in which the signal encoded in the input is converted to the output. The intermediate structure could be a duplex with a toehold that is complementary to the cellular target and displace the shorter strand in the duplex as an output. This released strand will then be the signal that triggers opening of the cage. However, the extra step of hybridisation may reduce the overall probability of cage opening because the output strand might not reach the cage, particularly in the compact cellular environment. Further investigations are required to assess whether the effects of reducing the steric hindrance outweigh the effects of introducing an extra step of hybridisation.

## 5.4 Single-stranded RNA

Most cellular RNAs have secondary structures (e.g. mRNA) or tertiary structures (e.g. ribosomal RNA) and they are bound by various enzymes in order to achieve their cellular functions. These factors might prevent the DNA cages from accessing the target regions. Therefore, the most ideal signalling candidate would be a short single-stranded RNA

(ssRNA). However, the challenge is how to express a high quantity of single-stranded RNA inside mammalian cells.

The ssRNA described here is most similar to an important class of cellular RNA called microRNA (miRNA). miRNAs are non-coding RNAs of 21-25 nucleotides long. Their main function is to down-regulate gene expression. They are partially complementary to a region of their target mRNA. Upon binding to their target mRNA in the form of an active RNA-induced silencing complex (RISC), this leads to either the cleavage of the mRNA or prevent further translation, and hence down-regulates protein expression.[123] MicroRNAs have been linked to a wide variety of diseases, such as cancer and heart disease.[124] For example, miR-21 has been reported to be up-regulated in breast cancer cells.[125]

According to the current model for the biogenesis of miRNA,[126,127] the miRNA gene is transcribed inside the nucleus and the resulting transcript is then processed and exported into the cytoplasm as a hairpin structure. The hairpin structure is then cleaved and it becomes a duplex. The duplex unwinds in the presence of specific enzymes in the RNAi pathway to form RISC, and only one strand will ultimately bind to the mRNA. Although mature miRNA is single-stranded, miRNA remains double-stranded throughout most of its biogenesis process.

Small RNAs, including microRNA, can be transiently expressed inside cells via the transfection of an expression vector.[128] In this section, I will investigate the possibility of expressing a high quantity of ssRNA inside mammalian cells. The vector system used here is called pU6-neo,[129] which is based on the U6 promoter[130] that can generate small RNAs in mammalian cells.

The general design principle of the insert for pU6-neo is shown in Figure 5-7a. The bold letters represent the compulsory bases of the insert and the series of Ns represents the desired sequence. The transcription starts with a G nucleotide and stops at the TTTT region. The insert sequence has two sections that are complementary to each other and they are separated by a region that is underlined. Because of that, the insert transcript will fold into a hairpin structure shown in Figure 5-7b. The underlined region forms the loop that links the two complementary regions of the transcript.

Herein, instead of expression of a hairpin structure, I examined the possibility of directly expressing short single-stranded RNA (ssRNA) via this vector system. The plasmid is called pU6-ssRNA.

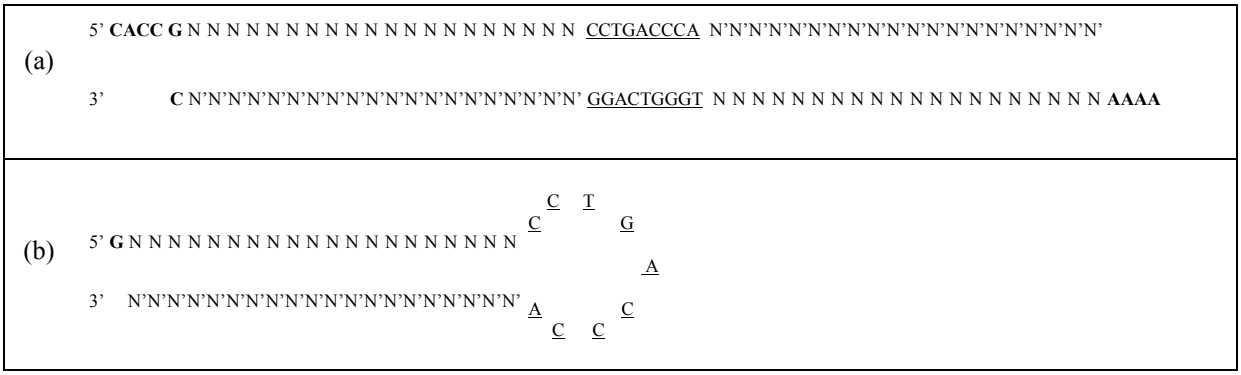


Figure 5-7: The insert design for the pU6-neo expression plasmid. (a) shows a general design of the DNA insert for the pU6-neo expression plasmid. Bold regions are compulsory to the expression system; the transcription starts with a G nucleotide and stops at the TTTT region. The region with a series of Ns is where the desired sequence is inserted. N and N' are complementary pairs. The underlined region represents the loop that will form in the transcript. (b) The hairpin structure of the transcript.

In pU6-ssRNA, the sequence cloned into the pU6-neo expression system was based on the signalling strand for OT744 discussed in Section 5.2. The sequence was incorporated into pU6-neo via the Bbsl restriction sites (Appendix A.23). The full construct was then purified from transformed *E. coli.* (Appendix A.19).

$7 \times 10^5$ cells were seeded in each well in the 6-well plate the night before the transfection. 4 µg of plasmid was transfected into mammalian cells with 10 µl Lipofectamine® 2000 and incubated overnight (Appendix A.15.1.3). The RNA extract was collected the following day (Appendix A.12) and examined in native PAGE to check whether the plasmid was expressed inside the transfected cells.

Firstly, I compared the RNA extract between untreated cells and cells transfected with an established expression system based on pU6-neo. The established system expresses small RNA against murine BACE 1, which is a protease that is important for Alzheimer's disease pathogenesis.[131] As a reminder to the reader, this construct folds into a hairpin shape when expressed.

This comparison would verify whether an extra band would be visible in native PAGE in the treated sample when the expression system was working. Figure 5-8a shows the RNA extracts of cells transfected with an established expression system based on pU6-neo (Lane 1) and untreated cells (Lane 2). 4 µl of RNA extract was loaded into each lane. An extra band was present in lane 1 (black arrow) which corresponded to the small RNA product from the expression system. Other bands present in both lanes were cellular RNA materials, such as mRNA and tRNA. This confirmed that when the pU6-neo expression system was working, the RNA extract should also have had an extra band. Although the small RNA against murine

BACE 1 was expressed strongly in this system, it was unlikely that it could be utilised to open the tetrahedron because it was in a hairpin conformation. The loop of the hairpin was only 9 nt, so it was not long enough to open the tetrahedron. The stem part was double stranded, so it would not interact with the tetrahedron either.

Then, I compared the RNA extracts between untreated cells and cells transfected with pU6-ssRNA. In Figure 5-8b, lane 1 was the RNA extract from the untreated cells and lane 2 was the extract from cells transfected with pU6-ssRNA plasmid. There was no extra band in lane 2, so the ssRNA was not expressed.

To further confirm that there was no ssRNA expressed, the same sample from lane 2 of Figure 5-8b - the extract from cells transfected with the ssRNA expression system, was incubated with OT744 to check if the extract would trigger any cage opening. 4 µl of RNA extract was mixed and incubated with 8 µl of gel purified OT744 at 37 ˚C for 3 hours. Figure 5-8c is a native PAGE gel which shows the results of the incubation. It was scanned in Alexa-488 channel, so if there were any opening in the sample, Alexa-488 signal would have been high and a strong band would have been visible. Lane 3 was OT744 with the RNA extract of cells transfected with the ssRNA expression system and this was the test case; lane 4 was the tetrahedra with the extract from untreated cells, which is the negative control; lane 5 was the pre-opened tetrahedra in Buffer A, which was the positive control and lane 6 was the closed tetrahedra in Buffer A, which was another negative control. There were no visible bands in all lanes, except lane 5 which contained the pre-opened tetrahedron. Since lanes 4 and 6 were the negative controls, no Alexa-488 signals were expected to be low. However, for lane 3, the lack of bands indicated no opening of OT744 was observed.

The preliminary experiments therefore showed that the attempt to overexpress short single-stranded RNA using this particular system was unsuccessful. Without the hairpin structure, the target construct was not detectable within the RNA extract. A possible explanation is that the loop within the hairpin structure of the transcript is essential for the post-processing of the product after the transcription and its export. Therefore, without the loop, the insert was not expressed.

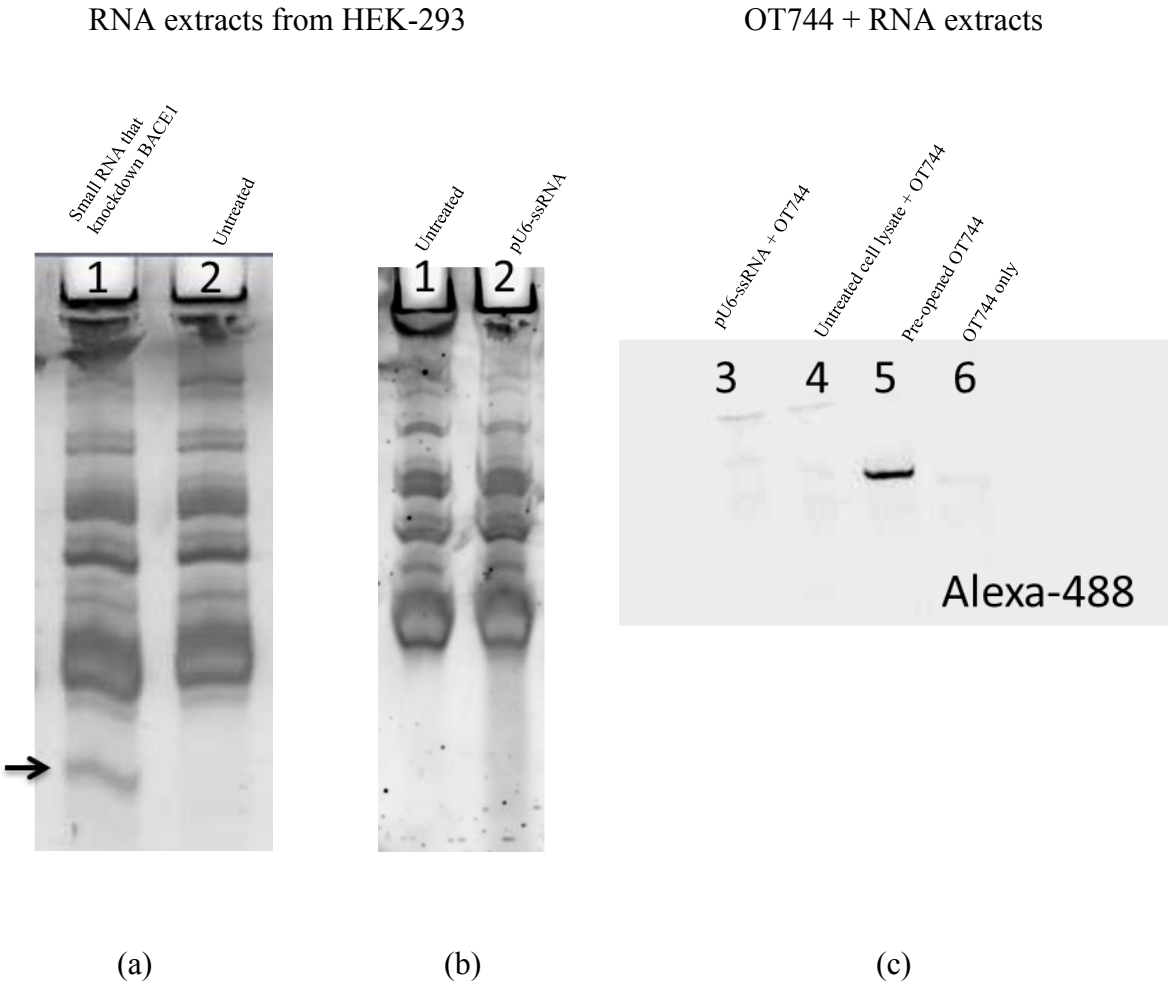


Figure 5-8: 29:1 10% native PAGE to verify the expression of pU6-ssRNA. (a) and (b) compare the RNA extracts of cells with different tratement. (a) Lane 1: cell lysate from HEK-293 expressing small RNA that knockdown BACE1; Lane 2: HEK-293 cell lysate. (b) Lane 1: HEK-293 cells lysate; lane 2: cell lysate from HEK-293 transfected with pU6-ssRNA. Both (a) and (b) were stained with SYBR® Gold. In (c), the gel is used to examine the extent of tetrahedron opening when OT744 was incubated at 37 °C with the RNA extracts. The gel was scanned in the Alexa-488 channel. OT744 was incubated with RNA extract from HEK-293 transfected with pU6-ssRNA (lane 3), RNA extract from untreated HEK-293 (lane 4). Lane 5 contains the pre-opened tetrahedron and lane 6 contains OT744 (closed), both in the tetrahedral assembly buffer, Buffer A. A strong Alexa-488 signal indicates the opening of the tetrahedron. Hence there is no opening in lane 3. These experimental results suggest that the expression of pU6-ssRNA was unsuccessful.

## 5.5 Conclusion

The feasibility of three cellular ribonucleic acids as the signalling molecules to trigger actuation of DNA cages was tested: mRNA, tRNA-RNA fusion and ssRNA.

The first candidate was Renilla luciferase mRNA. Within the mRNA, two regions were chosen to be the hybridisation targets. One out of the two regions successfully hybridised with the tetrahedral component strand. However, the DNA cage failed to be opened by the mRNA and I contributed that to be caused by the steric interference between the three-dimensional rigid DNA tetrahedron on the bulky mRNA. In order to overcome this challenge, a translator gate can be introduced into the system in future experiments. The translator gate would interact with the cellular RNA, producing an output that triggers the opening of the DNA tetrahedron.

The second candidate was the tRNA-RNA fusion product. Both the tRNA scaffold and the tRNA-RNA fusion were recombinantly expressed in *E .coli*. The tRNA-RNA fusion in the cell lysate was able to hybridise with a shorter version of the tetrahedral component strand. This opens up the possibilities to use a new class of RNA to interact with DNA nanostructures.

Finally, the possibility of expressing short single-stranded RNA (ssRNA) via the transfection of a small RNA expression plasmid was also investigated. The motivation behind was that the short ssRNA would experience the least steric hindrance when compared to mRNAs and

tRNAs, hence a good signalling candidate. The expression of such RNA failed. By altering the transcript from a hairpin structure to a single-stranded product severely alter the processing of the nuclear RNA. No ssRNA was detected in the RNA extract from cells.

# Chapter 6 Potential Biological Applications

## 6.1 Introduction

The majority of the research described so far has been focused the actuation of the DNA tetrahedra, but in this chapter, the focus will be shifted to the potential biological applications of DNA nanostructures. This chapter explores ways to utilise DNA cages as carriers for splice-correcting oligonucleotides to modulate gene expression and as chemical reactors to regulate the level of activity of the encapsulated proteins. In addition, other than the typical 20 base pairs (bp) edge tetrahedron, I will also discuss the synthesis of different wire-framed DNA nanostructures: the triangular prism and the small tetrahedron.

## 6.2 Antisense RNA carriers

Therapeutic oligonucleotides interfere with RNA processing inside cells and in turn regulate their gene expression.[132] Hence this is a promising class of therapeutic agent for genetic disorders such as muscular dystrophies.[133] DNA nanostructures could be effective carriers for these therapeutic oligonucleotides because they can be loaded onto the nanostructures via complementary base pairing.

In this section, I will discuss using DNA tetrahedra and triangular prisms as carriers for a particular class of therapeutic oligonucleotides. However, before I present the experimental data, I will first describe the biological mechanism involved and briefly explain how the therapeutic oligonucleotide works.

### 6.2.1 Splicing

In the cell nucleus, a DNA template is transcribed and the product is called the pre-mRNA. It must be processed before becoming a mature mRNA that encodes the sequence of a functional protein. One of the processing steps is called splicing, which removes parts of the pre-mRNA. A mutation in the pre-mRNA can lead to incorrect splicing, and an incorrect mature mRNA. This results in the synthesis of a non-functional protein.

#### 6.2.1.1 Splice-correcting oligonucleotides

Antisense is a synthetic and therapeutic RNA that is complementary to part of an mRNA. In this chapter, a particular type of antisense: splice-correcting oligonucleotide is investigated. The splice-correcting oligonucleotide binds to part of the pre-mRNA that are involved in pre-mRNA splicing and re-directs splicing to give an alternative form of mRNA.[134] In order to protect the oligonucleotide against nuclease degradation, the oligonucleotide has 2'-O-methyl modified bases with phosphorothioate backbone to increase its stability.

### 6.2.2 Model cell line

In this section, experiments were conducted in a model HeLa pLuc705 cell line.[98] It has an engineered mutation in the luciferase coding sequence so that functional luciferase is only expressed when a specific splice-correcting oligonucleotide (SCO) is successfully delivered to the nucleus and re-direct the splicing. This is a well-established model system with a sensitive positive-readout for gene delivery and low background noise. It has been used to evaluate the delivery efficiency of cell-penetrating peptides[97,135] and receptor ligands.[136]

### 6.2.3 Tetrahedra ($TET_{SCO}$)

The DNA tetrahedron is redesigned so that it carries one antisense (SCO - the red strand in Figure 6-1). The SCO used here is based on the original antisense reported by Kang et al,[98] but it has 13 extra nucleotides (nt) at the 5' end so that it can be attached to the tetrahedron via hybridisation. The extra nucleotides retain the splice-correcting property of the oligonucleotide (verified in Appendix C.6).

Successful delivery of DNA cages carrying the SCO should restore the luciferase production inside HeLa pLuc705 cells (HeLa705). Only a small quantity of SCO is required to induce a significant increase of luciferase expression. Since Walsh et al.[2] demonstrated successful uptake of tetrahedron into cells without the aid of transfection reagent, the naked $TET_{SCO}$ was tested here. It was reasonable to speculate that this sensitive reporter system might be able to detect the uptake of $TET_{SCO}$ into HeLa705 without a transfection reagent.

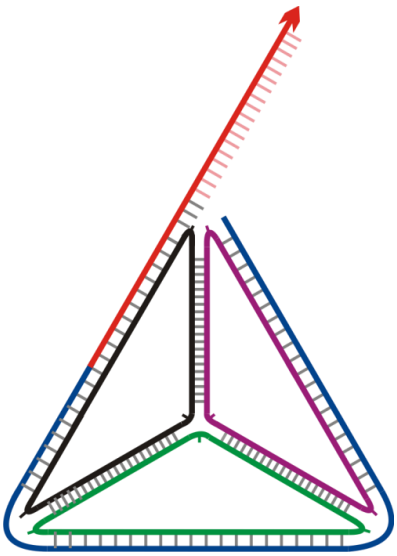

Figure 6-1: Schematic diagram of the tetrahedron carrying an SCO ($TET_{SCO}$). The sequences of the component strands are found in Appendix B.5.1.

### 6.2.3.1 Experimental Outline

The DNA nanostructures (TET or $TET_{SCO}$) were assembled at 2.5 µM concentration (Appendix A.2), ligated with T4 ligase (Appendix A.3) and purified from polyacrylamide gel (Appendix A.4) before their incubations with HeLa705. TET was a fully ligated tetrahedron, without the overhang. It acted as the negative control in this experiment because it did not contain the SCO sequence that induced splicing.

8 x $10^4$ HeLa705 cells were seeded in a 96-well plate the night before the experiment (Appendix A.9). Then, the samples were treated with 10 pmol of the tetrahedra with SCO ($TET_{SCO}$) for 24 hours (Appendix A.15.1.4). The two negative controls were the tetrahedra without SCO (TET) and solutions soaked with polyacrylamide gel. After the incubation, the luciferase expression in each sample was measured by the Promega

Luciferase Assay (Appendix A.24). The level of luciferase expression was normalised to the endogenous protein level by the Bradford Assay (Appendix A.25). The fold-increase in luciferase expression was compared between the treated and the untreated cells. Fold-increase of 1 meant that the treatment did not increase the luciferase expression in the treated cells.

#### 6.2.3.2 Results

Table 6-2 shows the results of the treatment without any transfection reagent (naked). $TET_{SCO}$ alone (bottom row) induced over 30-fold increase in luciferase expression. This seemed to suggest that TET alone was effective in delivering the SCO. However, the other two negative controls, gel and TET also produced an increase of luciferase expression when compared to the untreated cells. Since there was no SCO in those controls, the luciferase expression could not be related to splicing. Therefore, this must be an artefact, which might be related to some contaminations from gel purifications.

It is known that there is acrylamide contamination after gel purification: this is the reason why the concentrations of DNA gel purified products cannot be readily determined by their absorbance at 260 nm. The purified solution must pass through a spin column to exchange buffer in order to remove the contaminants; only then will the absorbance be accurate for its concentration measurement.

Similarly in the case of splicing, without buffer exchange, there was contamination from the gel purified solution which interfered with the experiment.

| | Fold-increase (naked, no buffer exchange) |
|---|---|
| TET | 11 |
| Gel | 33 |
| $TET_{SCO}$ | 35 |

Table 6-1: Luciferase fold-increases of HeLa705 cells. Cells were incubated with closed tetrahetra (TET), solution soaked in polyacrylamide gel (Gel) and the tetrahedra with antisense ($TET_{SCO}$) at 37˚C for 24 hr. All the tetrahedral structures were gel purified.

The experiment was repeated with gel purified samples that were passed through the spin columns for buffer exchange (Appendix A.26). There were two categories of treatment: with and without transfection reagent LF. The results are displayed in Table 6-2. The tetrahedron (TET) and the gel sample did not induce any luciferase expression in either category of treatment. This suggests the buffer exchange procedure significantly reduced the non-specific luciferase expression. Only when LF was used as a transfection reagent did $TET_{SCO}$ induce a 9-fold increase, but $TET_{SCO}$ alone did not.

In summary, $TET_{SCO}$ was not able to deliver the SCO without the aid of a transfection reagent. Either the DNA tetrahedra remained completely trapped in endosomes or there was insufficient uptake of the DNA nanostructures. Juul et al.[38] also reported the lack of DNA cages uptake in Sf9 insect cells without a transfection reagent. The discrepancy might be due to the use of different cell lines because Walsh et al.[2] used HEK-293 in the study. In addition, they also suggested that the nanostructures were trapped in

endosomes and little was escaped into the cytoplasm. If this was the case, then the SCO would not have been able to reach its target in the nucleus.

In addition, because this particular luciferase assay was cell-line specific, it would not be possible to explore how the effect varied between cell lines or to choose a more desirable cell line.

| | Fold-increase in luciferase expression | |
|---|---|---|
| | buffer exchange | |
| | Naked | LF |
| TET | 1 | 1 |
| Gel | 1 | 1 |
| $TET_{SCO}$ | 1 | 9 |

Table 6-2: Luciferase fold-increases of HeLa705 cells treated with sample that underwent buffer exchange before the incubations. One set of samples were transfected into the cells with the aid of the transfection reagenet LF and the other set without (naked). Cells were treated with closed tetrahetra (TET), solution soaked in polyacrylamide gel (Gel) and the tetrahedra with antisense ($TET_{SCO}$) at 37˚C for 24 hr.

### 6.2.4 Triangular Prisms (TP)

Fakhoury et al.[48] reported that DNA cages could maintain the effect of the antisense more effectively than the antisense alone. The system used in this publication was based on a triangular prism, which has six single-stranded DNA regions, 20 nt in length, that serve as loading sites for the phosphorothioated antisense oligonucleotide. Figure 6-2 shows a schemiatic diagram of a triangular prism (TP) loaded with six antisense strands (red). Their system was similar to the one discussed above and they also used a

transfection agent in their study. This is consistent with the result in the previous section that naked DNA nanostructures cannot effectively deliver antisense into cells.

However, differences include: firstly, the two nanostructures have different shapes, but both TET and TP are wire-framed nanostructures; secondly, a different antisense was used with a different sequence and modifications (SCO has additional 2' O-methyl modifications); thirdly, a triangular prism can carry six strands of antisense, while $TET_{SCO}$ can only carry one; fourthly, the reporter system relies on knockdown of luciferase expression rather than its induction.

Since the two systems are comparable, but with some differences, I decided to modify the TP system to carry the SCO, in order to examine whether any enhancement effect on luciferase induction would be observed. (Refer to Appendix B.5.3 for the sequences of the TP component strands.)

In the following two sections, I will first compare the formation yields of TET and TP (Section 6.2.4.1) and then investigate the performance of triangular prism as the antisense carrier (Section 6.2.4.2).

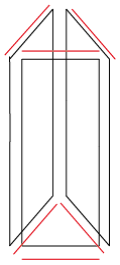

Figure 6-2: schematic diagram of TP_SCO, a triangular prisms (black) with six SCO strands (red).

### 6.2.4.1 Formation advantage of triangular prisms over tetrahedra

Formation of the triangular prisms (TP) was first reported by the Sleiman group.[89] Similar to the standard tetrahedron, each edge has 20 bases. However, it has six single-stranded edges and three double-stranded edges. At each vertex, each strand has four unbound thymines to relieve the strain. It has three component strands and each is 96 nt long. The synthesis process is similar to the DNA tetrahedra: equimolar component strands are mixed and annealed in Buffer A (Appendix A.2).

I examined the assembly yield for TET and TP under a range of component strands concentrations in native PAGE. Figure 6-3a shows the yield of the TP, with the component strands concentration ranging from 1 μM (lane 1) to 10 μM (lane 6). Even at 10 μM, the only strong band in the lane is the triangular prism. There is a smear band above the triangular prism band for formation concentration higher than 4μM, which might correspond to a dimer of the TP.

In contrast, the closed tetrahedron TET (Figure 6-3b), gives a dimer when assembled at 2 μM (lane 1) and a significant amount of DNA material accumulates in the well. In Lane 2, TP gives a strong monomer band when assembled in the same concentration.

Therefore, TP maintains a high yield over a wider range of concentrations, even at micromolar concentration. Being able to assemble with high yield at a high concentration is a useful property because this implies that gel purification might not be necessary. The gel purification step required for tetrahedron introduces acrylamide contamination (as discussed in Section 6.2.3) and further reduces the amount that can be synthesized. For TP, no further purification step is needed. In addition, the single-

stranded regions in the TP make it a versatile carrier because antisense (or other functional strands) can easily be added to the TP mix and the nanostructures will be antisense carriers. Overall, TP is a more suitable structure to be utilised as an SCO carrier.

However, the triangular prism is more prone to nuclease degradation than the DNA tetrahedron because of the single-stranded regions within the triangular prism. The former has a half-life of 2 hours [42] and the latter one is over 4 hours.[82] In the case of antisense delivery, structural integrity of the DNA nanostructure is not of utmost importance. Contrarily, for a targeted drug delivery system, structural integrity will become a more pressing consideration. Therefore, triangular prism may not be a better scaffold in other applications.

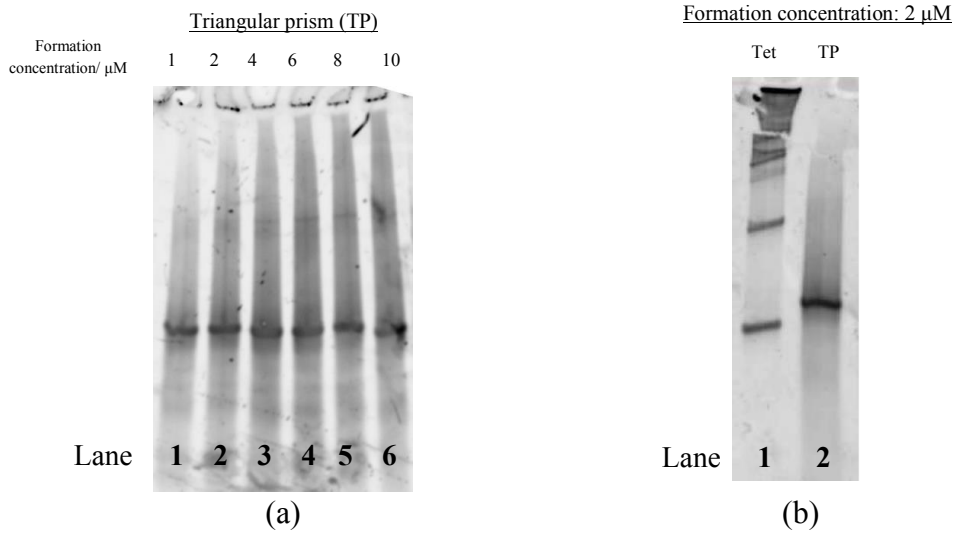


Figure 6-3: Native 29:1 6% PAGE to compare the formation of the triangular prism and the tetrahedron. Both gels have 15mM $MgCl_2$ and 2 pg of DNA was loaded into each lane. (a) To verify the formation of the triangular prisms at various formation concentrations. Lane 1: 1 μM. Lane 2: 2 μM. Lane 3: 4 μM. Lane 4: 6 μM. Lane 5: 8 μM. Lane 6: 10 μM. (b) To compare the yields between the tetrahedra and the triangular prisms. Lane 1: Tetrahedra formed at 2 μM. Lane 2: Triangular prisms formed at 2 μM.

### 6.2.4.2 Multiple splice-correcting oligonucleotide carriers

Fakhoury et al.[48] reported that the gene silencing was enhanced with the DNA scaffold when compared to a single-stranded antisense, in terms of the percentage of knockdown of luciferase and the duration of such effect. In their study, for the same amount of antisense strands, antisense loaded onto the DNA scaffold induced twice as much knockdown as the antisense strand alone. HeLa705 is a positive-readout system and the low background signal is low, so it should be more sensitive than the knockdown system in the original TP system.

In this section, the TP was modified to deliver the SCO (from Section 6.2.3) to induce luciferase expression in HeLa705 cells. The new nanostructure is called TP_SCO. The SCO was incubated with the pre-assembled TP_SCO overnight at room temperature and the antisense strands would hybridise to the single-stranded regions of the DNA nanostructures.

15 pmol of SCO or SCO hybridised with TP (TP_SCO) were incubated with HeLa705 for 24 hours in Opti-MEM® (Appendix A.15.1.4). The total amounts of SCO were the same in both samples. Figure 6-4a showed that TP_SCO transfected without the aid of LF, which is labelled as TP_SCO_N, did not induce any luciferase expression, which was consistent with the result of $TET_{SCO}$. When LF was used as a transfection reagent, both SCO and TP_SCO induced luciferase expression, but there was no enhancement effect by the DNA scaffold.

Next, the effects of the DNA scaffolds at 24 and 48 hours incubation were also examined. According to the experimental result shown in Figure 6-4b, the splicing

effect of SCO in HeLa705 cells was not enhanced by the use of the DNA triangular prism at either time points. After 24 hours of incubation, both TP_SCO and SCO had similar effect on the luciferase expression. However, after 48 hours, SCO alone induced more luciferase expression than TP_SCO.

(a)

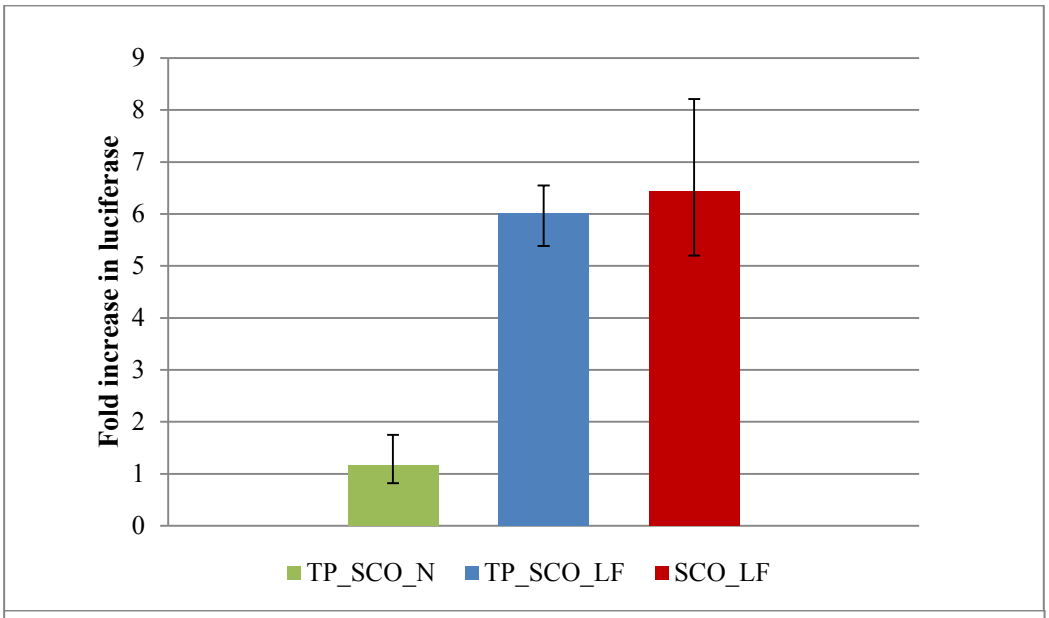


(b)

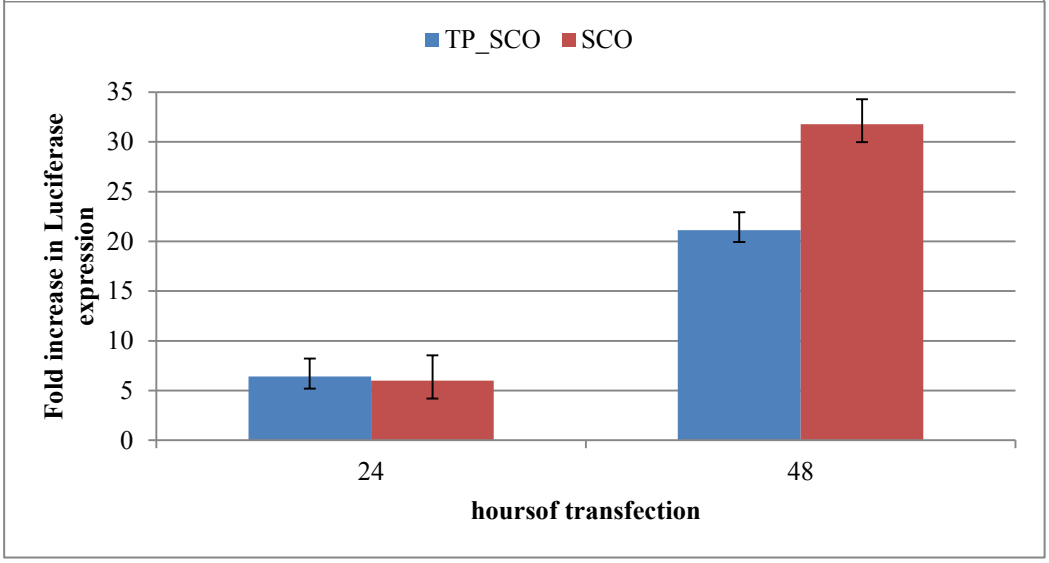


Figure 6-4: Splice-correction activity in terms of expression of luciferase fold increase in HeLa705 under different treatments. (a) Cells were incubated with TP_ SCO without LF (TP_SCO_N), TP_SCO with LF (TP_SCO_LF) and SCO alone with LF (SCO_LF) for 24 hr in Opti-MEM®. (b)TP_SCO and SCO were transfected with LF in Opti-MEM® and they were incubated for 24 hr and 48 hr.

### 6.2.5 Discussion

In summary, in the HeLa705 positive-readout system, the splicing effect of SCO was not enhanced by the use of a DNA scaffold. This is different to the data reported by Fakhoury et al.[48] and that might be due to the chemical modifications on the antisense used. The SCO has 2' O-methyl modifications in addition to the phosphorothioate backbones. It is more resistant to nuclease degradation than the phosphorothioated antisense oligonucleotide used in the paper. Neither of the DNA scaffold, triangular prisms or tetrahedra, offered enhancement in stability beyond that conferred by the nuclease-resistant 2′ O-methyl modification. Therefore, the extra DNA materials are unnecessary and likely to induce more cell stress[44] than delivering the antisense on its own. Cell viability assays, such as, MTT assays, could be used to test for adverse effects of DNA cage delivery.

## 6.3 Papain encapsulated inside a reconfigurable tetrahedron

DNA cages can be used as reaction chambers because guest molecules can be incorporated into the DNA nanostructures.[13,14] In this section, I will investigate whether the activity of the encapsulated molecule can be regulated via conformational changes of the DNA cage.

The system I used was based on a previously established system, which encapsulated papain inside a standard tetrahedron[137]. Moreover, it was reported that there was a reduction in the activity of the encapsulated papain.

Herein, the papain was encapsulated inside a reconfigurable DNA tetrahedron (OTpap, Appendix B.5.4 for the sequences of the component strands). Addition of opening strand (OS) would trigger opening of the tetrahedron. I hypothesised that when the DNA cage became open, the encapsulated papain would be more accessible to its substrates, leading to an increase in the enzymatic activity of the papain.

### 6.3.1 Experimental Outline

Papain was first covalently attached to a tetrahedral component strand (S1-pap, Appendix A.27). The DNA strand was modified with a thiol group at the 5' end and it was conjugated non-specifically to a surface lysine on papain using a heterobifunctional crosslinker. Then the conjugated product was mixed with the other three component strands and anneal to from a complete tetrahedron (Appendix A.28).

The papain activity was monitored by a fluorescence based reporter assay, the EnzChek® Protease Assay (Appendix A.29). The substrate was a casein derivative that was heavily labelled with a fluorescent dye, BODIPY FL and this resulted in self-quenching. As papain digested the substrate, this released segments of fluorescently labelled peptides. The fluorescence was no longer quenched and led to an increase in the fluorescence signals. A higher rate of increase of fluorescence signal indicated a higher level of activity of papain.

Comparisons of papain activity were always made between the same batches of OTpap in order to reduce potential variations between different batches of S1-pap. Addition of opening strand (OS) would trigger opening of the tetrahedron.

### 6.3.2 Results

Figure 6-5 shows the results of the protease assay of three samples: encapsulated papain in closed tetrahedron (blue, OTpap), encapsulated papain in open tetrahedron (green, OTpap OS) and encapsulated papain in the digested tetrahedron (red, OTpap DNAse I). Before the fluorescence reporter assay, the digested sample was incubated with DNase I, a non-specific endonuclease that digests DNA, so that the DNA cage was absent and hence the papain was no longer encapsulated (Appendix A.29.1).

As expected, encapsulated papain in the digested tetrahedron (red) had the highest enzymatic activity because there was no obstruction to the active sites of the papain. On the other hand, the open and closed samples had reduced activities in comparison to the digested sample, but they had a similar level of activity. This implied the configurations of the cage did not influence on the papain activity. Otherwise, opening of the cages should partially restore the papain activity. I suspect that the wire-framed DNA cage was too “leaky” for the substrate, so it could access the papain inside the cage, regardless of the cage configuration. The substrate in the EnzChek® assay was a casein derivative, with a molecular weight of approximately 20 kDa. It might be small enough to cross the tetrahedron barrier and access the encapsulated papain. This explanation was consistent with the observation that the actuation of the DNA cages failed to regulate the activity of the encapsulated papain.

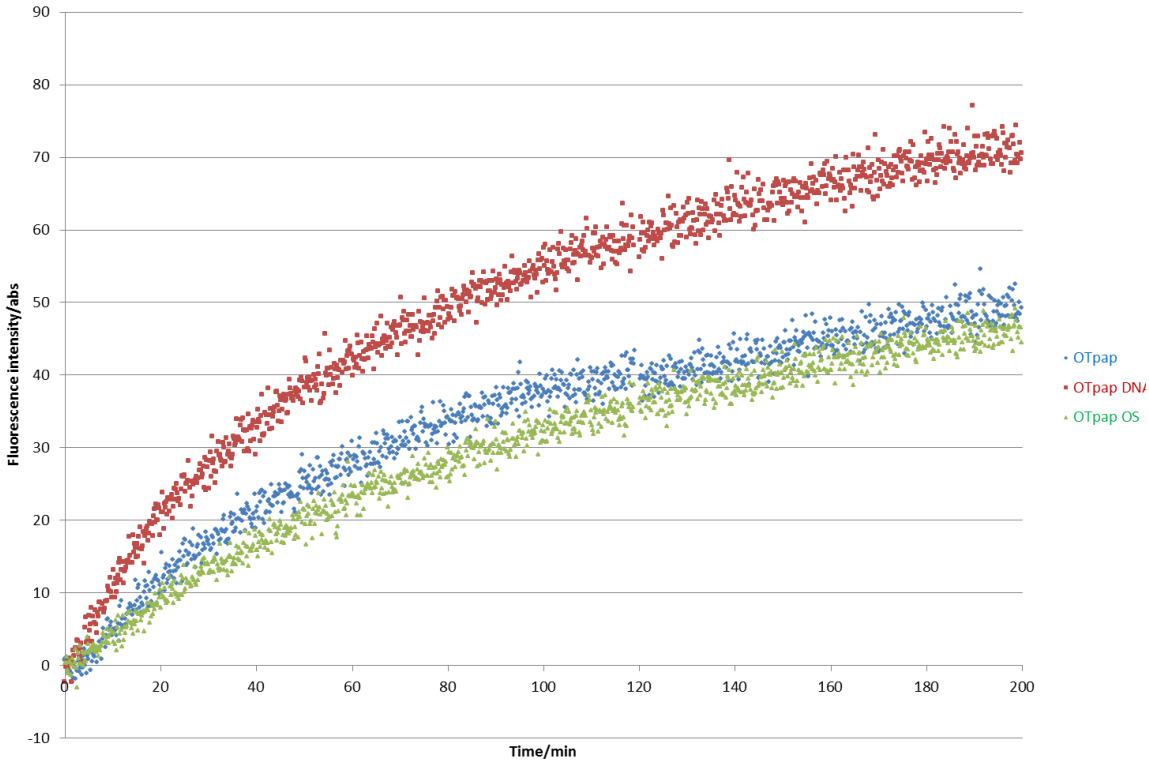


Figure 6-5: Fluorescence measurements of the Enzchek® protease reporter assay, to examine the activity of papain. The rate of fluorescence increase correlates to the papain activity. Blue is the tetrahedron with the encapsulated papain (OTpap); Red is the tetrahedron with the encapsulated papain incubated with DNase I (OTpap DNase I), hence the DNA cages are digested and the papain is no longer encapsulated; green is the open tetrahedra with the encapsulated papain (OTpap OS).

### 6.3.2.1 DNA-papain conjugation reduces the enzymatic activity

This then leads to another question: what caused the reduction in the papain activity when it was encapsulated in the cage? I suspected that reduction of enzymatic activity might be caused by the conjugation between papain and the DNA strand. I therefore compared the activities of S1-pap when the conjugated stand was intact and when the strand was digested by DNase I. Similarly, the enzyme activity was monitored by the Enzchek® Protease Assay (Appendix A.29.2).

In Figure 6-6, 40 µl of DNA papain-conjugated products were added to the cuvettes with 150 µl of reporter substrate. The red sample was incubated with DNase I before the start of the experiment and the green sample was not, so the former had no DNA strands and the latter had intact DNA strands. The former (red) had a higher enzyme activity than the intact S1-pap (green). This suggested that the DNA-papain conjugation process might impair the enzyme activities. The conjugation employed here targeted any lysine residues on the papain, so it was not site-specific. Conjugation could occur at locations close to the active site of papain. The DNA strand might also obstruct the access to the active sites of the papain. This explanation is consistent with the lack of regulatory effect observed for the actuation of DNA cages.

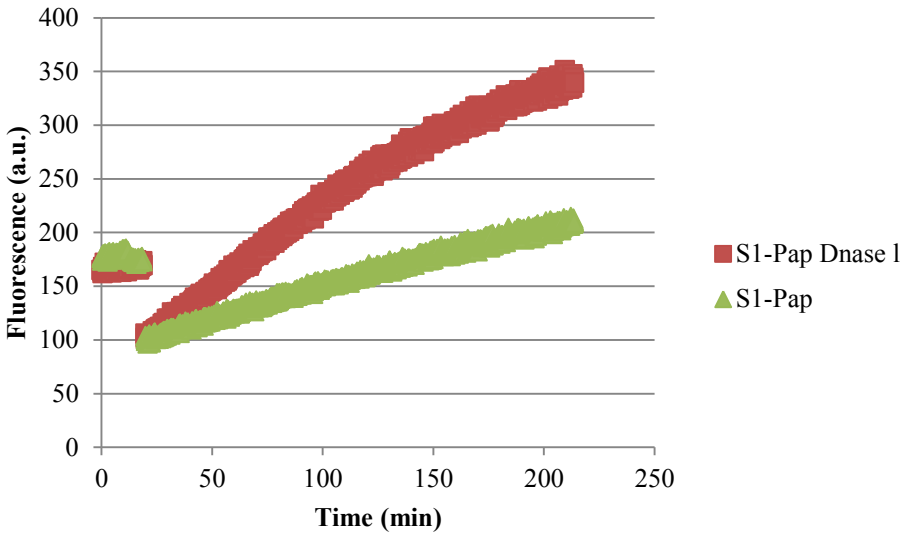


Figure 6-6: Fluorescence measurements of the Enzchek® protease reporter assay, to examine the effect of conjugation between the DNA oligo and papain. One of the DNA conjugated papain sample (red, S1-pap DNase I) was incubated with DNAse I before the start of the measurement (red). The other sample had no DNase I treatment, so it had intact DNA (green, S1-pap). At 20 mins, both samples were added into the assay and S1-pap (green) had a slower enzymatic activity than the sample without DNA (red).

### 6.3.3 Future experiments

In the current experimental design, papain activity cannot be regulated by the actuation of cages and I suspected that was due to the size of the substrate. A macromolecule that has a dimension bigger than 7 nm would be a better choice of substrate. One of the main industrial applications of papain is to digest antibodies to produce Fab fragments[138] from immunoglobulin, such as IgG and IgM. IgG has a molecular weight of 150 kDa and it should not be able to access the encapsulated papain. Therefore, immunoglobulin could be used as the substrate for future experiments.

Another challenge faced in this project was the low yield of the papain-conjugated DNA strand (S1-pap), which led to an even lower yield of the tetrahedra with encapsulated

papain. There are two ways to improve the synthesis of S1-pap: firstly, to improve the purification method for S1-pap. Size exclusion columns may be used instead of gel purifications; secondly, to choose a recombinant protein with a poly-histidine tag or to express the protein from a recombinant plasmid, so that a poly-histidine tag can be included. This would then widen the purification options available for the protein-conjugated oligonucleotides products.

## 6.4 Small Tetrahedra

In this section, I will discuss the synthesis of a small tetrahedron. The motivation behind is to study the effect of size and shape of DNA nanostructures on cellular uptake. Many studies have reported that cellular uptake is influenced by the geometry of the nanoparticles. For example, sharp edges in nanoparticles are advantages for delivery;[139] transferrin-coated gold nanoparticles with diameters of 50 nm have the highest uptake;[140] nanoparticles with high aspect ratio, such as nanotubes, have enhanced uptake and endosomal escape.[141] However, none of these studies specifically focus on DNA nanostructures. With the precise control of size and shape we have with synthesised DNA nanostructures comes great opportunity to investigate such properties systematically. It will also allow us to rationally design the DNA-based-drug-carrier.

In addition, successful formation of small tetrahedra could potentially reduce the cost of synthesis because the component strands of a small tetrahedron, each strand being 33-nt long, does not require HPLC purification. In contrast, each component strand of the standard 20-bp-edge tetrahedron is 63 nt long and it requires HPLC purifications. The

potential economic benefit becomes more prominent for the chemically modified strands, such as a thiol modified strand for covalent conjugation between oligonucleotide and protein. Without the need for HPLC purification, there will be ten times more starting material for this procedure. To my knowledge, the smallest three-dimensional DNA nanostructure published is a triangular prism, which each edge being one complete turn of a DNA double helix,[142] i.e. 10 bp. Therefore, the formation of the smaller tetrahedron should be feasible.

### 6.4.1 Synthesis

The synthesis of the small tetrahedron was the same as the standard tetrahedron (Appendix A.2). Four component strands were annealed at a final concentration of 250 nM in Buffer A. The formation of tetrahedron was examined in native PAGE (Appendix A.7.1).

### 6.4.2 Design 1- $Tet_{small}$

The initial design of the small tetrahedron is shown in Figure 6-7a. All nicks are in the middle of the edge, with 5 bp on either side. (For sequences see Appendix B.5.5)

Figure 6-7b shows the native PAGE of various combinations of the component strands. Lanes 1 and 2 are the component strands alone. Lanes 3 and 4 are the two-strand complexes, S2•S4 and S2•S3 respectively. Since they each had a band higher than the component strand alone (lanes 1 and 2), the two-strand complexes were formed successfully. Each of those two pairs had a 10 bp edge complementary with each other, so they could hybridise with each other as designed.

Lane 5 is S1+S2+S3, which was supposed to represent the three-strand complex, but such formation failed. The strong band in lane 5 was in the same position as bands in lanes 3 and 4, which corresponded to the two-strand complex. The faint band corresponded to a component strand alone. As S2 and S3 shared a 10 bp edge, but neither with S1, the strong band was the S2•S3 product and S1 was the component strand alone. Lane7 has all four strands, which should represent a fully assembled small tetrahedron. However, there was no clear band in lane 6, so the assembly of the small tetrahedron was unsuccessful.

Since S1 does not share a 10 bp edge with any of the other three strands, I suspect that it cannot form a stable duplex with the other component strands, so it cannot be incorporated into the structure. The face of the tetrahedron that S1 runs round is only held together by 6 sets of 5 bp interactions and this is not strong enough to keep all four strands together. Indeed, any complex that involved S1 failed to form (lane 6 and 7).

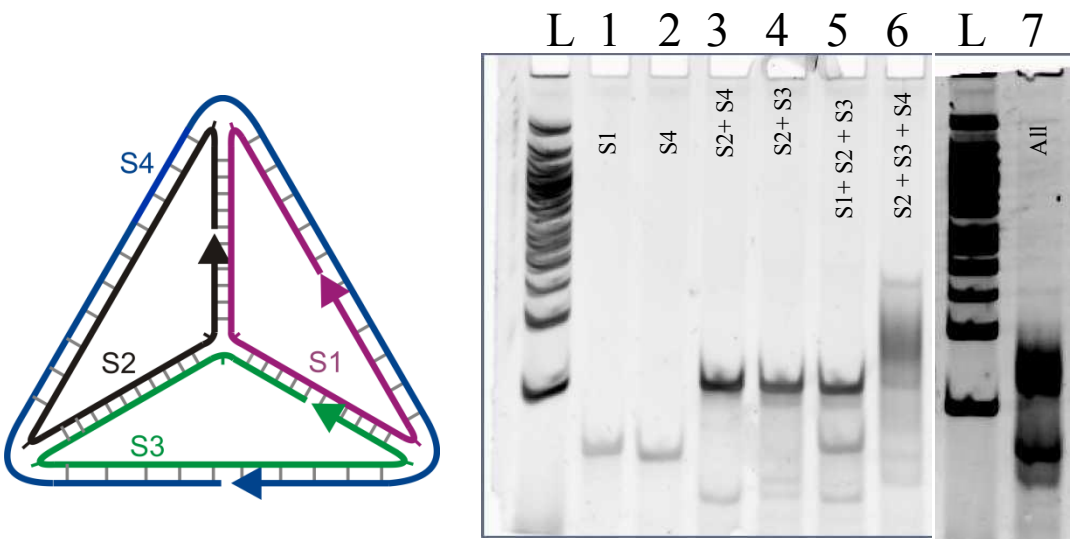


(a) (b)

Figure 6-7: The initial design of the small tetrahedron and its formation analysis. (a) Schematic diagram for the 10 bp edge small tetrahedron, with all nicks in the middle ($Tet_{small}$). Arrows indicate 3' end. (b) 29:1 10% native PAGE to examine the formation of the small tetrahedron. L: 50 bp NEB ladder. Lane 1: S1. Lane 2: S4. Lane 3: S2 + S4. Land 4: S2 +S3. Lane 5: S1 + S2 + S3. Lane 6: S2 +S3 +S4. Lane 7: All four strands.

### 6.4.3 Design 2 – $Tet_{small}2$

In the light of the result above, each component strand needs to have at least one 10 bp edge with another component strand in the revised version. This is less important for the standard 20 bp edge tetrahedron because when a nick is in the middle of the edge, each section would be 10 bp long and this provides sufficient binding strength compared to the thermal fluctuation.

Therefore, the nick of S3 was moved from the edge with S1 to S2, so that the nick would be on the edge with S2 (Figure 6-8a). S1 and S3b now form a 10 bp complementary edge. However, this is not yet sufficient for the small tetrahedron to form because there is no 10 bp edge between the two-strand complexes: S2•S4 and S1•S3. Therefore, S4 was redesigned to S4b with its nick at a vertex. The final design of $Tet_{small}2$ is shown in Figure 6-8b. (For sequences see Appendix B.5.6)

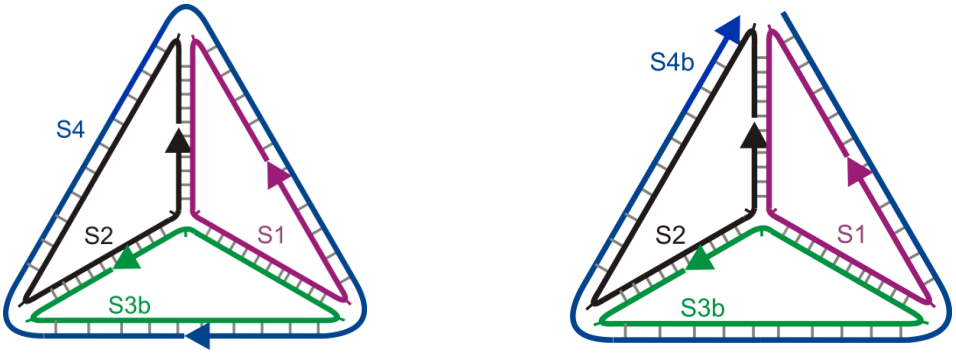


(a) (b)

Figure 6-8: Different modifications of small tetrahedron. (a) Schematic diagram for the modified small tetrahedron with the new strand S3b and the nick is at new positions (b) Schematic diagram for $Tet_{small}2$, the modified small tetrahedron with nicks at new positions.

Figure 6-9a shows the results of formation with various combinations of the component strands in native PAGE. Lane 1 has S1, so it is the component strand alone. Lane 2 is S1+S4b and it has two bands that correspond to the component strand alone. This indicates the two strands fail to hybridise because S1 and S4b do not have a full 10 bp

edge. This lane is to illustrate the necessity of a 10-bp-edge between the two-strand complexes Lanes 3 and 4 are the two-strand complexes that formed successfully. Lanes 5 and 6 are the three-strand complexes. Lane 7 has all the component strands; it has a clear band that has the least mobility and is only visible when all four component strands are present. Therefore, it confirms the successful formation of the small tetrahedron.

#### 6.4.3.1 Ligation by T4 ligase

Ligation of the nicks in S1, S2 and S3b can improve the stability of the small DNA tetrahedron from exonuclease degradations. (The nick of S4 is at a vertex, so the T4 ligase would not be able to ligate that.) I therefore incubated $Tet_{small}2$ with T4 ligase at room temperature overnight (Appendix A.3) and examined the samples with the native PAGE (Figure 6-9b). Lane 1 is $Tet_{small}2$ without the ligation, lane 2 is the three-strand complex without ligation and lane 3 is $Tet_{small}2$ with ligation. Interestingly, a bigger structure was formed in lane 3. The band was in a position similar to a standard 20 bp tetrahedron. This suggests that the three nicks between S1, S2 and S3b were not stable. Instead of stabilising the monomer, the ligase might have joined the small tetrahedron with another tetrahedron forming a dimer. In addition, the smeary appearances of the bands in lanes 1 and 2 implied that the small tetrahedron structure was not very stable. All the samples were only 1-day-old.

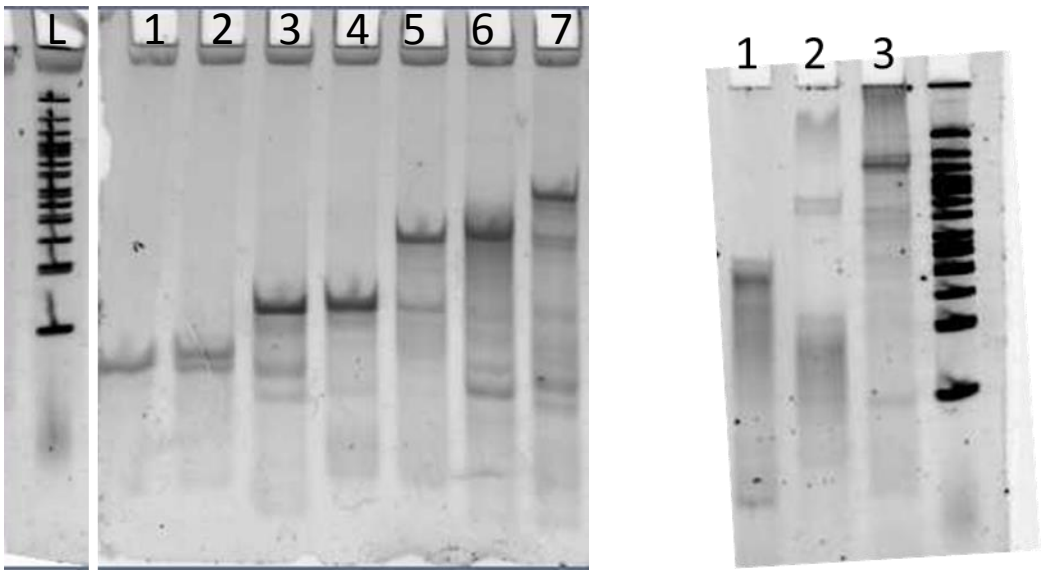


(a) (b)

Figure 6-9: 29:1 10% native PAGE to verify the formation and the stability of $Tet_{small}2$. (a) To examine the formation of $Tet_{small}2$, with the modified S3b and S4b. L is the 50 bp NEB ladder. Lane 1: S1, land 2: S1 + S4b, lane 3: S2 + S4b, lane 4: S3b + S4b, lane 5: S1 + S3b + S4b, lane 6: S2 + S3b+ S4b, lane 7: all (S1 + S2 + S3b + S4b). (b) To examine the effect of the overnight ligation by T4 ligase on $Tet_{small}2$. Lane 1: $Tet_{small}2$ without ligation., lane 2: S1 + S3b + S4b without ligation, lane 3: $Tet_{small}2$ with ligation.

### 6.4.4 Discussion

The small tetrahedron was shown to form successfully, but found not to be as stable as the standard tetrahedron.

He et al.[142] reported the successful formation of a10-bp-edge triangular prism. Such structure can be assembled from annealing 5 component strands with nicks at the middle of the edge. The difference between their reported result and the investigation in this section might be due to geometry of the DNA nanostructures. He et al. used a

triangular prism instead of a tetrahedron, and the former structure might be under less strain. In the same study, the small triangular prism could also be constructed from one single-stranded DNA and there would only be one nick in the system. This may further stabilise the small triangular prism.

For the small tetrahedron described here, further redesigning is necessary to form a stable structure. I suggest redesigning the component strands so that all the nicks are at the vertices and chemical ligations might be able to ligate the strands with nicks at the vertices to form a more stable structure.

However, the consequence of restricting the nicks positions is that the small tetrahedron loses its ability to control the position and the orientation of the chemical modifications, because modifications are often introduced at either the 3' or 5' ends. For example, the nick position was used to control whether the conjugated enzyme was on the inside or the outside of the tetrahedron.[13]

Going back to the motivations described at the beginning of this section, the small tetrahedron could be useful in the study of the effect of size and shape of DNA nanostructures on cellular uptake. However, it is unlikely that it could be used as a cage to encapsulate molecules because of the restricted nick positions of the component strands.

## 6.5 Conclusion

According to the experimental results in Section 6.2, using DNA nanostructures as a scaffold to deliver antisense has few additional benefits. The scaffold offers no enhancement in stability beyond that conferred by the nuclease-resistant 2′ O-methyl modification. The extra DNA materials are unnecessary and likely to induce more cell stress[44] than delivering the antisense on its own.

The DNA triangular prism (TP) and the DNA tetrahedron were also compared. The TP has two main advantages over the tetrahedron. Firstly, the TP can be formed at micromolar concentration without the need of gel purification, but the tetrahedron cannot. Secondly, the TP is a more versatile DNA nanostructure than the tetrahedron because of the single-stranded regions, where ligands, aptamers, antisense or other functionalised strands can readily be loaded into the preassembled nanostructures. Therefore, TP is a potentially better carrier for therapeutic oligonucleotides.

In Section 6.3, experimental data shows that actuation of DNA cages did not regulate papain activity. The level of enzymatic activity was the same in an open and in a closed cage. The previously reported reduction of enzymatic activity of encapsulated papain might be caused by the DNA-papain conjugation. In hindsight, the cage was too ’leaky’ for the substrates. The choice of the protein, the cage and the substrate should be reviewed before proceeding further.

In Section 6.4, the formation of the 10 bp tetrahedron was successful. It was not possible to have all four nicks in the middle of the edge and at least one of the nicks

needed to be at the vertex. Otherwise, the small tetrahedron would not assemble. However, the structure was found to be unstable because in the presence of T4 ligase, the monomeric small tetrahedron formed a bigger structure.

In all these side projects, the functions and results of DNA nanostructures did not meet its original aims and goals, but the process of investigation has given insight into what the feasible biological applications of DNA nanotechnology might be.

# Chapter 7 Summary and discussion

## 7.1 Summary

In this chapter, I will summarise the results presented, the progress made in this research project and my view on the future of DNA nanotechnology in biomedical application.

Chapter 2 to 4 focus on the actuations of the DNA nanostructures inside mammalian cells. Chapter 5 explores the possibilities to trigger conformational changes in the DNA tetrahedra via cellular RNA signals. Chapter 6 discusses the synthesis of the small tetrahedron and two applications of DNA nanostructures, firstly as antisense carriers to control gene expression in cells and secondly as chemical reactors to control the level of activity of an encapsulated enzyme.

In the work of this thesis, the main system is based on a reconfigurable DNA tetrahedron. It can be opened via toehold-mediated strand displacement with an opening strand. In Chapter 2, I assessed the stability of the reconfigurable DNA tetrahedron in tissue culture medium, in which the concentration of the magnesium ions was lower than the assembly buffer and its supplement contained nucleases that degraded DNA nanostructures. Because of these two factors, DNA nanostructures that were stable in

the assembly buffer might not necessary be stable in the tissue culture medium. The tissue culture medium mimics the physiological conditions. The first design of the reconfigurable tetrahedron OT2.2 was open in the absence of the opening strand due to the low magnesium ions level in the medium. I strengthened the closing mechanism by increasing the number of base pairs that kept the cage closed to avoid unintentional opening in low magnesium ions. The DNA tetrahedron can be degraded within hours of incubation in medium supplemented with serum. A closed tetrahedron had a longer lifetime than an open tetrahedron. Serum-free medium was therefore used for the transfection of the DNA cages in the rest of the experiments in this thesis to avoid potential degradation during the incubation.

In Chapter 3, I established the positive (open) and negative (closed) controls inside mammalian cells. The DNA tetrahedra were transfected with Lipofectamine®2000 in serum-free medium. According to the confocal micrographs, DNA tetrahedra were stable inside cells for eight hours because the two controls were clearly distinguishable within this timescale. However, the DNA tetrahedra remained trapped in compartments and this suggested inefficient escape from endosomes to the cytoplasm. Next, the chemically modified synthetic oligonucleotides were transfected into cells a few hours after the DNA tetrahedra and this induced the actuation of a small proportion of DNA tetrahedra inside mammalian cells. This work represents the first examples of the actuation of DNA tetrahedron by an external signal inside mammalian cells.

Since only a small proportion of DNA tetrahedra were open by the separately transfected synthetic strands, it was important to increase the strength of the fluorescence signal. A simplified model system – a DNA duplex was therefore used

instead of the DNA tetrahedron system in Chapter 4. The transfection efficiency was also improved by using XtremeGENE HP rather than Lipofectamine®2000. Experiments where cells were first transfected with the duplex DNA and then subsequently transfected with an opening strand confirmed that strand displacement can take place within cells. Both flow cytometry and confocal microscopy showed a gradual increase in the fluorescence signal that measured the extent of strand displacement. The increase was larger when the opening strand had been chemically modified. With the current experimental data, I speculate that the DNA nanostructure and opening strand are initially localised to separate endosomes which fuse at the periphery of the nucleus and trigger strand exchange. In order to answer this question, I designed a two-colour experiment that simultaneously localise the DNA nanostructures and the opening strands, but it was unsuccessful and extracellular aggregation of fluorophore-labelled nucleic acids was observed. This demonstrates the need for a more effective washing protocol to remove the extracellular DNA nanostructures that remain after the transfection. Dextran sulphate[53] or acidic glycine buffer[103] have been used to remove the extracellular nucleic acids in tissue culture, but they are not used to remove DNA nanostructures that are in complex with transfection reagent. They might also affect the uptake in the second round of transfection with the opening strands. In conclusion, their effectiveness and potential undesired effect require further examination.

In retrospect, a simplified model is a good starting point. It should have been introduced at the beginning of the work in this thesis. It would have provided us with more information in a shorter timescale regarding the appropriate parameters of the system,

such as the concentration of the nanostructures, the timescale of the experiments and the various ways to transfect them into cells.

In Chapter 5, I investigated possibilities of using cellular RNA to interact with the DNA nanostructures. Messenger RNA, modified tRNA and short single-stranded RNA were tested. Regions of weak secondary structure within the luciferase mRNA were targeted. The tetrahedral component strand successfully hybridised with the mRNA and this indicated that the particular region mRNA was accessible to the single-stranded DNA. However, the mRNA failed to interact with the assembled tetrahedron, possibly because of the steric hindrance between the three-dimensional structure of the DNA tetrahedron and the mRNA. There are two challenges here: the first one is about selecting an appropriate target region and the second one is the effect of steric hindrance upon strand displacement reactions between rigid or bulky bodies. Firstly, live cell imaging of mRNA has been achieved, so target regions can be found from publications. However, the probes used are mostly either single-stranded or in the form of a molecular beacon. For future experiments, one needs to test if it is possible for a duplex with a toehold to interact with the mRNA in live cell condition because strand displacement is part of the process of inducing conformational changes in this current design. Secondly, I speculate that steric hindrance is the reason why the DNA cages fail to be opened by the mRNA. Further investigation into the effect of steric hindrance is necessary. The three-dimensional structure of the DNA tetrahedron is likely to have an impact on the strand displacement reaction. Experiments that systematically increase in the size of the opening signals would be informative.

The second cellular RNA candidate was the modified tRNA with the opening signal encoded in its anticodon region. The modified tRNA was successfully expressed in bacteria and the RNA extract hybridised with one of the tetrahedral strands. This opens up the potential to use tRNA as the signal to trigger opening and more investigation is required. In addition, a translator gate[122] could be incorporated into the opening mechanism. The translator gate would interact with the cellular RNA, producing an output that triggers the opening of the DNA tetrahedron. This might overcome the difficulties caused by steric hindrance.

The third cellular RNA candidate was the short single-stranded RNA, it failed to be translated, mostly likely because the inserted sequence lacked a hairpin structure and it was not compatible with the expression system. There are microRNA expression vectors that one could use in the future to over express the targeting signal.[143]

Chapter 6 is the miscellaneous chapter, but it points to the bigger picture and the future applications of the DNA nanotechnology. Based on the report that DNA tetrahedra could enter cells without any transfection reagent,[2] I tested the use DNA nanostructures as the antisense carriers to induce luciferase expression in HeLa pLuc705 cells. However, there was no detectable increase in luciferase expression when transfection reagent was not used. When transfection reagent was used, the DNA nanostructure scaffold had no additional enhancement effect when compared to antisense transfected without the nanostructures. I concluded that there was little benefit in using DNA nanostructures as the antisense carrier. The second potential application I investigated was using the DNA tetrahedron as a chemical reactor to regulate the activity of the encapsulated molecule. Papain was encapsulated inside a reconfigurable tetrahedron.

The hypothesis was that the DNA tetrahedral wire-framed structure would obstruct the access of the substrates to the active sites of papain, so the tetrahedral structure would inhibit the enzymatic activity of papain. However, according to the fluorescence-based reporter assay, the papain activity was the same regardless of the states of the cage (open and closed). It was therefore concluded that the wire-framed nanostructure was too leaky and so it was insufficient to obstruct the access of the substrates to papain. Finally, I studied the synthesis of the first reported 10-bp-edge tetrahedron. The formation of the small tetrahedron was successful, but found not to be stable if the nicks were in the middle of the edge, so all the nicks should be at the vertex. This restriction limited its potential to be a chemical reactor that can encapsulate molecules.

## 7.2 Discussion

### 7.2.1 Cell entry

In this project, a significant proportion of time was spent in establishing the open and closed state of the tetrahedron. However, this was only possible with the use of transfection reagent. Walsh et al.[2] reported that DNA tetrahedron could enter HEK-293 cells simply by incubating the sample in serum-free medium and the uptake was comparable to the sample which a transfection reagent was used. If this were true, this would have been a major advantage of a DNA based drug delivery system because those structures could be taken up by cells without additional chemicals or modifications. Bujold et al.[24] also reported the uptake of a similar DNA nanostructure, DNA cube, into LNCaP cells and HeLa cells. According to their flow cytometry data in

the supplementary information, the fluorescence signal of the naked DNA cube is only twice of that of the background, which is 10-fold less than the uptake with transfection reagent Lipofectamine® 2000. In both of these cases, the DNA nanostructures are incubated with cells in serum-free media. The possibility of extracellular degradation of the nanostructures is therefore excluded. However, I could not detect any uptake of the DNA tetrahedron into cells by fluorescence imaging with the confocal microscopy or by measuring luciferase induction using the antisense system discussed in Chapter 6. Juul et al.[38] reported a lack of uptake of the temperature-controlled DNA nanostructures into Sf9 insect cells.

Pei et al.[3] reported using the reconfigurable tetrahedra to detect changes in ATP concentration in intracellular environment. This implied that the tetrahedra were inside cells. Le et al.[4] used single-particle tracking to investigate the uptake pathway of a naked DNA tetrahedron with a Cy3 fluorophore at each of the four vertices. However, in both of these two studies, the incubation medium contains nucleases that degrade DNA nanostructures and this might separate the fluorophores from the nanostructures. Since the fluorophores are hydrophobic, they can cross the plasma membrane and enter the cells and give rise to artefact signals.

I am sceptical of the claims that there is a robust uptake of DNA nanostructures into cells without any chemical modifications or transfection reagent. When those results were compared to the standard transfection reagent, their uptake was minute and the only evidence available was florescence signal, rather than having a biological effect, such as protein expression.

### 7.2.2 Alternative efficient delivery methods

Overall, through the work of this DPhil, progress has been made in exploring the technical difficulties of building a targeted drug delivery system based on DNA. The positive and negative controls were only established with the use of transfection reagents. For most of the commercially available transfection reagents, their exact compositions are not published. The unknown nature of these reagents makes them less attractive to basic research. In addition, the delivered nanostructures remained trapped in compartment bound features, so the endosomal escape into the cytosol is not effective. This limits the possibility of the DNA nanostructures reaching its signalling target.

An alternative method that can effectively deliver DNA nanostructures into cytosol is therefore the key to achieve the goal of targeted drug delivery. Functionalising DNA nanostructures with chemical groups, such as folic acids[50] and hydrophobic dendritic chains,[24] to promote uptake into specific cells have been reported. DNA nanostructures may also require other chemical modifications to enhance their nuclease resistance.

Moreover, RNA aptamer is an attractive candidate to delivery DNA nanostructures. In recent years, it has made much progress on cell-types-specific aptamer delivery. For example, an RNA aptamer A9g is reported to be internalised specifically by prostate cancer cells. In addition, the aptamer itself exhibits therapeutic effects and inhibit the cancer metastases.[144] In principle, it should be relatively simple to introduce RNA aptamers to DNA nanostructures via Watson-Crick base pairing. As discussed in the introduction, when the aptamer binds to its target, it undergoes conformational changes.

This property of the aptamer has been used as to open a DNA icosahedron upon a chemical trigger,[36] but that was done outside cells. I think in future, there will be more work that utilise both aptamers and DNA nanostructures as part of cell-targeted therapies.

Finally, the most important question is what additional values will the DNA nanostructures bring to these therapies? If chemical modifications are necessary for the DNA nanostructures, what is the additional benefit of introducing those modifications to the DNA nanostructures rather than the therapeutic agents? I suspect that DNA nanostructures may not play a significant part in the targeted-drug delivery system. Nevertheless, I believe DNA nanostructures will play a key role in other important biomedical applications, including the development of ultrasensitive diagnostic tools, to deepen the understanding of multiple scientific disciplines. For example, in molecular biology, DNA nanostructures have been used to study the cellular uptake of nanoparticles and the pH in various endosomal compartments;[65] in biochemistry, DNA encapsulation technology could be further utilised to study protein-protein interactions in a highly organised and crowded environment.[16] Promising progress has been made in functionalising biosensors with rigid DNA nanostructures to improve the detection limits for microRNA[145,146] and small chemicals.[147]

# Appendix A Materials and Methods

## A.1 Materials

All synthetic nucleic acids were purchased from Integrated DNA Technologies (IDT). They are resuspended in Milli-Q water to 100 μM and stored at 4ºC. Tissue culture related products were from Life Technologies, kindly provided by the Wood group in the Department of Physiology, Anatomy and Genetics, Oxford. These included tissue media Gibco® DMEM, Opti-MEM®, cell dissociation reagents TrypLE™ and PBS for cell washing. Mammalian cells were maintained in a 37 ˚C incubator with 5% humidified $CO_2$. Mammalian cells and plasmids (psiCheck2.2 and pU6-neo) were gifts from the Wood group. DNA ladder, T4 ligase and restriction enzymes were purchased from New England Biolabs (NEB). Unless specified, the rest of the chemicals were from Sigma.

### A.1.1 Opti-MEM®

Opti-MEM is a commercial serum-free media that is optimised for cationic lipid transfection. The exact composition is not available, but it is based on Eagle's Minimum Essential Media (MEM), buffered with sodium bicarbonate and HEPES. MEM contains various inorganic salts, vitamins, amino acids and glucose. In the context that is relevant to Section 2.3.3.1.1,

MEM has 0.8 mM of $Mg^{2+}$. The complete formulation for MEM can be found in http://www.sigmaaldrich.com/life-science/cell-culture/learning-center/media-formulations/mem.html.

### A.1.2 Dulbecco's Modified Eagle's Medium (DMEM)

DMEM is a commercial media that contains various inorganic salts, vitamins, amino acids and glucose. The complete formulation for MEM can be found in http://www.lifetechnologies.com/uk/en/home/technical-resources/media-formulation.170.html. It is supplemented with fetal bovine serum to support cell growth in tissue cultures.

## A.2 General synthetic scheme for DNA nanostructures

Unless specified, all DNA nanostructures, including DNA tetrahedra, triangular prisms and duplexes, involved the same synthesis scheme. Equimolar concentrations of the component strands at specified concentrations were mixed in Buffer A (10 mM Tris-HCl, 15 mM $MgCl_2$, pH 7.4). The mixture was heated to 91 ˚C for 3 minutes followed by cooling to 4 ˚C in approximately 4 minutes with a thermal cycler (Mastercycler personal, Eppendorf). DNA tetrahedra were ligated with T4 ligase (A.3) and gel purified (A.4) before the experiments.

In Chapters 2 and 3, tetrahedra were synthesised at final concentration of 2.5 μM. In Chapter 4, the duplexes were synthesised at 4 μM.

## A.3 Ligation with T4 DNA Ligase

Tetrahedral component strands with 5' phosphorylated ends were ligated with T4 ligase (M0202, NEB) at room temperature overnight in 1x T4 ligase buffer. 2 µl of T4 ligase was used for every 100 µl reaction mix after the annealing process.

## A.4 Gel purifications of DNA tetrahedra

Sample was first run on a 6% 29:1 native PAGE with the broad comb at 215V for 40 minutes. DNA tetrahedra used in this thesis were labelled with fluorophores, so they were visualised using a Bio-Rad gel scanner with the appropriate settings to image the fluorescence. The desired band was cut out by the gel cutter. The band was transferred into a 1.5 ml Eppendorf tube and crushed by a pipette tip. The crushed pieces were covered with sufficient Buffer A (100 µl of Buffer A for one band across the whole Bio-Rad mini-gel). The sample was soaked overnight and then they were transferred to a Millipore Ultrafree-MC HV centrifugal filter. The tube was spun at 12000 g for 2 hours to elute the solution containing the purified tetrahedron.

## A.5 Measuring the concentration of gel-purified Cy5-labelled DNA tetrahedron

8 µl of the purified DNA tetrahedron from A.4 was examined in 10% 29:1 native PAGE, alongside with 8 µl of the Cy5-labelled component strand (S3), ranging from 100 nM to 800

nM. The gel was visualised using a gel scanner with the corresponding fluorescence setting. Quantity One® 1-D analysis software was used to detect the band in the image and measured their intensities. A calibration curve with intensity against concentration was plotted with the component strand samples. Concentration of the DNA cages was then determined from its intensity according to the linear fitting of the calibration curve. The final concentration of the purified tetrahedron ranged from 300 nM to 800 nM.

As a note of clarification, the concentration of any gel-purified product could not be accurately determined by the absorbance at 260 nm because of the acrylamide contamination from the gel. It distorted the absorbance curve and overestimated the concentration of the DNA sample. If this method is to be sued, the sample must first pass through a spin column for buffer exchange (A.26) before measuring the absorbance. However, this required at least 20 µl of the sample and introduced further decrease of the yield because the recovery process was not 100%.

## A.6 Ensemble fluorescence measurement

All ensemble fluorescence measurements were taken with the Cary Eclipse Fluorescence Spectrophotometer (Varian). It has been mainly used in measuring the actuation of the DNA tetrahedra.

The fluorescence signals recorded were Cy3 (excitation 550nm, emission 565 nm), Cy5 (excitation 650nm, emission 665 nm) and Alexa-488 (excitation 495nm, emission 519 nm).

Samples were loaded into glass cuvettes with a minimum volume of 120 µl. The slit width was set to 5 nm and the voltage of the detector was set between 600 and 900 V.

Unless specified, 20 µl of tetrahedral sample was added into 120 µl of Buffer A. When a separate opening strand was involved, the opening strand would have been diluted from the 100 µM stock concentration to the specified concentration in Buffer A.

## A.7 Gel electrophoresis

### A.7.1 Native Polyacrylamide Gel Electrophoresis (PAGE)

Native PAGEs were used to analyse DNA nanostructures held together by Watson-Crick interactions. The formation and the states of DNA nanostructures were examined in native PAGE throughout the work of this thesis.

A polyacrylamide gel consists of a mixture of acrylamide and bisacrylamide to form a gel matrix with pores. The pore sizes depend on the concentration of acrylamide and the ratio between acrylamide and bisacrylamide. In the work of this thesis, all gels were either 6% or 10% of acrylamide concentration, 29: 1 ratio of acrylamide to bisacrylamide. The gel mix was buffered with Tris Acetate-EDTA (TAE).

An electric field was applied across the gel, so the mobility of the samples depended on their charges and sizes. All PAGE experiments were run in a Mini-PROTEAN 3 (Bio-Rad) at 4˚C to prevent the heating of the gel due to the applied voltage. An applied voltage of 180-240V

of range was applied for time ranging from 30 to 90 minutes. Unless specified, sample was mixed with loading dye in the ratio of 5:1. The composition of the loading dye was 0.25 % bromophenol blue and 30% glycerol in water.

#### A.7.1.1 Magnesium Chloride

Some DNA nanostructures were not stable in Native PAGE without $Mg^{2+}$. Therefore, 15 mM of $MgCl_2$ was added into the gel mix and the buffer solution, so that the magnesium ions concentration would be the same as the assembly buffer, Buffer A.

### A.7.2 Agarose gel

1 g of agarose was dissolved in 100 ml of TAE. Before loading the DNA sample into the well, the sample was mixed in the ratio of 5:1 with the loading dye. Gel was run at 80V for approximately an hour at room temperature. Gels were run in a Wide Mini-Sub Cell GT Cell (Bio-Rad).

Agarose gel was used instead of polyacrylamide when the nucleic acid sample was too big to migrate into a polyacrylamide gel.

#### A.7.2.1 Agarose gel shift experiment

Agarose gel shift experiment was used in Section 5.2.1.3 to verify the accessibility of particular regions within the mRNA. If the mRNA was accessible to a single-stranded DNA, then it would displace the single-stranded DNA from its original position in the gel.

In Section 5.2.1.3, 2 μM of mRNA was incubated with 400 nM of the tetrahedral component strand (S4_744 or S4_990) in Buffer A at 37 ˚C for 1 hour. 4 μl of each sample was loaded into each lane. The gel was run at 80V for 1 hour.

### A.7.3 Visualisation of bands in gel

All gels were scanned by Pharos FX plus Molecular Imager (Bio-Rad) and Quantity One® 1-D analysis software was used to operate the gel scanner.

#### A.7.3.1 SYBR Gold

For PAGE, each gel was soaked in water with 2ul of SYBR® Gold Nucleic Acid Gel Stain (Life Technologies) for 5 minutes. Then the gel was rinsed with water once before scanning.

#### A.7.3.2 Fluorophores on DNA nanostructures

Some of the DNA nanostructures were formed with fluorophore-labelled component strands, for example, Cy3, Cy5, FAM or Alexa-488. Those bands can be directly visualised in the Pharos FX plus Molecular Imager, which had appropriate lasers and filers to excite and image the corresponding fluorescence.

## A.8 Degradation of DNA materials in complete medium

Complete medium was Dulbecco's Modeified Eagle's Medium GlutaMAX$^{TM}$ (GIBCO), supplemented with 10 % heat inactivated fetal bovine serum (FBS). Equal volume of DNA sample and complete medium was combined and the mix was incubated at 37˚C. Mixes

began their incubations at different time and the integrities of the DNA materials were examined in native PAGE at the same time.

In Section 2.3.4, the final concentration of strand S3 Cy5 in the mix was 500 nM and approximately 200 nM for the tetrahedral samples. 8 µl of the sample was loaded into each lane.

In Section 2.4, $O_c$ was diluted from the 100 µM stock to 1µM in PBS. Then equal volume of $O_c$ was mixed with complete medium. After the incubation, 8 µl from each mix was loaded onto a lane.

## A.9 Seeding cells

Cells were grown in Corning® T-75 Flasks with DMEM medium supplemented with 10% heat inactivated FBS, 1% penicillin and streptomycin, in a 37 ˚C incubator with 5% humidified $CO_2$. This composition of this medium is called growth medium. For each experiment, cells were seeded onto new plates the night before the treatment. Growth medium was removed and the cells were washed with PBS three times. Then cells were incubated with 4 ml of trypsin replacement (TrypLE™ Express Replacement Enzyme, Life Technologies) at the 37˚C incubator for 10 minutes. Cell became detached from the surface of the flask and 6 ml of growth medium was added to inactivate the trypsin. Solution was pipetted up and down gently to ensure cells were in suspension. The 10ml was transferred to a 15ml falcon tube and it was centrifuged for 3 minutes at 2500 rpm. After centrifugation, the supernatant was removed and cells were re-suspended in 1 ml of growth medium. 5 µl of cell

was mixed with 195 µl of Trypan Blue solution; 10 µl of the blue cell mix was loaded onto a haemocytometer and it was examined under a microscope. The cell density of the suspension was calculated and an appropriate amount of cells was mixed with the corresponding volume of growth medium. Then, the cell mix would be added into each well, for example 500µl per well in a 24-well plate.

## A.10 Degradation of DNA tetrahedron in cell lysate (see Section 2.3.5)

Degradation of DNA cages in cell lysate was examined in Chapter 2. $10^5$ MCF-7 cells were seeded in a well in 24-well plate the night before in growth medium. The next day, cell medium was removed and cells were washed with PBS three times. Then 300 µl of 1x Cell Culture Lysis Reagent (CCLR, E1531, Promega) was added. The plate was left on a shaker at room temperature for 30 minutes. The cell mix was transferred into an Eppendorf tube. Cell membrane and debris were separated from the lysate by centrifuging the sample at 300 g for 5 minutes. 6 µl of the supernatant was mixed with 6 µl of DNA cages. The mix was incubated at 37˚C for various periods of time and all the samples were examined in native PAGE at the same time.

## A.11 Degradation of $O_c$ inside cells (see Section 2.4.2)

7 x$10^5$ of MCF-7 and HEK-293 cells were seeded in two separate 35 mm petri dishes the night before in growth medium. The next day, cell medium was removed and cells were washed with PBS 3 times. 1.5 ml of fresh growth medium was added into each dish.

300 pmole of $O_c$ was transfected into the mammalian cells with the aid of Lipofectamine® 2000 (LF) overnight. 3 µl of 100 µM $O_c$ was added to 247 µl OpiMEM. 10 µl of LF was diluted in 240 µl of Opti-MEM® and the mix was incubated at room temperature for 5 minutes. The diluted $O_c$ was then combined with the diluted LF and incubated for 25 minutes at room temperature. The total volume of 500 µl complex was added into each well containing cells and 1 ml of medium.

The following day, the cells were thoroughly washed with PBS in order to remove any $O_c$ that were not taken up by cells. Then, the RNA extract from the transfected cells was collected with a miRNeasy mini kit (Qiagen), according to the manufacture's instruction (A.12). 2 columns were used for each 35 mm petri dish of cells. The RNA extract was examined in native PAGE. 5 µl of the RNA extract was added into each lane.

The RNA extract containing $O_c$ was also used to open DNA cages in Section 2.4.2.2. 20 µl of the RNA extract was added to a solution of 30 nM DNA cages in Buffer A with a final volume of 150 µl. The fluorescence signals were monitored in the fluorimeter (Appendix A.6).

## A.12 Small RNA extraction

miRNeasy Mini Kit (Qiagen) was used to prepare RNA extraction from mammalian cells in Sections 2.4.1 and Section 2.4.2, following manufacturer's instruction. In brief, cells were first lysed and homogenised. Chloroform was then added and the sample was mixed by vortex and centrifuged. The sample separated into three phases and the upper aqueous phase containing the RNA. It was extracted carefully by a pipette and it was passed through the RNeasy Mini spin column. Pure RNA was eluted in RNase-free water. For a 6-well plate experiment, 2 spin columns would be used per well of cells. 50 - 100 µl of pure RNA extract would be eluted from each column.

As for tRNA extraction from BL21 (DE3*) E. coli*, the bacteria were grown in 5 ml LB for 18 hours in a shaker. Bacterial culture was then harvested by centrifuging at 6000 x g for 15 minutes. The supernatant was poured away and the pellet was resuspended in 700 µl of QIAzol lysis reagent. The rest was following the manufacturer's instruction.

## A.13 Confocal Microscopy

Cells were seeded in either 24-well glass-bottom plates (MatTek glass no. 1.5, uncoated) or Ibidi µ-Slide 8-well (IbiTreat with no. 1.5 polymer coverslip) the night before. They are both chambers especially for confocal microscopy. Cells were grown to approximately 80% confluent at the time of transfection.

Immediately before imaging, cell medium was removed and the cells were washed with PBS three times. Fresh colourless DMEM medium (21063-019, Life Tehnologies) was added. The

samples were than imaged using a LSM 510 META inverted fluorescence confocal microscope (Carl Zeiss) in the Sir William Dunn School of Pathology, Oxford. The microscope, which was designed for live cell imaging, had a 37ºC chamber supplied with 5% humidified $CO_2$.

Cy3 was excited by the HeNe543 laser and the emission was collected between 560 and 615 nm; Cy5 was excited by the HeNe633 laser and the emission was collected from 650 nm onward. HeNe543 and HeNe633 lasers were switched on one hour before the imaging began, in order to stabilise the laser power output. Nucleic acid stain Hoechst was excited by the Diode 405-30 laser and the emission was collected between 422 and 465 nm. All images displayed in this thesis were taken with a 63x / 1.40 Plan-Apochromat Ph3 (oil) objective.

### A.13.1 Nucleus stain

Nucleic acid stain (Hoechst 34580, Invitrogen) was used to stain the nuclei of mammalian cells in confocal microscopy. For a well in the 24-well plate, 1.5µg of Hoechst was added to the cell medium and incubated at 37˚C in a humidified 5% $CO_2$ atmosphere for 30 minutes. Then the medium was removed and fresh imaging medium was added. Staining could be done at least 6 hours prior imaging or immediately before imaging.

## A.14 Flow Cytometry

Cells were seeded in each well in a 24-well plate in growth medium the night before the transfections. At the time for cellular fluorescence measurement, cell medium was removed and cells were washed thoroughly with PBS. Cells were then incubated with 200 µl of trypsin

replacement at 37˚C for 10 minutes. Solution was pipetted up and down gently to ensure cells were in suspension. Then the plate was taken to the Dunn School for flow cytometry measurements. 200 µl of PBS was added into each well to dilute the sample. The samples were analysed using FACS Calibur flow cytometer (BD Biosciences). 20 000 cells were analysed per sample. Fluorescence channel FL1 was used to measure signal for Alexa-488 and FL4 for the Cy5 signal.

Data was analysed using a MATLAB script (Flow Cytometry GUI for MATLAB).[1] Gating was used to remove unwanted data points, such as dead cells and clumps of cells. A sample of untreated cells was used as a reference to select single cells populations. Based on the side-scattered signal (SSC) and the forward-scattered signal (FSC) of the sample, a region that represented the single cells population was drawn. Then, the signal from the normalisation fluorophore (usually Cy5 for the tetrahedron) was used to select the population of cells that had any uptake of the DNA nanostructures.

[1]: http://www.mathworks.co.uk/matlabcentral/fileexchange/38080-flow-cytometry-gui-for-matlab

# A.15 Transfection of nucleic acids

## A.15.1 Lipofectamine® 2000 (LF)

### A.15.1.1 DNA cages only

For the incubation of DNA tetrahedra in a 24-well plate format: firstly, diluted 0.2 µg of DNA tetrahedron up to 50 µl of Opti-MEM® in an Eppendorf tube. Then in a separate tube,

2 µl of LF was added to 48 µl of Opti-MEM® and the mix was incubated for 5 minutes at room temperature. Then, 50 µl of DNA tetrahedron was combined with 50 µl diluted LF. The two were mixed gently and incubated at room temperature for 1 hour. Next, the 100 µl complex was added to a well of cells containing 400 µl of Opti-MEM®. The plate was then returned to the incubator (37˚C with humidified 5% $CO_2$) for several hours. For experiment in other plate format, the materials were scaled according to the area of the well.

### A.15.1.2 DNA cages and the opening strands (see Chapter 3)

In Section 3.3, experiments involved two rounds of transfection. The first round was with the DNA cage and the second round was the signalling strand. In the first round of transfection, the procedure was exactly the same as the one described in A.15.1.1. The cages were incubated with for 3 hours. The medium was removed and cells were washed with PBS three times. Fresh growth medium was added and incubated with cells for an hour before it was removed again and be replaced with Opti-MEM®. Then, the new transfection complex would be added. The multiple washes between the two rounds of transfection were employed to remove any remaining DNA cages there were not internalised by the cells.

During the one-hour wait, the preparation of the second round of transfection began. The signalling strand was diluted to 2.4 µM in 50 µl of Opti-MEM®. 2 µl of LF was mixed with Opti-MEM® so that the final volume was also 50 µl and it was incubated for 5 minutes at room temperature. Then, the diluted DNA was mixed gently with the diluted LF and incubated at room temperature for 20 minutes. Next, the 100 µl complex was added to a well

containing 400 µl of Opti-MEM®. The plate was returned to the incubator (37˚C with humidified 5% $CO_2$) for a fixed period of time.

### A.15.1.3 DNA plasmid

In the 24-well plate format, 0.8 µg of plasmid diluted in 50µl of Opti-MEM® was transfected with 2µl of LF in 50µl of Opti-MEM®. The mix was mixed and incubated at room temperature for 20 minutes before adding into a well containing mammalian cells and 400 µl of Opti-MEM®. For experiment in other plate format, the materials were scaled according to the area of the well.

### A.15.1.4 Transfection for splicing experiments (see Section 6.2)

Splicing experiments discussed in Chapter 6 were done in 96-well plates. 8 x $10^4$ HeLa705 cells were seeded in each well in a 96-well plate in growth medium the night before.

For DNA tetrahedra (TET or $TET_{SCO}$), 15 µl of the purified sample (700 nM) was mixed with 5 µl Opti-MEM® containing 0.1 µl LF. The 20 µl complex was incubated at room temperature for 1 hour and added into each well. The final volume of the well was 100 µl. For the negative control, which was the solution soaked with polyacrylamide gel, 15 µl was used in place of the DNA tetrahedra.

For DNA TP, 15 pmoles was diluted up to 9 µl in Opti-MEM®. Then it was combined with 5 µl Opti-MEM® containing 0.1 µl LF. LF DNA complex was incubated at room temperature for 30 minutes. The mix was added to a well with final volume being 100ul.

### A.15.2 X-trememGENE HP DNA transfection reagent (XG)

Similar to LF, some experiments with XG had one or two rounds of transfection. The flow of the experiments was the same: 3 hours incubation with the duplex or the tetrahedron, then medium was removed and cells were washed. After an hour, the medium was replaced again and the second transfection complex was added.

Therefore, I would only outline the procedure involved in forming the transfection complex between DNA and XG. XG was stored at -20˚C, so firstly, XG was warmed to room temperature before adding into the DNA mixes. For the tetrahedral incubation in Chapter 3, 0.2 μg of DNA tetrahedra was diluted in 194 μl of Opti-MEM® and 6 μl of XG was then added to the mix; for the opening strand, 1.2 μl of 100 μM was diluted in 93.8 μl Opti-MEM® and 5 μl of XG was added to the mix. The final volume of all the XG-DNA mix was 200 μl in a 24-well plate experiment.

For DNA duplex in Chapter 4, 12.5 μl of 4 μM of duplex L•Q was diluted in 194 μl of Opti-MEM®; for the signalling strand, 1 μl of the 100 μM was diluted in 194 μl of Opti-MEM®. Then 5 μl of XG was added into the mix.

The XG-DNA mix was always incubated at room temperature for 30 minutes. Then the 200 μl complex was added to a well of cells containing 300 μl of Opti-MEM®.

## A.16 *In vitro* transcription (see Section 5.2.1)

MEGAscript® T7 Transcription Kit (AM 1333, Life Technologies) was used to produce a large amount of pure Renilla luciferase mRNA *in vivo* from the DNA plasmid psiCheck 2.2 (B.4.1). The plasmid has a T7 promoter and the enzyme mix from the kit contained the T7 RNA polymerase that was used to synthesise the desired mRNA.

The plasmid was first linearised by restriction enzyme EcoR1. Then according to the manufacturer's instruction, the linear DNA template was incubated with the enzyme mix and other starting materials provided in the kit at 37˚C for 6 hours. The mRNA was recovered by lithium chloride precipitation and re-suspended in nuclease-free water. The mRNA concentration was measured by absorbance at 260 nm.

## A.17 Construction of tRNA expression plasmid (see Section 5.3)

### A.17.1 tRNA Scaffold

#### A.17.1.1 Preparation of the insert

The double-strand DNA (dsDNA) insert for the plasmid was purchased from IDT as two phosphorylated oligonucleotides. They were resuspended in Milli-Q water at 100 μM. The two oligonucleotides were combined at 5 μM final concentration in Buffer A. The mix was incubated at 95 ˚C for 5 minutes in the thermal cycler and it was switched off to allow the two strands to anneal by slow cooling for approximately 30 minutes. The dsDNA was diluted to 200 nM in PBS.

### A.17.1.2 Preparation of the backbone psiCheck2.2

The construction of tRNA expression plasmid was modified from psiCheck2.2. psiCheck2.2 was first cut by restriction enzyme BglII and Xhol (NEB). 1 µg of psiCheci2.2 was mixed and incubated with 1 µl of BglII and 1 µl of Xhol in 30 µl of 1x NEB Buffer 3.1 at 37 ˚C for 2 hours. The enzyme was heat inactivated at 65 ˚C for 20 minutes.

The product was then purified with QIAquick PCR Purification Kit and examined on an agarose gel. The correct band was cut and purified.

### A.17.1.3 Combining the backbone and the insert

Then the synthetic double-stranded DNA insert was incubated with the purified backbone in the ratio of 3:1 overnight at room temperature. The following day, the mix was incubated with T4 ligase at room temperature for 2 hours. The insert had the necessary sequence for the expression of the tRNA scaffold, which included the T7 promoter, the tRNA scaffold sequence and the T7 terminator. The insert was joined to the plasmid via complementary bases generated by the cuts of the restriction enzymes.

The modified plasmid was then transformed into *E. coli* (D5Hα), followed by plasmid purifications the next day with the Qiagen Miniprep. Plasmid sequencing was done to check whether the plasmid had the intended modified sequence. The new plasmid was called psiCheck_tRNA6.

### A.17.1.4 Further modifications

Plasmid psiCheck_tRNA6 contained the tRNA scaffold, but it had two EagI restriction sites: one within the tRNA scaffold, and the other one from the backbone psiCheck2.2 (between XholI and Bam HI). Since EagI was planned to be the site of insertion for the opening sequence, the other EagI site that was outside the tRNA scaffold must be removed. Restriction enzymes XhoI and Bam HI were used to remove the unwanted EagI site.

Then DNA Polymerase I, Large (Klenow) Fragment was used to fill in the ends of the plasmid to form two blunt ends. Then, the plasmid was ligated by T4 ligase at room temperature overnight. Next, the modified plasmid was transformed into *E. coli* and followed by a miniprep for plasmid purifications. Plasmid sequencing was done to ensure the plasmid had the intended sequence. The final plasmid was called ptRNA6cut2, which only had one EagI restriction site.

## A.17.2 tRNA-RNA insert into the tRNA scaffold

The insert containing the opening sequences was prepared as described in A.17.1.1. The plasmid tRNA6cut2 was incubated with EagI as A.17.1.2. The two products were combined as A.17.1.3. Plasmid sequencing was done to check whether the plasmid had the intended modified sequence.

## A.18 Transformation of bacteria with plasmid DNA

Competent bacteria from -80˚C was thawed on ice. 25 µl of competent bacteria was mixed with 20 ng of plasmid in an Eppendorf tube. The mix was left on ice for an hour. Then, the bacteria were heat shock at 42 ˚C for 30 seconds. The tube was placed on ice for 5 minutes to recover. 400 µl of SOC medium was added into the tubes and mixed gently. 50 µl of the mix was plated and spread on a LB plate with ampicillin by sterile plastic beads. The beads were removed and the plate was incubated at 37˚C overnight.

## A.19 Plasmid purification

NEB 5-alpha competent *E. coli* (C2987I) was transformed according to the procedure described in A.18. A single colony was picked from the LB plate and it was inoculated in 3 ml of LB medium with ampicillin. It was incubated overnight at 37 ˚C with shaking. QIAprep Spin Miniprep Kit (Qiagen) was used to isolate plasmid from the bacteria culture following manufacturer's instructions.

## A.20 tRNA plasmid expression

For tRNA to be expressed, a T7 expression host, BL21 (DE3*) E. coli* was used. The bacteria was transformed and plated on LB plate with ampicillin (A.18). The plate was incubated at 37˚C overnight. In the following day, a single colony was picked and resuspended in 5 ml LB

medium with ampicillin overnight. 40 µl of 100mM IPTG was also added to the medium to induce T7 expression. RNA was extracted with miRNeasy Mini Kit the following day (A.12).

## A.21 Agilent 2100 Bioanalyzer

In Section 5.3, the RNA extracts from the bacteria were examined via the Agilent 2100 Bioanalyzer with the Small RNA Analysis Kits. The Small RNA Analysis Kit was suitable for samples with RNA samples of size 6 and 150 nucleotides (nt). The tRNA and tRNA-RNA fusion product were within this range.

The results were completed with the kind assistance of the facility manager Sheena Lee and the analysis kits were provided by the Wood group. I provided the facility manager with RNA extracts of concentrations ranging from 200 to 2000 ng/µl and the samples were ran under 1 in 100 dilutions.

The Bioanalyzer functions as an automatic RNase-free station for on-chip gel electrophoresis to perform RNA analysis. It provides automated sizing and quantification of the fragments. In brief, an appropriate chip was loaded into the Bioanalyzer and in this case, it was a chip from the Small RNA Analysis Kits. The chip contained 16 wells for 15 samples and a ladder to be loaded. The wells are interconnected by micro-channels that are filled with a siever polymer and nucleic acids fluorescence dye. The polymer forms a matrix with a suitable density for the size range of the RNA samples to be examined. With the samples loaded, the chip becomes an integrated circuit. Similar to gel electrophoresis, a voltage is applied to separate

RNAs of different sizes because they travelled at different speed. The RNA molecules are detected by the laser-induced fluorescence and the outputs are translated into gel-like images.

## A.22 RNase inhibitor

1 µl of RNase inhibitor (Roche, N808-0119) was added to 20 µl of sample mix in Section 5.3.2 to prevent potential degradation of the RNA extract.

## A.23 Construction of pU6-ssRNA plasmid (see Section 5.4)

Plasmid pU6-ssRNA was modified from pU6-neo, which was a gift from the Wood group.

### A.23.1 Preparation of the insert

The double-strand DNA (dsDNA) insert for the plasmid was purchased from IDT as two phosphorylated oligonucleotides. They were resuspended in Milli-Q water at 100 µM. The two oligonucleotides were combined at 5 µM final concentration in 1 x T4 ligase buffer. The mix was incubated at 95 ˚C for 5 minutes in the thermal cycler and it was switched off to allow the two strands to anneal by slow cooling for approximately 30 minutes. The dsDNA was diluted to 200 nM in PBS.

### A.23.2 Preparation of the pU6-neo

pU6-neo was cut by restriction enzyme Bbs1 (NEB, R0539S). 1 µg of pU6-neo was mixed and incubated with 2 µl of Bbs1 in 30 µl of 1x NEB Buffer 2 at 37 ˚C for 1 hour. The enzyme was heat inactivated at 65 ˚C for 20 minutes.

Then, the 5' phosphate from the cut plasmid was removed by Antarctic Phosphatase (NEB, M0298S) to prevent the re-joining of the plasmid to itself in the next step. 4 µl of 10x Antarctic Phosphatase Reaction Buffer, 1 µl of Antarctic Phosphatase and 5 µl of Milli-Q water were added to the mix. The mix was incubated at 37 ˚C for 1 hour. The enzyme was heat inactivated at 65 ˚C for 20 minutes.

### A.23.3 Ligation of the insert into pU6-neo

The dsDNA insert and the prepared pU6-neo were mixed in the ratio of 3:1 and incubated at room temperature for 1 hour. 1 µl of T4 ligase, 2 µl of 10 x T4 ligase buffer was added to 17 µl of sample mix and incubated overnight at room temperature before transformation (A.18).

## A.24 Luciferase Assay (see Section 6.2)

Cells were seeded in a 96-well plate the night before the antisense transfection. After specified period of treatment, luciferase expression in Hela705 was quantified by Promega Luciferase Assay System (E1500). Cell Culture Lysis Reagent (CCLR) and Luciferase Assay Reagent (LAR) were stored at -20˚C, so the appropriate amounts of chemicals were defrosted immediately before the experiment. Cell medium was removed and cells were washed with

PBS three times. Then, cells in each well were lysed with 40 µl of CCLR. The plate was left shaking at room temperature for 20 minutes. Immediately before the bioluminescence measurement, 20 µl of LAR was mixed with 20 µ of cell lysate in a black 96-well plate. The measurement was conducted in a multi-label plate reader (Perkin Elmer Victor3 1420).

## A.25 Bradford Assay (see Section 6.2)

Protein content in each sample was measured by the Bradford Assay, so that the luciferase expression of each sample would be normalised to their protein contents. Bradford Reagent (Sigma, B916) was stored at 4˚C. An appropriate amount was taken out to equilibrate in the dark to room temperature before use. 250 µl of the Bradford reagent was mixed with 5 µl of cell lysate in a transparent 96-well plate. The plate was incubated at room temperature for 10 minutes and it was covered with aluminium foil to avoid light during the incubation. Absorbance at 595 nm of the solution in each well was measured in a multi-label plate reader (Perkin Elmer Victor3 1420).

The amount of protein present was deduced from a BSA calibration curve that was measured at the same time and plotted in the range of 0.2 – 1 mg/ml.

## A.26 Buffer Exchange

Bio-Gel P-6 Column (Bio-Rad, 732-6200) was used to exchange buffer in a sample. In Section 6.2.3, contaminants from the gel purified tetrahedra led to an artefact in the experiments. Spin columns were used to remove the contaminants in the buffer. Initially, the

gel in the spin column was suspended in SSC buffer (150 mM sodium chloride, 17.5 mM sodium citrate, pH 7.0). However, it was important for the tetrahedra to remain in Buffer A. Therefore, the suspended buffer was first replaced from SSC buffer into Buffer A by three rounds of centrifugations according to the instruction given in the manual. Then 20 – 70 µl of sample was loaded into the spin column and it was centrifuged at 1000 x g for 4 minutes.

## A.27 DNA conjugation with papain (S1-pap)

Strand S1 was modified with a 5' $C_6$ thiol modification (commercially available in IDT). It was re-suspended to 100 µM in Milli-Q water. An aliquot of DNA was incubated with reducing agent TCEP in the ratio of 10 : 1 by volume for 90 minutes, in order to reduce the disulphide bond. TECP was then removed by passing the sample through a size-exclusion spin column once (A.26).

Papain (P4762, SIGMA) was dissolved in PBS to form a 100 µM solution. Sulfo-SMCC linker (Thermo Scientific, 22622 no-weigh$^{TM}$ format) was first dissolved to 20 mM in DMSO and then an equal volume of PBS was added. Sulfo-SMCC and papain was mixed in 1.5 : 1 by moles and incubated at room temperature for 1 hour. Excess linker was removed using a spin column (A.26). Papain and S1 strands were combined in 25 : 1, molar excess of papain. The mixture was left at 4˚C overnight and the product was examined in PAGE the following day. The sample was stored at 4˚C and used within a week. Gel purification (A.4) was employed to purify the product with only one DNA strand conjugated to a papain. Other products included unconjugated papain and papain conjugated with multiple DNA strands.

## A.28 Synthesis of DNA tetrahedron with papain attached (OTpap)

Equimolar S2 and S4 were mixed in excess to S1-pap in Buffer A. The mixture was annealed from 54˚C, cools down to 4˚C in approximately 3 minutes. The sample was stored at 4˚C and used within a week.

## A.29 EnzChek® protease assay

Papain activity was measured by EnzChek® protease assay (E6638, Molecular Probes). The substrate was a casein derivative that was heavily labelled with BODIPY FL. The fluorescence of BODIPY FL was self-quenched due to the heavy labelling. In the presence of papain, the substrate was digested into highly fluorescent peptides. The fluorescence was monitored by the fluorimeter (A.6) with excitation wavelength at 485 nm and emission at 530nm.

There are two components in this kit: the BODIPY FL casein substrate and the 20 x digestion buffer (containing 200 mM Tris-HCl, 2 mM sodium azide, pH7.8). The substrate was provided in vials in lyophilised form. 200 µl of PBS was added to one of the vials and the stock solution would have a concentration 1.0 mg/ml. The stock solution was stored at 4˚C and used within 4 weeks.

1x digestion buffer was prepared by addition of an appropriate volume of Milli-Q water to the 20x digestion buffer. Magnesium chloride was also added to a final concentration of 15 mM to prevent unintentional opening of the tetrahedron (discussed in Chapter 2).

Immediately before the fluorimeter experiment, the working solution was prepared by diluting the stock solution of BODIPY FL by 100-fold with the 1x digestion buffer.

In addition, adsorption of the casein substrate to the surface of the cuvette was reported by Diana Di Paolo (a DTC project student in 2012). This influenced the rate of digestion in the first 30 minutes of the assay. In order to avoid this, the cuvette was filled with 150 µl of 2mg/ml BSA solution for an hour, and then rinsed and dried overnight the day before the protease assay.

### A.29.1 OTpap

Prior to the experiment in Figure 6-5, the three samples were treated differently. For 'OTpap', it contained 60 µl of OTpap, 13 µl of 1x digestion buffer; 'OTpap DNase I' contained 60 µl of OTpap, 2 µl DNase I, 7 µl 10x DNase I Reaction Buffer and 4 µl of 1x digestion buffer; 'OTpap OS' contained 60 µl of OTpap, 2 µl of 10 µM opening strand, 11 µl of 1x digestion buffer. All three samples were incubated at 37˚C for an hour before the protease assay.

In the protease assay, each cuvette contained 70 µl of the working solution and 70 µl of the treated sample described above. 600 µl of mineral oil as added to each cuvette to prevent evaporation.

### A.29.2 S1-pap

In the second experiment that involved S1-pap (Figure 6-6), 80 µl of S1pap was mixed with 2 µl of DNase I, 9.34 µl of 10x DNase I Reaction Buffer and 2 µl of Milli-Q water. For the intact S1-pap, the DNase I was replaced with water. The samples were incubated at 37˚C for an hour before the protease assay. In the protease assay, 40 µl of the treated sample was mixed with 150 µl of 1x working solution in each cuvette. 600 µl of mineral oil as added to each cuvette to prevent evaporation.

## A.30 Digestion of samples with DNase I

DNase I (NEB) digests DNA non-specifically into di-, tir- and oligonucleotide products. It was used in Section 6.3 to digest DNA in the tetrahedron and S1-Pap. In both cases, DNA sample was in 1x DNase I Reaction buffer with 2 µl DNase I for 70-80 µl of sample, incubated at 37˚C for an hour.

## A.31 Rate constant fitting for the strand displacement reaction (See Section 2.3.6)

Strand displacement reaction is being modelled as a second-order rate reaction.

$L{\bullet}S + I \rightarrow L{\bullet}I + S$

Assuming the amount of backward reaction is negligible, the rate constant for the forward reaction is k.

$$\frac{d[L \bullet S]}{dt} = -k[L \bullet S][I] \qquad (1)$$

[A] means the concentration of A. $[A]_0$ is the initial concentration of A.

Since $[I] = [I]_0 - [L \bullet I]$ , substitute this to equation (1)

$$\frac{d[L \bullet S]}{dt} = -k[L \bullet S]([I]_0 - [L \bullet I]) \qquad (2)$$

Also, $[L \bullet I] = [L \bullet S]_0 - [L \bullet S]$, substitute this to equation (2)

$$\frac{d[L \bullet S]}{dt} = -k[L \bullet S]([I]_0 - [L \bullet S]_0 + [L \bullet S]) \qquad (3)$$

Approximating the initial concentrations of products are the same, i.e. $[I]_0 = [L \bullet S]_0$

$$\frac{d[L \bullet S]}{dt} = -k[L \bullet S]^2$$

Solving the differential equation, gives the following solution:

$$[L \bullet S] = \frac{[L \bullet S]_0}{1 + k[L \bullet S]_0 t} \qquad (4)$$

Since [L•I] is the product that gives the fluorescence signal, change the subject of equation (4) to [L•I] gives:

$$[L \bullet S]_0 - [L \bullet I] = \frac{[L \bullet S]_0}{1 + k[L \bullet S]_0 t}$$

By transforming the equation,

$$\frac{1}{[L \bullet S]_0 - [L \bullet I]} = kt + \frac{1}{[L \bullet S]_0}$$

A straight line graph was plotted, with the y-axis being $\frac{1}{[L\bullet S]_0 - [L\bullet I]}$ and *t* being the x-axis.

k is the gradient of the straight line graph and the data was fitted with a straight line equation in Excel.

## A.32 Quantitative analysis in Chapter 3 (See Section 3.2.3.2)

Quantitative analysis of confocal microscopy images was conducted in MATLAB. A confocal image that imaged through the centre of the cells was taken for analysis. Each image had 4 channels: Cy3, Cy5, Hoechst and phase contrast. They were split into 4 images in ImageJ[102] and only the Cy3 and Cy5 images were loaded as separate matrices into MATLAB.

A control image of untreated cells was used to set the lower thresholds for the Cy3 and Cy5 images independently. Each threshold was set as the level that 95% of the signals in the control image were below, so that most of the noise would be eliminated.

The image was taken in 12-bits, so the saturated value was 4096; the upper threshold was set to be 4090. Pixels that had a value between the upper and lower threshold were selected.

Cy3: Cy5 ratio of each pixel was calculated. The frequency of each Cy3:Cy5 value was weighted with the Cy5 intensity because the number of tetrahedron was proportional to the Cy5 intensity. A higher Cy5 signal meant more tetrahedra were present in the pixel. Then, a histogram of Cy3:Cy5 ratios were plotted. The distributions for opened and closed tetrahedra were compared.

# Appendix B DNA Sequences

## B.1 Oligos used in Chapter 2

### B.1.1 DNA tetrahedron 2.2 (OT2.2)

| Strand name | Sequences 5'…3' | Structure |
|---|---|---|
| S1 | */Phos/* AGG CAG TTG AGA CGA ACA TTC CTA AGT CTG AAA TTT ATC ACC CGC CAT AGT AGA CGT ATC ACC | 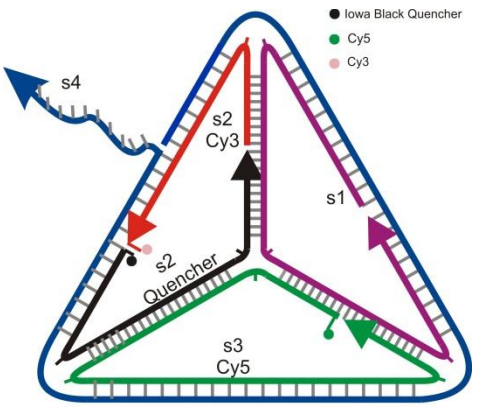 |
| S2 Cy3 | */Phos/* AGG AAT GTT CGA ATG TGA GTT TCG A /Cy3/ | |
| S2 Quencher (Iowa Black FQ) | */BkFQ/* GCC GCA GCG ATT ACA GCT TGC TAC ACG ATT CAG ACT T | |
| S3 Cy5 | /Cy5/ GGT GAT AAAACG TGT AGC AAG CTG TAA TCG ACG GGA AGA GCA TGC CCA TCC ACT ACT ATG GCG | |
| S4 | CTC ACA TAC TCA ACT GCC TGG TGA TAC GAG GAT GGG CAT GCT CTT CCC GAC TGC GGC TCG AAA ATG TTA GGGT | |
| Opening strand | ACC CTA ACA TTT TCG A | |

## B.1.2 DNA tetrahedron 6.3 (OT6.3)

| Strand name | Sequences 5'…3' | Structure |
|---|---|---|
| S1 | */Phos/* AGG CAG TTG AGA CGA ACA TTC CTA AGT CTG AAA TTT ATC ACC CGC CAT AGT AGA CGT ATC ACC | 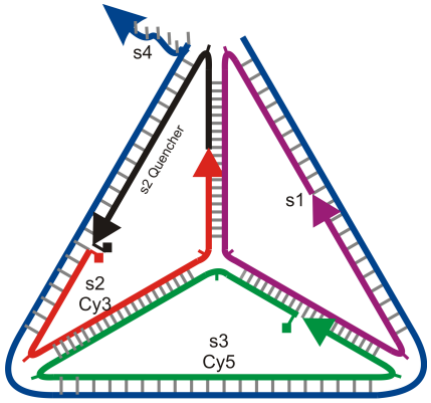 |
| S2 Cy3 | /5Cy3/GCC GCA GCG ATT ACA GCT TGC TAC ACG ATT CAG ACT T | |
| S2 Quencher (Iowa Black FQ) | /5Phos/ AGG AAT GTT CGA ATG TGA GTT TCG A */BkFQ/* | |
| S3 Cy5 | */Cy5/* GGT GAT AAAACG TGT AGC AAG CTG TAA TCG ACG GGA AGA GCA TGC CCA TCC ACT ACT ATG GCG | |
| S4 | CTCAACTGCCTGGTGATACGAGGATGGGC ATGCTCTTCCCGACTGCGGCTCGAAACTC ACATATGTTA | |
| CT_S4* | /Phos/ GCTCTTCCCGACTGCGGCTCGAAACTCAC ATACTCAACTGCCTGGTGATACGAGGATG GGCAT | |
| Opening strand[#] | TAA CAT ATG TGA GTT TCG A | |



*For the closed tetrahedron (CT), only S4 is modified, so that it can be ligated and the closed tetrahedron has no overhang.

[#] This strand is called $O_{neg}$ in Chapters 3 and 4.

## B.1.3 OT6.3SCO

| Strand name | Sequences 5'…3' | Structure |
|---|---|---|
| S1 | */Phos/* AGG CAG TTG AGA CGA ACA TTC CTA AGT CTG AAA TTT ATC ACC CGC CAT AGT AGA CGT ATC ACC | 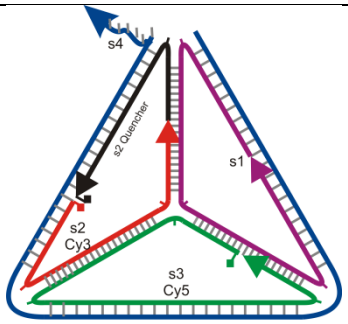 |
| S2 Cy3 | /5Cy3/GCCGCAGACGATTACAGCTTGCTACACGATTC AGACTT | |
| S2 Quencher (Iowa Black FQ) | /Phos/ AGGAATGTTCGAACCTCAGTTACAT */BkFQ/* | |
| S3 Cy5 | */Cy5/* GGT GAT AAAACG TGT AGC AAG CTG TAA TCG ACG GGA AGA GCA TGC CCA TCC ACT ACT ATG GCG | |
| S4 | CTCAACTGCCTGGTGATACGAGGATGGGCATGCTCT TCCCGACTGCGGCTTGTAACTGAGGTAAGAGG | |
| Opening strand $O_c$ | /phos/ ACCCTCGCATG ATT GmC*mC* mU*mC*mU* mU*mA*mC* mC*mU*mC* mA*mG*mU* mU*mA*mC* mA | |



m-2' O methyl bases; * - phosphorothioate backbone modification

## B.2 Oligos used in Chapter 3

| Strand name | Sequences 5'…3' | Structure |
|---|---|---|
| S1 | */Phos/* AGG CAG TTG AGA CGA ACA TTC CTA AGT CTG AAA TTT ATC ACC CGC CAT AGT AGA CGT ATC ACC | 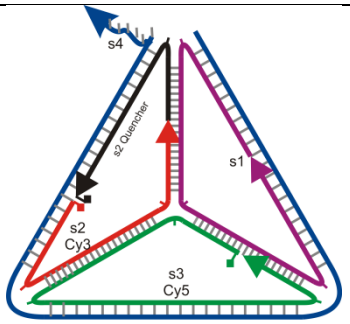 |
| S2 Cy3 | /5Cy3/GCCGCAGACGATTACAGCTTGCTACACGATTC AGACTT | |
| S2 Quencher (Iowa Black FQ) | /Phos/ AGGAATGTTCGAACCTCAGTTACAT */BkFQ/* | |
| S3 Cy5 | */Cy5/* GGT GAT AAAACG TGT AGC AAG CTG TAA TCG ACG GGA AGA GCA TGC CCA TCC ACT ACT ATG GCG | |
| S4 | CTCAACTGCCTGGTGATACGAGGATGGGCATGCTCT TCCCGACTGCGGCTTGTAACTGAGGTAAGAGG | |
| Opening strand $O_c$ | /phos/ ACCCTCGCATG ATT GmC*mC* mU*mC*mU* mU*mA*mC* mC*mU*mC* mA*mG*mU* mU*mA*mC* mA | |
| $O_{neg}$ (negative control) | ACTACAACGCCTACCTTCG | |

## B.3 Oligos used in Chapter 4

| Strand name | Sequences 5'…3' |
|---|---|
| L | TGTAACTGAGGTAAGAGGCAAT/cy5/ |
| Q (Iowa Black RQ) | /Bk RQ/ ATTGCCTCTTACCTCA |
| O | /Phos/ACCCTCGCATGATTGCCTCTTACCTCAGTTACA |
| $O_c$ | /Phos/ACCCTCGCATG ATTGmC*mC* mU*mC*mU* mU*mA*mC* mC*mU*mC* mA*mG*mU* mU*mA*mC* mA |
| O_Cy3 | /Phos/ ACCCTCGCATGATTGCCTCTTACCTCAGTTACA /Cy3/ |
| $O_{neg}$ (negative control) | ACTACAACGCCTACCTTCG |

# B.4 Oligos used in Chapter 5

## B.4.1 Plasmid psiCheck2.2

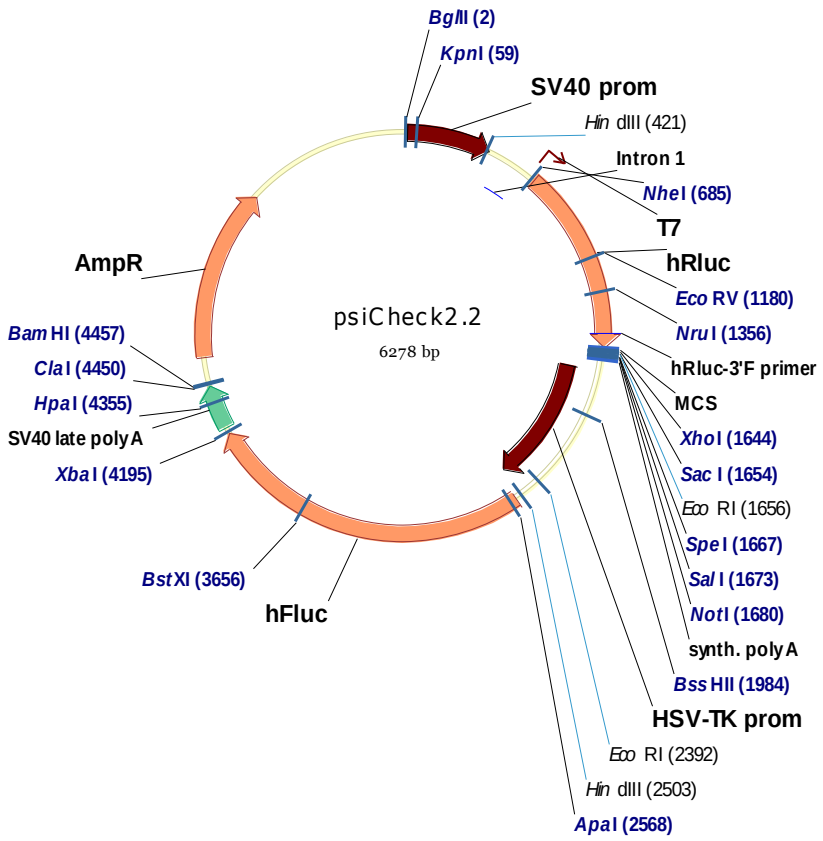


agatctgcgcagcaccatggcctgaaataacctctgaaagaggaacttggttaggtaccttctgaggcggaaagaaccagctgtgga
atgtgtgtcagttagggtgtggaaagtccccaggctccccagcaggcagaagtatgcaaagcatgcatctcaattagtcagcaaccag
gtgtggaaagtccccaggctccccagcaggcagaagtatgcaaagcatgcatctcaattagtcagcaaccatagtcccgcccctaact
ccgcccatcccgcccctaactccgcccagttccgcccattctccgccccatggctgactaatttttttatttatgcagaggccgaggccg
cctcggcctctgagctattccagaagtagtgaggaggctttttggaggcctaggcttttgcaaaaagcttgattcttctgacacaacagt
ctcgaacttaagctgcagaagttggtcgtgaggcactgggcaggtaagtatcaaggttacaagacaggtttaaggagaccaatagaaa
ctgggcttgtcgagacagagaagactcttgcgtttctgataggcacctattggtcttactgacatccactttgcctttctctccacaggtgtc
cactcccagttcaattacagctcttaaggctagagtacttaatacgactcactataggctagccaccatggcttccaaggtgtacgaccc
cgagcaacgcaaacgcatgatcactgggcctcagtggtgggctcgctgcaagcaaatgaacgtgctggactccttcatcaactactat
gattccgagaagcacgccgagaacgccgtgatttttctgcatggtaacgctgcctccagctacctgtggaggcacgtcgtgcctcacat
cgagcccgtggctagatgcatcatccctgatctgatcggaatgggtaagtccggcaagagcgggaatggctcatatcgcctcctggat
cactacaagtacctcaccgcttggttcgagctgctgaaccttccaaagaaaatcatctttgtgggccacgactgggggcttgtctggcc
tttcactactcctacgagcaccaagacaagatcaaggccatcgtccatgctgagagtgtcgtggacgtgatcgagtcctgggacgagt
ggcctgacatcgaggaggatatcgccctgatcaagagcgaagagggcgagaaaatggtgcttgagaataacttcttcgtcgagacca

tgctcccaagcaagatcatgcggaaactggagcctgaggagttcgctgcctacctggagccattcaaggagaagggcgaggttaga
cggcctaccctctcctggcctcgcgagatccctctcgttaagggaggcaagcccgacgtcgtccagattgtccgcaactacaacgcct
accttcgggccagcgacgatctgcctaagatgttcatcgagtccgaccctgggttcttttccaacgctattgtcgagggagctaagaagt
tccctaacaccgagttcgtgaaggtgaagggcctccacttcagccaggaggacgctccagatgaaatgggtaagtacatcaagagctt
cgtggagcgcgtgctgaagaacgagcagtaattctaggcgatcgctcgaggagctcgaattcccgggactagtgtcgacgcggccg
ctggccgcaataaaatatctttattttcattacatctgtgtgttggttttttgtgtgaggatctaaatgagtcttcggacctcgcgggggccgc
ttaagcggtggttagggtttgtctgacgcgggggggaggggaaggaacgaaacactctcattcggaggcggctcgggtttggtctt
ggtggccacgggcacgcagaagagcgccgcgatcctcttaagcacccccccgccctccgtggaggcgggggtttggtcggcgggt
ggtaactggcgggccgctgactcgggcgggtcgcgcgccccagagtgtgacctttcggtctgctcgcagacccccgggcggcgc
cgccgcggcggcgacgggctcgctgggtcctaggctccatggggaccgtatacgtggacaggctctggagcatccgcacgactgc
ggtgatattaccggagaccttctgcgggacgagccgggtcacgcggctgacgcggagcgtccgttgggcgacaaacaccaggacg
gggcacaggtacactatcttgtcacccggaggcgcgagggactgcaggagcttcagggagtggcgcagctgcttcatccccgtggc
ccgttgctcgcgtttgctggcggtgtccccggaagaaatatatttgcatgtctttagttctatgatgacacaaaccccgcccagcgtcttgt
cattggcgaattcgaacacgcagatgcagtcggggcggcgcggtcccaggtccacttcgcatattaaggtgacgcgtgtggcctcga
acaccgagcgaccctgcagcgacccgcttaaaagcttggcattccggtactgttggtaaagccaccatggccgatgctaagaacatta
agaagggccctgctcccttctaccctctggaggatggcaccgctggcgagcagctgcacaaggccatgaagaggtatgccctggtg
cctggcaccattgccttcaccgatgcccacattgaggtggacatcacctatgccgagtacttcgagatgtctgtgcgcctggccgaggc
catgaagaggtacggcctgaacaccaaccaccgcatcgtggtgtgctctgagaactctctgcagttcttcatgccagtgctgggcgcc
ctgttcatcggagtggccgtggcccctgctaacgacatttacaacgagcgcgagctgctgaacagcatgggcatttctcagcctaccgt
ggtgttcgtgtctaagaagggcctgcagaagatcctgaacgtgcagaagaagctgcctatcatccagaagatcatcatcatggactcta
agaccgactaccagggcttccagagcatgtacacattcgtgacatctcatctgcctcctggcttcaacgagtacgacttcgtgccagagt
ctttcgacagggacaaaaccattgccctgatcatgaacagctctgggtctaccggcctgcctaagggcgtggccctgcctcatcgcac
cgcctgtgtgcgcttctctcacgcccgcgaccctattttcggcaaccagatcatccccgacaccgctattctgagcgtggtgccattcca
ccacggcttcggcatgttcaccaccctgggctacctgatttgcggctttcgggtggtgctgatgtaccgcttcgaggaggagctgttcct
gcgcagcctgcaagactacaaaattcagtctgccctgctggtgccaaccctgttcagcttcttcgctaagagcaccctgatcgacaagt
acgacctgtctaacctgcacgagattgcctctggcggcgccccactgtctaaggaggtgggcgaagccgtggccaagcgctttcatct
gccaggcatccgccagggctacggcctgaccgagacaaccagcgccattctgattaccccagagggcgacgacaagcctggcgc
cgtgggcaaggtggtgccattcttcgaggccaaggtggtggacctggacaccggcaagaccctgggagtgaaccagcgcggcga
gctgtgtgtgcgcggccctatgattatgtccggctacgtgaataaccctgaggccacaaacgccctgatcgacaaggacggctggctg
cactctggcgacattgcctactgggacgaggacgagcacttcttcatcgtggaccgcctgaagtctctgatcaagtacaagggctacc
aggtggccccagccgagctggagtctatcctgctgcagcaccctaacattttcgacgccggagtggccggcctgcccgacgacgat
gccggcgagctgcctgccgccgtcgtcgtgctggaacacggcaagaccatgaccgagaaggagatcgtggactatgtggccagcc
aggtgacaaccgccaagaagctgcgcggcggagtggtgttcgtggacgaggtgcccaagggcctgaccggcaagctggacgccc
gcaagatccgcgagatcctgatcaaggctaagaaaggcggcaagatcgccgtgtaataattctagagtcggggcggccggccgctt
cgagcagacatgataagatacattgatgagtttggacaaaccacaactagaatgcagtgaaaaaaatgctttatttgtgaaatttgtgatg
ctattgctttatttgtaaccattataagctgcaataaacaagttaacaacaacaattgcattcattttatgtttcaggttcagggggaggtgtg
ggaggttttttaaagcaagtaaaacctctacaaatgtggtaaaatcgataaggatccaggtggcacttttcggggaaatgtgcgcggaa
cccctatttgtttatttttctaaatacattcaaatatgtatccgctcatgagacaataaccctgataaatgcttcaataatattgaaaaaggaag
agtatgagtattcaacatttccgtgtcgcccttattcccttttttgcggcattttgccttcctgtttttgctcacccagaaacgctggtgaaagt
aaaagatgctgaagatcagttgggtgcacgagtgggttacatcgaactggatctcaacagcggtaagatccttgagagttttcgccccg
aagaacgttttccaatgatgagcacttttaaagttctgctatgtggcgcggtattatcccgtattgacgccgggcaagagcaactcggtcg
ccgcatacactattctcagaatgacttggttgagtactcaccagtcacagaaaagcatcttacggatggcatgacagtaagagaattatg
cagtgctgccataaccatgagtgataacactgcggccaacttacttctgacaacgatcggaggaccgaaggagctaaccgcttttttgc
acaacatgggggatcatgtaactcgccttgatcgttgggaaccggagctgaatgaagccataccaaacgacgagcgtgacaccacg
atgcctgtagcaatggcaacaacgttgcgcaaactattaactggcgaactacttactctagcttcccggcaacaattaatagactggatg

gaggcggataaagttgcaggaccacttctgcgctcggcccttccggctggctggtttattgctgataaatctggagccggtgagcgtgg
gtctcgcggtatcattgcagcactggggccagatggtaagccctcccgtatcgtagttatctacacgacggggagtcaggcaactatg
gatgaacgaaatagacagatcgctgagataggtgcctcactgattaagcattggtaactgtcagaccaagtttactcatatatactttagat
tgatttaaaacttcatttttaatttaaaaggatctaggtgaagatccttttgataatctcatgaccaaaatcccttaacgtgagttttcgttcca
ctgagcgtcagaccccgtagaaaagatcaaaggatcttcttgagatcctttttttctgcgcgtaatctgctgcttgcaaacaaaaaaaccca
ccgctaccagcggtggtttgtttgccggatcaagagctaccaactctttttccgaaggtaactggcttcagcagagcgcagataccaaat
actgttcttctagtgtagccgtagttaggccaccacttcaagaactctgtagcaccgcctacatacctcgctctgctaatcctgttaccagt
ggctgctgccagtggcgataagtcgtgtcttaccgggttggactcaagacgatagttaccggataaggcgcagcggtcgggctgaac
gggggttcgtgcacacagcccagcttggagcgaacgacctacaccgaactgagatacctacagcgtgagctatgagaaagcgcc
acgcttcccgaagggagaaaggcggacaggtatccggtaagcggcagggtcggaacaggagagcgcacgagggagcttccagg
gggaaacgcctggtatctttatagtcctgtcgggtttcgccacctctgacttgagcgtcgatttttgtgatgctcgtcaggggggcggagc
ctatggaaaaacgccagcaacgcggccttttacggttcctggccttttgctggccttttgctcacatggctcgac

*The gene for Renilla luciferase is highlighted in blue and the sequence for regions 744 and 990 are underlined.*

## B.4.2 OT990 and OT744

| Strand name | Sequences 5'…3' | Structure |
|---|---|---|
| S1 | */Phos/* AGG CAG TTG AGA CGA ACA TTC CTA AGT CTG AAA TTT ATC ACC CGC CAT AGT AGA CGT | 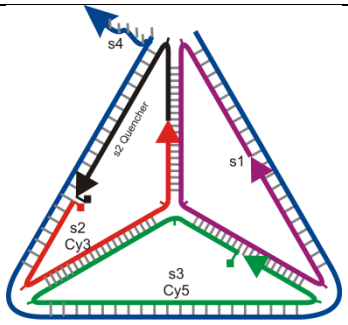 |
| S2 Cy3 | /5Cy3/GCCGCAGACGATTACAGCTTGCTACACGATTC AGACTT | |
| S3 Cy5 | */Cy5/* GGT GAT AAAACG TGT AGC AAG CTG TAA TCG ACG GGA AGA GCA TGC CCA TCC ACT ACT ATG GCG | |
| S2 Quencher 744 (Iowa Black FQ) | /5Phos/ AGGAATGTTCGAACGCCTACCTTCG /BkFQ/ | |
| S2 Quencher 990 (Iowa Black FQ) | /5Phos/ AGGAATGTTCGACCGGGACTAGTGT / BkFQ/ | |
| S4_744 | CTCAACTGCCTGGTGATACGAGGATGGGCATGCTCT TCCCGACTGCGGCCGAAGGTAGGCGTTGTAGT | |
| S4_990 | CTCAACTGCCTGGTGATACGAGGATGGGCATGCTCT TCCCGACTGCGGCACACTAGTCCCGGGAATTC | |

OT990 and OT744 share the same S1, S2 Cy3, S3 Cy5

### B.4.3 ptRNA6cut2

AGATCTCGATCCCGCGAAATTAATACGACTCACTATAGGGGCCCGGATAGCTCAGTCGGTAGAGC
AGCGGCCGCGGGTCCAGGGTTCAAGTCCCTGTTCGGGCGCCATAGCATAACCCCTTGGGGCCTCTA
AACGGGTCTTGAGGGGTTTTTTGCTCGAGGAGCTCGAATTGATCCAGGTGGCACTTTTCGGGGAAA
TGTGCGCGGAACCCCTATTTGTTTATTTTTCTAAATACATTCAAATATGTATCCGCTCATGAGACAA
TAACCCTGATAAATGCTTCAATAATATTGAAAAAGGAAGAGTATGAGTATTCAACATTTCCGTGTC
GCCCTTATTCCCTTTTTTGCGGCATTTTGCCTTCCTGTTTTTGCTCACCCAGAAACGCTGGTGAAAG
TAAAAGATGCTGAAGATCAGTTGGGTGCACGAGTGGGTTACATCGAACTGGATCTCAACAGCGGT
AAGATCCTTGAGAGTTTTCGCCCCGAAGAACGTTTTCCAATGATGAGCACTTTTAAAGTTCTGCTA
TGTGGCGCGGTATTATCCCGTATTGACGCCGGGCAAGAGCAACTCGGTCGCCGCATACACTATTCT
CAGAATGACTTGGTTGAGTACTCACCAGTCACAGAAAAGCATCTTACGGATGGCATGACAGTAAG
AGAATTATGCAGTGCTGCCATAACCATGAGTGATAACACTGCGGCCAACTTACTTCTGACAACGAT
CGGAGGACCGAAGGAGCTAACCGCTTTTTTGCACAACATGGGGGATCATGTAACTCGCCTTGATCG
TTGGGAACCGGAGCTGAATGAAGCCATACCAAACGACGAGCGTGACACCACGATGCCTGTAGCAA
TGGCAACAACGTTGCGCAAACTATTAACTGGCGAACTACTTACTCTAGCTTCCCGGCAACAATTAA
TAGACTGGATGGAGGCGGATAAAGTTGCAGGACCACTTCTGCGCTCGGCCCTTCCGGCTGGCTGGT
TTATTGCTGATAAATCTGGAGCCGGTGAGCGTGGGTCTCGCGGTATCATTGCAGCACTGGGGCCAG
ATGGTAAGCCCTCCCGTATCGTAGTTATCTACACGACGGGGAGTCAGGCAACTATGGATGAACGA
AATAGACAGATCGCTGAGATAGGTGCCTCACTGATTAAGCATTGGTAACTGTCAGACCAAGTTTAC
TCATATATACTTTAGATTGATTTAAAACTTCATTTTTAATTTAAAAGGATCTAGGTGAAGATCCTTT
TTGATAATCTCATGACCAAAATCCCTTAACGTGAGTTTTCGTTCCACTGAGCGTCAGACCCCGTAG
AAAAGATCAAAGGATCTTCTTGAGATCCTTTTTTTCTGCGCGTAATCTGCTGCTTGCAAACAAAAA
AACCACCGCTACCAGCGGTGGTTTGTTTGCCGGATCAAGAGCTACCAACTCTTTTTCCGAAGGTAA
CTGGCTTCAGCAGAGCGCAGATACCAAATACTGTTCTTCTAGTGTAGCCGTAGTTAGGCCACCACT
TCAAGAACTCTGTAGCACCGCCTACATACCTCGCTCTGCTAATCCTGTTACCAGTGGCTGCTGCCA
GTGGCGATAAGTCGTGTCTTACCGGGTTGGACTCAAGACGATAGTTACCGGATAAGGCGCAGCGG
TCGGGCTGAACGGGGGGTTCGTGCACACAGCCCAGCTTGGAGCGAACGACCTACACCGAACTGAG
ATACCTACAGCGTGAGCTATGAGAAAGCGCCACGCTTCCCGAAGGGAGAAAGGCGGACAGGTATC
CGGTAAGCGGCAGGGTCGGAACAGGAGAGCGCACGAGGGAGCTTCCAGGGGGAAACGCCTGGTA
TCTTTATAGTCCTGTCGGGTTTCGCCACCTCTGACTTGAGCGTCGATTTTTGTGATGCTCGTCAGGG
GGGCGGAGCCTATGGAAAAACGCCAGCAACGCGGCCTTTTTACGGTTCCTGGCCTTTTGCTGGCCT
TTTGCTCACATGGCTCGAC

### B.4.4 tRNA-RNA fusion

| Strand name | Sequences 5'…3' |
|---|---|
| tRNA scaffold insert | AGATCT CGATCCCGCGAAAT TAATACGACTCACTATA GGG GCCCGGATAG CTCAGTCGGT AGAGCAG CGGCCG CGGGTCCAGG GTTCAAGTCC CTGTTCGGGC GCCA TAGCATAACCCCTTGGGGCCTCTAAACGGGTCTTGAGGGGTTTTTTG CTCGAG |
| tRNA-RNA insert | CGGCCG CCTCC ACCTCTTACCTCAGTTACAA TCTCC CGGCCG |
| FAM-SCO' | /FAM/ GTAACTGAGGTAAGAGGCAATCATGCGAGGGT |

The tRNA is highlighted in blue and orange. The orange region is the restriction site for EagI. The pink region is the restriction sites of Bgl II and XhoI. The underlined regions are the T7 promoter and the T7 terminator.

### B.4.5 Short RNA

Forward sequence of the insert:
5' /5Phos/CAC CGA CTA CAA CGC CTA CCT TCG 3'
G is where the transcription starts

Backward sequence of the insert:
5' /5Phos/ AAA ACG AAG GTA GGC GTT GTA GTC 3'
AAA A is the termination signal for the U6 small nuclear RNA promoter

# B.5 Oligos used in Chapter 6

## B.5.1 $TET_{SCO}$

| Strand name | Sequences 5'…3' | Structure |
|---|---|---|
| S1 | */Phos/* AGG CAG TTG AGA CGA ACA TTC CTA AGT CTG AAA TTT ATC ACC CGC CAT AGT AGA CGT ATC ACC | 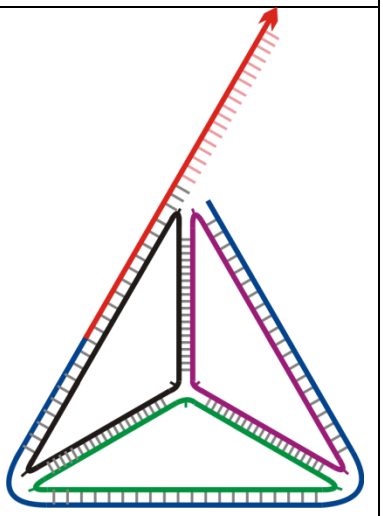 |
| S2 | /Phos/CTTGCTACACGATTCAGACTTAGGAATGTTCG ACATGCGAGGGTCCAATACCGACGATTACAG | |
| S3 | */Phos/* GGT GAT AAAACG TGT AGC AAG CTG TAA TCG ACG GGA AGA GCA TGC CCA TCC ACT ACT ATG GCG | |
| S4 partial | CTCAACTGCCTGGTGATACGAGGATGGGCATGCTCT TCCCGACGGTATTG | |
| SCO (same as $O_c$) | /phos/ ACCCTCGCATG ATT GmC*mC* mU*mC*mU* mU*mA*mC* mC*mU*mC* mA*mG*mU* mU*mA*mC* mA | |

m-2' O methyl bases; * - phosphorothioate backbone modification

## B.5.2 TET

| Strand name | Sequences 5'…3' |
|---|---|
| S1 | */Phos/* AGGCAGTTGAGACGAACATTCCTAAGTCTGAAATTTATCACCCGCCATAGTAGACGTATCACC |
| S2 | */Phos* /CTTGCTACACGATTCAGACTTAGGAATGTTCGACATGCGAGGGTCCAATACCGACGATTACAG |
| S3 | */Phos/* GGTGATAAAACGTGTAGCAAGCTGTAATCGACGGGAAGAGCATGCCCATCCACTACTATGGCG |
| S4 | */Phos/*CCCTCGCATGACTCAACTGCCTGGTGATACGAGGATGGGCATGCTCTTCCCGACGGTATTG GA |

### B.5.3 Triangular prism (TP)

| Strand name | Sequences 5'…3' |
|---|---|
| TP1 | TCGCTGAGTA TTTT TGTAACTGAGGTAAGAGGCA TTTT GCAAGTGTGGGCACGCACAC<br>TTTT TGTAACTGAGGTAAGAGGCATTTTCACAAATCTG |
| TP2 | CACTGGTCAGTTTTTGTAACTGAGGTAAGAGGCATTTTTACTCAGCGACAGATTTGTGTT<br>TTTGTAACTGAGGTAAGAGGCATTTTGGTTTGCTGA |
| TP3 | CCACACTTGCTTTT TGTAACTGAGGTAAGAGGCA TTTTCTGACCAGTGTCAGCAAACC<br>TTTTTGTAACTGAGGTAAGAGGCATTTTGTGTGCGTGC |

### B.5.4 Papain encapsulated tetrahedron (OTpap)

| Strand name | Sequences 5'…3' |
|---|---|
| S1(+2) Thiol | /ThioMC6D/<br>CCAGGCAGTTGAGACGAACATTCCTAAGTCTGAAATTTATCACCCGCCATAGTAGACGT<br>ATCA |
| S2 | /Phos/<br>GCCGCAGACGATTACAGCTTGCTACACGATTCAGACTTAGGAATGTTCGAATGTGAGTT<br>TCGA |
| S3 | /Phos/<br>GGTGATAAAACGTGTAGCAAGCTGTAATCGACGGGAAGAGCATGCCCATCCACTACTA<br>TGGCG |
| S4 | /Phos/<br>CTCACATACTCAACTGCCTGGTGATACGAGGATGGGCATGCTCTTCCCGACTGCGGCTC<br>GAAAATGTTAGGGT |
| Opening strand OS | ACCCTAACATTTTCGA |

### B.5.5 $Tet_{small}$

| Strand name | Sequences 5'…3' | Structure |
|---|---|---|
| S1 | /Phos/TTGAGACGAACATTCCATTTATCACCCAGGCAG | 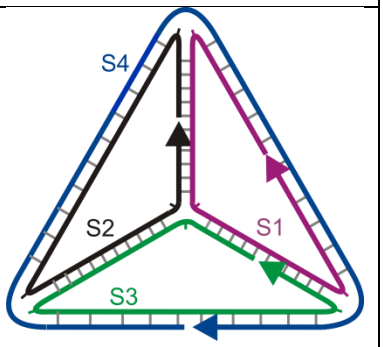 |
| S2 | /Phos/ GTTCGAATGCGAGGGTACGATTACAGCAGGAAT | |
| S3 | /Phos/ATAAAAGCTGTAATCGACGGGAAGAGCAGGGTG | |
| S4 | /Phos/ TCCCGAACCCTCGCATACTCAACTGCCAGCTCT | |



### B.5.6 $Tet_{small}2$

| Strand name | Sequences 5'…3' | Structure |
|---|---|---|
| S1 | /Phos/TTGAGACGAACATTCCATTTATCACCCAGGCAG | 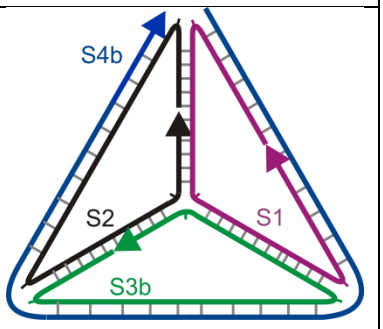 |
| S2 | /Phos/ GTTCGAATGCGAGGGTACGATTACAGCAGGAAT | |
| S3b | /phos/AATCGACGGGAAGAGCAGGGTGATAAAAGCTGT | |
| S4b | CTCAACTGCCAGCTCTTCCCGAACCCTCGCAT | |

# Appendix C Additional experimental results

## C.1 FRET signal within the tetrahedron

In Section 2.2.1, the use of the Cy3:Cy5 ratio to determine the fraction of open cages was explained. Since Cy3 and Cy5 is a FRET pair, it could interfere with the readout. Figure C-1 show that the FRET (green triangles) was detectable in the spectrometer, but it was not significant. The addition of opening strands led to over a 10 times increase of the Cy3 fluorescence, from 25 a.u. to 350 a.u., and the Cy5 signal was relatively stable (~220 a.u.). On the other hand, the FRET signals were below 30 a.u. throughout the experiment. Therefore, it is valid to use of the Cy3:Cy5 ratio to determine the fraction of open cages.

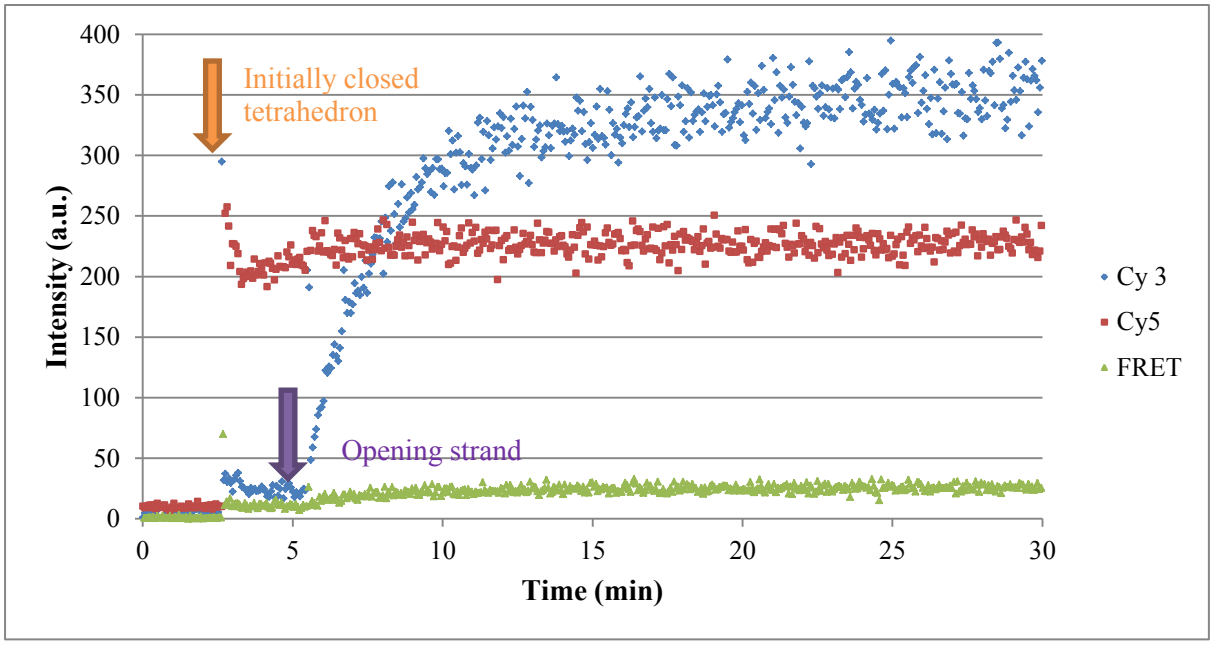


Figure C-1: Fluorescence measurements of the initially closed tetrahedron. In the beginning, there was 120 µl of Buffer A in the cuvette. At 3 mins, 20 µl of tetrahedron was added into the cuvette. The tetrahedron was in the closed state. The Cy5 signal (red squares) was high, which indicates the presence of the tetrahedron and the Cy3 signal (blue diamonds) was low because it was next to the quencher. The FRET signal between Cy3 and Cy5 was low, around 12 a.u. At 5 mins, 10 µl of 4 µM opening strand was added to the cuvette, which led to the opening of the cages. The FRET signal increased and stabilised to about 27 a.u. This demonstrates that there were FRET between the Cy3-Cy5 pair, but it was low when compared to the Cy3 and Cy5 signals alone.

## C.2 Effect of the addition of EDTA on OT2.2

Unintentional opening due to magnesium ion depletion was investigated further by stepwise addition of EDTA to the closed tetrahedron (OT2.2) in Buffer A. The fluorescence signals were monitored in the fluorimeter (Appendix A.6).

One EDTA molecule chelates with one $Mg^{2+}$, so the addition of EDTA decreases the concentration of magnesium ions. In Figure C-1, the Cy3:Cy5 ratio increased as $Mg^{2+}$ concentration decreased. This indicated that a growing proportion of the closed tetrahedra had become open. At 10 mM $MgCl_2$, the Cy3:Cy5 ratio was similar to a fully-opened sample. Further reductions in the levels of $Mg^{2+}$ did not increase the Cy3 signal. This suggested that all cages were already opened at a magnesium ion concentration that was 10 times more than the cytosolic concentration. Therefore, the supposedly closed tetrahedra would become open when transferred to the tissue culture. In agreement with the previous section, a new design was therefore needed.

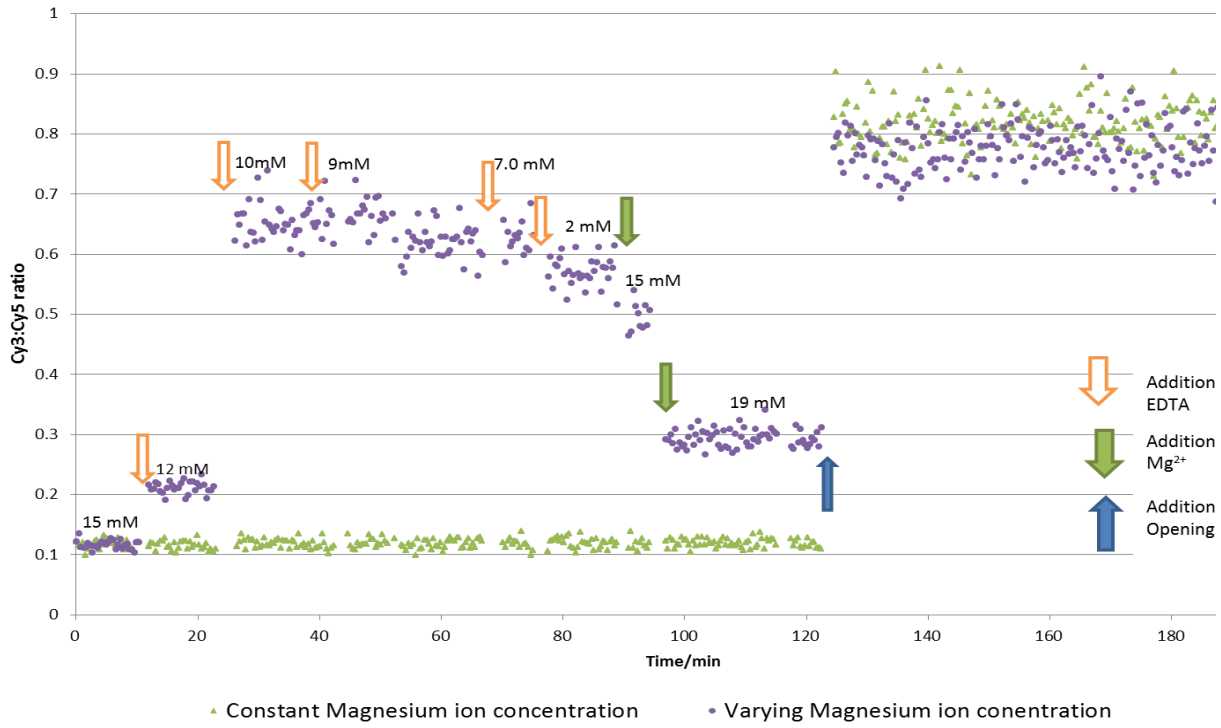


Figure C-2: Fluorescence measurement of closed tetrahedron (OT2.2). One sample (green triangle) had a constant magnesium ion concentration (15mM) throughout the experiment. The magnesium concentration of the other sample (represented by purple circles) was varied by adding EDTA. Initially, the buffer had 15mM magnesium ions and the cage was closed, hence the low Cy3:Cy5 fluorescence signal. By adding EDTA (the orange arrows), EDTA molecules chelated with magnesium ions and reduced the concentration of magnesium ions in the buffer. The subsequent magnesium ion concentrations are written on the figure next to the arrows. The Cy3:Cy5 signal increased as the magnesium ion concentration decreased. This suggests a proportion of the cage was not closed because the signal was no longer quenched by the quencher. The addition of magnesium ions (the green arrows) partially restored the Cy3: Cy5 ratio. Finally, adding the opening strand increased the Cy3: Cy5 ratio for both samples.

## C.3 Open and closed state in HEK-293 cells

In Section 3.2.2, I explained that the open and closed state of the DNA cages were established in both HEK-293 and MCF7 cells. Figure C-2 shows the flow cytometry results with HEK-293. 0.2 µg of DNA cages were transfected into HEK-293 cells with the aid of LF for 4 hr before the cellular fluorescence was determined by the flow cytometry.

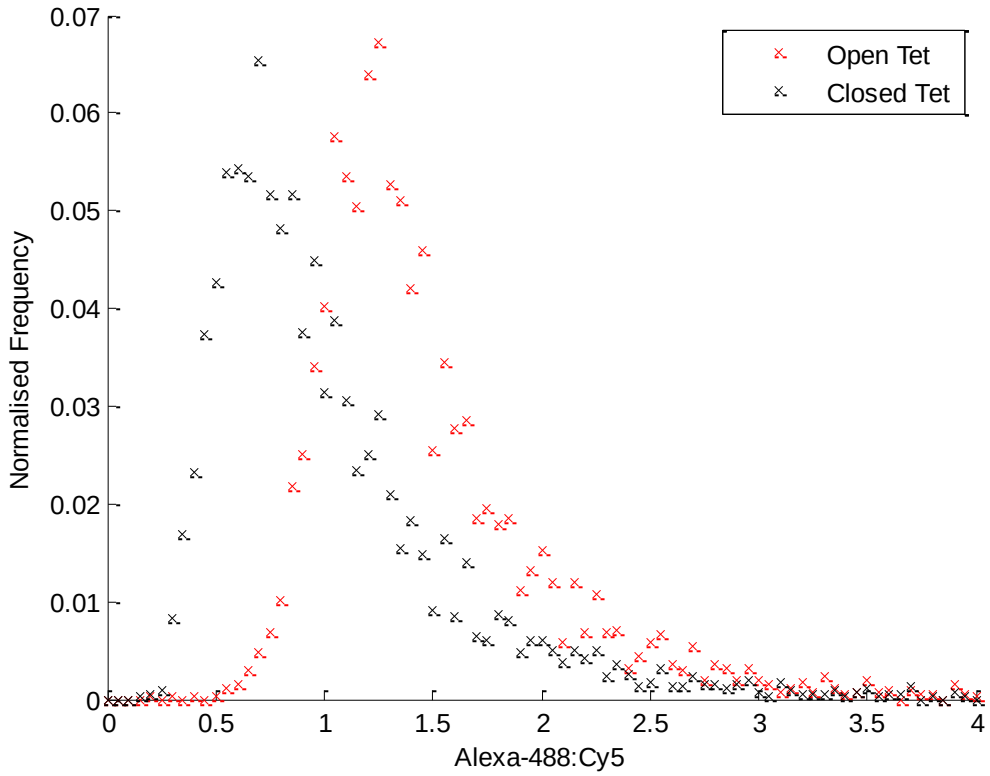


Figure C-3: Distributions of the Alexa-488:Cy5 in HEK-293. HEK-293 cells were transfected with the open (red) and closed (black) tetrahedra for 4 hr. The two distributions are clearly distinguishable and so the positive (open) and negative(closed) control were established in HEK-293 cells.

## C.4 Comparison between the cellular uptake of HEK-293 and HeLa cells

0.2 μg of DNA cages were transfected into HeLa and HEK-293 cells with the aid of LF and the samples were incubated for three hours. HeLa cellular fluorescence was approximately half of that in HEK-293, according to the flow cytometry measurement (Figure C-3). Therefore, the use of the HeLa cells was discontinued.

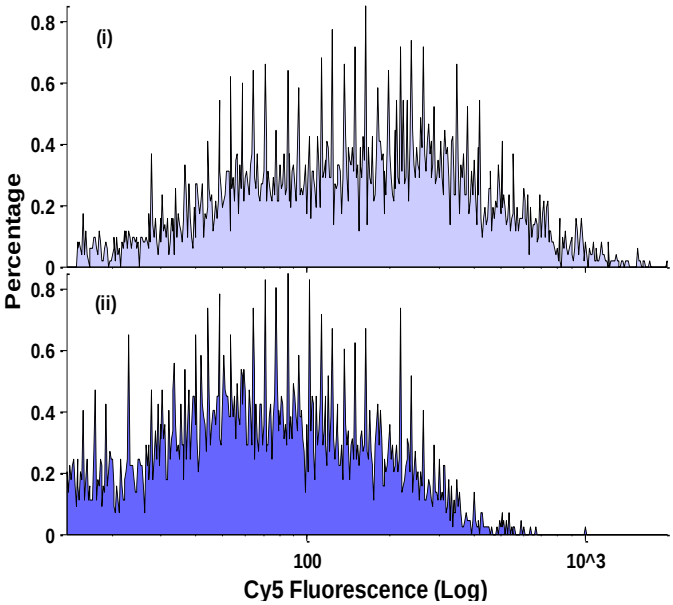


Figure C-4: Flow cytometry measurement to examine the uptake of cages into different cell lines. The uptake of Cy5-labelled tetrahedra into (i) HEK-293and (ii) HeLa cells. HEK-293 cells overall have more cages than HeLa cells because they have a higher Cy5 fluorescence. Therefore, HEK-293 was selected.

## C.5 FRET signal within L•O_Cy3

In Section 4.3.6, the signalling strand was modified with a Cy3 at the 3' end. It was designed to hybridise with Strand L and to displace Strand Q to form a new duplex called L•O_Cy3 (Figure C-5). The Cy3 and Cy5 are at the opposite ends of the duplex, 22 base pairs apart and that is approximately 7 nm.

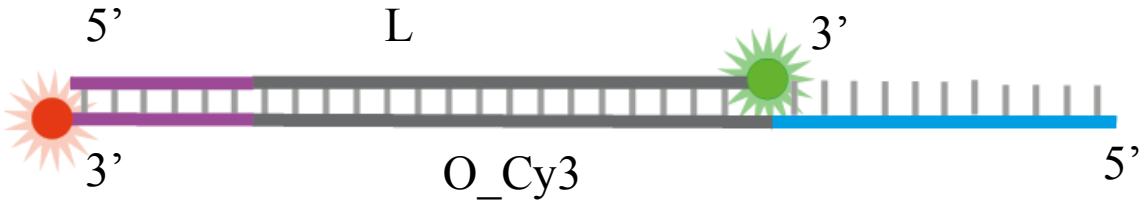


Figure. C-5: The schematic diagram of the duplex L•O_Cy3.

A fluorimeter experiment was conducted to measure the extent of FRET between the fluorophores (Figure C-6). Two measurements were taken for each sample: 1) emission at 665 nm with excitation at 650 nm, which corresponded to the Cy5 signal (blue diamonds and crosses); 2) emission at 665nm with excitation at 550 nm (red diamonds and crosses).

Initially, sample 1 contained 1 μM of O_Cy3 in Buffer A and sample 2 contained 1 μM of control strand with a Cy3 at its 3'. There was no Cy5 fluorophores in the sample, so both sample 1 and 2 had very low Cy5 signal. When both samples were excited at 550 nm, Cy3 was excited and emitted signals that bleedthrough to 650 nm. This was not a FRET signal because no Cy5 was present at this stage. The bleedthrough signal was less than 10% of the signal measured at Cy3 peak emission (565 nm). The data for emission at 565 nm was not

included in the figure below because the channel was saturated at 1000 a.u. throughout the experiment. (In addition, although both samples had the same concentration of Cy3, the control sample was 70% brighter. This could be attributed to a combination of pipetting discrepancy, slight variations between cuvettes and the age of the fluorophores. One sample might be bleached more than the other. However, this should not affect the conclusion of the data.)

Shortly after 7 minutes, 100 nM of L•Q was added into both samples. In sample 2, the control strand was not expected to interact with L•Q, so the Cy5 signal remained low (blue crosses). The Cy3 signal (red crosses) in sample 2 decreased slightly due to the dilution effect.

In sample 1, strand L was displaced from strand Q by O_Cy3, so there was a sharp increase of the Cy5 signal (blue diamonds) indicating L•O_Cy3 was formed. However, when sample 1 was excited at 550 nm, the emission at 650 nm (red diamond) remained similar to its previous level. This demonstrated that there was some, but insufficient amount of FRET between the two fluorophores under the current instrument setting.

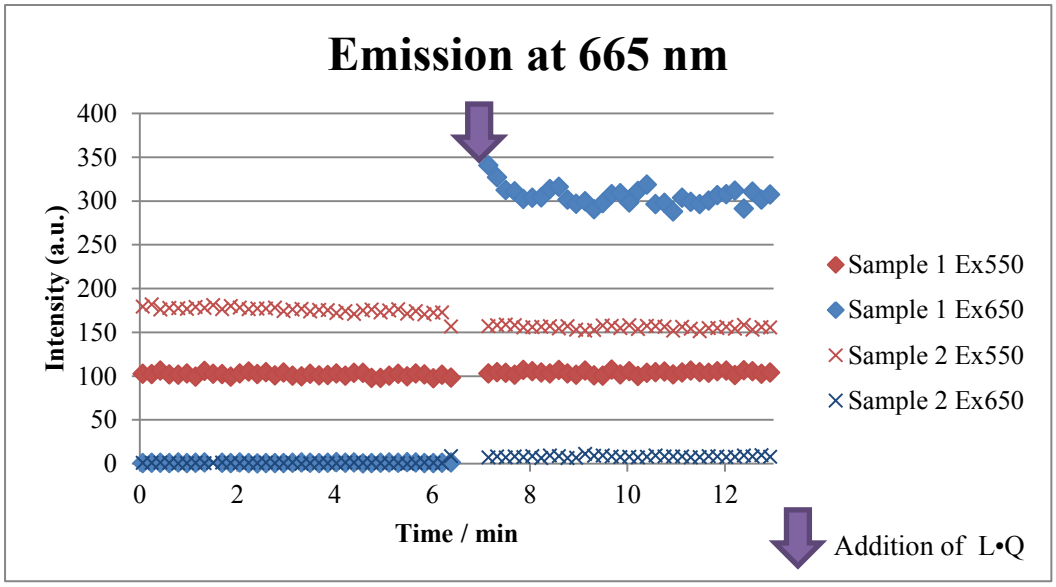


Figure. C-6: Fluorimeter measurement of FRET signals within L•O_Cy3. Initially, 1 µM of O_Cy3 was present in sample 1 (diamonds) and 1 µM of control strand with a Cy3 at its 3' end in sample 2 (crosses). Both samples had low emission at 665 nm when they were excited at 650 nm (blue); both had a detectable bleedthrough signal from Cy3 at 665 nm when it was excited at 550 nm. At 7 minutes, L•Q was added and this led to an increase in Cy5 signal in Sample 1 because Strand L was displaced from strand Q by O_Cy3. There was no significant increase of emission at 665 nm upon excitation at 550 nm. Therefore, it was concluded that the extent of FRET between Cy3 and Cy5 on L•O_Cy3 was small.

## C.6 Dose response of modified SCO

The SCO used in Chapter 6 was based on the original antisense reported by Kang et al,[98] but it had 13 extra nucleotides (nt) at the 5' end so that it could be attached to the tetrahedron via hybridisation. A dose response experiment was conducted to verify that the SCO retained its splice-correcting function with the extra nucleotides. 10 to 100 pmol of SCO was transfected to HeLa705 cells in a 96 well plate, with the aid of 0.5 µl of LF per well (Appendix A.15.1). The luciferase expression was measured after 24 hours of incubation (Appendix A.24).

Figure C-7 shows the fold-increase in luciferase expression in the treated cells when compared to the untreated cells. 20 pmol (100 nM) of SCO resulted in over 60-fold increase in luciferase expression when compared to the untreated cells. In the literature, 200n nM of the original splice-correcting oligo (without the extra nucleotides) induced a 70-fold increase in a similar experimental setting,[97] so the two values were comparable. Therefore, SCO retained the splice-correcting function.

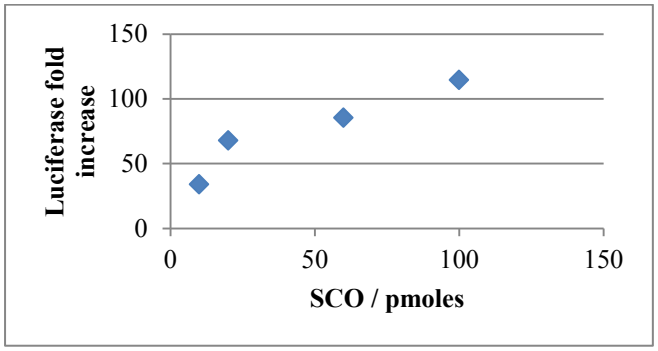


Figure. C-7: Dose response of SCO in HeLa705. SCO was transfected with the aid of LF and it retained its splice-correcting functionality.

# References


1. Bae YH, Park K. Targeted drug delivery to tumors: Myths, reality and possibility. *Journal of Controlled Release*. 2011;153:198-205. doi:10.1016/j.jconrel.2011.06.001.

2. Walsh AS, Yin H, Erben CM, Wood MJA, Turberfield AJ. DNA cage delivery to mammalian cells. In: *ACS Nano*. Vol 5. ; 2011:5427-5432. doi:10.1021/nn2005574.

3. Pei H, Liang L, Yao G, Li J, Huang Q, Fan C. Reconfigurable three-dimensional DNA nanostructures for the construction of intracellular logic sensors. *Angewandte Chemie - International Edition*. 2012;51:9020-9024. doi:10.1002/anie.201202356.

4. Liang L, Li J, Li Q, et al. Single-particle tracking and modulation of cell entry pathways of a tetrahedral DNA nanostructure in live cells. *Angewandte Chemie (International ed in English)*. 2014;53(30):7745-7750. doi:10.1002/anie.201403236.

5. Chen JH, Seeman NC. Synthesis from DNA of a molecule with the connectivity of a cube. *Nature*. 1991;350:631-633. doi:10.1038/350631a0.

6. Goodman RP, Berry RM, Turberfield AJ. The single-step synthesis of a DNA tetrahedron. *Chemical communications (Cambridge, England)*. 2004:1372-1373. doi:10.1039/b402293a.

7. He Y, Ye T, Su M, et al. Hierarchical self-assembly of DNA into symmetric supramolecular polyhedra. *Nature*. 2008;452:198-201. doi:10.1038/nature06597.

8. Bath J, Turberfield AJ. DNA nanomachines. *Nature nanotechnology*. 2007;2:275-284. doi:10.1038/nnano.2007.104.

9. Rothemund PWK. Folding DNA to create nanoscale shapes and patterns. *Nature*. 2006;440:297-302. doi:10.1038/nature04586.

10. Dietz H, Douglas SM, Shih WM. Folding DNA into twisted and curved nanoscale shapes. *Science (New York, NY)*. 2009;325:725-730. doi:10.1126/science.1174251.

11. Han D, Pal S, Nangreave J, Deng Z, Liu Y, Yan H. DNA origami with complex curvatures in three-dimensional space. *Science (New York, NY)*. 2011;332:342-346. doi:10.1126/science.1202998.

12. Ke Y, Ong LL, Shih WM, Yin P. Three-dimensional structures self-assembled from DNA bricks. *Science (New York, NY)*. 2012;338(6111):1177-1183. doi:10.1126/science.1227268.

13. Erben CM, Goodman RP, Turberfield AJ. Single-molecule protein encapsulation in a rigid DNA cage. *Angewandte Chemie - International Edition*. 2006;45:7414-7417. doi:10.1002/anie.200603392.

14. Crawford R, Erben CM, Periz J, et al. Non-covalent single transcription factor encapsulation inside a DNA cage. *Angewandte Chemie - International Edition*. 2013;52:2284-2288. doi:10.1002/anie.201207914.

15. Voigt N V, Tørring T, Rotaru A, et al. Single-molecule chemical reactions on DNA origami. *Nature nanotechnology*. 2010;5:200-203. doi:10.1038/nnano.2010.5.

16. Fu J, Liu M, Liu Y, Woodbury NW, Yan H. Interenzyme substrate diffusion for an enzyme cascade organized on spatially addressable DNA nanostructures. *Journal of the American Chemical Society*. 2012;134:5516-5519. doi:10.1021/ja300897h.

17. Fu Y, Zeng D, Chao J, et al. Single-step rapid assembly of DNA origami nanostructures for addressable nanoscale bioreactors. *Journal of the American Chemical Society*. 2013;135:696-702. doi:10.1021/ja3076692.

18. Minton a P. The influence of macromolecular crowding and macromolecular confinement on biochemical reactions in physiological media. *The Journal of biological chemistry*. 2001;276(14):10577-10580. doi:10.1074/jbc.R100005200.

19. Deeds E, Ashenberg O. Robust protein–protein interactions in crowded cellular environments. *Proceedings of the ...*. 2007;104(38):14952-14957. http://www.pnas.org/content/104/38/14952.short. Accessed June 27, 2015.

20. Zhang DY, Winfree E. Control of DNA strand displacement kinetics using toehold exchange. *Journal of the American Chemical Society*. 2009;131:17303-17314. doi:10.1021/ja906987s.

21. Srinivas N, Ouldridge TE, Šulc P, et al. On the biophysics and kinetics of toehold-mediated DNA strand displacement. *Nucleic Acids Research*. 2013;41:10641-10658. doi:10.1093/nar/gkt801.

22. Yurke B, Turberfield AJ, Mills AP, Simmel FC, Neumann JL. A DNA-fuelled molecular machine made of DNA. *Nature*. 2000;406:605-608. doi:10.1038/35020524.

23. Dittmer WU, Simmel FC. Transcriptional control of DNA-based nanomachines. *Nano Letters*. 2004;4:689-691. doi:10.1021/nl049784v.

24. Bujold KE, Fakhoury J, Edwardson TGW, et al. Sequence-responsive unzipping DNA cubes with tunable cellular uptake profiles. *Chemical Science*. 2014;5:2449-2455. doi:10.1039/c4sc00646a.

25. Ellington AD, Szostak JW. In vitro selection of RNA molecules that bind specific ligands. *Nature*. 1990;346:818-822. doi:10.1038/346818a0.

26. Tuerk C, Gold L. Systematic evolution of ligands by exponential enrichment: RNA ligands to bacteriophage T4 DNA polymerase. *Science (New York, NY)*. 1990;249:505-510. doi:10.1126/science.2200121.

27. Bock LC, Griffin LC, Latham JA, Vermaas EH, Toole JJ. Selection of single-stranded DNA molecules that bind and inhibit human thrombin. *Nature*. 1992;355:564-566. doi:10.1038/355564a0.

28. Stojanovic MN, De Prada P, Landry DW. Aptamer-based folding fluorescent sensor for cocaine. *Journal of the American Chemical Society*. 2001;123:4928-4931. doi:10.1021/ja0038171.

29. Huizenga DE, Szostak JW. A DNA aptamer that binds adenosine and ATP. *Biochemistry*. 1995;34:656-665. doi:10.1021/bi00002a033.

30. Bang GS, Cho S, Kim B-G. A novel electrochemical detection method for aptamer biosensors. *Biosensors & bioelectronics*. 2005;21:863-870. doi:10.1016/j.bios.2005.02.002.

31. Radi AE, Acero Sánchez JL, Baldrich E, O'Sullivan CK. Reagentless, reusable, ultrasensitive electrochemical molecular beacon aptasensor. *Journal of the American Chemical Society*. 2006;128:117-124. doi:10.1021/ja053121d.

32. Stojanovic MN, Landry DW. Aptamer-based colorimetric probe for cocaine. *Journal of the American Chemical Society*. 2002;124:9678-9679. doi:10.1021/ja0259483.

33. Liu X, Freeman R, Willner I. Amplified fluorescence aptamer-based sensors using exonuclease III for the regeneration of the analyte. *Chemistry (Weinheim an der Bergstrasse, Germany)*. 2012;18(8):2207-2211. doi:10.1002/chem.201103342.

34. Levy M, Cater SF, Ellington AD. Quantum-dot aptamer beacons for the detection of proteins. *Chembiochem : a European journal of chemical biology*. 2005;6(12):2163-2166. doi:10.1002/cbic.200500218.

35. Bayer TS, Smolke CD. Programmable ligand-controlled riboregulators of eukaryotic gene expression. *Nature biotechnology*. 2005;23:337-343. doi:10.1038/nbt1069.

36. Banerjee A, Bhatia D, Saminathan A, Chakraborty S, Kar S, Krishnan Y. Controlled release of encapsulated cargo from a DNA icosahedron using a chemical trigger. *Angewandte Chemie - International Edition*. 2013;52:6854-6857. doi:10.1002/anie.201302759.

37. Douglas SM, Bachelet I, Church GM. A Logic-Gated Nanorobot for Targeted Transport of Molecular Payloads. *Science*. 2012;335:831-834. doi:10.1126/science.1214081.

38. Juul S, Iacovelli F, Falconi M, et al. Temperature-controlled encapsulation and release of an active enzyme in the cavity of a self-assembled DNA nanocage. *ACS Nano*. 2013;7:9724-9734. doi:10.1021/nn4030543.

39. Cooper GM, Hausman RE. *The Cell: A Molecular Approach 2nd Edition*.; 2007:1-820.

40. McMahon HT, Boucrot E. Molecular mechanism and physiological functions of clathrin-mediated endocytosis. *Nature reviews Molecular cell biology*. 2011;12:517-533. doi:10.1038/nrm3151.

41. Parton RG, Simons K. The multiple faces of caveolae. *Nature reviews Molecular cell biology*. 2007;8:185-194. doi:10.1038/nrm2122.

42. Gruenberg J, Van der Goot FG. Mechanisms of pathogen entry through the endosomal compartments. *Nature reviews Molecular cell biology*. 2006;7:495-504. doi:10.1038/nrm1959.

43. Dalby B, Cates S, Harris A, et al. Advanced transfection with Lipofectamine 2000 reagent: primary neurons, siRNA, and high-throughput applications. *Methods (San Diego, Calif)*. 2004;33(2):95-103. doi:10.1016/j.ymeth.2003.11.023.

44. Lv H, Zhang S, Wang B, Cui S, Yan J. Toxicity of cationic lipids and cationic polymers in gene delivery. *Journal of Controlled Release*. 2006;114:100-109. doi:10.1016/j.jconrel.2006.04.014.

45. Akhtar S, Benter IF. Review series Nonviral delivery of synthetic siRNAs in vivo. 2007;117(12):3623-3632. doi:10.1172/JCI33494.following.

46. Hemphill J, Deiters A. DNA computation in mammalian cells: MicroRNA logic operations. *Journal of the American Chemical Society*. 2013;135:10512-10518. doi:10.1021/ja404350s.

47. Afonin K a, Viard M, Martins AN, et al. Activation of different split functionalities on re-association of RNA-DNA hybrids. *Nature nanotechnology*. 2013;8:296-304. doi:10.1038/nnano.2013.44.

48. Fakhoury JJ, McLaughlin CK, Edwardson TW, Conway JW, Sleiman HF. Development and characterization of gene silencing DNA cages. *Biomacromolecules*. 2014;15:276-282. doi:10.1021/bm401532n.

49. Ko SH, Liu H, Chen Y, Mao C. DNA nanotubes as combinatorial vehicles for cellular delivery. *Biomacromolecules*. 2008;9:3039-3043. doi:10.1021/bm800479e.

50. Lee H, Lytton-Jean AKR, Chen Y, et al. Molecularly self-assembled nucleic acid nanoparticles for targeted in vivo siRNA delivery. *Nature Nanotechnology*. 2012;7:389-393. doi:10.1038/nnano.2012.73.

51. Li J, Pei H, Zhu B, et al. Self-assembled multivalent DNA nanostructures for noninvasive intracellular delivery of immunostimulatory CpG oligonucleotides. *ACS Nano*. 2011;5:8783-8789. doi:10.1021/nn202774x.

52. Charoenphol P, Bermudez H. Aptamer-targeted DNA nanostructures for therapeutic delivery. *Molecular Pharmaceutics*. 2014;11:1721-1725. doi:10.1021/mp500047b.

53. Reyes-Reyes EM, Teng Y, Bates PJ. A new paradigm for aptamer therapeutic AS1411 action: Uptake by macropinocytosis and its stimulation by a nucleolin-dependent mechanism. *Cancer Research*. 2010;70:8617-8629. doi:10.1158/0008-5472.CAN-10-0920.

54. Soundararajan S, Wang L, Sridharan V, et al. Plasma Membrane Nucleolin Is a Receptor for the Anticancer Aptamer AS1411 in MV4-11 Leukemia Cells □. 2009:984-991. doi:10.1124/mol.109.055947.

55. Surana S, Bhatia D, Krishnan Y. A method to study in vivo stability of DNA nanostructures. *Methods*. 2013;64:94-100. doi:10.1016/j.ymeth.2013.04.002.

56. Bratu DP, Cha B-J, Mhlanga MM, Kramer FR, Tyagi S. Visualizing the distribution and transport of mRNAs in living cells. *Proceedings of the National Academy of Sciences of the United States of America*. 2003;100(23):13308-13313. doi:10.1073/pnas.2233244100.

57. Santangelo PJ, Nix B, Tsourkas A, Bao G. Dual FRET molecular beacons for mRNA detection in living cells. *Nucleic acids research*. 2004;32:57. doi:10.1093/nar/gnh062.

58. Weil TT, Parton RM, Davis I. Making the message clear: Visualizing mRNA localization. *Trends in Cell Biology*. 2010;20:380-390. doi:10.1016/j.tcb.2010.03.006.

59. Chang M, Yang CS, Huang DM. Aptamer-conjugated DNA icosahedral nanoparticles as a carrier of doxorubicin for cancer therapy. *ACS Nano*. 2011;5:6156-6163. doi:10.1021/nn200693a.

60. Zhao Y-X, Shaw A, Zeng X, Benson E, Nyström AM, Högberg B. DNA origami delivery system for cancer therapy with tunable release properties. *ACS nano*. 2012;6:8684-8691. doi:10.1021/nn3022662.

61. Jiang Q, Song C, Nangreave J, et al. DNA origami as a carrier for circumvention of drug resistance. *Journal of the American Chemical Society*. 2012;134:13396-13403. doi:10.1021/ja304263n.

62. Kim K-R, Kim D-R, Lee T, et al. Drug delivery by a self-assembled DNA tetrahedron for overcoming drug resistance in breast cancer cells. *Chemical communications (Cambridge, England)*. 2013;49:2010-2012. doi:10.1039/c3cc38693g.

63. Liu X, Xu Y, Yu T, et al. A DNA nanostructure platform for directed assembly of synthetic vaccines. *Nano Letters*. 2012;12:4254-4259. doi:10.1021/nl301877k.

64. Kole R, Krainer AR, Altman S. RNA therapeutics: beyond RNA interference and antisense oligonucleotides. *Nature Reviews Drug Discovery*. 2012. doi:10.1038/nrd3625.

65. Surana S, Bhat JM, Koushika SP, Krishnan Y. An autonomous DNA nanomachine maps spatiotemporal pH changes in a multicellular living organism. *Nature communications*. 2011;2:340. doi:10.1038/ncomms1340.

66. Gehring K, Leroy J, Guéron M. A tetrameric DNA structure with protonated cytosine-cytosine base pairs. 1993. http://www.nature.com/nature/journal/v363/n6429/abs/363561a0.html. Accessed June 13, 2015.

67. Modi S, Nizak C, Surana S, Halder S, Krishnan Y. Two DNA nanomachines map pH changes along intersecting endocytic pathways inside the same cell. *Nature nanotechnology*. 2013;8:459-467. doi:10.1038/nnano.2013.92.

68. Ishitsuka Y, Ha T. DNA nanotechnology: a nanomachine goes live. *Nature nanotechnology*. 2009;4:281-282. doi:10.1038/nnano.2009.101.

69. Nishikawa M, Mizuno Y, Mohri K, et al. Biodegradable CpG DNA hydrogels for sustained delivery of doxorubicin and immunostimulatory signals in tumor-bearing mice. *Biomaterials*. 2011;32:488-494. doi:10.1016/j.biomaterials.2010.09.013.

70. Mirkin CA, Letsinger RL, Mucic RC, Storhoff JJ. A DNA-based method for rationally assembling nanoparticles into macroscopic materials. *Nature*. 1996;382:607-609. doi:10.1038/382607a0.

71. Rosi NL, Giljohann DA, Thaxton CS, Lytton-Jean AKR, Han MS, Mirkin CA. Oligonucleotide-modified gold nanoparticles for intracellular gene regulation. *Science (New York, NY)*. 2006;312(5776):1027-1030. doi:10.1126/science.1125559.

72. Cutler JI, Zhang K, Zheng D, Auyeung E, Prigodich AE, Mirkin CA. Polyvalent nucleic acid nanostructures. *Journal of the American Chemical Society*. 2011;133:9254-9257. doi:10.1021/ja203375n.

73. Choi CHJ, Hao L, Narayan SP, Auyeung E, Mirkin C a. Mechanism for the endocytosis of spherical nucleic acid nanoparticle conjugates. *Proceedings of the National Academy of Sciences of the United States of America*. 2013;110:7625-7630. doi:10.1073/pnas.1305804110.

74. Storhoff JJ, Elghanian R, Mucic RC, Mirkin CA, Letsinger RL. One-Pot Colorimetric Differentiation of Polynucleotides with Single Base Imperfections Using Gold Nanoparticle Probes. *Journal of the American Chemical Society*. 1998;120(9):1959-1964. doi:10.1021/ja972332i.

75. Prigodich AE, Lee O-S, Daniel WL, Seferos DS, Schatz GC, Mirkin CA. Tailoring DNA structure to increase target hybridization kinetics on surfaces. *Journal of the American Chemical Society*. 2010;132(31):10638-10641. doi:10.1021/ja104859j.

76. Alhasan AH, Kim DY, Daniel WL, et al. Scanometric microRNA array profiling of prostate cancer markers using spherical nucleic acid-gold nanoparticle conjugates. *Analytical chemistry*. 2012;84(9):4153-4160. doi:10.1021/ac3004055.

77. Prigodich AE, Randeria PS, Briley WE, et al. Multiplexed nanoflares: mRNA detection in live cells. *Analytical chemistry*. 2012;84(4):2062-2066. doi:10.1021/ac202648w.

78. Zheng D, Giljohann DA, Chen DL, et al. Topical delivery of siRNA-based spherical nucleic acid nanoparticle conjugates for gene regulation. *Proceedings of the National Academy of Sciences*. 2012;109:11975-11980. doi:10.1073/pnas.1118425109.

79. Jensen SA, Day ES, Ko CH, et al. Spherical nucleic acid nanoparticle conjugates as an RNAi-based therapy for glioblastoma. *Science translational medicine*. 2013;5:209ra152. doi:10.1126/scitranslmed.3006839.

80. Cutler JI, Auyeung E, Mirkin CA. Spherical nucleic acids. *Journal of the American Chemical Society*. 2012;134:1376-1391. doi:10.1021/ja209351u.

81. Veronese ML, Bullrich F, Negrini M, Croce CM. The t(6;16)(p21;q22) chromosome translocation in the LNCaP prostate carcinoma cell line results in a tpc/hpr fusion gene. *Cancer Research*. 1996;56:728-732.

82. Douglas SM, Dietz H, Liedl T, Högberg B, Graf F, Shih WM. Self-assembly of DNA into nanoscale three-dimensional shapes. *Nature*. 2009;459:414-418. doi:10.1038/nature08165.

83. Martin TG, Dietz H. Magnesium-free self-assembly of multi-layer DNA objects. *Nature Communications*. 2012;3:1103. doi:10.1038/ncomms2095.

84. Peitsch MC, Polzar B, Stephan H, et al. Characterization of the endogenous deoxyribonuclease involved in nuclear DNA degradation during apoptosis (programmed cell death). *The EMBO journal*. 1993;12:371-377.

85. Houk BE, Hochhaus G, Hughes JA. Kinetic modeling of plasmid DNA degradation in rat plasma. *AAPS pharmSci*. 1999;1:E9.

86. Keum J-W, Bermudez H. Enhanced resistance of DNA nanostructures to enzymatic digestion. *Chemical communications (Cambridge, England)*. 2009:7036-7038. doi:10.1039/b917661f.

87. Mei Q, Wei X, Su F, et al. Stability of DNA origami nanoarrays in cell lysate. *Nano Letters*. 2011;11:1477-1482. doi:10.1021/nl1040836.

88. Hahn J, Wickham SFJ, Shih WM, Perrault SD. Addressing the Instability of DNA Nanostructures in Tissue Culture. *ACS nano*. 2014. doi:10.1021/nn503513p.

89. Conway JW, McLaughlin CK, Castor KJ, Sleiman H. DNA nanostructure serum stability: greater than the sum of its parts. *Chemical communications (Cambridge, England)*. 2013;49:1172-1174. doi:10.1039/c2cc37556g.

90. Perrault SD, Shih WM. Virus-inspired membrane encapsulation of DNA nanostructures to achieve in vivo stability. *ACS Nano*. 2014;8:5132-5140. doi:10.1021/nn5011914.

91. Stein IH, Schüller V, Böhm P, Tinnefeld P, Liedl T. Single-molecule FRET ruler based on rigid DNA origami blocks. *Chemphyschem : a European journal of chemical physics and physical chemistry*. 2011;12(3):689-695. doi:10.1002/cphc.201000781.

92. Murphy MC, Rasnik I, Cheng W, Lohman TM, Ha T. Probing Single-Stranded DNA Conformational Flexibility Using Fluorescence Spectroscopy. 2004;86(April):2530-2537.

93. Smith RM, Martell AE, Motekaitis RJ. *NIST Critically Selected Stability Constants of Metal Complexes Database*. National Institute of Standards & Technology; 1998.

94. Ahmad R, Arakawa H, Tajmir-Riahi H. A comparative study of DNA complexation with Mg (II) and Ca (II) in aqueous solution: major and minor grooves bindings. *Biophysical journal*. 2003;84(April):2460-2466. http://www.sciencedirect.com/science/article/pii/S0006349503750504. Accessed June 20, 2015.

95. Zanetti-Domingues LC, Tynan CJ, Rolfe DJ, Clarke DT, Martin-Fernandez M. Hydrophobic fluorescent probes introduce artifacts into single molecule tracking experiments due to non-specific binding. *PLoS ONE*. 2013;8. doi:10.1371/journal.pone.0074200.

96. Yurke B, Mills AP. Using DNA to power nanostructures. *Genetic Programming and Evolvable Machines*. 2003;4:111-122. doi:10.1023/A:1023928811651.

97. Ezzat K, El Andaloussi S, Zaghloul EM, et al. PepFect 14, a novel cell-penetrating peptide for oligonucleotide delivery in solution and as solid formulation. *Nucleic Acids Research*. 2011;39:5284-5298. doi:10.1093/nar/gkr072.

98. Kang SH, Cho MJ, Kole R. Up-regulation of luciferase gene expression with antisense oligonucleotides: implications and applications in functional assay development. *Biochemistry*. 1998;37:6235-6239. doi:10.1021/bi980300h.

99. Sandbichler AM, Aschberger T, Pelster B. A method to evaluate the efficiency of transfection reagents in an adherent zebrafish cell line. *BioResearch open access*. 2013;2:20-27. doi:10.1089/biores.2012.0287.

100. Hemphill J, Deiters A. DNA computation in mammalian cells: MicroRNA logic operations. *Journal of the American Chemical Society*. 2013;135:10512-10518. doi:10.1021/ja404350s.

101. Luzio JP, Pryor PR, Bright NA. Lysosomes: fusion and function. *Nature reviews Molecular cell biology*. 2007;8:622-632. doi:10.1038/nrm2217.

102. Schindelin J, Arganda-Carreras I, Frise E, et al. Fiji: an open-source platform for biological-image analysis. *Nature Methods*. 2012;9:676-682. doi:10.1038/nmeth.2019.

103. Kameyama S, Horie M, Kikuchi T, et al. Acid wash in determining cellular uptake of fab/cell-permeating peptide conjugates. In: *Biopolymers - Peptide Science Section*. Vol 88. ; 2007:98-107. doi:10.1002/bip.20689.

104. Silverstein SC, Steinman RM, Cohn ZA. Endocytosis. *Annual review of biochemistry*. 1977;46:669-722. doi:10.1146/annurev.bi.46.070177.003321.

105. Vercauteren D, Vandenbroucke RE, Jones AT, et al. The use of inhibitors to study endocytic pathways of gene carriers: optimization and pitfalls. *Molecular therapy : the journal of the American Society of Gene Therapy*. 2010;18:561-569. doi:10.1038/mt.2009.281.

106. Mousavi SA, Kjeken R, Berg TO, Seglen PO, Berg T, Brech A. Effects of inhibitors of the vacuolar proton pump on hepatic heterophagy and autophagy. *Biochimica et Biophysica Acta - Biomembranes*. 2001;1510:243-257. doi:10.1016/S0005-2736(00)00354-0.

107. Dunn WA, Hubbard AL, Aronson NN. Low temperature selectively inhibits fusion between pinocytic vesicles and lysosomes during heterophagy of 125I-asialofetuin by the perfused rat liver. *The Journal of biological chemistry*. 1980;255:5971-5978.

108. Bashirullah A, Cooperstock RL, Lipshitz HD. RNA localization in development. *Annual review of biochemistry*. 1998;67:335-394. doi:10.1146/annurev.biochem.67.1.335.

109. Church SL, Grant JW, Ridnour LA, et al. Increased manganese superoxide dismutase expression suppresses the malignant phenotype of human melanoma cells. *Proceedings of the National Academy of Sciences of the United States of America*. 1993;90:3113-3117.

110. Ding Y, Chan CY, Lawrence CE. Sfold web server for statistical folding and rational design of nucleic acids. *Nucleic Acids Research*. 2004;32. doi:10.1093/nar/gkh449.

111. Shao Y, Wu Y, Chan CY, McDonough K, Ding Y. Rational design and rapid screening of antisense oligonucleotides for prokaryotic gene modulation. *Nucleic Acids Research*. 2006;34:5660-5669. doi:10.1093/nar/gkl715.

112. Christoffersen RE, McSwiggen J, Konings D. Application of computational technologies to ribozyme biotechnology products. *Journal of Molecular Structure*. 1994;311:273-284.

113. Sixou S, Szoka FC, Green GA, Giusti B, Zon G, Chin DJ. Intracellular oligonucleotide hybridization detected by fluorescence resonance energy transfer (FRET). *Nucleic acids research*. 1994;22:662-668. doi:10.1093/nar/22.4.662.

114. Tyagi S. Imaging intracellular RNA distribution and dynamics in living cells. *Nature methods*. 2009;6:331-338. doi:10.1038/nmeth.1321.

115. Tsuji A, Koshimoto H, Sato Y, et al. Direct observation of specific messenger RNA in a single living cell under a fluorescence microscope. *Biophysical journal*. 2000;78:3260-3274. doi:10.1016/S0006-3495(00)76862-7.

116. Qiu L, Wu C, You M, et al. A targeted, self-delivered, and photocontrolled molecular beacon for mRNA detection in living cells. *Journal of the American Chemical Society*. 2013;135:12952-12955. doi:10.1021/ja406252w.

117. Ponchon L, Beauvais G, Nonin-Lecomte S, Dardel F. A generic protocol for the expression and purification of recombinant RNA in Escherichia coli using a tRNA scaffold. *Nature protocols*. 2009;4:947-959. doi:10.1038/nprot.2009.67.

118. Sunbul M, Jäschke A. Contact-mediated quenching for RNA imaging in bacteria with a fluorophore-binding aptamer. *Angewandte Chemie - International Edition*. 2013;52:13401-13404. doi:10.1002/anie.201306622.

119. Zadeh JN, Steenberg CD, Bois JS, et al. NUPACK: Analysis and design of nucleic acid systems. *Journal of Computational Chemistry*. 2011;32:170-173. doi:10.1002/jcc.21596.

120. Plochowietz a, Crawford R, Kapanidis a N. Characterization of organic fluorophores for in vivo FRET studies based on electroporated molecules. *Physical chemistry chemical physics : PCCP*. 2014:1-3. doi:10.1039/c4cp00995a.

121. Green SJ, Lubrich D, Turberfield AJ. DNA hairpins: fuel for autonomous DNA devices. *Biophysical journal*. 2006;91:2966-2975. doi:10.1529/biophysj.106.084681.

122. Seelig G, Soloveichik D, Zhang DY, Winfree E. Enzyme-free nucleic acid logic circuits. *Science (New York, NY)*. 2006;314:1585-1588. doi:10.1126/science.1132493.

123. Rana TM. Illuminating the silence: understanding the structure and function of small RNAs. *Nature reviews Molecular cell biology*. 2007;8:23-36. doi:10.1038/nrm2085.

124. Van Rooij E, Olson EN. MicroRNAs: Powerful new regulators of heart disease and provocative therapeutic targets. *Journal of Clinical Investigation*. 2007;117:2369-2376. doi:10.1172/JCI33099.

125. Iorio M V., Ferracin M, Liu CG, et al. MicroRNA gene expression deregulation in human breast cancer. *Cancer Research*. 2005;65:7065-7070. doi:10.1158/0008-5472.CAN-05-1783.

126. Lee Y, Ahn C, Han J, et al. The nuclear RNase III Drosha initiates microRNA processing. *Nature*. 2003;425:415-419. doi:10.1038/nature01957.

127. Yi R, Qin Y, Macara IG, Cullen BR. Exportin-5 mediates the nuclear export of pre-microRNAs and short hairpin RNAs. *Genes and Development*. 2003;17:3011-3016. doi:10.1101/gad.1158803.

128. Denti MA, Rosa A, Sthandier O, De Angelis FG, Bozzoni I. A new vector, based on the polII promoter of the U1 snRNA gene, for the expression of siRNAs in mammalian cells. *Molecular Therapy*. 2004;10:191-199. doi:10.1016/j.ymthe.2004.04.008.

129. Roberts TC. Duchenne muscular dystrophy: RNA-based therapeutics and microRNA biology. 2012.

130. Ohkawa J, Taira K. Control of the functional activity of an antisense RNA by a tetracycline-responsive derivative of the human U6 snRNA promoter. *Human gene therapy*. 2000;11:577-585. doi:10.1089/10430340050015761.

131. Alvarez-Erviti L, Seow Y, Yin H, Betts C, Lakhal S, Wood MJA. Delivery of siRNA to the mouse brain by systemic injection of targeted exosomes. *Nature biotechnology*. 2011;29:341-345. doi:10.1038/nbt.1807.

132. Goodchild J. Therapeutic oligonucleotides. *Methods in Molecular Biology*. 2011;764:1-15. doi:10.1007/978-1-61779-188-8_1.

133. Lu QL, Mann CJ, Lou F, et al. Functional amounts of dystrophin produced by skipping the mutated exon in the mdx dystrophic mouse. *Nature medicine*. 2003;9:1009-1014. doi:10.1038/nm897.

134. Bauman J, Jearawiriyapaisarn N, Kole R. Therapeutic potential of splice-switching oligonucleotides. *Oligonucleotides*. 2009;19:1-13. doi:10.1089/oli.2008.0161.

135. Asseline U, Gonçalves C, Pichon C, Midoux P. Improved nuclear delivery of antisense 2'-Ome RNA by conjugation with the histidine-rich peptide H5WYG. *The journal of gene medicine*. 2014;33:1-25. doi:10.1002/jgm.2773.

136. Alam R, Dixit V, Kang H, et al. Intracellular delivery of an anionic antisense oligonucleotide via receptor-mediated endocytosis. *Nucleic Acids Research*. 2008;36:2764-2776. doi:10.1093/nar/gkn115.

137. Walsh AS. Biological applications of DNA cages. 2011.

138. Newkirk MM, Edmundson A, Wistar R, Klapper DG, Capra JD. A new protocol to digest human IgM with papain that results in homogeneous Fab preparations that can be routinely crystallized. *Hybridoma*. 1987;6:453-460. doi:10.1089/hyb.1987.6.453.

139. Chu Z, Zhang S, Zhang B, et al. Unambiguous observation of shape effects on cellular fate of nanoparticles. *Scientific reports*. 2014;4:4495. doi:10.1038/srep04495.

140. Chithrani BD, Chan WCW. Elucidating the mechanism of cellular uptake and removal of protein-coated gold nanoparticles of different sizes and shapes. *Nano Letters*. 2007;7:1542-1550. doi:10.1021/nl070363y.

141. Ji Z, Wang X, Zhang H, et al. Designed synthesis of CeO2 nanorods and nanowires for studying toxicological effects of high aspect ratio nanomaterials. *ACS nano*. 2012;6:5366-5380. doi:10.1021/nn3012114.

142. He X, Dong L, Wang W, Lin N, Mi Y. Folding single-stranded DNA to form the smallest 3D DNA triangular prism. *Chemical communications (Cambridge, England)*. 2013;49:2906-2908. doi:10.1039/c3cc39266j.

143. Hu T, Fu Q, Chen P, Ma L, Sin O, Guo D. Construction of an artificial microRNA expression vector for simultaneous inhibition of multiple genes in mammalian cells. *International Journal of Molecular Sciences*. 2009;10:2158-2168. doi:10.3390/ijms10052158.

144. Dassie JP, Hernandez LI, Thomas GS, et al. Targeted inhibition of prostate cancer metastases with an RNA aptamer to prostate specific membrane antigen (PSMA). *Molecular therapy : the journal of the American Society of Gene Therapy*. 2014. doi:10.1038/mt.2014.117.

145. Ge Z, Lin M, Wang P, et al. Hybridization chain reaction amplification of microRNA detection with a tetrahedral DNA nanostructure-based electrochemical biosensor. *Analytical Chemistry*. 2014;86:2124-2130. doi:10.1021/ac4037262.

146. Wen Y, Pei H, Shen Y, et al. DNA Nanostructure-based Interfacial engineering for PCR-free ultrasensitive electrochemical analysis of microRNA. *Scientific reports*. 2012;2:867. doi:10.1038/srep00867.

147. Sheng Q, Liu R, Zhang S, Zheng J. Ultrasensitive electrochemical cocaine biosensor based on reversible DNA nanostructure. *Biosensors and Bioelectronics*. 2014;51:191-194. doi:10.1016/j.bios.2013.07.053.

# Appendix D